Elements of Fracture Mechanics

Prashant Kumar
Former Professor
Department of Mechanical Engineering
IIT Kanpur

McGraw Hill Education (India) Private Limited
NEW DELHI

McGraw Hill Education Offices
New Delhi New York St Louis San Francisco Auckland Bogotá Caracas
Kuala Lumpur Lisbon London Madrid Mexico City Milan Montreal
San Juan Santiago Singapore Sydney Tokyo Toronto

McGraw Hill Education (India) Private Limited

Published by McGraw Hill Education (India) Private Limited,
P-24, Green Park Extension, New Delhi 110 016.

Seventh reprint 2014
RLZXCRCURQZAR

ISBN (13): 978-0-07-065696-3
ISBN (10): 0-07-065696-7

Managing Director: *Kaushik Bellani*

Asst. Manager—Production: *Sohan Gaur*
Manager—Sales & Marketing: *S Girish*
Product Manager—Science, Technology and Computing: *Rekha Dhyani*
General Manager—Production: *Rajender P Ghansela*

Typeset at Script Makers, 19, A1-B, DDA Market, Paschim Vihar, New Delhi 110 063 and printed at AP Offset Pvt. Ltd., Delhi 110 095

Cover Printer: AP Offset Pvt. Ltd.

Cover Designer: Kapil Gupta

To

Many excellent teachers who motivated me from my school days to PhD program. Some of them are:

K. Kumar, Lucknow Montessori School, Lucknow (1956-57)
T. Joshi, Lucknow Christian College, Lucknow (1960-62)
N. C. Dahl, IIT Kanpur, Visiting from MIT, USA (1963-64)
A. J. Erickson, IIT Kanpur, Visiting from MIT, USA (1963-65)
P. W. Fay, IIT Kanpur, Visiting from Cal. Tech., USA (1965-66)
C. W. Radcliff, University of California, Berkeley, USA (1967-68)
Y. Takahashi, University of California, Berkeley, USA (1967-68)
R. J. Clifton, Brown University, USA (1970-77)
L. B. Freund, Brown University, USA (1971-74)
A.C. Pipkin, Brown University, USA (1972-73)
P.C. Paris, Brown University, Visiting from Lehigh University, USA (1973-74)
Barton Roessler, Brown University, USA (1973-74)
J.R. Rice, Brown University, USA (1972-73)

and

My uncle Dr. Ram Krishan and aunt Mrs. Sheela Krishan who raised me and played the most pivotal role in shaping my thought process.

Preface

There are many components of machines, process plants and household goods that fail through fatigue and fracture, which can be avoided by applying *fracture mechanics*. Although the modern fracture mechanics was born in 1948–49, its acceptability was quite slow for several decades because of its complex mathematics and involved concepts. Initially, the fracture mechanics was applied to high-risk products like nuclear plants, airplanes, space vehicles, submarines, etc. Now this field is becoming popular at the grassroot levels too. Therefore, it is important to explain this concept in simple, well-disposed and easy-to-understand manner without compromising on the rigor—this book is intended to do the same.

The book has gone through several phases of revisions to improve its readability further. Several analogies and anecdotes placed appropriately in this book have also helped in accomplishing this goal. Two most important mechanisms—fatigue failure and environment-assisted fracture that result in the growth of subcritical cracks to catastrophic failure of structural components—have been discussed in Chapter 9. Along with that, an additional chapter has talked about various non-destructive test methods for identifying cracks in the structural components. The detailed illustrations developed with the help of latest graphic software have added more clarity in understanding the concept.

This book has adopted the approach of different courses on fracture mechanics at the advanced undergraduate and postgraduate levels. The readers novice in this field can explore this complex but beautiful concept effortlessly through this book. The responses of students have directed me in choosing the right pace and the appropriate levels while presenting the subject. Readers with prior knowledge of fracture mechanics may find it rudimentary at few places. But with experience I have learned to be on elementary side rather than leaving a reader confused.

Unlike in most books on fracture mechanics where basic concepts are discussed shortly usually leaving the reader confused, this book gradually discusses the fundamental theory with the results and their applications. With my industrial experience and interest in product design, I view the theories of fracture mechanics as useful tools to be applied to practical problems. Once the fundamentals of fracture mechanics are mastered properly, the reader can easily move to advanced books or research journals. Therefore, special tricks involving highly complex mathematics to solve problems of minor interest are not included here.

I hope this book will be appreciated by the readers for its salient features like lucid content, articulation, anecdotes, and presentation of the subject in small and effective steps, and will prove to be beneficial in introducing the subject in general.

PRASHANT KUMAR

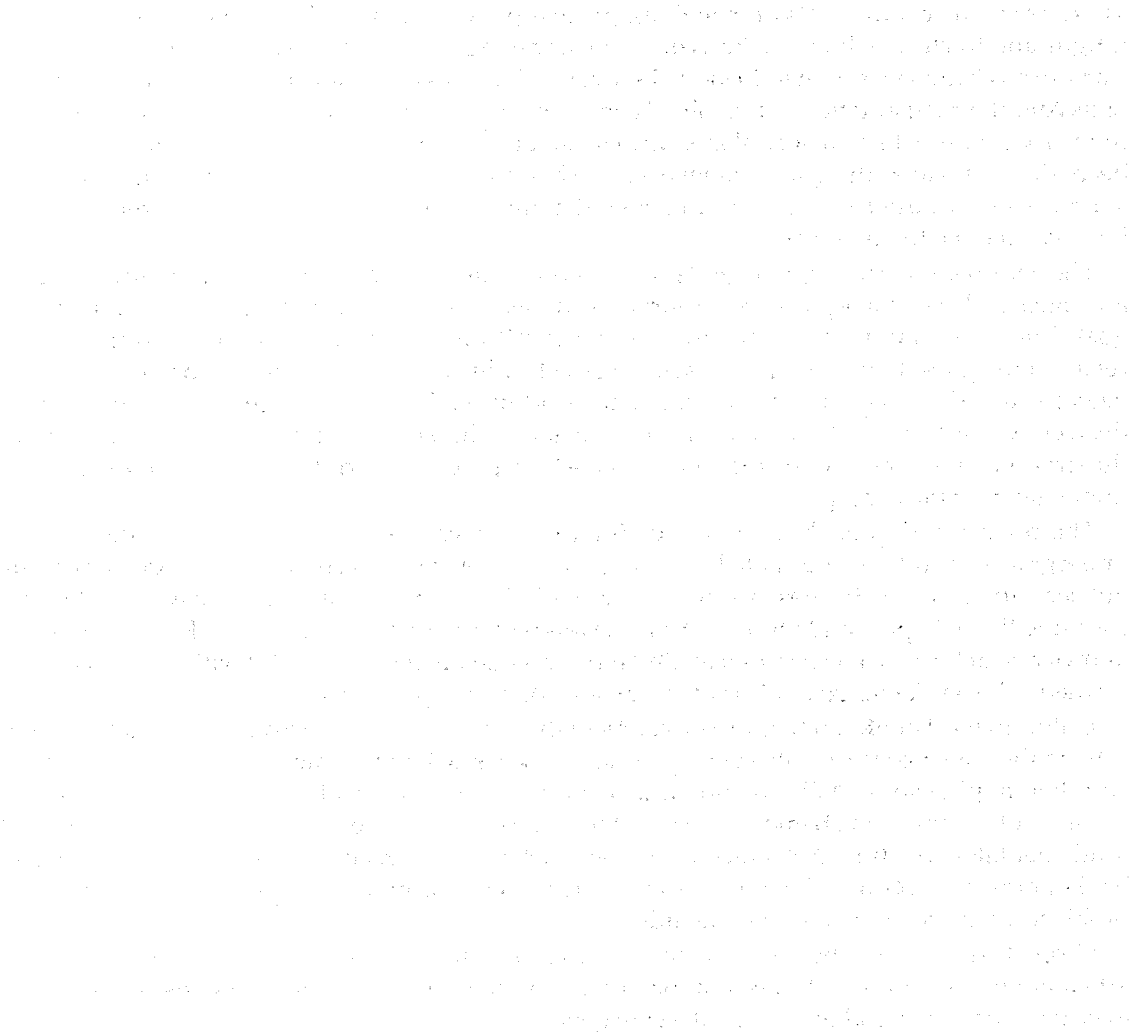

Acknowledgements

- IIT Kanpur for encouragement and financial support to prepare the manuscript
- ARDB, Sena Bhavan, New Delhi for supporting various research grants in the field of fracture mechanics
- Prof. N.N. Kishore (IIT Kanpur) for contributing a chapter in the book
- Prof. Raju Sethuraman (IIT Madras) for contributing a chapter in the book
- Prof. K. Ramesh (IIT Madras) for contributing a figure on photoelastic fringes
- Profs. Bishakh Bhattacharya, J. Ramkumar and K. K. Kar for constructive criticism of the manuscript
- Raj Mulani, Rahul Ranjan Pandey, Ramesh Chandra and Yatendra for preparing the illustrations using latest graphic softwares
- Vinay Pahlajani and Rajamanohar for their help in graphics through latest softwares
- Mr. Divakar to coordinate various activities in preparing the manuscript
- Mr. Anurag Goel to meet various needs of the manuscript preparation
- Mrs. Sandhya Agnihotri and S.L. Yadav for typing the manuscript
- Mr. Kalyan Kumar Singh for constructive suggestions and help in proof reading
- My son Saurabh Vishal on persistent encouragement to have the book published
- McGraw-Hill Education (India) Ltd. for publishing the book

Contents

Chapter 1

Background

I learned there that innovation is a very difficult thing in the real world.

R.P. Feynman

1.1 Kinds of Failure

Some people suffer from hypertension and are susceptible to heart attacks. Many, unfortunately, suffer from diabetes and take special precautions to avoid or delay its destructive effects. On an average, a person in our society is vulnerable to one or two of such diseases as cancer, arthritis, asthma, hepatitis, gastritis, tuberculosis, etc. and is conscious about it. Similarly, a component in a structure may be susceptible to one, two or more kinds of failure. For example, under given load conditions a roller bearing is most likely to fail through fatigue of its rollers after a certain number of rotations.

We should thus know the different conditions that can cause the failure of a structural component. Some of the common causes of failure are:

- Yielding
- Deflection beyond a certain stage
- Buckling
- Fatigue
- Fracture
- Creep
- Environmental degradation
- Resonance
- Impact
- Wear

A component is designed so as to avoid yielding of the worst loaded point (critical point). Safety against yield failure is considered to be the basic requirement of any design and is taught in all courses on 'strength of materials' at undergraduate level. Although stress tensor is quite complex with six independent components, criteria like Mises or Tresca are adopted to obtain a

scalar number (e.g., maximum shear stress in Tresca criterion). The scalar number is then compared with a limiting value which is determined through experiments. In simple cases, the worst loaded point may easily be identified, whereas it may be difficult to find where exactly the worst loaded point is in a general case. These days excellent computer packages based on finite element analysis are available. In a finite element simulation, the body of the component can be divided into different colors; for example, red color shows the portion where the stresses are maximum, green color shows the lowest stresses and other colors for intermediate stresses. However, it has been found that often a structural component fails even when the worst loaded point is well within the yield stress. Thus we conclude that a design of a work-component based entirely on avoiding yielding is not adequate in certain cases. The component may be susceptible to crack growth!

All engineering materials deform on loading. A structural component may be deformed to such an extent that its performance is affected. Certain plastics have been developed to possess high strength, but they may not be suitable for many structural components because of their low stiffness, i.e., about 1% of steel's stiffness. If the wings of an airplane are made of a polymer, they may droop down so much that the tip of the wings would touch the ground. In fact, many components of conventional engineering materials (steel, aluminum, and the like) are designed to meet constraints of deflection, although the stress of the worst loaded point is considerably lower than yield stress. These kinds of components are thus susceptible to failure through deflection beyond a certain value. If a crack grows in a component, its stiffness decreases and the deformation may exceed the allowable limit.

A thin member under a compressive load or a thin tube under torsion or lateral compression may be susceptible to buckling, and the design should be checked against likely failure through buckling.

Many components of the modern industrial world are subjected to fluctuating loads and consequently may fail through fatigue. In fact, failure through fatigue is so common that more than 80% failures are caused by fluctuating loads. Many investigators are currently working for the development of this field. However, convenient and effective methods to control fatigue-failures are still not adequately developed. A critical structural component should be regularly checked to detect fatigue cracks through non-destructive tests. This has led to the development of excellent methods of crack identification, such as ultrasonic crack detection, X-ray or radiation filming, detecting through monitoring acoustic emission, magnetic flux method, decoration of surface cracks through dye-penetration, etc.

Fracture mechanics is based on the implicit assumption that there exists a crack in a work-component. The crack may be man-made such as a hole, a notch, a slot, a re-entrant corner, etc. The crack may exist within a component due to manufacturing defects like slag inclusion, cracks in a weldment or heat affected zones due to uneven cooling and presence of foreign particles. A dangerous crack may be nucleated and grown during the service of the component (fatigue generated cracks, nucleation of notches due to environmental dissolution). Fracture mechanics deals with the question—is a known crack likely to grow under a certain given loading condition? Fracture mechanics is also applied to crack growth under fatigue loading. Initially, the fluctuating load nucleates a crack, which then grows slowly and finally the crack growth rate per cycle picks up speed. Thereafter comes the stage when the crack-length is long enough to be considered critical for a catastrophic fracture failure.

About 50–60 years ago, when accurate analysis for predicting the growth of a crack was not available, a reasonably high factor of safety was chosen to account for unforeseen factors. A large

part of this ambiguity has been cleared with the development of fracture mechanics and understanding the causes and effects of fatigue failure. This now enables a designer to use a much lower factor of safety, thus reducing cost of such structural components. Simultaneously, the weight of these components is reduced and their reliability is enhanced.

Other ways of failure (creep, environmental degradation, wear, etc.) are also as important and must be looked into and analyzed, so that the component may not develop snags on their account. However, one thing should also be borne in mind, that a component is usually not likely to fail through more than two or three ways. Therefore, susceptibility should be kept in mind at the time of designing a component.

1.2 Historical Aspects

For a long time, we always had some idea about the role of a crack or a notch. While cutting a tree, we would make a notch with an axe at its trunk and then pull it down with a rope. While breaking a stick we would make a small notch with a knife before bending it. Swords played an important role in the pre-industrial society. Good swords were made by folding a thin metal sheet at the centre line and then hammering it to make it thin again so that it could be further folded. Thus, a sword would have many layers. If a crack develops in one of the layers, it is not likely to move to another, thus making the sword very tough.

Leonardo da Vinci (1452–1519) was the first person to make a setup to measure the strength of a wire. He found out that the strength of a wire depended on its length. A wire in his time were not of high quality and a long wire was likely to posses many cracks. However, fracture mechanics was not studied as a separate discipline for a long time.

The Industrial Revolution opened a new vista for us and many different kinds of machines and structures were designed and built. If we look back and study, we would find that many bridges, boilers, buildings, ships, were failed due to fracture in nineteenth century [1.1]. Locomotives, a very important industry in those days, used to face innumerable accidents due to failure of wheels, axles of wheels, and rails. Wohler [1.2] was one of the earliest investigators (1860), who investigated fatigue of locomotive axles by applying controlled cyclic loads. This led to development of S-N Diagram and finding endurance limit of steel [1.3].

In nineteenth century and early part of twentieth century, the entire industry was obsessed with production. Even the failure theories were developed quite late: Tresca in (1864) and Mises (1913). However, World War II accelerated the industrial production at a very rapid rate, due to unusually high demands of war. Within six years of the war, the know-how of aircraft making improved dramatically. Also, the ships, which were earlier made by joining plates together through the process of riveting, were changed to welded frames. Many cargo ships, known as liberty ships, were rolled out from American docks within a short span. However, soon there were complications regarding welded structures. Many of these failed in the cold temperatures of the North Atlantic Ocean [1.1]. As a matter of fact some of these broke up into two parts. However, ships made by riveting plates did not display such failures. If a crack nucleated and grew in a plate, it would only split that plate into two parts; the crack would not grow into another plate. A welded structure is a large single continuous part and therefore, if the crack becomes critical, it will run through the entire hull of the ship.

Jet planes were developed initially as small fighter planes, which would fly at high altitudes. When this technology was used for the construction of large body passenger planes, it was found that the planes were exploded in the air. An investigating team was appointed to look into the failures of the Comet Jetliner right in the early fifties. It was found that a fatigue crack, initiated near an opening in the fuselage [1.4], ran through its entire body especially at high altitudes, where the outside atmospheric pressure was low and the interior of the airplane was pressurized for the comfort of passengers. In fact, a jetliner flying over a height of 10,000 m (32,800 ft) works like a pressurized balloon with the wall of its fuselage under high tensile stresses.

With the development of large ships made of welding plates and high capacity jet airplanes, new problems arose; the predominant question asked was—what causes the failure? Can we contain the failure? And then a new discipline of engineering, called 'fracture mechanics' was developed. In fact, Griffith [1.5, 1.6] developed the right ideas for the growth of a crack in the 1920s. Using atomistic models, he estimated the strength of a structural material and found that it should be of the order of its modulus. However, the strength of engineering materials was experimentally found to be of two to three lower orders. He went ahead and developed the ideas of energy requirements in growing a crack. However, his work was not taken seriously at that time because engineers were busy in increasing production and making money. This period was followed by the Great Depression which had many problems of its own. Further, Griffith was not able to invent a convenient parameter to predict the load on a component that would cause the growth of a crack.

For all practical purposes, modern fracture mechanics was born in 1948 when George Irwin [1.7] formulated fracture mechanics by devising workable parameters like stress intensity factor and energy release rate. Once the breakthrough took place, many investigators started taking interest in it and fracture mechanics became a separate and important discipline with several reputed journals and text books. Irwin's development was mainly for brittle or less ductile materials. The analysis was conservative for most engineering materials which are generally ductile. Other parameters, like Crack Tip Opening Displacement by Wells [1.8] in 1961 and J-Integral by Rice [1.9] in 1968, were developed to account for the large plastic zone at the crack-tip in ductile materials.

Fracture mechanics is now applied extensively to important fields like nuclear engineering, piping, space ships, rockets, offshore structures, etc. Critical components in nuclear power plants are made from very tough materials; but they too have failed catastrophically once in a while.

1.3 Brittle and Ductile Fracture

Some materials are known as brittle because a crack moves easily through components made of such materials. If we investigate a fractured surface of a brittle failure to determine the depth up to which the material is affected by the crack growth, we find that material was influenced to a very shallow depth. Rest of the material remains unaffected. On the contrary, a ductile fracture causes a large amount of plastic deformation to a significant depth.

Brittle fracture in crystalline metals can be classified into two broad groups—intergranular and transgranular. A crack tip of intergranular failure grows along the grain boundaries as shown in [Fig. 1.1 (a)]. Transgranular fracture, on the other hand, occurs through the crack tip propagating within grains [Fig. 1.1 (b)]. However, cleavage failure within a grain occurs along a weak crystallographic plane. In fact, cleavage fracture is the most brittle form of a fracture and it hardly

damages the fractured surfaces. Once the cleavage crack reaches the grain boundary, it finds another favorable orientation in the next grain.

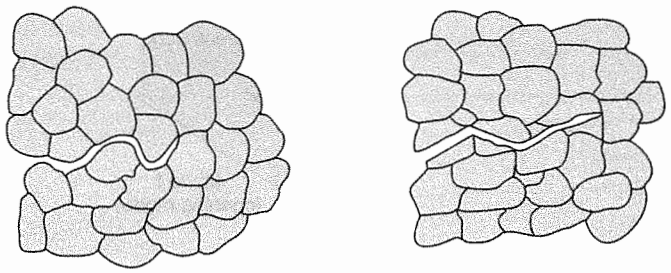

(a) Intergranular (b) Transgranular

Fig. 1.1 Brittle fracture

Ductile fracture growth occurs due to substantial plastic deformation and creation of microvoids in the vicinity of the crack tip. The material deforms plastically due to micromechanisms, such as nucleation and motion of dislocations, formation of twins, etc. Engineering materials generally contain second phase particles. Tiny voids are formed at the sides of these particles under the influence of the tensile field of the crack tip. Dislocation motion helps in the formation of these voids. The ductile crack growth occurs by the coalescence of these voids. Fractured surface of a ductile failure shows tiny dimples and gives the surface a rather rough look. In fact, around one such dimple, a second phase particle can be identified. The plastic deformation and coalescence of voids absorb a large amount of energy and, therefore, a crack does not grow easily in ductile materials.

Often it has been found that materials normally ductile at room temperature in ordinary conditions behave as brittle materials under certain special conditions. Steel, which is quite ductile at room temperature, becomes brittle at low temperatures. This explains why welded structures of Liberty ships in World War II failed in the cold waters of the North Atlantic Ocean. Also, the toughness of certain materials is affected considerably by the rate of loading (strain rate).

A thick plate of a regular ductile material may also allow the growth of a crack in a brittle manner. The portion that is deep inside the thick plate (away from free surfaces) is constrained from all sides and large plastic deformations are not possible in the vicinity of the crack-tip. In comparison to thick plates, thin plates are more resistant to crack growth. These aspects will be discussed in detail in subsequent chapters.

1.4 Modes of Fracture Failure

A crack front in a structural component is a line usually of varying curvature. Thus, the state of stress in the vicinity of the crack front varies from one point to another. A segment of the crack front can be divided into three basic modes as shown in Fig. 1.2. Mode I is the opening mode and the displacement is normal to the crack surface. Mode II is a sliding mode and the displacement is in the plane of the plate—the separation is antisymmetric and the relative displacement is normal to the crack front. Mode III also causes sliding motion but the displacement is parallel to the crack front, thereby causing tearing.

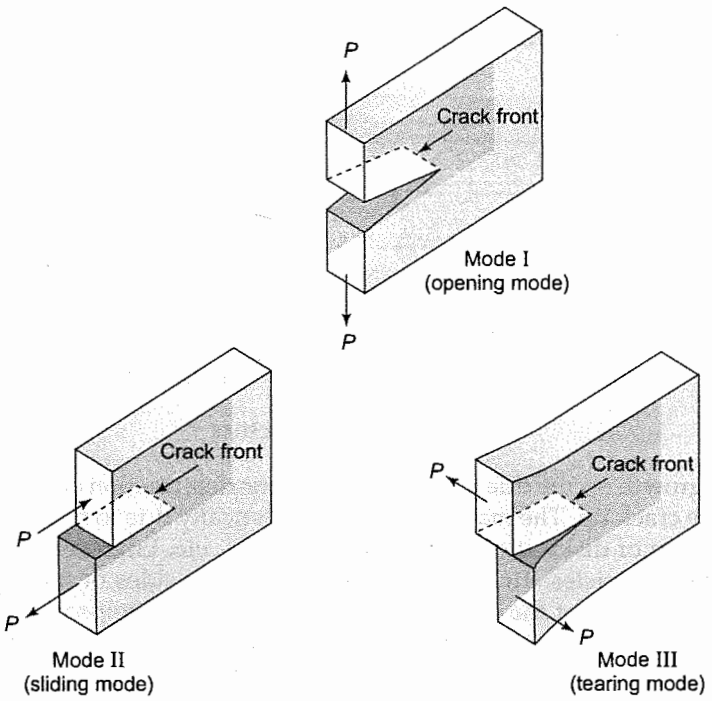

Fig. 1.2 The three modes of fracture

An inclined crack front in a component can be modeled as a superposition of the three basic modes and then, the effect of loading by each mode can be analyzed separately. Mode I usually plays a dominant role in many engineering applications and is considered to be the most dangerous. However, in certain applications, components fail through the dominant roles played by Mode II or Mode III. Mode I has been analyzed most so far. Also, elaborate experimental methods have been developed to determine toughness in Mode I; in fact, detailed codes have been prepared for these experimental methods and they are internationally accepted.

1.5 How Potent Is a Crack?

Designers are always interested to know whether a crack is likely to grow if the geometry of a crack in a structural component, loads and other boundary conditions are known. We should, therefore, have a parameter to measure crack potency or crack extension force.

The analysis of fracture mechanic problem is done through different approaches, each having its own parameter [1.10–1.12]. All of them are well accepted to measure the potency of a crack; only one is needed to solve a problem. The parameter Energy Release Rate (G) is energy based and is applied to brittle or less ductile materials. Stress Intensity Factor (K) is stress based, also developed for brittle or less ductile materials. J-Integral (J) has been developed to deal with ductile materials. Its formulation is quite general and can be applied to brittle materials also. Crack Tip Opening Displacement ($CTOD$) parameter has been also developed for ductile materials and, as the name suggests, it is displacement based.

Depending upon the application, an appropriate parameter is chosen to analyze the given problem. For critical components of nuclear reactors, airplanes, submarines, locomotives, turbine blades, etc., a sophisticated fracture mechanics analysis is recommended and one may gain by investing more money for accurate analysis and experimental tests. In this book, all four parameters are developed and discussed.

1.6 Point of View

Fracture mechanics problems are studied through two different points of views: (a) material science and (b) applied mechanics. Material scientists like to study microscopic mechanisms near the crack front, such as dislocation generation and motion, role of grain boundaries, formulation of twins, role of second phase particles, nucleation and growth of voids and their coalescence, etc. They also study texture of the fractured surfaces. In this short book, we have taken the applied mechanics approach and the material is assumed to be continuous, ahead of the crack-tip. However, some discussion on micromechanisms has been included at a few places.

1.7 Damage Tolerance

Problems of fracture mechanics are solved using two different approaches. In the first approach, component geometry which includes the length, location and orientation of the crack is given along with boundary conditions. The objective is to find the upper limit of the applied load that would not cause catastrophic failure of the component.

In the second approach, known as damage tolerance, the maximum load on a component is known; the objective is to find the longest length of a crack that remains dormant. Once we know the length, the structural component can be thoroughly checked with an appropriate non-destructive test. In the case of fluctuating loads applied on the component, a fatigue crack may be nucleated even at a surface which was previously crack free. This crack may grow with fluctuating loads. In such situations, critical components are checked regularly. If a crack that is likely to grow and become critical is detected, then the component is repaired or replaced. On the other hand, detection of a small crack should not cause panic because its length may be much smaller than the maximum length of crack allowed in damage tolerance analysis.

These days many companies have started believing in avoiding a likely catastrophic failure by regular non-destructive tests of critical components. For example, a chemical company making urea in Kanpur city maintains an excellent nondestructive test department. Its engineers mostly face problems at the pipe-joints and thus they regularly check the joints, identify cracks and take necessary actions. In the long run, it saves considerable expenses because a catastrophic failure through the growth of a crack may cause extensive damage to other parts, besides causing shut-down of the plant and loss of human lives in some cases.

References

1.1 Broek, D. (1982). *Elementary Engineering Fracture Mechanics*, Martinus Nijhoff Publishers, The Hague.

1.2 Wöhler, A. (1860). Versuche über die Festigkeit der Eisenbahnwagenachsen *Zeitschrift für Bauwesen*. 10; English summary (1967), *Engineering*, 4, pp. 160–161.
1.3 Goodman, J. (1899). *Mechanics Applied to Engineering*, London: Longmans Green.
1.4 Barsom, J.M. and Rolfe, S.T. (1987). *Fracture and Fatigue Control in Structures*, Prentice Hall, Inc., Englewood Cliffs, New Jersey.
1.5 Griffith, A.A. (1921). The Phenomena of Rupture and Flow in Solids, *Philosophical Transactions of the Royal Society of London*, A 221, pp. 163–197.
1.6 Griffith, A.A. (1924). The Theory of Rupture, *Proceedings of the First International Conference of Applied Mechanics*, Delft.
1.7 Irwin, G.R. (1948). Fracture Dynamics, *Fracturing of Metals*, American Society for Metals, Cleveland, pp. 147–166.
1.8 Wells, A.A. (1961). Unstable Crack Propagation in Metals: Cleavage and Fracture, *Proceedings of the Crack Propagation Symposium*, College of Aeronautics, Cranfield, 1. pp. 210–230.
1.9 Rice, J.R. (1968). A Path Independent Integral and the Approximate Analysis of Strain Concentration by Notches and Cracks, *Journal of Applied Mechanics*, Transactions of ASME, 35, pp. 379–386.
1.10 Ramesh, K. (2007). *E-Book on Engineering Fracture Mechanics*, IIT Madras, URL: http//apm.iitm.ac.in/smlab/kramesh/book_4.htm.
1.11 Liu, A. (2005). *Mechanics and Mechanisms of Fracture—An Introduction*, ASM International, Ohio, USA.
1.12 Anderson, T.L. (2004). *Fracture Mechanics: Fundamentals and Applications*, CRC, Press-Book.

Chapter

2

Energy Release Rate

A man in passion rides a horse that runs away with him.

C.H. Spurgeon

2.1 Introduction

Whether a crack in a component is likely to grow under given load conditions is of vital importance to fracture mechanics.

The problem has been analyzed through several approaches—stress, displacement or energy methods [2.1–2.7]. Each approach defines a suitable parameter. A limit on the parameter defines the toughness of the material. For a prescribed load condition, if the value of the parameter exceeds the limit, the crack may grow.

This chapter deals with the energy method. The advantage of this energy approach is that there is no need to account for the large stresses that are developed in the vicinity of a crack-tip. The energy method conveniently avoids any analysis close to the crack-tip. The approach is similar to solving the problem of a body sliding down on a frictionless slope in which one is interested to know only the velocity of the body. It is determined by invoking the conservation of kinetic and potential energies, irrespective of the slope of the slide, which may vary from one point to another along the path.

2.2 Griffith's Dilemma

Griffith, in the early 1920s [2.8, 2.9], developed some basic concepts. He was aware of the analytical solution, developed by Inglis [2.10], which determines stress field around an elliptical hole in a large plate, loaded under the tensile stress σ_0 as shown in Fig. 2.1. He noted that the maximum stress develops at point A of the ellipse and is given by

$$\sigma_{22}^{\max} = \sigma_0\left(1+\frac{2a}{b}\right) \tag{2.1}$$

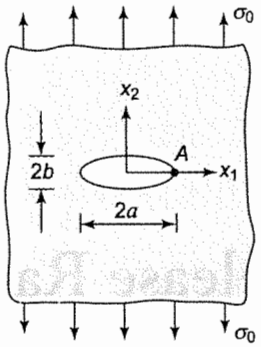

Fig. 2.1 An elliptical hole in a stretched plate

For a circular hole, σ_{22}^{max} is three times greater than σ_0. But for an elliptical hole where the major axis a is much longer than the minor axis b, σ_{22}^{max} becomes quite large; so much so that for a sharp crack with minor axis tending to be very small (of the order of interatomic distances), no real material can sustain the stress. Thus, even for a small applied stress σ_0, Eq. (2.1) suggests that σ_{22}^{max} would be very large and would exceed the ultimate strength of the material. Equation (2.1) further suggests that even a sharp crack of small length may grow and break the component into two pieces. However, this is contrary to our observations. Griffith thus concluded that some other mechanisms must be existing which helped materials to sustain solid forms.

2.3 Surface Energy

Similar to the surface tension of a liquid, all solid surfaces are associated with surface energies or free energies. These energies are developed because atoms close to a surface behave differently from atoms at the interior of the solid. The interior atoms are attracted or repulsed by the neighboring atoms more or less uniformly from all directions. On the contrary, an atom on the free surface has no neighboring atoms towards the exterior side of the surface, thus resulting in a different equilibrium. In fact, atoms at the surface, as well as atoms just under them, have to re-adjust to form the equilibrium and this develops a strain in the material close to the free surface. Such surface deformation requires energy and is known as surface energy.

2.4 Griffith's Realization

Griffith realized that a crack in a body would not grow unless energy was released to overcome the energy needs of forming two new surfaces, one below and one above the crack plane. The surface energy of a material depends on the material properties. However, its magnitude is rather small, of the order of 1 J/m^2. Table 2.1 lists the surface energy of some of commonly encountered solids.

Surface energy of the order of 1 J/m^2 is considered insignificant (1 J energy will raise the temperature of one teaspoon of water by 0.05° C only). In brittle materials such as silica, glass and diamond, advancing cracks require small energies of the order of surface energies, and, therefore

once a crack starts advancing, it runs through the body easily, causing catastrophic failure. But some additional mechanisms operate on most materials which do not allow cracks to grow at low energies. These mechanisms will be discussed subsequently in this chapter.

TABLE 2.1 Surface energy of some commonly used materials

Material	*Surface Energy (J/m^2)*
Copper	0.98
Mild Steel	1.20
Aluminum	0.60
NaCl	1.35
MgO	3.30
Glass pane	2.30
Ice	0.07
Diamond	5.50

2.5 GRIFFITH'S ANALYSIS

Let us consider a plate with no prior crack [Fig. 2.2(a)]. It is pulled and then maintained in tension between two rigid supports [Fig. 2.2(b)]. Now, with a knife, a crack is cut at the centre of the plate with the crack plane normal to the tensile stress. The crack length is increased gradually with the help of the knife. A critical stage reaches when the crack starts growing on its own; i.e., without any further need of the knife. How long is this critical length? How to predict it?

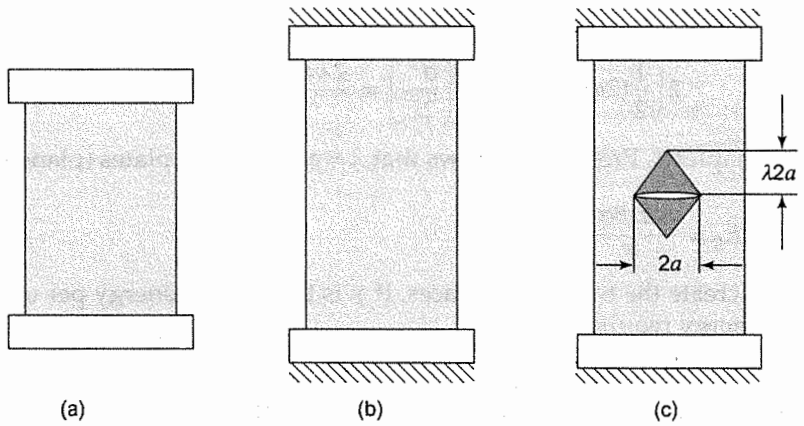

Fig. 2.2 (a) A unstretched plate, (b) the stretched plate, and (c) introducing a crack at the center

Before we answer these questions, we would like to point out that the plate becomes less stiff as the crack advances. Consequently, for this case of the plate with ends held rigidly, the stress within the plate decreases and the strain energy stored in the plate is reduced. The energy thus released is available for the crack to grow.

To convince ourselves, a simple experiment may be conducted by taking a discarded tube of a bicycle wheel and cutting it along the length to obtain a plate sheet. The sheet is stretched and mounted on a frame. We can even use the arm-rests of a chair for the purpose. A small crack is introduced with a blade or knife normal to the stretching direction and the crack is enlarged gradually. At the critical length, the crack starts advancing slowly on its own and the knife is withdrawn. The crack slowly picks up the speed and runs all the way to the side edges, thus, snapping the rubber sheet into two pieces.

Finding a rigorous solution to the problem shown in Fig. 2.2(c) is a difficult task at this stage. To understand Giriffith's analysis, we will carry an approximate analysis in this section. The plate is chosen to have its dimensions much larger than the longest crack to be considered. Then, the stress at points far away from the crack is assumed to remain constant.

Most of the energy release, as the crack advances, comes from those parts of the plate which are adjacent to the cracked surfaces, because they are traction free. For the sake of convenience, the major area of the plate where its strain energy is released may be taken as a triangle on each side of the crack plane as shown in Fig. 2.2 (c). In fact, other shapes such as a parabola will serve the purpose; we have chosen it to be triangular to keep the algebra simple. With the increase in crack length the base and the height of both triangles increase and, therefore, the area from which the strain energy is released is proportional to the square of the crack length.

The height of a triangle is $\lambda(2a)$ where λ is a constant. Then, the total release of energy E_R is determined by multiplying the area of both triangles with plate thickness B and the strain energy density $\sigma^2/2E$ where σ is the tensile stress and E is the Young's modulus. Thus, released energy is given by

$$E_R = (\text{Volume of triangles}) \times \left(\frac{\sigma^2}{2E}\right)$$

$$= 2\left(\frac{1}{2}(2a)(2\lambda a)B\right) \times \left(\frac{\sigma^2}{2E}\right) = \frac{2\lambda a^2 B\sigma^2}{E}$$

Rigorous analysis (Chapter 4, Problem 8) shows that $\lambda = \pi/2$ for thin plates (plane stress) giving

$$E_R = \frac{\pi a^2 B\sigma^2}{E} \tag{2.2}$$

Energy is required to create the two new surfaces. If γ is the surface energy per unit area of one surface, the surface energy required E_S is

$$E_S = 2(2a)B\gamma = 4aB\gamma \tag{2.3}$$

The relations of Equations (2.2) and (2.3) are shown graphically in Figure 2.3. E_R increases parabolically whereas E_S increases linearly with increasing crack length a. Consider a small crack length, $2a_0$ whose length is incremented by Δa. The slope of E_R is smaller than the corresponding slope E_S and, therefore, the energy release ΔE_R in advancing the crack-tip by distance Δa is not sufficient to meet the energy needs of new surfaces (ΔE_S). The crack would not grow and would remain subcritical. In fact, the crack would be dormant unless energy is supplied by an external agency, the operator of the knife in this case.

As the operator gradually continues cutting the crack further, the slope of E_R increases, while the slope of E_S remains the same. A stage is reached when the slope of E_R becomes equal to the

slope of E_S. The crack now becomes critical, because for an incremental advance of crack length, energy release equals the energy required. Therefore, for the crack to become critical

$$\frac{dE_R}{da} \geq \frac{dE_S}{da} \tag{2.4}$$

A question may be raised here—why does the crack grow in this experiment even when $E_R < E_S$? Note that the difference in these two energies has already been supplied by the operator of the knife. In fact, this difference is an extremely useful quantity because of which many small cracks in a body do not grow and they remain dormant.

If the plate had been pulled to a higher tension prior to the introduction of the crack, the E_R would increase with the crack length at a faster rate (Fig. 2.3) and then even the cracks of smaller lengths would become critical. In order to determine the critical crack length a_c we substitute E_R [Eq. (2.2)] and E_S [Eq. (2.3)] in Inequality 2.4 to obtain

$$\frac{2\pi a_c B\sigma^2}{E} \geq 4B\gamma$$

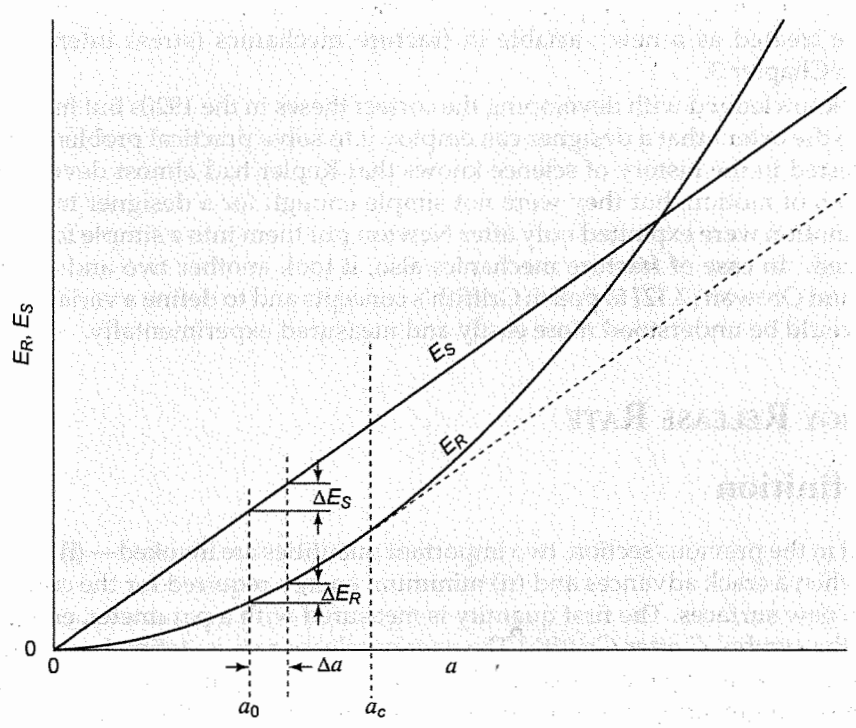

Fig. 2.3 Variation of energy release E_R and required surface energy E_S with crack length

For a safe crack,

$$a_c \leq \frac{2E\gamma}{\pi\sigma^2} \tag{2.5}$$

If we want to know how much stress is required to advance a given crack for plane stress cases, the inequality is rearranged to

$$\sigma_c \geq \left[\frac{2E\gamma}{\pi a}\right]^{1/2} \tag{2.6}$$

For plane strain (thick plate), E is replaced by $E/(1-\nu^2)$ and the relation becomes

$$\sigma_c \geq \left[\frac{2E\gamma}{\pi(1-\nu^2)a}\right]^{1/2} \tag{2.7}$$

where ν is the Poisson's Ratio.

We deduce, from Inequalities 2.6 and 2.7, that the critical stress depends on modulus E, surface energy γ and crack length a. As expected, the higher value of the surface energy of a material increases the critical stress whereas a longer crack reduces it. Larger modulus means that the plate is capable of storing less energy, thereby resulting into smaller energy release which, in turn requires higher stress for making the crack critical. One may also note from Inequality 2.6 that the product $\sigma_c\sqrt{a}$ depends only on material properties (elastic constants E and ν and surface energy γ). Therefore, $\sigma\sqrt{a}$ may be treated as a new variable in fracture mechanics (stress intensity factor) to be developed in Chapter 3.

Griffith acknowledged with developing the correct theses in the 1920s but his analysis was not developed to the extent that a designer can employ it to solve practical problems. For example, a reader interested in the history of science knows that Kepler had almost developed everything about the laws of motion, but they were not simple enough for a designer to make a machine. The laws of motion were exploited only after Newton put them into a simple form with variables clearly defined. In case of fracture mechanics also, it took another two and a half decades for Irwin [2.11] and Orowan [2.12] to polish Griffith's concepts and to define a variable, energy release rate, which could be understood more easily and measured experimentally.

2.6 Energy Release Rate

2.6.1 Definition

As discussed in the previous section, two important quantities are invoked— (i) how much energy is released when a crack advances and (ii) minimum energy required for the crack to advance in forming two new surfaces. The first quantity is measured with a parameter, energy release rate, denoted by the symbol G after Griffith. The energy release rate is defined as energy release per unit increase in area during crack growth. The word "rate" is sometimes confusing to beginners because in most engineering applications, rate signifies differentiation with respect to time. In the definition of G the rate is defined with respect to change in crack area. Another aspect of the definition is that the energy release rate can be calculated even for the cracks which cannot grow under a given load condition. That is, if there is a virtual growth of the crack, energy equal to G would be released from the system per unit extension of area.

The energy requirement for a crack to grow per unit area extension is called crack resistance and is usually denoted by the symbol, R. Note that symbol R is used in place of surface energy γ discussed in the previous section because during crack growth an anelastic deformation

(e.g., plastic deformation in metals) also occurs up to a certain depth of the cracked surfaces. R, in fact, is the sum of the energies required, (i) to form two new surfaces and (ii) to cause anelastic deformation. Like energy release rate, the crack resistance is also a rate but it is rather unfortunate that the word 'rate' has not been included in its nomenclature.

Both parameters, energy release rate as well as crack resistance, are important to study the possibility of a crack becoming critical. Obviously, the energy release rate of a crack must be greater than the crack resistance for the crack to have a chance to grow. In fact, this is not the only condition; other conditions will be discussed subsequently. We would like to compare the growth of crack with a young man trying to purchase a car. If he does not have enough money, he cannot own the car. If he has just enough money to buy the car, he will make the purchase and bring the car home. In case, he has money in excess, not only he will purchase the car, but he can drive around at fast speeds to far away places and may even break road regulations and be dangerous to other vehicles. Similarly, if the energy release rate exceeds the crack resistance, the crack acquires kinetic energy and may grow at a speed faster than the speed of a supersonic airplane.

2.6.2 Mathematical Formulation

With an advancing crack, the following happens in a general case:

1. Strain energy in the component decreases or increases.
2. Stiffness of the component decreases.
3. The points of the component, at which external loads are applied, may or may not move. Work is being done on the component by these forces if the points move.
4. Energy is being consumed to create two new surfaces.

Formulation for energy release rate is carried out by invoking the conservation of energy. Consider the case of an incremental increase in the crack area ΔA. To cause this crack growth, an incremental external work ΔW_{ext} is done by the external forces and the strain energy within the body of the component increases by ΔU. Then, the available energy, $G\Delta A$, provides the energy balance as follows:

$$G\Delta A = G\Delta W_{ext} - \Delta U \tag{2.8a}$$

Dividing the equation by ΔA and taking the limit $\Delta A \to 0$, we obtain

$$G = -\frac{d}{dA}(U - W_{ext}) \tag{2.8b}$$

The negative sign has been deliberately taken out of the differential term because $(U - W_{ext})$ is commonly known as potential energy Π. Therefore, the equation is written as

$$G = -\frac{d\Pi}{dA} \tag{2.9}$$

The above equation is quite powerful to evaluate the energy release rate of a system. The equation may be viewed from a different angle; that is, energy is available from the system if the potential energy decreases. Note that G is always positive for a crack studied for its probable growth.

In many engineering applications, fracture mechanics is applied to plates of uniform thickness and then ΔA can be expressed as $B\Delta a$, where B is the thickness and Δa is the increment in crack length. Equation (2.9) is then modified to

$$G = -\frac{1}{B}\frac{d\Pi}{da} \tag{2.10}$$

Before we show an application of the equation, we would like to modify it for dynamic crack propagation. As a crack moves rapidly, some energy is being consumed to the impart kinetic energy to cracked portions of the body and to generate stress waves. Therefore, Eq. (2.8a) is modified to

$$G\Delta A = \Delta W_{ext} - \Delta U - \Delta T$$

where ΔT is the incremental increase in kinetic energy in the body. On taking the limit, the equation becomes

$$G = -\frac{d}{dA}(U - \Delta W_{ext}) - \frac{dT}{dA} \tag{2.11}$$

Equation (2.9) looks simple but one still has to worry for external forces and change in internal energy. Can we simplify the equation further? For some cases we can. Two approaches are developed: (i) change in compliance, (ii) change in internal energy.

2.6.3 Change in Compliance Approach

In a component, decrease in stiffness with an increasing crack length may be simple to visualize, but in fracture mechanics, it is easier to deal with compliance which is the inverse of stiffness. Thus, compliance of a body increases with the increase in the crack length.

Consider a general case of a body with a crack and load P as shown in Fig. 2.4. The displacement u of the point at which the load is applied can be expressed as

$$u = CP \tag{2.12}$$

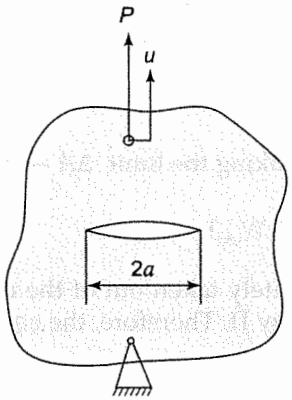

Fig. 2.4 Component with a crack

where C is the compliance. The objective now is to find the energy release rate G in terms of change of compliance with respect to the crack length a.

In order to provide a feel to the reader, we have chosen the case of a double cantilever beam (DCB), which is made by splitting a beam on one end (Fig. 2.5). However, the proof is general and

the results can be applied to other problems. Further, we have chosen the case in which the crack is at mid-plane of the beam, with both cantilevers having identical geometry.

This problem is solved for two extreme cases: (i) constant load P in which the displacement of load point increases as the crack grows and (ii) constant displacement where load decreases with crack growth.

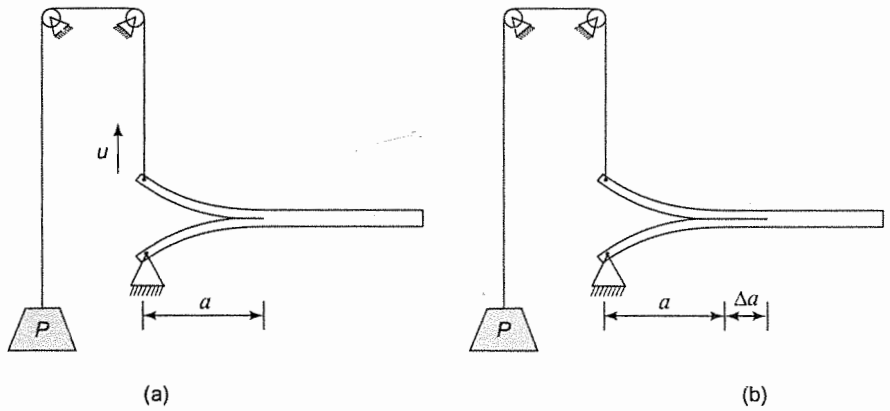

Fig. 2.5 DCB specimen loaded with a constant load

Constant Load: In the case of a constant load (Fig. 2.5), the cantilever ends move away from the crack plane with the advancing crack and thus work Pu is being done on the specimen. Consequently, the cantilevers are flexed more and they absorb a part of energy out of the external work. The remaining energy is utilized to extend the crack by Δa. For this system strain energy U and work done W_{ext} are

$$U = \frac{1}{2} Pu$$

$$W_{ext} = Pu$$

The potential energy becomes

$$\Pi = U - W_{ext} = \frac{1}{2} Pu - Pu = -\frac{1}{2} Pu \tag{2.13}$$

Substituting the expression of Π in Eq. (2.10) and making use of the fact that P remains constant, we obtain:

$$G = \frac{P}{2B}\frac{du}{da}$$

Substituting u from Eq. (2.12), we obtain:

$$G = \frac{P^2}{2B}\frac{dC}{da} \tag{2.14}$$

The equation provides another way to determine the energy release rate—just by finding the rate of change of compliance. Also, the simple expression of this equation justifies our choice of displacement-load equation in terms of compliance rather than in stiffness.

Fixed Grip: The analysis for the case of fixed grip is quite different; but the result would indeed be the same. As the crack advances, no external work is done on the system because the external load is not allowed to move (Fig. 2.6). What is the mechanism of energy release required for the crack growth? With the increase in the crack length, the cantilevers of Fig. 2.6a are relaxed to acquire a smaller curvature (Fig. 2.6b). The configuration of Fig. 2.6b has less strain energy because the energy stored in a cantilever is proportional to the square of the curvature. The body, therefore, continuously releases its strain energy with increasing crack length and if the release is large enough to meet the demands of producing two new surfaces, the crack may grow. The potential energy of the system is:

$$\Pi = \frac{1}{2} Pu$$

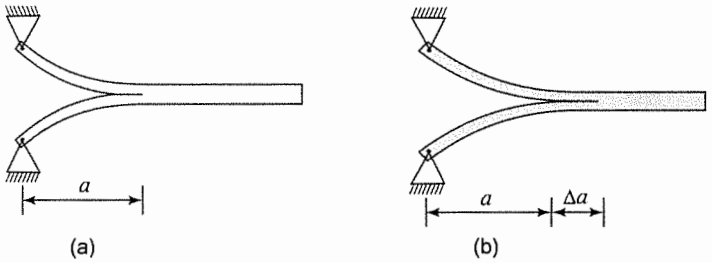

Fig. 2.6 DCB specimen with fixed grips

Substituting in Eq. (2.10), we obtain:

$$G = -\frac{u}{2B}\frac{dP}{da}$$

Substituting P from Eq. (2.12) and realizing u remains constant, we obtain:

$$G = \frac{u^2}{2BC^2}\frac{dC}{da}$$

which, on eliminating u using Eq. (2.12), provides:

$$G = \frac{P^2}{2B}\frac{dC}{da}$$

It is worth noting that the result is same as that of the constant load case.

We deliberately solved the two cases separately to make the reader aware that energy to propagate a crack may come from different sources. In the case of a constant load, energy requirements of the crack surfaces are met by the external work done on the body. In fact, the external work done is split into two parts, first part [50%, Eq. (2.13)] increases the strain energy, as the cantilever deforms to higher curvature and the second part is released for the crack growth. In the case of a fixed grip, the entire energy needed for the advancement of the crack is met by the decrease in existing strain energy.

In practical applications, the cases are mixed. If P and u are changing simultaneously, as shown in Fig. 2.7, it can be argued that, for a short while, P is changed by ΔP at constant u and, then, u is

changed by Δu with constant P. Such successive changes approximately follow the actual loading path. Since there is no constraint on the magnitude of Δu and ΔP, they can be made as small as we like; so much so that the actual load-displacement curve is approached exactly. Since the expression for finding G is same for either case, Eq. (2.14) is valid for any general kind of loading.

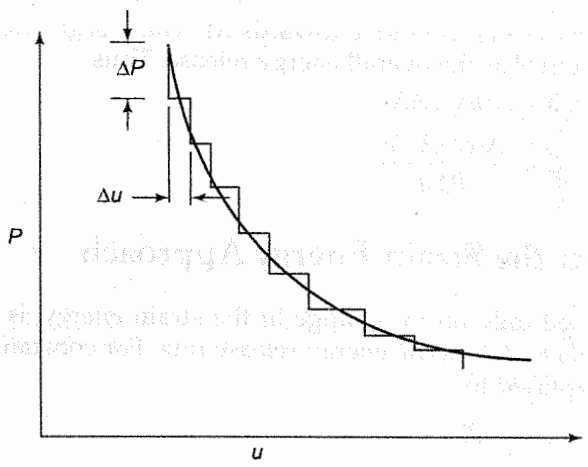

Fig. 2.7 General case

The parameter G is often chosen by many researchers to determine interlaminar toughness of a composite laminate. A *DCB* specimen is pulled in a tensile machine at a slow cross-head speed (Fig. 2.8a). A stage is reached (state A in the load-displacement curve of Fig. 2.8b) when the crack starts growing. It is allowed to grow by a small distance ($\approx$ 5 to 10 mm) to state M, and the machine is stopped and unloaded. From A to M, load decreases due to reduced stiffness, and distance u increases because the machine is continuously pulling the cantilever all along. The slope of the unloading curve MO is smaller than that of the loading curve OA. With this data in our hand, we could now evaluate the energy release rate. In fact, we will prove that the area OAM is the energy released when the crack moves through distance Δa.

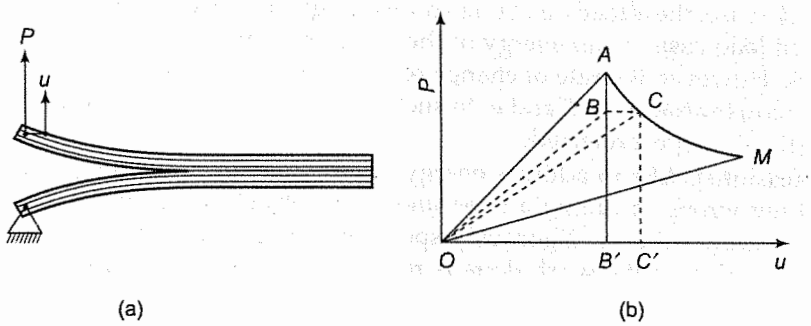

Fig. 2.8 DCB specimen of a polymer composite laminate

Line AM is split into horizontal and vertical segments as shown. From A to B, the crack advances with constant displacement, and, therefore, the energy equivalent to the area of ΔOAB is released.

Along BC the crack propagates at constant load, adding external work given by the rectangle $BCC'B'$. Half of it is used to increase the strain energy of the cantilever given by the area of ΔOBC. The rest is available as energy release for the growth of the crack, which is also equal to the area of ΔOBC. Thus, by moving from point A to C, the energy release is equivalent to the sum of the areas of triangles OAB and OBC. The remaining segments along AM, with the same argument, provide the energy release as we move towards M. These segments can be made as small as possible, giving area OAM as the overall energy release. Thus,

$$GB\Delta a = \text{Area } OAM$$

yielding,

$$G = \frac{\text{Area } OAM}{B\Delta a}$$

2.6.4 Change in the Strain Energy Approach

Another method, based only on the change in the strain energy, is also found convenient for linear elastic materials to determine energy release rate. For constant displacement (fixed grip) case, Eq. (2.8b) is simplified to:

$$G = -\frac{dU}{dA} \tag{2.15}$$

This equation states that the decrease in the existing strain energy per unit area extension of crack is the energy release rate. In case of a constant load case, we have already seen that:

$$\frac{dW_{ext}}{dA} = 2\frac{dU}{dA} \tag{2.16}$$

This, in fact, is a general theorem for linear elastic materials and is known as Clapeyron's Theorem. Substituting Eq. (2.16) in Eq. (2.8b), we have,

$$G = \frac{dU}{dA} \tag{2.17}$$

We thus obtain the same form for G in both cases, except with a difference of the negative sign. In the fixed grip case, the already existing strain energy decreases as the crack advances, whereas in the constant load case, strain energy of the component increases, which is equal to half of he external work. However, the rate of change of internal energy does not give G in the mixed case with simultaneous variation of P and u. In such cases, the method of finding the rate of change of compliance [Eq. (2.14)] is preferred.

Some professionals like to address energy release rate as strain energy release rate (SERR). There is nothing wrong in calling a phenomenon or object by any name as long as there is no confusion in communication. Rigorously speaking, strain energy is not released in a constant load case; only a part of the work done is released. We will, therefore, not be using SERR for energy release rate in this book.

Example 2.1 Determine the energy release rate for an edge crack loaded as shown in Fig. 2.9.
Solution: This is a case of constant load and, therefore, we can determine G using Eq. (2.17). For each cantilever,

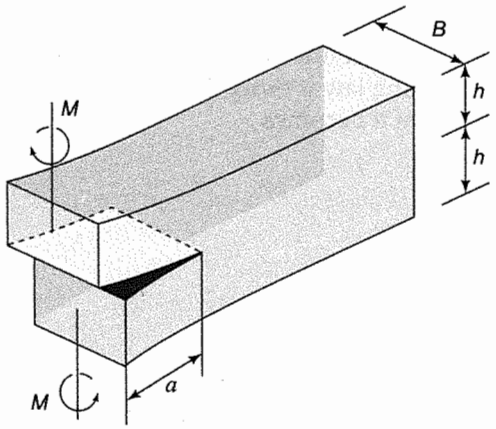

Fig. 2.9 Edge-cracked body of Example 2.1

$$U = \int \frac{1}{2} M\kappa \, da$$

where κ is the curvature of the beam and obtained as:

$$\kappa = \frac{M}{EI} = \frac{M}{E(hB^3/12)} = \frac{12M}{EhB^3}$$

where E is the modulus and I the moment of inertia of the beam's cross-section. Accounting for strain energy in both the cantilevers,

$$U = 2\int_0^a \frac{1}{2} M\left(\frac{12M}{EhB^3}\right) da = \frac{12M^2 a}{EhB^3}$$

Invoking Eq. (2.17), we have

$$G = \frac{1}{B}\left(\frac{dU}{da}\right) = \frac{12M^2}{EhB^4}$$

2.7 Energy Release Rate of DCB Specimen

The energy release rate can be obtained if the variation of compliance with respect to crack length is known. For some cases, a relation between the applied force P and the displacement u can be obtained by using field equations of solid mechanics. Then, by differentiating the ratio of u/P and substituting in Eq. (2.14), the energy release rate is determined. In this section, we would apply the method to a DCB specimen.

The deflection of a cantilever beam, δ, caused by load P applied at the free end is well-known and is given as,

$$\delta = \frac{1}{3}\frac{P}{E}\frac{l^3}{I}$$

where l, E and I are the length, modulus, and moment of inertia of the beam's cross-section, respectively. For a DCB specimen with one cantilever-end attached to a fixed jaw of a tensile machine, the deflection of the moving jaw is twice the deflection of one cantilever and, therefore, for crack length a, the displacement u becomes

$$u = \frac{2}{3}\frac{P}{E}\frac{a^3}{I} \tag{2.18}$$

leading to,

$$C = \frac{u}{P} = \frac{2a^3}{3EI} \tag{2.19}$$

For the rectangular cross-section of cantilevers, $I = Bh^3/12$, where h is the depth of a cantilever and B is the thickness of the DCB specimen. Substituting I in Eq. (2.19) we obtain

$$C = 8\frac{a^3}{EBh^3}$$

Differentiating and substituting in Eq. (2.14), we obtain

$$G_I = \frac{12}{E}\frac{a^2}{B^2}\frac{P^2}{h^3} \tag{2.20}$$

The depth h plays a dominant role because deflection of the cantilever depends prominently upon its depth. A cantilever of high depth flexes only by a small amount and therefore has a poor capability of storing strain energy. It is to be noted here that energy release rate depends on the capacity of the body to store strain energy. When the crack extends with fixed grip condition, the energy release comes from the decrease in strain energy and if the capability to store energy is small, the energy release rate is also small. In case of a constant load, the release of energy comes from the external work, but it is equal to increase in strain energy. Therefore, a body with low capability of storing strain energy provides small values of energy release rate.

The thickness B also controls the deflection of the cantilever and therefore a beam of larger thickness would make the beam less flexible and provide a smaller energy release rate. Similarly, material property, modulus E, also governs the deflection; a stiff material like steel does not allow large deflection and, therefore, releases less energy in comparison to low modulus materials like glass fiber composites or aluminum.

From Eq. (2.20), we should make one more observation which is disturbing from the designers' point of view. If load P is maintained constant, energy release rate keeps on increasing with the square of the crack length, whereas the surface energy required per unit surface area does not depend much on the crack length for most engineering applications. Because of the excess energy, which increases rapidly with the crack length, the crack is likely to attain high velocity causing catastrophic failures. Designers find it very difficult to devise effective and practical methods to arrest cracks that have become unstable. Therefore, while designing a component, an all-out effort is made not to allow a crack to become unstable. In critical components, like an axle of a locomotive wagon, the entire body is scanned with modern techniques (ultrasonic flaw detector, etc.) to make sure that it does not contain a crack longer than the predetermined safe length.

Example 2.2 Determine the critical energy release rate of a DCB specimen loaded in a tensile testing machine. The thickness of the DCB specimen is 30 mm, depth of each cantilever 12 mm and crack length 50 mm. It is made of a hardened steel with the modulus of 207 GPa and the crack is about to propagate at 15405 N pulling load.

Solution Invoking Eq. (2.20), we have

$$G_{Ic} = \frac{12}{E}\frac{a^2}{B^2}\frac{P^2}{h^3} = \frac{12 \times (0.050\ \text{m})^2 \times (15405\ \text{N})^2}{(207 \times 10^9\ Pa) \times (0.030\ \text{m})^2 \times (0.012\ \text{m})^3}$$

$$= 22.1\ \text{kJ/m}^2$$

Example 2.3 Determine the shape of the DCB specimen if G_I is to remain constant with the growth of the crack. The specimen is loaded in the constant load mode. Determine the depth h of the specimen beyond the crack tip if thickness of the specimen remains constant ($B = 30$ mm). The initial crack length is 50 mm, modulus 207 GPa and depth of each cantilever 12 mm up to the initial crack length.

Solution: For G_I to remain constant in Eq. (2.20)

$$G_I = \frac{12a^2P^2}{EB^2h^3} = \text{constant}$$

leading to,

$$\frac{a^2}{h^3} = \frac{EB^2G_I}{12P^2} = \text{constant}$$

But the constant is determined with initial conditions as

$$\text{constant} = \frac{a_0^2}{h_0^3} = \frac{(0.050\ \text{m})^2}{(0.012\ \text{m})^3} = 1447\ \text{m}^{-1}$$

yielding to,

$$h = \frac{a^{2/3}}{(1447)^{1/3}} = 0.0884a^{2/3}$$

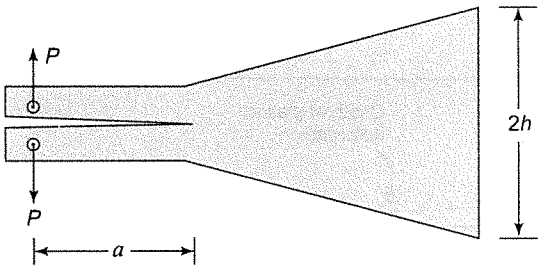

Fig. 2.10 DCB specimen with constant G_I

For $a = 0.08$ m, the above relation gives $h = 0.0164$ m (=16.4 mm). The resulting shape of the specimen is shown in Fig. 2.10. Note that the cantilever depth increases with the growing crack; the cantilever with larger depth releases smaller energy because its capacity to store energy is smaller, thus compensating the effect of increased crack length.

2.8 Anelastic Deformation at Crack-tip

To advance a crack, Griffith correctly identified that energy is required which is consumed in forming two new surfaces. As discussed earlier in this chapter, the surface energy of solids is quite small and only cracks in brittle materials (e.g., diamonds, window glass panes) advance by such criterion. For most of the engineering materials (metals, polymer, etc.), a lot more energy is required in addition to the surface energy in order to grow a crack. Therefore, besides surface energy of the solids, some other mechanisms are also operative, which absorb large amounts of energy.

Inglis [2.10] showed that the stresses at crack-tips are quite large; so large that they cause an anelastic deformation in front of the crack-tip. The anelastic deformation, such as plastic flow in metals, is mostly irreversible and if the stresses are released the body will not attain its original configuration near the crack-tip. The energy that causes this anelastic behavior is eventually converted into heat energy and is lost to the surroundings. Thus, the anelastic deformation dissipates work energy into heat energy.

In metals, the plastic deformation in the vicinity of the crack-tip is caused mainly by motion and generation of dislocations, rotation of grains and grain boundaries, formation of voids, etc. If the material is of low yield stress, the size of the plastic zone is large.

The plastic zone is very useful to designers who like to avoid fracture failure in machine components. A large plastic zone means that a large amount of energy is required to advance a crack-tip because a newer portion of the component is being continuously subjected to plastic deformation. The energy is thus continuously being dissipated by the advancing crack tip to the plastic deformation. This is analogous to the preparation of an agricultural field with a plough which goes on throwing soil on either side. If the plough is dug deeper, more soil is upturned and this requires more energy. On the contrary, if the plough is not inserted into the ground at all, hardly any energy is required. The plastic deformation is thus a boon in disguise. A large plastic zone introduces plastic deformation to greater depth in the cracked surfaces as shown in Fig. 2.11. To understand the concepts, one may even express overall surface energy γ as sum of natural surface energy γ_n which a surface possesses even if it has not been subjected to any plastic deformation and the surface energy γ_p which is caused by the plastic deformation near the cracked surfaces. The simple relation is written as,

$$\gamma = \gamma_n + \gamma_p \tag{2.21}$$

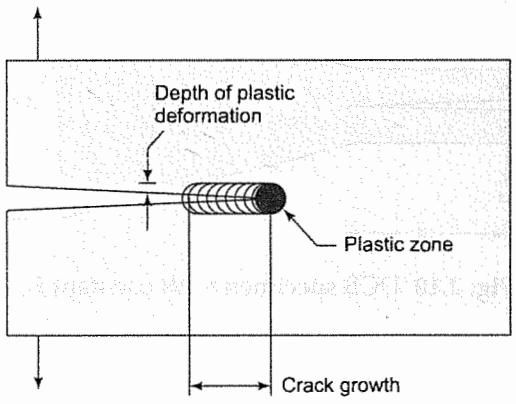

Fig. 2.11 Increase of the effective surface energy due to plastic deformation

For most structural metals used in our daily life, γ_p is several orders higher than γ_n and, therefore, γ_n may as well be ignored (Table 2.2). However, Eq. (2.21) is not a convenient way to formulate problems in fracture mechanics because there is always an uncertainty in the magnitude of γ_p.

TABLE 2.2 Representative values of γ_n and γ_p for some common materials

Material	γ_n (J/m^2)	γ_p (J/m^2)
Mild Steel	1.20	125,000
Alloy Steel	1.20	15,000
Aluminum Alloy	0.60	4,000

In case of non-metals such as polymers, anelastic deformation near the crack tip is governed by mechanisms different from those in metals. For example, polymer chains align themselves parallely to each other under high stress and dissipate energy. The energy dissipation is several orders more than the natural surface energy.

To sum up, the anelastic deformation in front of a crack-tip demands a large energy release rate. Therefore, for most of the cracks in a body, the energy release rate is not high enough to make them critical. Consequently, the cracks remain sleeping or dormant.

2.9 Crack Resistance

For a crack to grow, the crack resistance (R) is the energy required by the crack per unit increase in area. It characterizes the material behavior. For most engineering materials, crack resistance increases with the crack length as shown in Fig. 2.12. A minimum value R_i is needed to make the crack grow. Crack resistance depends on the plastic zone size. In a crack with a large plastic zone size, high energy is required to grow the crack as more material is subjected to plastic deformation. A substantial portion of the energy is lost eventually to the surroundings.

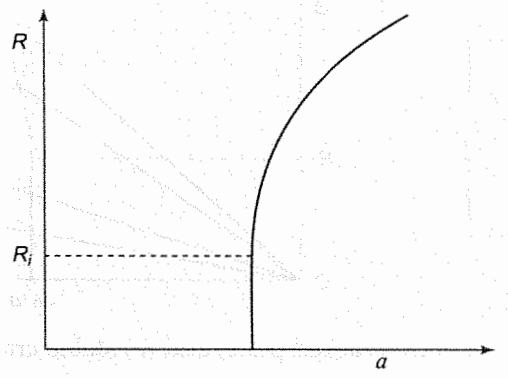

Fig. 2.12 R-curve of ductile materials

Why does R increase with a? As the crack advances, plastic zone size becomes larger which, in turn, requires higher energy for crack growth. Interestingly, the shape of the R-curve is not found

to depend much on the initial length of a crack for most of the engineering materials. However, R-curve depends considerably on the temperature and the thickness of a plate. The dependence on temperature is understandable because many other properties (yield stress, etc.) depend on temperature. Dependence of the R-curve on a plate's thickness involves a geometrical parameter and makes it difficult to define toughness as an intrinsic property of a material. This aspect will be taken up again in this chapter.

2.10 Stable and Unstable Crack Growth

We have already realized that for a crack to grow the energy release rate of a crack must be greater than the crack resistance. We have now developed an adequate background to explore other requirements for a crack to become unstable.

Consider a large plate with a centre crack length $2a$, loaded in Mode I by stress σ (Fig. 2.13). We would explore how much energy is released at a constant stress σ_1 if the crack length is varied. It will be shown in Chapter 4 that $G = \sigma^2 \pi a/E$ for plane stress and $G = (1 - \nu^2)\, \sigma^2 \pi a/E$ for plane strain cases. Note that G increases with crack length as shown in Fig. 2.13. If stress σ_1 is small and the G-curve intersects the R-curve below R_i, the crack will not propagate because the energy release rate is not adequate. The curve of higher stress σ_2 just passes through R_i and still the crack does not advance because with Δa increase in crack length, the energy release is smaller than the requirement. If the stress is further increased to σ_3, G exceeds R for crack having length between a_0 and a_3 and the crack is likely to grow. However, with the increase in crack length the difference between G and R diminishes to zero at point B. There will not be any further advancement of the crack. Therefore, the crack may advance from length a_0 to length a_3 only.

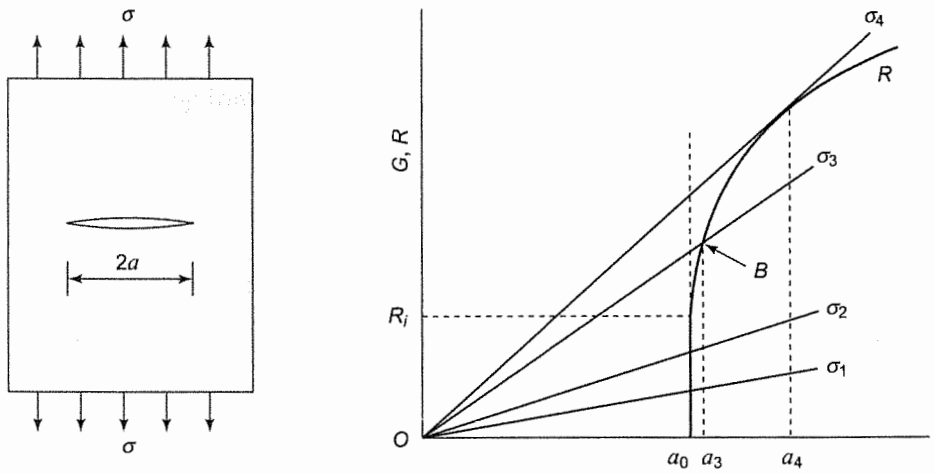

Fig. 2.13 (a) Centre-cracked plate, and (b) stable crack growth

If the applied stress increases gradually, point B shifts to the right (Fig. 2.13). In other words, the crack grows slowly (stable crack growth). For stress σ_4, G-curve just touches the R-curve which means energy release rate is higher for all crack lengths except, of course, at the crack length a_4 where they are equal. Even a slightly higher stress or a perturbation makes the crack

grow. As soon as the crack length increases, the difference between G and R grows, which provides excess energy to the crack. As a result, the crack gains velocity, ending up in a catastrophic failure. Thus, for a crack to grow and become critical, two conditions are necessary

$$G \geq R \tag{2.21a}$$

$$\frac{dG}{da} \geq \frac{dR}{da} \tag{2.21b}$$

The stable crack growth, at times, is useful in detecting a potential danger. Once a stable crack is detected in a component, a remedial action should be taken either by finding ways to arrest the crack or replacing the defective component with a new component.

Even if the above two conditions are fulfilled, the crack may not extend. The local conditions at the crack-tip are quite important. If the tip is blunt, stresses at the crack-tip are not very high as it is clear from the Inglis solution [Eq. (2.1)]. Then, the crack is unlikely to propagate, although the energy criteria are met. An analogy may be drawn with some stone pieces placed right in front of the tires of a car—the powerful engine finds itself helpless although the car is capable of moving once the stone pieces are removed.

A designer should not feel assured in cases where cracks are of long lengths, satisfying inequalities 2.21, but have blunt ends such as a hole at the crack-tip. Such cases are like sitting on a volcanic mountain which may erupt at any time. On the surface of a blunt crack front, a small length crack with a sharp tip may develop due to some unforeseen factors such as bad workmanship, fatigue or environmental degradation. The effective crack length then is the sum of the length of the blunt and the small crack. Under such conditions the crack may grow easily.

2.11 R-Curve for Brittle Cracks

In a brittle material, the size of the plastic zone in the vicinity of a crack tip is negligible and even the growth of the plastic zone is negligible with the advancement of the crack. Consequently, the R-curve rises vertically at the given crack length (Fig. 2.14) and then turns horizontal like a step function.

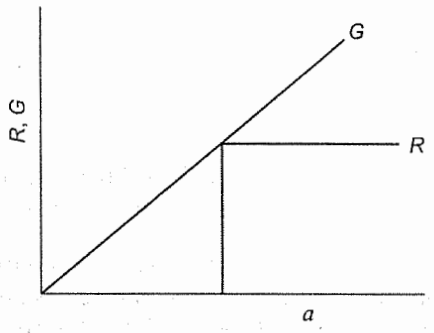

Fig. 2.14 R-curve of brittle materials

As soon as the stress is large enough to make G overcome R, the crack advances. Note that stable growth does not occur. The difference between G and R increases rapidly with increasing crack length and the crack runs catastrophically.

2.12 Thin Plate vs Thick Plate

From the point of view of fracture, which plate is tougher, thick or thin? Once I organized a trekking trip in the Grand Canyon, USA. We went down, right up to the Colorado river; i.e., 5000 ft. down and then we climbed up 5000 ft. in a day covering a distance of nearly 45 km. One of my team-mates, who, even after being a little overweight was fit enough to be admitted in the Indian Army, had a very hard time climbing up the 5000 ft. On the other hand, there was another fellow, extremely lean and thin, climbed without any problem and that too two hours ahead of the other trekkers. From this incident the reader might have guessed by now that the thin plate is tougher; but the question still remains, why?

It has already been argued that because of plastic deformation at the crack-tip, a large amount of energy is dissipated near the cracked surfaces. If the material yields easily and the plastic zone size is large at the crack-tip, the crack will not grow at low values of the energy release rate. We shall prove that in a thin plate (plane stress) the plastic zone size is considerably bigger than the plastic zone size in a thick plate (plane strain). If this is so, a thin plate is tougher against crack growth.

We will first consider yielding in the vicinity of the crack-tip in a thin plate. Both the free surfaces of the plate are traction free and, therefore, the three stress components σ_{33}, σ_{31} and σ_{32} (Fig. 2.15a) are zero on the surfaces. Also, they are negligible small even at all interior points for most of the engineering applications because the plate is thin. Note the σ_{33} becomes one of the three principal stresses and will hence forth be called σ_3.

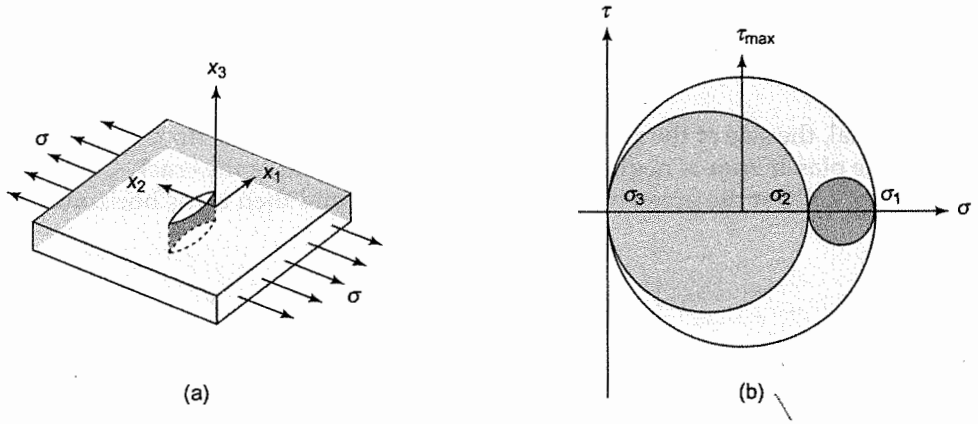

Fig. 2.15 (a) A thin plate with a center crack and (b) principal stresses with a large value of maximum shear stress

Other two principal stresses σ_1 and σ_2 lie in the plane of the plate. To avoid complex algebra and emphasize more on the concepts, we explore the nature of stresses on points which are ahead of the crack-tip and are close to the plane of the crack for Mode I cases. Shear stresses are small near this plane due to the symmetry of the problem.

Normal stress σ_{22} is large and tensile, contributing dominantly to the highest principal stress σ_1. The other normal stress σ_{11} is also tensile as the material is not free to move in the plane of the plate. It contributes to next highest principal stress σ_2 as shown in Fig. 2.15b. For estimating the

size of the plastic zone, we will now make use of Tresca Yield Criterion, which is based on maximum shear stress. The maximum shear stress can easily be obtained by drawing all the three Mohr circles. σ_1 being the largest is on the far right in Fig. 2.15b and σ_3 at the origin with σ_2 lying in between. The radius of the largest Mohr circle, between σ_1 and σ_3, provides the maximum shear stress τ_{max}. It is worth noting that τ_{max} is quite large in cases of thin plates resulting in the generation of a plastic zone of a large size.

A thick plate with a Mode I crack, σ_2 and σ_1 are again tensile stresses as they are for the thin plate. Due to tensile σ_1 and σ_2, the material tends to stretch in the plane of the plate, which in turn tends to make the plate thinner. However, the plate is thick and constrained; the material is not able to flow in x_3 direction. As a result, tensile stress develops along x_3 direction. Fig. 2.16 shows all the three Mohr circles. For plane strain (thick plate), σ_3 is finite and only marginally smaller than σ_1 making the largest Mohr circle substantially smaller than the largest Mohr circle of plane stress. Thus, τ_{max} is considerably lower in a thick plate. In fact, the material in front of the crack-tip is locked and is not free to deform. In other words, thick plates do not allow the generation of large plastic zone sizes. Hence, they are not as capable of dissipating energy as thin plates are. These aspects will be discussed in detail in Chapter 5.

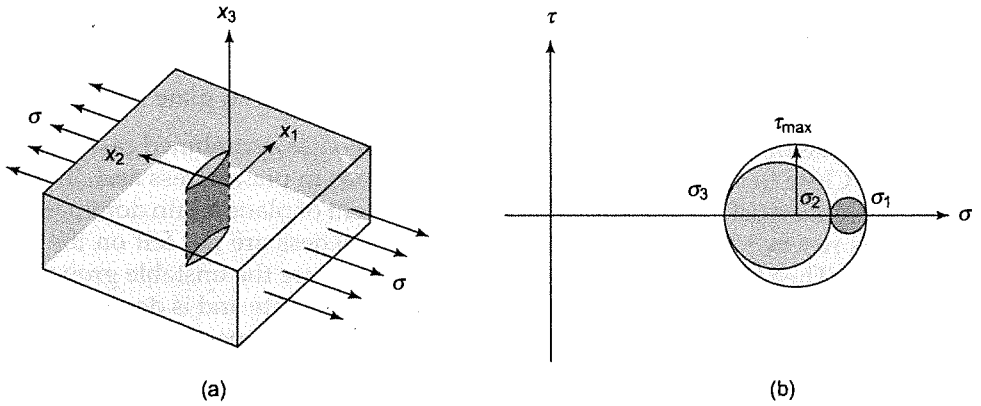

Fig. 2.16 (a) A thick plate with a center crack and (b) principal stresses with a low value of maximum shear stress

When the Alaska pipeline to transport crude oil from the interiors of the Alaska state to the sea-shore was being designed, there was a constant tussle between the conventional designers and the modern experts of fracture mechanics. The conventional designers wanted the pipe line to be made of thick wall so that stresses will be smaller and the material would not fail due to yielding. The experts of fracture mechanics wanted to choose smaller wall thickness because then the wall of the pipe would be loaded in the plane stress and be tough against crack growth.

2.13 Critical Energy Release Rate

R-curve depends on the thickness of a plate if it is loaded in a plane stress. Figure 2.17 shows three *R*-curves for plane stress for three thicknesses, with the corresponding critical energy release rates $G_c^{(1)} G_c^{(2)}$ and $G_c^{(3)}$.

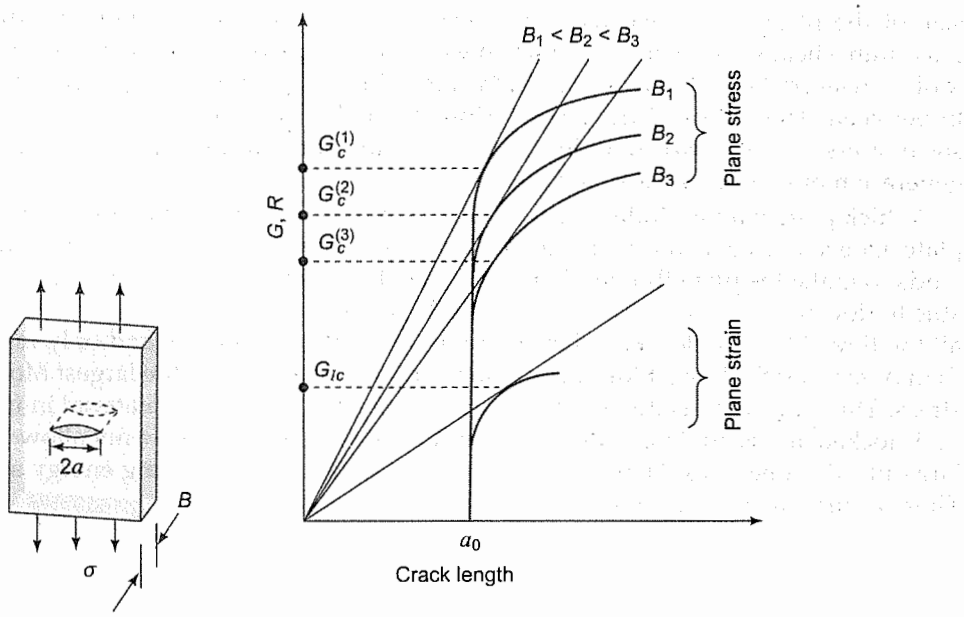

Fig. 2.17 Critical energy release rate of plane strain and plate stress

When the thickness of the plate is increased further, it becomes a combined case of plane stress and plane strain. Close to the free surfaces, material deforms in plane stress and, in the interior, plane strain conditions exist. On thicker plates, the component of plane strain dominates; so much so, that a stage is reached beyond which the effects of thickness are not felt on the R-curve as shown in Fig. 2.17. Then the energy release rate required to cause the unstable growth no longer depends on plate thickness. This is called critical energy release rate and is denoted by G_{Ic} where 'I' stands for Mode I. The critical energy release rate becomes the property of a material. Table 2.3 provides representative values of plane strain G_{Ic} of some widely used engineering materials.

Design engineers like to use components made of thin cross-sections so that they are loaded in plane stress. For example, the web and the flange of an I-beam should be made of small thicknesses. An irony is that, when designers refer to literatures or handbooks, the critical energy release rate is available only for plane strain and not for plane stress. One may argue that by using the critical energy release rate of plane strain we have conservative design. But, the resulting design may sometimes turn out to be over-designed and non-feasible. For example, the structure of an airplane is designed with a low factor of safety for restricting its dead weight. In such cases, the critical energy release rate is determined for the thickness of the sheet chosen by the designers.

Experimental techniques to determine the critical energy release rate are not developed well except in some special cases like determining the interlaminar G_c of fiber composite laminates. Details of experimental techniques are presented in Chapter 8.

The concept of the energy release rate is not conveniently applicable to materials with large plastic zone at the vicinity of the crack tip. In the analysis discussed so far in this chapter, the material is assumed to be linearly elastic and if the plastic zone is small, its effect may be neglected in determining the energy release rate. However, with a large plastic zone at the crack tip, the analysis should be done more carefully by accounting for the constitutive relations of plasticity within the plastic zone. The parameter J-Integral deals with such problems more effectively (Ch. 6).

TABLE 2.3 Representative plane strain G_{Ic} of some common materials

Material	G_{Ic} (J/m^2)
Mild Steel	≈250,000
Alloy Steel (σ^*_{ys} = 1070)	30,000
EN 24 (U.K.)	
4340 (U.S.A.)	
40Ni2Cr1Mo28 (I.S.)	
Aluminum 7075-T6	8,000
Titanium Ti-6Al-4V	29,000
Perspex (PMMA)	800
PVC	4,500
* Yield Stress in MPa	

2.14 CLOSURE

In this chapter, the problem of fracture has been discussed purely through energy approach without worrying about existence of very large stresses in the vicinity of the crack tip. To sum up, there should be an energy release from the system to make a crack move. The energy release is measured by the parameter, energy release rate (G). Also, energy is required to form two new cracked surfaces and is accounted by another parameter, crack resistance (R). The necessary requirements for the crack advance are (i) $G \geq R$ and (ii) $dG/da \geq dR/da$. The value of G, which satisfies these two conditions, becomes the material property known as critical energy release rate. For thin plates, the critical energy release rate depends on the thickness of a plate, whereas it is independent of the thickness of thick plates.

QUESTIONS

1. Why is the surface of a solid associated with surface energy (or free energy)? What is an approximate value of free energy of the surface of a metal?
2. Actual energy required in a ductile material to create two new surfaces through the crack growth is several orders higher than the surface energy of solids. Why so?
3. Why does the compliance of a component increase with the growth of a crack?
4. Does the strain energy of a component increase with the crack growth?
5. Why does negative sign appear in the expression of G defined through Eq. (2.9)?
6. How does the rate of change of strain energy give G for constant load case or constant deflection case? Is this approach valid for non-linear elastic materials?
7. Why is failure catastrophic once a crack starts growing in a DCB specimen?
8. What are different mechanisms of anelastic deformation in a polymer?
9. If the load is increased gradually on a component made of a ductile material, why do we obtain stable crack growth before the catastrophic failure?

10. Why does a brittle material not have stable crack growth?
11. Why are thin plates tougher in comparison to thick plates?
12. Why is critical energy release rate not given in handbooks for thin plates?

PROBLEMS

1. Determine the energy release rate of a DCB specimen through change in strain energy approach for constant load.
2. Determine the energy release rate, using elementary beam analysis, for the configurations given in Fig. 2.18 ($h<<a$).

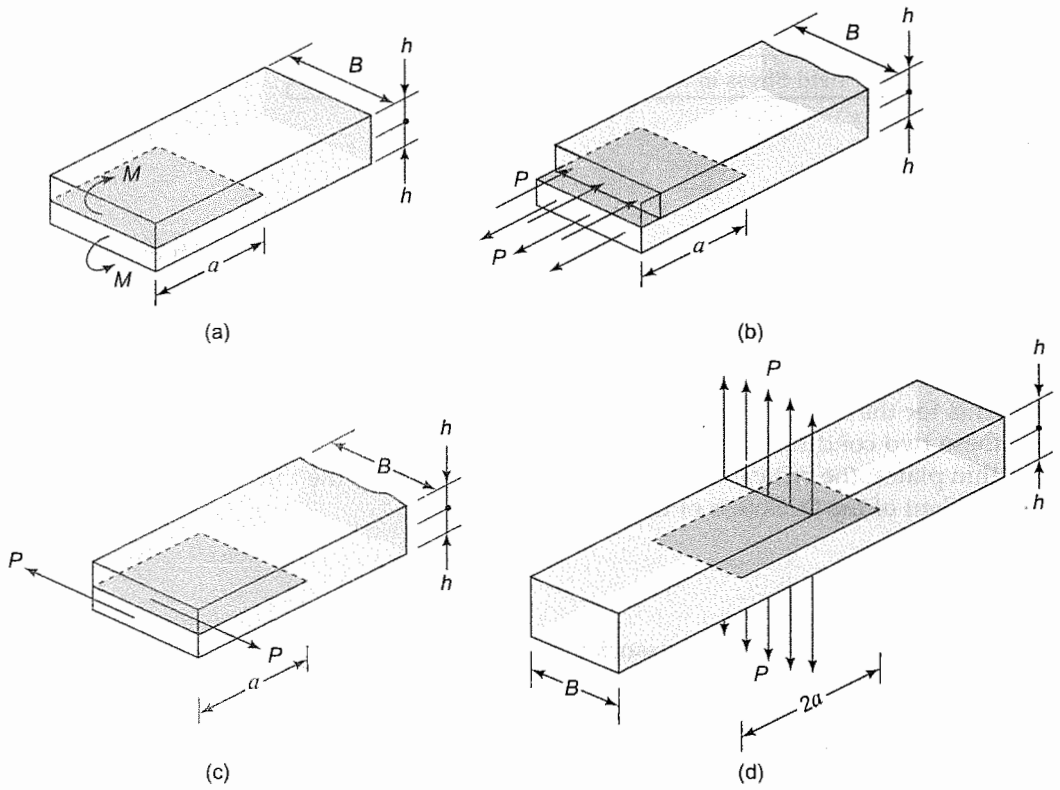

Fig. 2.18 The figure of Problem 2

3. G_I is determined for a DCB specimen with a load at the end of each cantilever in Section 2.7 by neglecting the effect of the shear stress. If the strain energy of the shear force is also considered, find G_I.

4. Consider a plate with a crack of length a and lateral load P acting on the corners as shown in Fig. 2.19. Find the energy release rate.
   [$\theta = TL / K\mu$ where θ is the angle of twist, T twisting moment, L length, μ shear modulus and

$$K = \frac{bh^3}{16}\left[\frac{16}{3} - 3.36\frac{h}{b}\left(1 - \frac{h^4}{12b^4}\right)\right]$$

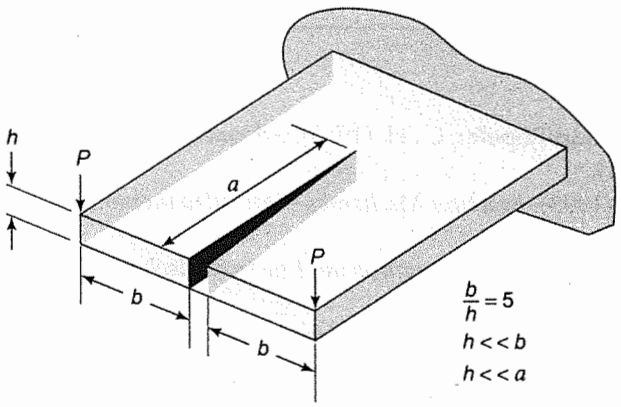

Fig. 2.19 The figure of Problem 4

5. The load on a 30 mm thick plate with an edge crack of 50 mm length was increased very slowly and the displacement of the load point was monitored. It was observed that at the load of 2100 N and displacement $u = 4.1$ mm, the crack started growing. The rate of crack growth was much faster than the rate at which the load increased and therefore the crack essentially was grown at the load of 2100 N. Through an optical recording using a rapid camera it was found that the crack grew up to 65 mm length with the rapid increase in displacement to $u = 7.5$ mm. Determine the critical energy release rate.
6. A large plate of 36 mm thickness with an edge crack of $a = 32$ mm length is pulled very slowly under displacement control loading. At the displacement of 7.2 mm, when the recorded load is 2750 N, the crack starts growing. At $a = 41.7$ mm, the crack is arrested and the load decreases to 1560 N. Determine the critical energy release rate.
7. A double cantilever beam of a fiber composite laminate with an initial pre-crack is loaded under displacement control to the critical load and the crack is allowed to grow by a small length. Then, the specimen is unloaded to zero load. Now, the specimen with a larger crack length is loaded again to the new critical load and allowed to grow further by a small length. Such load cycles are repeated five times and compliance is obtained during each cycle. The data is summarized in Table 2.4. The load displacement curve remains elastic up to the critical point and the thickness of the specimen is $B = 30$ mm. Determine the critical strain energy rate for each segment of crack growth through the approach of finding the area enclosed in the corresponding triangle of the load-displacement recording.

TABLE 2.4 The table of Problem 7

Crack length a (mm)	*Compliance C (m/N)*	*Critical load P (N)*
32	33.5×10^{-6}	94.3
42	68.9×10^{-6}	78.8
50	121.0×10^{-6}	64.0
58	191.0×10^{-6}	53.5
67	294.0×10^{-6}	44.0

REFERENCES

2.1 Kanninen, M.F. and Popelar, C . H. (1985). *Advanced Fracture Mechanics*, Oxford University Press, New York.

2.2 Gdoutos, E.E. (1993). *Fracture Mechanics—An Introduction*, Kluwer Academic Publishers, Dordrecht.

2.3 Broek, D. (1982). *Elementary Engineering Fracture Mechanics*, Martinus Nijhoff Publishers, The Hague.

2.4 Meguid, S.A. (1989). *Engineering Fracture Mechanics*, Elsevier Applied Science, London.

2.5 Barsom, J. M. and Rolfe, S.T. (1987). *Fracture and Fatigue Control in Structures*, Prentice-Hall, Inc., Englewood Cliffs, New Jersey.

2.6 Hertzberg, R. W. (1989). *Deformation and Fracture Mechanics of Engineering Materials*, John Wiley and Sons, New York.

2.7 Knott, J.F. (1973). *Fundamentals of Fracture Mechanics*, John Wiley and Sons, New York.

2.8 Griffith, A.A. (1921). The Phenomena of Rupture and Flow in Solids, Philosophical Transactions of the Royal Society of London, A 221, pp 163–169.

2.9 Griffith, A.A. (1924). The Theory of Rupture, *Proceedings of the First International Conference of Applied Mechanics*, Delft.

2.10 Inglis, C. E. (1913). Stress in a Plate due to the Presence of Cracks and Sharp Corners, Transactions of the Institute of Naval Architects, 55, pp. 219–241.

2.11 Irwin, G. R. (1948). *Fracture Dynamics: Fracturing of Metals*, American Society for Metals, Cleveland, pp. 147–166.

2.12 Orowan, E. (1948). *Fracture and Strength of Solids*, Reports on Progress in Physics, XII, p. 185.

2.13 Anderson, T. L. (2004). *Fracture Mechanics: Fundamentals and Applications*, CRC, Press-Book.

2.14 Sanford, R. J. (2003). *Principles of Fracture Mechanics*, Prentice Hall, Upper Saddle River.

2.15 Janssen, M., Zuidema, J. & Wanhill, R.J.H. (2004). *Fracture Mechanics*, Spon Press, Abingdon.

2.16 Ramesh, K. (2007). *e-Book on Engineering Fracture Mechanics*, IIT Madras, URL: http//apm.iitm.ac.in/smlab/kramesh/book_4_htm.

Chapter

3

Stress Intensity Factor

... nature is intelligent because it is too complicated to be called anything else.

Deepak Chopra

3.1 Introduction

3.1.1 Why Should Investigations be Closer to the Crack Tip?

Today, thinking big often implies focusing on minute details. Huge amounts of atomic energy is generated, both for peaceful and destructive purposes, by manipulating atoms which are invisible even under powerful microscopes. Similarly, in order to understand how crystalline materials (e.g., metals) deform plastically, we should understand the behavior of dislocations, which are imperfections and look like threads. Dislocations too are very small in diameter, but can be viewed under a powerful microscope. A crack front exists within a material, like a line running from one region of the body to another. The vicinity of a crack tip offers interesting information as the magnitudes of stress components are extremely high. When we want to break a wooden stick by bending it we make a notch. The notch creates high stresses, which in turn make the notch tip move rather easily.

Knowing the stress or displacement field in the vicinity of a crack tip is very useful. A material scientist may devise ways to develop new materials which can diffuse high stresses at the crack tip. A designer may modify some features such as notches, cutouts, keyways, etc., to minimize stresses. An experimentalist can think of methods of characterizing cracks by measuring stresses or strains near the crack tip. One of the biggest advantages is that stress analysis leads to define a parameter, stress intensity factor (SIF) to characterize a crack. In comparison to energy release rate, SIF is simpler for a designer and easier for laboratory measurements, so as to determine material properties.

3.1.2 Linear Elastic Fracture Mechanics (LEFM)

In a brittle material, the material remains elastic even at the crack tip where stresses are high. Most engineering materials do not fall in this category. Diamonds are known to be quite brittle

(elastic) even in the vicinity of a crack tip. Other brittle materials like window panes are known to have some anelastic deformation close to the crack tip. This chapter develops analysis of brittle materials only; the analysis does not account for plastic deformation close to the crack tip. A natural question arises—when most materials are not brittle, why should we make detailed analysis of brittle materials? Obviously, analysis of brittle materials is far simpler than the analysis of a material having a plastic zone at the crack tip. The presence of a plastic zone means that two kinds of stress-strain behaviors should be incorporated, plastic behavior inside the plastic zone and elastic behavior outside it. At the same time, it is difficult to evaluate the interface between the two zones. Furthermore, the material behavior inside the plastic zone is complex to model and in some materials, especially those which exhibit pronounced Bauschinger effect, the material behavior is extremely difficult to account for. Therefore, for the analysis of elastic-plastic fracture mechanics (EPFM), problems are usually solved through numerical analysis.

By confining our attention to elastic (or brittle) materials, we would be able to obtain closed form solutions to many problems. Also, we will learn how to deal with the singularity (infinite stresses at the crack tip) involved. There is another advantage in developing solutions of elastic crack problems. In many real life cases where the plastic zone size is quite small in comparison to the crack length, the contribution of the plastic zone in an elastic analysis may be neglected. That is, if stress fields in such cases are determined for purely elastic and elastic-plastic cases separately, the difference between the two is small enough to be considered negligible. A large number of engineering problems of practical applications fall in this category and consequently elastic analysis is good enough. This leads to an important subfield—linear elastic fracture mechanics (LEFM), where only elastic analysis is carried out to determine stress and displacement fields near a crack tip with characterizing parameters like the SIF. It is worth mentioning here that the energy release rate (G) has also been formulated for LEFM.

3.2 Stress and Displacement Fields in Isotropic Elastic Materials

On what parameters does the stress field depend in the vicinity of the crack tip? It, of course, depends on the external load, generally denoted by the far-field stress σ. The name, far field, may mislead some readers; it refers to stress at points of the body where the influence of the high stresses generated at the crack tip is negligible. The second important parameter, as discussed in Chapter 2, is the crack length a. We also realize that the stress field varies near the tip significantly from point to point and one must specify the coordinates at which stress components are to be determined. Generally, polar coordinates (r, θ) are employed for describing the location of the point. Further, the stress field depends upon geometry i.e., whether the crack is at the centre of the body, at the edge, or at the off-centre. Under geometrical considerations, the effect of the overall size of the specimen with respect to the crack length would also be included.

Let us express stress component σ_{ij} in the vicinity of crack tip as

$$\sigma_{ij} = f(\sigma, a, r, \theta, \text{geometry})$$

where i, j are the suffixes representing various stress components like σ_{11}, σ_{22}, σ_{12}, σ_{33}, etc. There is a separate relation (function f) for each stress component.

In engineering applications, most of the hardware components are in the form of plates. Commonly used sections like angles, I-beams, channels, rectangular tubes, etc., are made of flat plate sections. Even in a circular tube with a crack having its length much smaller than the diameter

of the tube, the region around the crack tip may be regarded as a flat plate. Thus, a study of crack in a flat plate encompasses many engineering applications.

In most problems of this book, x_1-axis is chosen along the crack length, x_3-axis along the normal of the plate and x_2-axis in the plane of the plate and normal to the crack length [Fig. 3.1(a)]. Also, we have chosen to denote stress components with two suffixes because that is a better way of representing the stress tensor. Consequently, we would be using symbol σ for shear stress components also; the suffixes will only differentiate shear components from normal components. Further, we prefer to use suffixes 1, 2 and 3 in place of x, y and z, as used in many books.

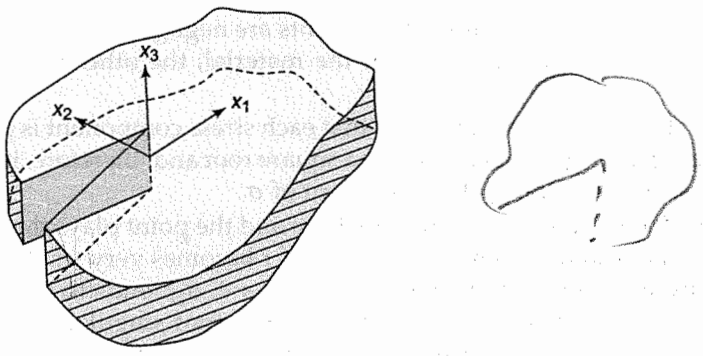

Fig. 3.1 Axes with respect to the crack in a plate

Solving equations of solid mechanics to obtain expressions for σ_{ij} in the vicinity of the crack tip is mathematically involved and, therefore, only the results would be presented and discussed in this section. The derivations would be presented in Sections 3.4 and 3.5.

To present results, we have chosen the common case of a flat plate with a crack of length $2a$ and far field stress σ as shown in Fig. 3.2(a). The stress field at a general point H near the crack tip for isotropic and linear elastic material in the flat plate for this Mode I case is

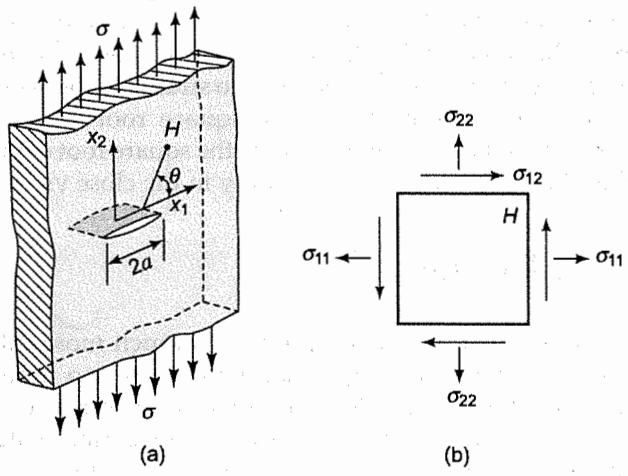

Fig. 3.2 (a) Infinite plate with a crack of length $2a$ subjected to a far field stress σ, and (b) definition of stress components at point H

$$\sigma_{11} = \frac{\sigma(\pi a)^{1/2}}{(2\pi r)^{1/2}} \cos\frac{\theta}{2}\left[1 - \sin\frac{\theta}{2}\sin\frac{3\theta}{2}\right] \tag{3.1a}$$

$$\sigma_{22} = \frac{\sigma(\pi a)^{1/2}}{(2\pi r)^{1/2}} \cos\frac{\theta}{2}\left[1 + \sin\frac{\theta}{2}\sin\frac{3\theta}{2}\right] \tag{3.1b}$$

$$\sigma_{12} = \frac{\sigma(\pi a)^{1/2}}{(2\pi r)^{1/2}} \sin\frac{\theta}{2}\cos\frac{\theta}{2}\cos\frac{3\theta}{2} \tag{3.1c}$$

For a thin plate, other stress components are negligible. In case of a thick plate $\sigma_{33} = \nu(\sigma_{11} + \sigma_{22})$ where ν is the Poisson's Ratio of the material; the other two stress components (σ_{13}, σ_{23}) are negligible.

It is clear from these equations that each stress component is proportional to the far field stress σ. The crack length appears under a square root and, therefore, its influence on stress components is also prominent, but not to the extent of σ.

The distance (r) between the crack tip and the point plays the most important role. It sits in the denominator under a square root sign. If r becomes very small, the stress components, specially σ_{22} goes up steeply, so much so that for $r \to 0$, σ_{22} tends to be infinite. Such solutions are called singular. In this case, it is known as square root singularity. In some special cases of fracture mechanics, other kinds of singularities are encountered.

Displacement field for a plane strain near the crack tip for Mode I of Fig. 3.2(a) is given by

$$u_1 = \frac{\sigma(\pi a)^{1/2}}{\mu}\left(\frac{r}{2\pi}\right)^{1/2} \cos\frac{\theta}{2}\left[1 - 2\nu + \sin^2\frac{\theta}{2}\right] \tag{3.2a}$$

$$u_2 = \frac{\sigma(\pi a)^{1/2}}{\mu}\left(\frac{r}{2\pi}\right)^{1/2} \sin\frac{\theta}{2}\left[2 - 2\nu + \cos^2\frac{\theta}{2}\right] \tag{3.2b}$$

$$u_3 = 0 \tag{3.2c}$$

where μ is the shear modulus. The above equations do not contain any singularity, because displacement is finite near the crack tip. Mathematically, displacement components are obtained from stress equations by converting stress components to strain components and then integrating the resulting expressions. During integration, the square root singularity disappears and displacement components turn out to be proportional to the square root of the distance r. However, one should note here that the Eqs (3.2a–c) are valid only in the close vicinity of the crack tip.

3.3 Stress Intensity Factor

In the engineering field, a problem with two variables is much more difficult to solve than a problem of one variable. A question may be raised here—can two independent variables be combined to form a new independent variable? If the answer is yes, the solution to the problem is likely to become much simpler. In the case of a wave propagation, solution even along one dimension becomes complex because two variables, space (x) and time (t), are involved. In such wave problems, we usually combine two variables to form a new variable, ($x - ct$), where c is the

velocity of the sound. There are many other similar cases such as linear kinetic energy combining two variables to one, linear momentum combining two variables to one, Reynolds Number in fluid mechanics combining four independent variables to one, and Sommerfield Number in journal bearing combining five variables into one.

If we look carefully into Eqs (3.1) and (3.2), we find that for a given geometry there are two main variables, the far field stress σ and the crack length a. Furthermore, in all the equations of stress and displacement, σ and a coexist as $\sigma\sqrt{a}$. Can this product be called by a different variable? Now with several decades of research work, we find that it is advantageous to do so. This credit goes to Irwin [3.1], who defined the new variable, stress intensity factor, and used the symbol K after the name of his collaborator Kies [3.2]. He defined K as

$$K_I = \sigma\,(\pi a)^{1/2} \tag{3.3}$$

There is no reason to have π in the above definition. It was included in the expression because of some historical reasons which shall be explained in the next chapter. However, the stress intensity factor K_I is formally defined as

$$K_I = (2\pi r)^{1/2}\,\sigma_{22}\,(r,\,\theta = 0) \text{ as } r \to 0 \tag{3.4}$$

This definition can be checked easily by substituting Eq. (3.1b) in the formal definition [Eq. (3.4)], the resulting expression will be the same as of Eq. (3.3).

We realize that, for stress or displacement fields, magnitude of σ or a is immaterial as long as $\sigma(\pi a)^{1/2}$ is same. This means a small crack length in a plate with high far field stress is equivalent to a large crack length with small far field stress, provided K remains same. This combination of σ and a to form a new variable is regarded as a breakthrough in the field of fracture mechanics. For Modes I–III, the stress intensity factor is written as K_I, K_{II} and K_{III} respectively, with subscript in Roman numbers.

The stress and displacement Eqs (3.1) and (3.2) may now be written in terms of the stress intensity factor. For Mode I problems of plane strain, they become

$$\sigma_{11} = \frac{K_I}{(2\pi r)^{1/2}} \cos\frac{\theta}{2}\left[1 - \sin\frac{\theta}{2}\sin\frac{3\theta}{2}\right] \tag{3.5a}$$

$$\sigma_{22} = \frac{K_I}{(2\pi r)^{1/2}} \cos\frac{\theta}{2}\left[1 + \sin\frac{\theta}{2}\sin\frac{3\theta}{2}\right] \tag{3.5b}$$

$$\sigma_{12} = \frac{K_I}{(2\pi r)^{1/2}} \sin\frac{\theta}{2}\cos\frac{\theta}{2}\cos\frac{3\theta}{2} \tag{3.5c}$$

$$u_1 = \frac{K_I}{\mu}\left(\frac{r}{2\pi}\right)^{1/2} \cos\frac{\theta}{2}\left[1 - 2\nu + \sin^2\frac{\theta}{2}\right] \tag{3.5d}$$

$$u_2 = \frac{K_I}{\mu}\left(\frac{r}{2\pi}\right)^{1/2} \sin\frac{\theta}{2}\left[2 - 2\nu + \cos^2\frac{\theta}{2}\right]. \tag{3.5e}$$

The stress intensity factor elegantly characterizes a crack, similar to energy release rate, G, developed in Chapter 2. Equations (3.5a–e) need to be modified for bodies which are of finite dimensions or where the crack tip is close to one of the free edges of the component. Closed form expression for stress intensity factor is available only for simple cases and, therefore, determining

the stress intensity factor becomes a challenge for many practical cases. These days, numerical techniques are widely used for this very purpose. However, for a body with a crack and known boundary conditions, once the stress intensity factor is determined, the crack is characterized for a designer and then, he can predict whether a crack in the work-component is likely to grow or not.

Stress and displacement equations for the center-cracked body are similar for other modes. For Mode II in plane strain and far field stress $\sigma_{12} = \tau$ (Fig. 3.3) with $K_{II} = \tau\sqrt{\pi a}$,

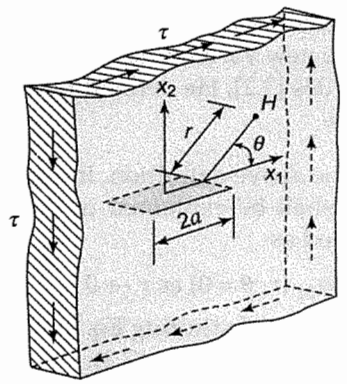

Fig. 3.3 A centre-crack in an infinite plate loaded in Mode II

we have

$$\sigma_{11} = -\frac{K_{II}}{(2\pi r)^{1/2}} \sin\frac{\theta}{2}\left[2 + \cos\frac{\theta}{2}\cos\frac{3\theta}{2}\right]$$

$$\sigma_{22} = \frac{K_{II}}{(2\pi r)^{1/2}} \sin\frac{\theta}{2}\cos\frac{\theta}{2}\cos\frac{3\theta}{2}$$

$$\sigma_{12} = \frac{K_{II}}{(2\pi r)^{1/2}} \cos\frac{\theta}{2}\left[1 - \sin\frac{\theta}{2}\sin\frac{3\theta}{2}\right]$$

$$u_1 = \frac{K_{II}}{\mu}\left(\frac{r}{2\pi}\right)^{1/2} \sin\frac{\theta}{2}\left[2 - 2\nu + \cos^2\frac{\theta}{2}\right]$$

$$u_2 = \frac{K_{II}}{\mu}\left(\frac{r}{2\pi}\right)^{1/2} \cos\frac{\theta}{2}\left[-1 + 2\nu + \sin^2\frac{\theta}{2}\right]$$

$$u_3 = 0.$$

For Mode III and far field stress $\sigma_{23} = \tau$ (Fig. 3.4) with $K_{III} = \tau\sqrt{\pi a}$, we have

$$\sigma_{11} = \sigma_{22} = \sigma_{33} = \sigma_{12} = 0$$

$$\sigma_{13} = -\frac{K_{III}}{(2\pi r)^{1/2}} \sin\frac{\theta}{2}$$

$$\sigma_{23} = \frac{K_{III}}{(2\pi r)^{1/2}} \cos\frac{\theta}{2}$$

$$u_1 = u_2 = 0$$

$$u_3 = \frac{K_{III}}{\mu}\left(\frac{2r}{\pi}\right)^{1/2} \sin\frac{\theta}{2}$$

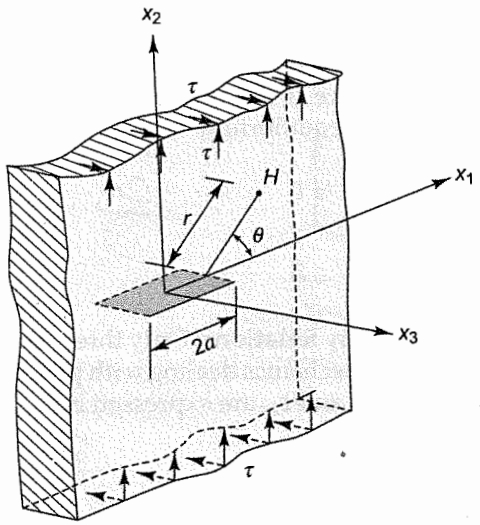

Fig. 3.4 A centre-crack in an infinite plate loaded in Mode III

3.4 Background for Mathematical Analysis

In the previous section, stress and displacement fields in the vicinity of a crack tip were presented without providing proofs. This section would develop the mathematical base and the following section would solve problems of all the three modes for simple geometries.

Although the field equations of solid mechanics are quite well-known, they would be presented for plane problems for the sake of completeness. The solution to fracture problems would be obtained by solving field equations of solid mechanics. Of course, proper boundary conditions would be incorporated, including zero traction conditions (free surface) of the cracked faces. To a beginner, some parts of this section may look strange and may be a bit difficult in the first reading because such analysis is not usually seen in other fields of mechanics of solids. A straightforward and simple analysis is not possible because the problem deals with a singularity. We would proceed slowly as if we are trying to reach the centre of a flower bud by taking one petal out gently at a time. This, of course, comes at a risk of annoying some of the readers who are already conversant with this field.

3.4.1 Field Equations

There are three kinds of field equations [3.3] which are solved for a set of given boundary conditions of a component. They are: (i) equilibrium equations relating to stress components, (ii) strain-displacement relations and (iii) stress-strain relations for the given material of the component. In case the problem is solved with stress or strain components as dependent variables, an additional set of equations must be satisfied to ensure that during the deformation, a continuous body remains continuous. This condition is called compatibility [3.4]. We will develop it because most problems would be solved in stress components. In fact, the compatibility condition provides the governing differential equation for many problems.

Equilibrium Equations: Equilibrium equations within a body are developed in any textbook of solid mechanics and, therefore, they will not be derived here. For problems dealing with plates, variation of stress components in the thickness direction is assumed to be negligible. For most fracture mechanics problems, body force is not important and, therefore, we are left with the following two differential equations of equilibrium:

$$\frac{\partial \sigma_{11}}{\partial x_1} + \frac{\partial \sigma_{12}}{\partial x_2} = 0 \tag{3.6a}$$

$$\frac{\partial \sigma_{12}}{\partial x_1} + \frac{\partial \sigma_{22}}{\partial x_2} = 0 \tag{3.6b}$$

Strain-Displacement and Compatibility Relations: Only three strain-displacement relations are involved in most problems of fracture mechanics dealing with plates. If u_1 and u_2 are displacement components, strain components ε_{11}, ε_{22} and ε_{12} are expressed by well known relations, as:

$$\varepsilon_{11} = \frac{\partial u_1}{\partial x_1} \tag{3.7a}$$

$$\varepsilon_{22} = \frac{\partial u_2}{\partial x_2} \tag{3.7b}$$

$$\varepsilon_{12} = \frac{1}{2}\left[\frac{\partial u_2}{\partial x_1} + \frac{\partial u_1}{\partial x_2}\right] \tag{3.7c}$$

It is to be noted here that the tensorial strain has been chosen, whose normal components are the same as the normal components of the engineering strain, but a shear component is half the corresponding shear component of the engineering strain. The compatibility conditions (necessary relation between strain components) are obtained by eliminating u_1 and u_2 from the above equations. Differentiating the equations, we have

$$\frac{\partial^2 \varepsilon_{11}}{\partial x_2^2} = \frac{\partial^3 u_1}{\partial x_1 \partial x_2^2}$$

$$\frac{\partial^2 \varepsilon_{22}}{\partial x_1^2} = \frac{\partial^3 u_2}{\partial x_1^2 \partial x_2}$$

$$\frac{\partial^2 \varepsilon_{12}}{\partial x_1 \partial x_2} = \frac{1}{2}\left[\frac{\partial^3 u_2}{\partial x_1^2 \partial x_2} + \frac{\partial^3 u_1}{\partial x_1 \partial x_2^2}\right]$$

By substituting the first two equations in the last equation, and rearranging the terms, we obtain

$$\frac{\partial^2 \varepsilon_{11}}{\partial x_2^2} + \frac{\partial^2 \varepsilon_{22}}{\partial x_1^2} - 2\frac{\partial^2 \varepsilon_{12}}{\partial x_1 \partial x_2} = 0 \tag{3.8}$$

This relation between the strain components ensures compatibility.

Stress-Strain Relations: For the linear isotropic materials deforming elastically, the stress-strain relations are well known as

$$\varepsilon_{11} = \frac{1}{E}\left[\sigma_{11} - \nu(\sigma_{22} + \sigma_{33})\right] \tag{3.9a}$$

$$\varepsilon_{22} = \frac{1}{E}\left[\sigma_{22} - \nu(\sigma_{11} + \sigma_{33})\right] \tag{3.9b}$$

$$\varepsilon_{33} = \frac{1}{E}\left[\sigma_{33} - \nu(\sigma_{11} + \sigma_{22})\right] \tag{3.9c}$$

$$\varepsilon_{12} = \frac{\sigma_{12}}{2\mu} = \frac{(1+\nu)}{E}\sigma_{12} \tag{3.9d}$$

where E is the Young's Modulus, μ is the shear modulus and ν is the Poisson's Ratio.

Plane Deformation: Consider a thin plate that is deformed in plane stress. On the free surfaces, the out of plane stresses are zero and they are usually negligible in the interior points of the plate. We thus assume

$$\sigma_{13} = \sigma_{23} = \sigma_{33} = 0$$

Therefore, the plate carries only in-plane stresses. The stress-strain relations are simplified to

$$\varepsilon_{11} = \frac{1}{E}\left[\sigma_{11} - \nu\sigma_{22}\right] \tag{3.10a}$$

$$\varepsilon_{22} = \frac{1}{E}\left[\sigma_{22} - \nu\sigma_{11}\right] \tag{3.10b}$$

$$\varepsilon_{12} = \frac{\sigma_{12}}{2\mu} = \frac{(1+\nu)}{E}\sigma_{12}. \tag{3.10c}$$

On the other hand, the plane strain case corresponds to a sufficiently thick plate for which (i) displacement in x_3 direction is restricted ($u_3 = 0$) and (ii) variation in x_3 direction is zero $\left(\frac{\partial}{\partial x_3} = 0\right)$.

These two conditions yield

$$\varepsilon_{13} = \varepsilon_{23} = \varepsilon_{33} = 0$$

Therefore, for plane strain cases, simplified stress-strain equations are obtained by setting $\varepsilon_{33} = 0$ in Eq. (3.9c) to have

$$\sigma_{33} = \nu(\sigma_{11} + \sigma_{22})$$

Substituting σ_{33} in Eqs (3.9a) and (3.9b) and rearranging the terms, we have

$$\varepsilon_{11} = \frac{(1-\nu^2)}{E}\left[\sigma_{11} - \frac{\nu}{1-\nu}\sigma_{22}\right] \tag{3.11a}$$

$$\varepsilon_{22} = \frac{(1-\nu^2)}{E}\left[\sigma_{22} - \frac{\nu}{1-\nu}\sigma_{11}\right] \tag{3.11b}$$

Also, Eq. (3.9d) is manipulated to

$$\varepsilon_{12} = \frac{(1-\nu)}{E}\frac{(1-\nu)}{(1-\nu)}\ \sigma_{12} = \frac{1-\nu^2}{E}\left(1+\frac{\nu}{1-\nu}\right)\ \sigma_{12} \tag{3.11c}$$

In the above equations, we define

$$E' = \frac{E}{1-\nu^2} \tag{3.11d}$$

$$\nu' = \frac{\nu}{1-\nu} \tag{3.11e}$$

Then, stress-strain relations for the plane strain become:

$$\begin{aligned}
\varepsilon_{11} &= \frac{1}{E'}\left[\sigma_{11} - \nu'\sigma_{22}\right] \\
\varepsilon_{22} &= \frac{1}{E'}\left[\sigma_{22} - \nu'\sigma_{11}\right] \\
\varepsilon_{12} &= \frac{1+\nu'}{E'}\sigma_{12}.
\end{aligned} \tag{3.12}$$

We thus note that the form of these equations is exactly the same as that of the corresponding equations for plane stress cases [Eqs (3.10)].

Biharmonic Differential Equation: When we glance at the field equations, we find that they are too many of them to compute. Therefore, we shall reduce the number of equations by going to the higher order of differential equations.

The analysis of determining stress field in the vicinity of a crack tip can be done either in stress, strain or displacement components. Based on experience we find that it is convenient to solve the differential equations with stress components as dependent variables for many problems of fracture mechanics. This is because the boundary conditions, especially at the cracked faces, are usually known in stress components. In fact, the cracked surfaces are generally traction free, thereby making several stress components zero (e.g., $\sigma_{22} = \sigma_{12} = 0$).

Since we are planning to develop the differential equations in terms of stress components, compatibility conditions should be invoked. Thus, the compatibility condition of Eq. (3.8), which relates strain components should be changed into a relation between stress components. This is done by substituting stress-strain relations [Eq. (3.10)] into the compatibility relation [Eq. (3.8)]. Thus, we have

$$\frac{\partial^2}{\partial x_2^2}(\sigma_{11} - \nu\sigma_{22}) + \frac{\partial^2}{\partial x_1^2}(\sigma_{22} - \nu\sigma_{11}) - 2(1+\nu)\frac{\partial^2\sigma_{12}}{\partial x_1 \partial x_2} = 0 \tag{3.13}$$

This equation has three dependent variables σ_{11}, σ_{22}, σ_{12} and is still cumbersome to solve. To make it manageable a new function Φ, known as Airy's Stress Function, is defined as:

$$\sigma_{11} = \frac{\partial^2 \Phi}{\partial x_2^2}$$

$$\sigma_{22} = \frac{\partial^2 \Phi}{\partial x_1^2} \tag{3.14}$$

$$\sigma_{12} = -\frac{\partial^2 \Phi}{\partial x_1 \partial x_2}$$

There is a definite purpose in coming to such a definition—they satisfy the equilibrium equations. Therefore, we will not worry for the equilibrium conditions any more. Substituting Eq. (3.14) in Eq. (3.13) and simplifying, we obtain the governing differential equation as

$$\frac{\partial^4 \Phi}{\partial x_1^4} + \frac{2\partial^4 \Phi}{\partial x_1^2 \partial x_2^2} + \frac{\partial^4 \Phi}{\partial x_2^4} = 0 \tag{3.15a}$$

This equation is generally written in more compact form by making use of the symbol

$$\nabla^2 = \frac{\partial^2}{\partial x_1^2} + \frac{\partial^2}{\partial x_2^2}$$

Then, Eq. (3.15a) is expressed as

$$\nabla^2 (\nabla^2 \Phi) = 0$$

or

$$\nabla^4 \Phi = 0 \tag{3.15b}$$

which is known as Biharmonic Equation.

If the above analysis is carried out for a plane strain [using Eq. (3.12) in place of Eq. (3.10)], the governing differential equation turns out to be the same. This is because the stress-strain equations of the plane stress and the plane strain have identical forms. The biharmonic solution may appear to be deceptively simple in appearance, but the solution to even simple problems is often not straightforward, because it involves fourth order partial derivatives.

3.4.2 Elementary Properties of Complex Variables

Stress and displacement fields in the vicinity of a crack tip have been obtained in several ways by various investigators. Some like to solve it through complex variable techniques and others without it. We will solve it through complex variables, as presented by Westergaard [3.5] in 1939. Some of the readers may hesitate in the beginning to play with complex numbers but we feel that it provides a short and simple route. It is like somebody travels from Delhi to Mumbai by an airplane instead by a train; the airplane takes only one tenth of time, but is more complex.

It has been found convenient to form a complex variable z as

$$z = x_1 + ix_2$$

In fact, by combining two independent variables x_1 and x_2 into one complex variable z, we reduce our difficulties of dealing with two independent variables in solving the biharmonic equation.

If $F(z)$ is a complex function of variable z, it can be written as

$$F(z) = \mathrm{Re}F_1 + i\,\mathrm{Im}F$$

In fact, $F(z)$ forms a surface on the complex plane (Fig. 3.5). The function is analytic at a point z if the derivative is the same in all directions [3.6]. This fact is quite useful and we equate derivative of $F(z)$ in x_1 direction with its derivative in ix_2 direction to obtain

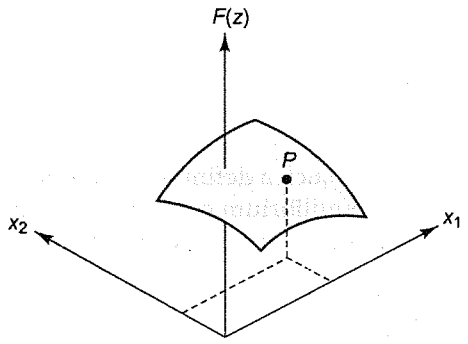

Fig. 3.5 Surface $F(z)$ on a complex plane

$$F'(z) = \frac{\partial F}{\partial x_1} = \frac{\partial \mathrm{Re}F}{\partial x_1} + i\frac{\partial \mathrm{Im}F}{\partial x_1}$$

$$F'(z) = \frac{\partial F}{i\partial x_2} = -i\frac{\partial \mathrm{Re}F}{\partial x_2} + \frac{\partial \mathrm{Im}F}{\partial x_2}$$

Since $F'(z) = \mathrm{Re}\,F' + i\,\mathrm{Im}F'$, the equations are rewritten as

$$F'(z) = \mathrm{Re}F' + i\,\mathrm{Im}F' = \frac{\partial \mathrm{Re}F}{\partial x_1} + i\frac{\partial \mathrm{Im}F}{\partial x_1}$$

$$F'(z) = \mathrm{Re}F' + i\,\mathrm{Im}F' = -i\frac{\partial \mathrm{Re}F}{\partial x_2} + \frac{\partial \mathrm{Im}F}{\partial x_2}$$

Comparing real and imaginary parts, we obtain (Cauchy–Riemann relations):

$$\begin{aligned}
\frac{\partial \mathrm{Re}F}{\partial x_1} &= \mathrm{Re}F' \\
\frac{\partial \mathrm{Im}F}{\partial x_1} &= \mathrm{Im}F' \\
\frac{\partial \mathrm{Re}F}{\partial x_2} &= -\mathrm{Im}F' \\
\frac{\partial \mathrm{Im}F}{\partial x_2} &= \mathrm{Re}F'
\end{aligned} \tag{3.16}$$

All the four equations are useful for analysis because they provide the method for differentiating the real and imaginary parts of $F(z)$ with respect to x_1 and x_2.

3.5 WESTERGAARD'S APPROACH

One way to solve the biharmonic equation is to express Φ in terms of another complex function $Z_I(z)$ for Mode I problems. In other words, $Z_I(z)$ is an intermediate solution which satisfies the biharmonic equation. It is chosen appropriately by Westergaard to suit the general characteristics of Mode I problems. Then to solve a specific problem, the form of $Z_I(z)$ is chosen to satisfy all the boundary conditions of the problem. An analogy is drawn here with an airplane that goes from Delhi to Bangalore. The intermediate solution $Z_I(z)$ is analogous to the airplane's flight which does a major job of taking passengers from a far away distance to the city. Then, dispersing passengers from the airport to various different parts of the city is analogous to solving various problems of Mode I.

Similarly, there is a Westergaard intermediate solution Z_{II} for the biharmonic equation for Mode II problems. Since general characteristics of Mode II problems are different from those of Mode I, Z_{II} has a different form. In the analogy of air flights the airplane goes from Delhi to Bangalore for Mode I problems whereas it flies from Delhi to Mumbai for Mode II problems.

The case of Mode III problems is usually simpler and can be managed without taking the help of the biharmonic equation. The problem can be solved in terms of displacement component u_3, thus avoiding the compatibility equations. It would be shown that the governing differential equation consists of only second order partial derivatives.

3.5.1 Mode I (Opening Mode)

For Mode I problems, Φ is expressed as

$$\Phi = \text{Re}\,\bar{\bar{Z}}_I + x_2\,\text{Im}\,\bar{Z}_I \tag{3.17}$$

where, $Z_I = d\bar{Z}_I / dz$ and $\bar{Z}_I = d\bar{\bar{Z}}_I / dz$

We shall show that this expression of Φ satisfies the biharmonic equation. Also, components σ_{11}, σ_{22} and σ_{12} would be expressed in terms of $Z_I(z)$ with the help of Eq. (3.14). What are the advantages in constructing the Westergaard function $Z_I(z)$? For many complex looking differential equations, such as the biharmonic equation, there are no set ways of solving them. We keep trying various solutions on the basis of feel, intuition or clairvoyance until one satisfies the differential equation. Westergaard is credited here for offering a simple solution. The integrals of $\bar{Z}$ and $\bar{\bar{Z}}$ do not cause difficulties in determining the stress field of a problem, because $Z_I(z)$ is differentiated at least twice and in the process, integrals are eliminated.

The proof of showing that the expression of Φ satisfies the biharmonic equation is straightforward, but it is carried out below for the sake of completeness. We would be adopting the convention

$$Z_I' = \frac{dZ_I}{dz}; \quad Z_I'' = \frac{dZ_I'}{dz} \text{ and } Z_I''' = \frac{dZ_I''}{dz}.$$

We differentiate Eq. (3.17) by making liberal use of Eq. (3.16) to obtain

$$\frac{\partial \Phi}{\partial x_1} = \text{Re}\,\bar{Z}_I + x_2\,\text{Im}\,Z_1$$

$$\frac{\partial^2 \Phi}{\partial x_1^2} = \text{Re}\,Z_I + x_2\,\text{Im}\,Z_I'$$

$$\frac{\partial^4 \Phi}{\partial x_1^4} = \text{Re}\, Z_I'' + x_2 \,\text{Im}\, Z_I'''$$

$$\frac{\partial \Phi}{\partial x_2} = -\,\text{Im}\,\bar{Z}_I + x_2 \,\text{Re}\, Z_I + \text{Im}\,\bar{Z}_I = x_2 \,\text{Re}\, Z_I \tag{3.18}$$

$$\frac{\partial^2 \Phi}{\partial x_2^2} = -\,x_2 \,\text{Im}\, Z_I' + \text{Re}\, Z_I$$

$$\frac{\partial^3 \Phi}{\partial x_2^3} = -\,x_2 \,\text{Re}\, Z_I'' - \text{Im}\, Z_I' - \text{Im}\, Z_I' = -\,x_2 \,\text{Re}\, Z_I'' - 2\,\text{Im}\, Z_I'$$

$$\frac{\partial^4 \Phi}{\partial x_2^4} = x_2 \,\text{Im}\, Z_I''' - \text{Re}\; Z_I'' - 2\text{Re}\, Z_I'' = x_2 \,\text{Im}\, Z_I''' - 3\,\text{Re}\, Z_I''$$

$$\frac{\partial^2 \Phi}{\partial x_1 \partial x_2} = x_2 \,\text{Re}\; Z_I'$$

$$\frac{\partial^4 \Phi}{\partial x_1^2 \partial x_2^2} = -\,x_2 \,\text{Im}\; Z_I''' + \text{Re}\, Z_I''$$

Substituting in the biharmonic Eq. (3.15a) to have the left hand side as

$$\text{Re}\, Z_I'' + x_2 \,\text{Im}\, Z_I''' - 2x_2 \,\text{Im}\, Z_I''' + 2\text{Re}\, Z_I'' + x_2 \,\text{Im}\, Z_I''' - 3\text{Re}\, Z_I'' \to 0$$

The differential equation is thus satisfied. Substitution of the relevant partial derivatives of Eq. (3.18) in Eq. (3.14) leads to

$$\sigma_{11} = \text{Re}\, Z_I - x_2 \,\text{Im}\, Z_I' \tag{3.19a}$$

$$\sigma_{22} = \text{Re}\, Z_I + x_2 \,\text{Im}\, Z_I' \tag{3.19b}$$

$$\sigma_{12} = -\,x_2 \,\text{Re}\, Z_I' \tag{3.19c}$$

In order to solve a given problem, the proper form of the Westergaard function $Z_I(z)$ is chosen such that the stress components, determined through Eq. (3.19), satisfy all the boundary conditions. Once such a function is obtained, the stress field in the vicinity of the crack tip can be easily obtained through Eq. (3.19). The Westergaard function does not solve a problem completely; it only aids in solving a problem. We still have to guess the form of the complex function $Z_I(z)$ in a specific problem.

To determine the displacement field (u_1, u_2) in the vicinity of the crack tip, we convert the stress field to the strain field with the help of appropriate stress-strain relations (Eq. (3.10) for plane stress problems and Eq. (3.12) for plane strain cases). Strains are then integrated for determining displacements.

We first take the case of plane stress. Substituting Eqs (3.19a–c) in Eqs (3.10a–c), we have

$$\frac{\partial u_1}{\partial x_1} = \varepsilon_{11} = \frac{1}{E}\left[\left(\text{Re}\, Z_I - x_2 \,\text{Im}\, Z_I'\right) - \nu\left(\text{Re}\, Z_I + x_2 \,\text{Im}\, Z_I'\right)\right] \tag{3.20a}$$

$$\frac{\partial u_2}{\partial x_2} = \varepsilon_{22} = \frac{1}{E}\left[\left(\mathrm{Re}\, Z_I + x_2\, \mathrm{Im}\, Z_I'\right) - \nu\left(\mathrm{Re}\, Z_I - x_2\, \mathrm{Im}\, Z_I'\right)\right] \tag{3.20b}$$

$$\frac{1}{2}\left[\frac{\partial u_1}{\partial x_2} + \frac{\partial u_2}{\partial x_1}\right] = \varepsilon_{12} = -\, x_2\, \frac{\mathrm{Re}\, Z_I'}{2\mu} \tag{3.20c}$$

Rearranging terms and making use of the relation $\mu = E/[2(1 + \nu)]$, we simplify the first two equations to

$$\frac{\partial u_1}{\partial x_1} = \frac{1}{2\mu}\left[\frac{(1-\nu)}{(1+\nu)}\, \mathrm{Re}\, Z_I - x_2\, \mathrm{Im}\, Z_I'\right]$$

$$\frac{\partial u_2}{\partial x_2} = \frac{1}{2\mu}\left[\frac{(1-\nu)}{(1+\nu)}\, \mathrm{Re}\, Z_I + x_2\, \mathrm{Im}\, Z_I'\right]$$

We integrate both the partial differential equations using relations of Eq. (3.16) to obtain:

$$u_1 = \frac{1}{2\mu}\left[\frac{(1-\nu)}{(1+\nu)}\, \mathrm{Re}\, \bar{Z}_I - x_2\, \mathrm{Im}\, Z_I\right] + f(x_2) \tag{3.21a}$$

$$u_2 = \frac{1}{2\mu}\left[\frac{2}{(1+\nu)}\, \mathrm{Im}\, \bar{Z}_I - x_2\, \mathrm{Re}\, Z_I\right] + g(x_1) \tag{3.21b}$$

where, $f(x_2)$ is the constant of integration which can be the function of x_2 only. Similarly $g(x_1)$ is the function of x_1 only. We shall be showing that for the fracture mechanics problems, function $f(x_2)$ and $g(x_1)$ can be equated to zero without losing any generality. To prove it, we substitute Eqs (3.21a and b) into Eq. (3.20c) to find that all terms involving Z_I cancel each other, leaving only the following equation:

$$\frac{\partial f(x_2)}{\partial x_2} + \frac{\partial g(x_1)}{\partial x_1} = 0$$

The equation is rearranged as

$$\frac{\partial f(x_2)}{\partial x_2} = -\frac{\partial g(x_1)}{\partial x_1} = A$$

where A is a constant. On integration,

$$f(x_2) = Ax_2 + B$$

$$g(x_2) = -Ax_1 + C$$

Again B and C are constants of integration. If we substitute these equations into Eqs (3.21a and b) and study them carefully, we note that all the points of the component are displaced by the same distance, given by $u_1 = B$ and $u_2 = C$. Therefore, B and C correspond to rigid body translation and they may be set to zero without losing any generality. Furthermore, rigid body rotation ω is governed by the equation

$$\omega = \frac{1}{2}\left[\frac{\partial u_1}{\partial x_2} - \frac{\partial u_2}{\partial x_1}\right]$$

and the contribution of function f and g towards rigid body rotation becomes

$$\omega = \frac{1}{2}(A + A) = A$$

Therefore, A corresponds to a rigid body rotation of the component and may be set equal to zero without losing any generality. Thus, for the plane stress cases,

$$u_1 = \frac{1}{2\mu}\left[\frac{(1-\nu)}{(1+\nu)}\operatorname{Re}\bar{Z}_I - x_2 \operatorname{Im} Z_I\right] \tag{3.22a}$$

$$u_2 = \frac{1}{2\mu}\left[\frac{2}{(1+\nu)}\operatorname{Im}\bar{Z}_I - x_2 \operatorname{Re} Z_I\right] \tag{3.22b}$$

For plane strain problems, we substitute Eqs (3.19a–c) in Eq. (3.12) to obtain

$$\frac{\partial u_1}{\partial x_1} = \frac{1}{E'}\left[(1-\nu')\operatorname{Re} Z_I - (1+\nu')x_2 \operatorname{Im} Z_I'\right]$$

$$\frac{\partial u_2}{\partial x_2} = \frac{1}{E'}\left[(1-\nu')\operatorname{Re} Z_I + (1+\nu')x_2 \operatorname{Im} Z_I'\right]$$

Substituting the values of E' and ν' [Eqs (3.11d and e)] in the above equations and then integrating them, we obtain the results for the plane strain cases as:

$$u_1 = \frac{1}{2\mu}\left[(1-2\nu)\operatorname{Re}\bar{Z}_I - x_2 \operatorname{Im} Z_I\right] \tag{3.23a}$$

$$u_2 = \frac{1}{2\mu}\left[2(1-\nu)\operatorname{Im}\bar{Z}_I - x_2 \operatorname{Re} Z_I\right] \tag{3.23b}$$

Thus, we have expressed all the stress and displacement components in terms of the Westergaard function Z_I, which still is an unknown function.

The Westergaard function does not solve a problem completely. The function solves it to a stage from where we have a much better chance to guess the form of Z_I by looking at the boundary conditions of a problem. The Westergaard approach comes out handy for the problems of an infinite plate because we do not have to concentrate much on satisfying boundary conditions of far field stress.

Now, we take up the problem of an infinite plate with through-the-thickness crack length of $2a$, loaded under a biaxial field of stress σ as shown in Fig. 3.6. Usually, if the exterior dimensions of the plate are much larger than the crack length, the plate is considered to be infinite. The boundary conditions that should be met while choosing the Westergaard function are:

(i) At the crack tip

$$\sigma_{22} = \infty$$

(ii) On cracked surfaces ($x_2 = 0, -a < x_1 < a$)

$$\sigma_{22} = 0, \quad \sigma_{12} = 0$$

(iii) Far away from the crack (large $|z|$)

$$\sigma_{11} = \sigma, \quad \sigma_{22} = \sigma, \quad \sigma_{12} = 0$$

While guessing the form of the Westergaard function for this problem we study Eq. (3.19) in light of the boundary conditions. The function which satisfies all the boundary conditions is

$$Z_I(z) = \frac{\sigma z}{(z-a)^{1/2}(z+a)^{1/2}} = \frac{\sigma z}{(z^2-a^2)^{1/2}} \tag{3.24}$$

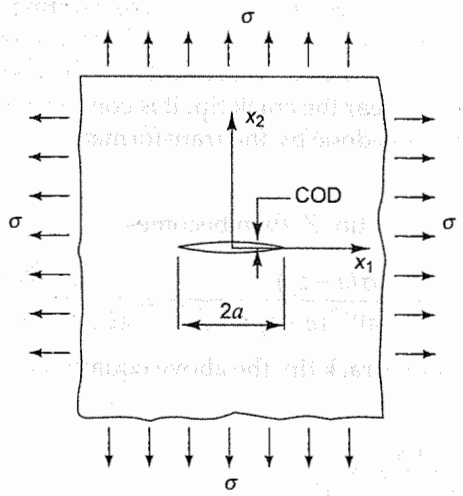

Fig. 3.6 A centre-crack in an infinite plate subjected to a biaxial stress field

Now we shall check whether the form of $Z_I(z)$ satisfies the boundary conditions. For checking the first boundary condition, using Eq. (3.19b), we find σ_{22} for $x_1 \geq 0$ and $x_2 = 0$ as

$$\sigma_{22} = \frac{\sigma x_1}{(x_1^2 - a^2)^{1/2}}$$

Clearly for $|x_1| \to a$, the stress component σ_{22} tends towards infinity, thus satisfying the first boundary condition. On cracked surfaces with x_2 negligibly small ($\simeq 0$), Z_I is simplified to

$$Z_I(z) = \frac{\sigma x_1}{(x_1^2 - a^2)^{1/2}} \tag{3.25}$$

Then, the stress components are

$$\sigma_{22} = \text{Re}\, Z_I$$
$$\sigma_{12} = 0.$$

Z_I is imaginary on the cracked surfaces because x_1 lies between $-a$ and a, making Re $Z_I = 0$. Thus the second boundary condition on the cracked surfaces is satisfied. In order to check the third boundary condition, we take $|z| \to \infty$ in Eq. (3.24) to have

$$Z_I(z) = \frac{\sigma}{\left(1 - a^2/z^2\right)^{1/2}} = \frac{\sigma}{\left(1 - \left(a^2/|z|^2\right)e^{-2i\theta}\right)^{1/2}}$$

leading to $Z_I(z) = \sigma$ for $\frac{a}{|z|} << 1$.

The differentiation of Eq. (3.24) gives

$$Z_I'(z) = -\frac{\sigma a^2}{\left(z^2 - a^2\right)^{3/2}} \tag{3.26}$$

which gives $Z_I'(z) = 0$ when $|z| \to \infty$. Substitution of the limiting values of $Z_I(z)$ and $Z_I'(z)$ in Eq. (3.19) leads to $\sigma_{11} = \sigma$, $\sigma_{22} = \sigma$ and $\sigma_{12} = 0$, thus satisfying the far field boundary conditions. Therefore, the chosen form of $Z_I(z)$ is the correct solution to the problem.

For determining the stress field near the crack tip, it is convenient to transform the origin from the centre of the crack to its tip. It is done by the transformation

$$z = a + z_o \tag{3.27}$$

where z_o is measured from the crack tip. Z_I then becomes

$$Z_I(z_o) = \frac{\sigma(a + z_o)}{(a + z_o - a)^{1/2}(a + z_o + a)^{1/2}} = \frac{\sigma\sqrt{a}[1 + z_o/a]}{(2z_o)^{1/2}[1 + z_o/2a)^{1/2}} \tag{3.28}$$

Since $|z_o| << a$ in the vicinity of the crack tip, the above equation is simplified to the approximate relation

$$Z_I(z_o) \simeq \frac{\sigma\sqrt{\pi a}}{(2\pi z_o)^{1/2}} = \frac{K_I}{(2\pi z_o)^{1/2}} \tag{3.29}$$

Expressing z_o in polar coordinates as $z_o = r(\cos\theta + i\sin\theta)$, it is modified to

$$Z_I = \frac{K_I}{(2\pi r)^{1/2}}\left(\cos\frac{\theta}{2} - i\sin\frac{\theta}{2}\right) \tag{3.30}$$

Similarly, the transformation $z = z_o + a$ changes Eq. (3.26) to

$$Z_I'(z_o) = -\frac{\sigma a^2}{z_o^{3/2}\left(z_o + 2a\right)^{3/2}} \simeq -\frac{\sigma a^2}{z_o^{3/2}\left(2a\right)^{3/2}}$$

$$= \frac{-K_I}{2(2\pi)^{1/2} r^{3/2}}\left(\cos\frac{3\theta}{2} - i\sin\frac{3\theta}{2}\right) \tag{3.31}$$

Substituting $Z_I(z_o)$ and $Z_I'(z_o)$ in Eq. (3.19) and realizing $x_2 = r\sin\theta$, we obtain

$$\sigma_{11} = \frac{K_I}{(2\pi r)^{1/2}}\cos\frac{\theta}{2} - \frac{r\sin\theta}{2}\frac{K_I}{(2\pi)^{1/2} r^{3/2}}\sin\frac{3\theta}{2}$$

$$= \frac{K_I}{(2\pi r)^{1/2}}\cos\frac{\theta}{2}\left(1 - \sin\frac{\theta}{2}\sin\frac{3\theta}{2}\right) \tag{3.32a}$$

Similarly,

$$\sigma_{22} = \frac{K_I}{(2\pi r)^{1/2}}\cos\frac{\theta}{2}\left(1 + \sin\frac{\theta}{2}\sin\frac{3\theta}{2}\right) \tag{3.32b}$$

$$\sigma_{12} = \frac{K_I}{(2\pi r)^{1/2}} \sin\frac{\theta}{2} \cos\frac{\theta}{2} \cos\frac{3\theta}{2} \tag{3.32c}$$

For determining the displacement field in the vicinity of the crack tip, $\bar{Z}_I(z_o)$ is obtained from Eq. (3.29) as

$$\bar{Z}_I(z_o) = \left(\frac{2}{\pi}\right)^{1/2} K_I \sqrt{z_o} = \left(\frac{2r}{\pi}\right)^{1/2} K_I \left(\cos\frac{\theta}{2} + i\sin\frac{\theta}{2}\right)$$

Now, it is a simple matter of substituting $Z_I(z_o)$ and $\bar{Z}_I(z_o)$ in Eq. (3.22) and simplifying it to obtain the displacement field in the vicinity of the crack tip for the plane stress as:

$$u_1 = \frac{K_I}{\mu}\left(\frac{r}{2\pi}\right)^{1/2} \cos\frac{\theta}{2}\left(\frac{(1-\nu)}{(1+\nu)} + \sin^2\frac{\theta}{2}\right) \tag{3.33a}$$

$$u_2 = \frac{K_I}{\mu}\left(\frac{r}{2\pi}\right)^{1/2} \sin\frac{\theta}{2}\left(\frac{2}{1+\nu} - \cos^2\frac{\theta}{2}\right) \tag{3.33b}$$

For the plane strain, substitution of $Z_I(z_o)$ and $Z_I(z_o)$ in Eqs (3.23a and b) gives:

$$u_1 = \frac{K_I}{\mu}\left(\frac{r}{2\pi}\right)^{1/2} \cos\frac{\theta}{2}\left(1 - 2\nu + \sin^2\frac{\theta}{2}\right) \tag{3.34a}$$

$$u_2 = \frac{K_I}{\mu}\left(\frac{r}{2\pi}\right)^{1/2} \sin\frac{\theta}{2}\left(2 - 2\nu - \cos^2\frac{\theta}{2}\right) \tag{3.34b}$$

Unlike the stress components, the displacement components are finite and there is no square root singularity. One should not get misled by noting that u_1 and u_2 keep on increasing with increasing r; the above solution is valid only in the close vicinity of the crack tip. Also, note that u_1 does not depend on the sign of θ; it is expected because Mode I problem is symmetric about the crack plane. However, as expected, u_2 changes its sign as θ is replaced by $-\theta$.

The distance between the two crack faces, known as the crack opening displacement (*COD*), is useful for carrying out experiments and for defining the parameter, crack tip opening displacement (*CTOD*) which is introduced in Chapter 7. *COD* of a centre-cracked plate when subjected to plane stress loading (Fig. 3.6) will be obtained by invoking Eq. (3.22b) for $x_2 = 0$. For this problem Z_I and $\bar{Z}_I$ simplify to

$$Z_I = \frac{\sigma z}{(z^2 - a^2)^{1/2}} = \frac{-i\sigma x_1}{\sqrt{a^2 - x_1^2}}$$

$$\bar{Z}_I = \sigma(z^2 - a^2)^{1/2} = i\sigma\sqrt{a^2 - x_1^2}$$

Substituting Z_I and $\bar{Z}_I$ in Eq. (3.22b) and realizing the shear modulus as $\mu = E/2(1 + \nu)$ we obtain

$$COD = 2u_2 = 2 \times \frac{1}{2\mu}\left[\frac{2\sigma}{(1+\nu)}\sqrt{a^2 - x_1^2}\right] \tag{3.35}$$

$$= \frac{4\sigma}{E}\sqrt{a^2 - x_1^2}$$

with the maximum crack opening equal to $4\sigma a/E$ at $x_1 = 0$.

In fracture mechanics problems, if $Z(z_o)$ is expressed with the crack tip as origin, $\sqrt{z_o}$ appears in the denominator of all the three modes. Another formal definition of K [3.7], which is an alternative yet equivalent to the two definitions already presented through Eqs (3.3) and (3.4), is

$$K = \lim_{z_o \to 0} \sqrt{2\pi z_o}\, Z(z_o) \tag{3.36}$$

If this definition is applied to Eq. (3.29), we have the familiar result, $K_I = \sigma\sqrt{\pi a}$.

We realize that the simple expression of Eq. (3.29) was obtained by neglecting some terms from Eq. (3.28). Some of us may, at this stage, like to split hairs and be interested in knowing how approximate the results are for the relation of Eq. (3.29). To have some idea, we would explore how σ_{22} differs from the correct solution on $x_2 = 0$ plane. For the biaxial case under consideration, the rigorous solution of Eq. (3.24) is simplified for $x_2 = 0$ to

$$Z_I(z) = \frac{\sigma x_1}{\left(x_1^2 - a^2\right)^{1/2}} \quad \text{for } |x_1| > a.$$

Substituting in Eq. (3.19b) leads to

$$\frac{\sigma_{22}}{\sigma} = \frac{x_1}{\left(x_1^2 - a^2\right)^{1/2}}$$

The origin is moved to the crack tip by the transformation $x_1 = a + x_o$ and, with some manipulation, we obtain

$$\frac{\sigma_{22}}{\sigma} = \frac{\left(1 + x_o/a\right)}{\left(2x_o/a\right)^{1/2}}\left(1 + \frac{x_o}{2a}\right)^{-1/2}$$

The approximate value of σ_{22} is obtained from Eq. (3.32b) for $\theta = 0$ as

$$\frac{\sigma_{22}}{\sigma} = \frac{1}{\left(2x_o/a\right)^{1/2}}$$

The percentage difference between the two values, rigorous and approximate (labeled as 'no approximation' and 'one term' respectively in Fig. 3.7), increases with the increase in distance from the origin on the crack plane. At the distance where $x_o/a = 0.15$, the difference is 9.8%.

The approximate relation of Eq. (3.29) can be improved by retaining higher terms in the expansion of $(1 + z_o/2a)^{-1/2}$ of Eq. (3.28). In fact, the form of $Z_I(z_o)$ changes to

$$Z_I = \frac{K_I}{\left(2\pi z_o\right)^{1/2}} + A_1 z_o^{1/2} + A_2 z_o^{3/2} + A_3 z_o^{5/2} + \cdots \tag{3.37}$$

where A_1, A_2, A_3, etc. are real numbers. If we retain the first two terms, σ_{22} is modified to

$$\sigma_{22} = \frac{K_I}{\left(2\pi r_o\right)^{1/2}} \cos\frac{\theta}{2}\left(1 + \sin\frac{\theta}{2}\sin\frac{3\theta}{2} + \frac{3r}{4a}\left(1 - \sin^2\frac{\theta}{2}\right)\right)$$

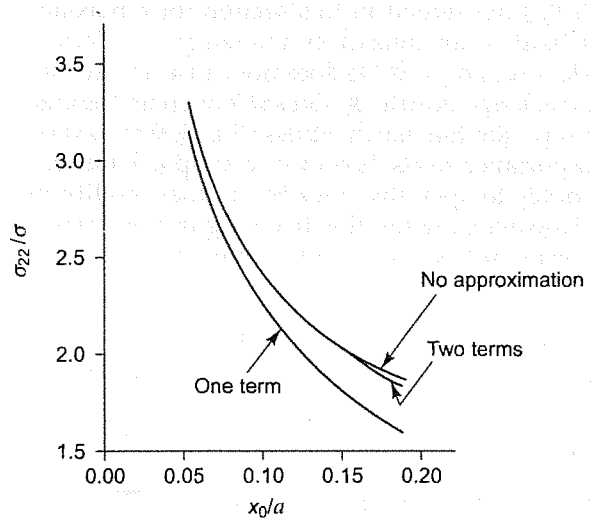

Fig. 3.7 σ_{22} on the crack plane for biaxial loading

In Fig. 3.7 the solution of 'two terms' is also plotted for σ_{22} from the above results for $\theta = 0$. It shows that the inclusion of one more term considerably reduces the difference between the rigorous and approximate values. For the biaxial loading problem, Fig. 3.8(a) shows the photo-elastic fringes (simulated on a computer) in the approximate case of using only the first term in Eq. (3.37). The lobes of the fringes are almost normal to the crack plane. Figure 3.8(b) shows the fringes when two terms are used and it is evident that the lobes of the fringes are inclined. This result is close to the fringes observed in real life cases.

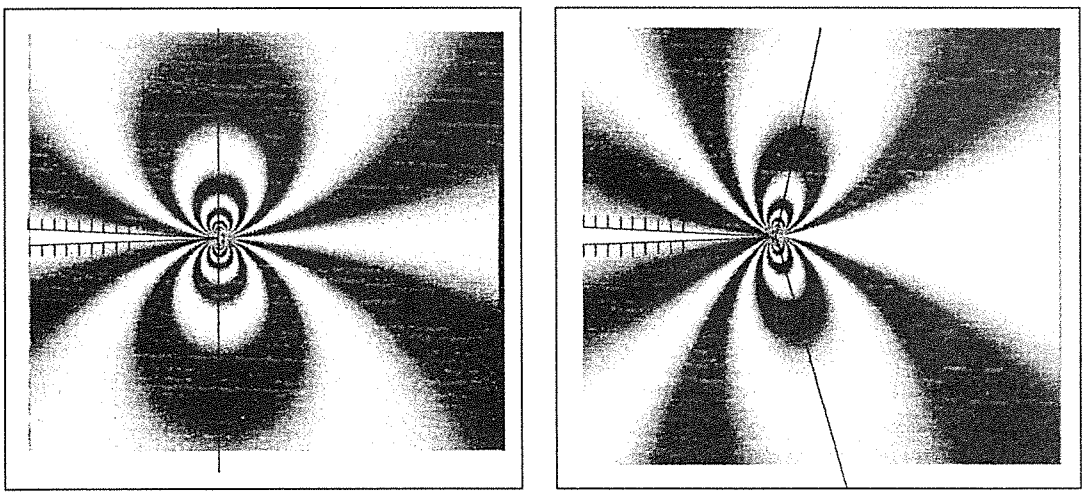

Fig. 3.8 Photoelastic fringes for the biaxial loading case with analysis of (a) one term, and (b) two terms (*Courtesy:* Dr K. Ramesh, Dept. of Applied Mechanics, IIT Madras)

The stress field [Eq. (3.32)] developed in this section for a biaxially loaded plate is usually claimed to be the stress field of an uniaxially loaded plate (Secs 3.2 and 3.3). What is the contribution of the far field stress $\sigma_{11} = \sigma$? It does not cause any substantial change in the stress field in the vicinity of the crack tip because σ_{11} does not open up the crack. Invoking the principle of superposition, we can separate the biaxial stress (Fig. 3.9) to two configurations, (a) and (b). Configuration (a) is of importance to us; however, a simple solution to it is still not available. Configuration (b) does not try to open the crack but it does modify the stress field to a certain extent near the crack tip. However, the solution to configuration (b) is not simple and we usually neglect its effect in engineering solutions to fracture mechanics.

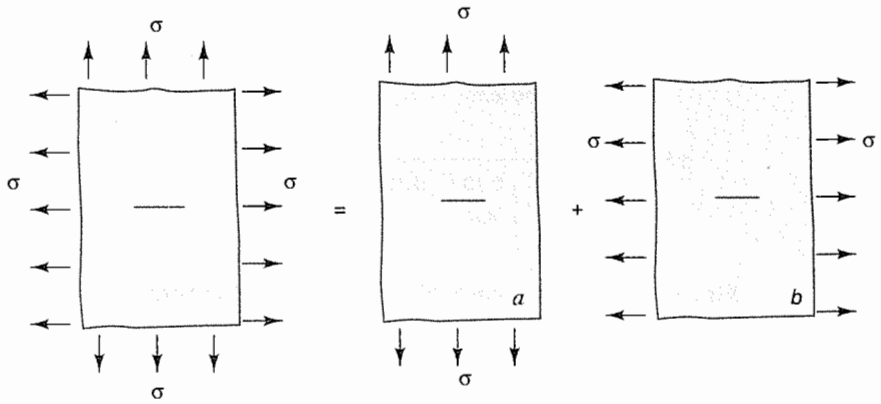

Fig. 3.9 Separating biaxial loading case to configs (a) and (b)

We close this subsection by realizing that the exact Westergaard solution is not available for a centre crack in a plate loaded uniaxially in the direction normal to the crack plane. However, a simple Westergaard function is available for biaxially loaded plates whose stress field in the vicinity of the crack tip is not substantially different from the case of an uniaxially loaded plate. Therefore, for most of the practical purposes, the solution of a biaxially loaded plate is employed for both uniaxially and biaxially loaded problems.

3.5.2 Mode II (Sliding Mode)

A centre-cracked problem in an infinite plate for Mode II loading is considered, as shown in Fig. 3.3(a). It has been found that the following expression of the Airy Stress Function ϕ is convenient:

$$\Phi = -x_2 \operatorname{Re} \bar{Z}_{II} \tag{3.38}$$

where, $\bar{Z}_{II}$ is a complex function and its form would be so chosen such that all the boundary conditions are satisfied. One can easily show that the above expression for Φ satisfies the biharmonic equation and the stress field is given by

$$\sigma_{11} = 2 \operatorname{Im} Z_{II} + x_2 \operatorname{Re} Z'_{II} \tag{3.39a}$$

$$\sigma_{22} = -x_2 \operatorname{Re} Z'_{II} \tag{3.39b}$$

$$\sigma_{12} = \operatorname{Re} Z_{II} - x_2 \operatorname{Im} Z'_{II} \tag{3.39c}$$

Further, stress components are converted to strain components and then integrated to yield for plane strain cases as

$$u_1 = \frac{1}{2\mu}\left[2(1-\nu)\,\mathrm{Im}\,\bar{Z}_{II} + x_2\,\mathrm{Re}\,Z_{II}\right] \tag{3.40a}$$

$$u_2 = \frac{1}{2\mu}\left[-1(1-2\nu)\,\mathrm{Re}\,Z_{II} - x_2\,\mathrm{Im}\,Z_{II}\right] \tag{3.40b}$$

For the case of Mode II, as shown in Fig. 3.3, the Westergaard function is given as:

$$Z_{II} = \frac{\tau z}{\left(z^2 - a^2\right)^{1/2}} \tag{3.41}$$

which satisfies all the boundary conditions. They are similar to boundary conditions of the Mode I problem [Fig. 3.2(a)]. Like in the case of Mode I, we transform the origin to the crack tip by the transformation relation $z = a + z_o$ and obtain the simplified but approximate relation as

$$Z_{II} = \frac{\tau(\pi a)^{1/2}}{(2\pi z_o)^{1/2}} \tag{3.42}$$

Invoking the definition of the stress intensity factor [Eq. (3.36)], we obtain:

$$K_{II} = \tau\sqrt{\pi a}$$

Substitution of Z_{II} and its derivative in Eqs (3.39a–c), leads to:

$$\sigma_{11} = \frac{-K_{II}}{(2\pi r)^{1/2}}\sin\frac{\theta}{2}\left(2 + \cos\frac{\theta}{2}\cos\frac{3\theta}{2}\right)$$

$$\sigma_{22} = \frac{K_{II}}{(2\pi r)^{1/2}}\cos\frac{\theta}{2}\sin\frac{\theta}{2}\cos\frac{3\theta}{2} \tag{3.43}$$

$$\sigma_{12} = \frac{K_{II}}{(2\pi r)^{1/2}}\cos\frac{\theta}{2}\left(1 - \sin\frac{\theta}{2}\sin\frac{3\theta}{2}\right)$$

Substitution of Z_{II} and $\bar{Z}_{II}$ in Eqs (3.40a and b) gives the displacement field for a plane strain problem as

$$u_1 = \frac{K_{II}}{\mu}\left(\frac{r}{2\pi}\right)^{1/2}\sin\frac{\theta}{2}\left(2 - 2\nu + \cos^2\frac{\theta}{2}\right) \tag{3.44a}$$

$$u_2 = \frac{K_{II}}{\mu}\left(\frac{r}{2\pi}\right)^{1/2}\left(-\cos\frac{\theta}{2}\right)\left(1 - 2\nu - \sin^2\frac{\theta}{2}\right) \tag{3.44b}$$

With the similar procedure, the displacement field for a plane stress field can be obtained as

$$u_1 = \frac{K_{II}}{\mu}\left(\frac{r}{2\pi}\right)^{1/2}\sin\frac{\theta}{2}\left(\frac{2}{1+\nu} + \cos^2\frac{\theta}{2}\right) \tag{3.45a}$$

$$u_2 = \frac{K_{II}}{\mu}\left(\frac{r}{2\pi}\right)^{1/2}\left(-\cos\frac{\theta}{2}\right)\left(\frac{1-\nu}{1+\nu} - \sin^2\frac{\theta}{2}\right) \tag{3.45b}$$

3.5.3 Mode III (Tearing Mode)

A large plate with a centre crack, subjected to a far field shear stress $\sigma_{23} = \tau$ (Fig. 3.4), is considered. For this case of Mode III,

$$u_1 = 0$$
$$u_2 = 0$$
$$u_3 = w(x_1, x_2).$$

For this displacement field, components of strain tensor turn out to be

$$\varepsilon_{11} = \varepsilon_{22} = \varepsilon_{33} = \varepsilon_{12} = 0$$
$$\varepsilon_{13} = \frac{1}{2}\frac{\partial w}{\partial x_1};\ \varepsilon_{23} = \frac{1}{2}\frac{\partial w}{\partial x_2}$$

leading to,

$$\sigma_{11} = \sigma_{22} = \sigma_{33} = \sigma_{12} = 0$$
$$\sigma_{13} = 2\mu\,\varepsilon_{13} = \mu\frac{\partial w}{\partial x_1} \tag{3.46a}$$
$$\sigma_{23} = 2\mu\,\varepsilon_{23} = \mu\frac{\partial w}{\partial x_2} \tag{3.46b}$$

It should be kept in mind that the problem of Mode III is not a case of plane stress or plane strain. It is considerably simpler because many components of displacement, stress and strain are zero. We would, therefore, not be using the biharmonic equation. Instead, the problem will be solved with displacement component w as the dependent variable and then there is no need to worry for compatible conditions any more. Out of the three equilibrium equations, only the last one provides the non-trivial equation,

$$\frac{\partial \sigma_{13}}{\partial x_1} + \frac{\partial \sigma_{23}}{\partial x_2} = 0.$$

Converting it into displacement components using Eqs (3.46a and b)

$$\frac{\partial^2 w}{\partial x_1^2} + \frac{\partial^2 w}{\partial x_2^2} = 0$$

which is the well known Laplace equation and is also written as

$$\nabla^2 w = 0$$

The Westergaard approach is also applicable to this differential equation by choosing w in the form of

$$w = \frac{1}{\mu}\,\mathrm{Im}\, Z_{\mathrm{III}} \tag{3.47}$$

where Z_{III} is a complex function of variable z. Again one can show that the above expression satisfies the governing differential equation. Also, substituting w in Eqs (3.46a and b), we obtain stress components as

$$\sigma_{13} = \mathrm{Im}\, Z'_{\mathrm{III}} \tag{3.48a}$$
$$\sigma_{23} = \mathrm{Re}\, Z'_{\mathrm{III}} \tag{3.48b}$$

The form

$$Z'_{III} = \frac{\tau z}{\left(z^2 - a^2\right)^{1/2}}$$

satisfies all the boundary conditions. Z'_{III} is transformed to the origin at the crack with relation $z = a + z_o$ and after neglecting the small terms, we obtain:

$$Z'_{III} = \frac{\tau\sqrt{a}}{\left(2z_o\right)^{1/2}}. \tag{3.49}$$

Using $\tau\sqrt{\pi a} = K_{III}$ and expressing z_o in polar coordinates, the equation is simplified to

$$Z'_{III} = \frac{K_{III}}{\left(2\pi r\right)^{1/2}}\left(\cos\frac{\theta}{2} - i\sin\frac{\theta}{2}\right). \tag{3.50}$$

Substituting Z'_{III} in Eq. (3.48), we obtain the stress field as

$$\sigma_{13} = -\frac{K_{III}}{\left(2\pi r\right)^{1/2}}\sin\frac{\theta}{2} \tag{3.51a}$$

$$\sigma_{23} = \frac{K_{III}}{\left(2\pi r\right)^{1/2}}\cos\frac{\theta}{2} \tag{3.51b}$$

Integrating Eq. (3.49) and substituting $\tau\sqrt{\pi a} = K_{III}$, we have

$$Z_{III} = \left(\frac{2}{\pi}\right)^{1/2} K_{III}\left(z_o\right)^{1/2} = K_{III}\left(\frac{2r}{\pi}\right)^{1/2}\left(\cos\frac{\theta}{2} + i\sin\frac{\theta}{2}\right)$$

which on substitution in Eq. (3.47), gives the displacement field as

$$u_3 = \frac{K_{III}}{\mu}\left(\frac{2r}{\pi}\right)^{1/2}\sin\frac{\theta}{2}$$

with $u_1 = 0$ and $u_2 = 0$

3.6 Concluding Remarks

We determined the stress and displacement fields around a crack tip in infinite plates for all the three modes. These results are quite useful to a designer, because in many practical applications a crack in a plate is quite small in comparison to the lateral extent of the plate.

The Westergaard's approach adopted in this chapter is not the general way of solving problems. In fact, problems of infinite plates are easier to solve because stress fields far away from the crack are simple; we mainly focus our attention to the cracked faces and with some luck we may be able to guess a solution, which satisfies all the boundary conditions. In the case of work-components,

which have their edge/edges close to the crack, the job of guessing a Westergaard function, which not only satisfies conditions at cracked faces but also meets the requirements at the edges, becomes a difficult task. Problems dealing with bodies of finite dimensions will be taken up in Chapter 4.

QUESTIONS

1. What is a singularity? What kind of singularity describes a stress field near the vicinity of a crack tip in LEFM? Is it expected to be different for elastic-plastic fracture mechanics?
2. Stress field is the same for plane stress and plane strain problems. Why is it not so for displacement fields?
3. In problems of plates, stress components are expressed in the Cartesian coordinate system whereas the location at which stress is considered is defined in polar coordinates. Why is such a mixed approach adopted?
4. For many problems of practical applications, solutions of infinite plates are applicable. Justify the statement.
5. Displacement near the crack tip is determined by integrating strain components. Why do we equate integration constants to zero?
6. Mode I case has been solved for a biaxial case and its stress and displacement fields are taken to be approximately the same as of an uniaxial case. Justify.
7. Why do we not use biharmonic equation to solve Mode III problems for a centre crack in an infinite plate?

PROBLEMS

1. Show that $\Phi = -x_2 \operatorname{Re} \bar{Z}_{II}$, chosen for the Mode II problem, satisfies the biharmonic equation. Determine stress components and displacement components (plane stress) in terms of Z_{II}.
2. For a centre crack in an infinite plate loaded in Mode II, determine stress components and displacement components (plane stress) near the vicinity of a crack tip in terms of K_{II}.
3. Show that $w = \frac{1}{\mu} \operatorname{Im} Z_{III}$, chosen for the Mode III problem for a centre-cracked infinite plate, satisfies the Laplace equation $\nabla^2 w = 0$. Determine stress components and all displacement components in terms of Z_{III}. Also, determine stress and displacement fields in the vicinity of the crack tip in terms of K_{III}.
4. In a large plate, a crack of length $2a$ is inclined with an angle α with x_1-axis (Fig. 3.10). The plate is loaded in x_2 direction with $\sigma_{22} = \sigma$.
   (i) Find the stress intensity factors.
   (ii) For $\sigma = 80$ MPa, $2a = 20$ mm and $\alpha = 30°$, determine K_I and K_{II}.
5. Determine stress at point H of Problem 4, if $r = 1$ mm and $\theta = 45°$.
6. Determine the critical crack length in a centered-cracked plate, loaded in Mode I, if critical stress intensity factor $K_{Ic} = 60$ MPa $\sqrt{m}$ and far field stress is 120 MPa.
7. Determine stress components (σ_{rr}, $\sigma_{\theta\theta}$, $\sigma_{r\theta}$) and displacement components (u_r, u_θ) in polar coordinates for plane stress of Mode I.

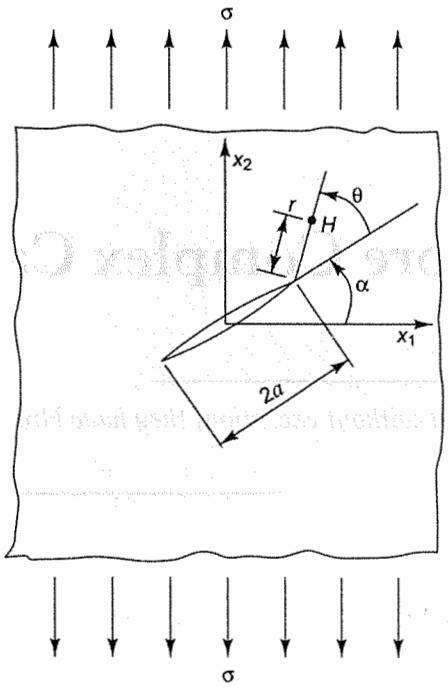

Fig. 3.10 The figure of Problem 4

REFERENCES

3.1 Irwin, G.R. (1958). *Fracture, Handbuch der Physik*, S. Flugge (ed.), Springer–Verlag, Berlin, Vol. VI, pp. 551–590.

3.2 Kanninen, M.F. and Popelar, C.H. (1985). *Advanced Fracture Mechanics*, Oxford University Press, New York.

3.3 Sokolnikoff, I.S. (1956). *Mathematical Theory of Elasticity*, McGraw-Hill Book Company, New York.

3.4 Fung, Y.C. (1965). *Foundation of Solid Mechanics*, Prentice-Hall Inc., Englewood, New Jersey.

3.5 Westergaard, H.M. (1939). "Bearing Pressures and Cracks," *Journal of Applied Mechanics*, 61, pp. A49–53.

3.6 Carrier, G.F., Krook, M. and Pearson, C.E. (1966). *Functions of a Complex Variable*, McGraw-Hill Book Company, New York.

3.7 Gdoutos, E.E. (2005). *Fracture Mechanics—An Introduction*, Springer, The Netherland.

3.8 Anderson, T.L. (2004). *Fracture Mechanics: Fundamentals and Applications*, CRC, Press-Book.

3.9 Sanford, R.J. (2003). *Principles of Fracture Mechanics*, Prentice Hall, Upper Saddle River.

3.10 Janssen, M., Zuidema, J. & Wanhill, R.J.H. (2004). *Fracture Mechanics*, Spon Press, Abingdon.

3.11 Ramesh, K. (2007). *e-Book on Engineering Fracture Mechanics*, IIT Madras, URL: http//apm.iitm.ac.in/smlab/kramesh/book_4.htm.

Chapter

4

SIF of More Complex Cases

Models are useful, but without exception, they have blind spots built into them.

Deepak Chopra

4.1 Other Applications of Westergaard Approach

We have so far solved the basic problems of Modes I, II and III in the previous chapter through the approach made available by Westergaard. The chapter defined stress intensity factor and determined stress and displacement fields near a tip of a crack in an infinite plate loaded with a far field stress. In this section, we would take up some more problems which are also important for the practical cases.

4.1.1 Wedge Loads on Cracked Surfaces

Consider the problem of two wedge loads P (per unit length), acting symmetrically on each cracked

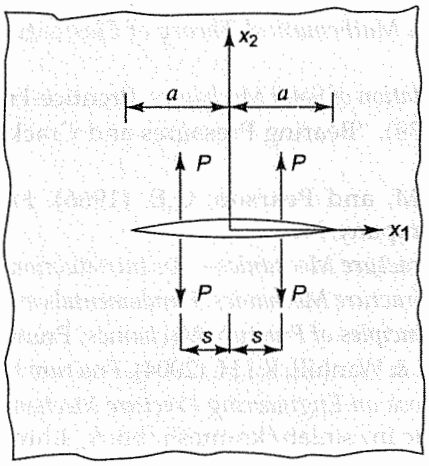

Fig. 4.1 Symmetrically applied wedge loads on the surfaces of a crack

surface (Fig. 4.1) at a distance s from the centre of the crack. The problem has applications to riveted joints. For this case, the Westergaard function is known to be

$$Z_I = \frac{2Pz\left(a^2 - s^2\right)^{1/2}}{\pi\left(z^2 - s^2\right)\left(z^2 - a^2\right)^{1/2}}$$

which leads to

$$K_I = \frac{2P}{\pi}\frac{(\pi a)^{1/2}}{\left(a^2 - s^2\right)^{1/2}} \tag{4.1}$$

Another case of wedge loads on one side only (Fig. 4.2) is more general, and stress intensity factors are known to be [4.1]:

$$K_I^A = \frac{P}{\sqrt{\pi a}}\left[\frac{a+s}{a-s}\right]^{1/2} \tag{4.2a}$$

$$K_I^B = \frac{P}{\sqrt{\pi a}}\left[\frac{a-s}{a+s}\right]^{1/2} \tag{4.2b}$$

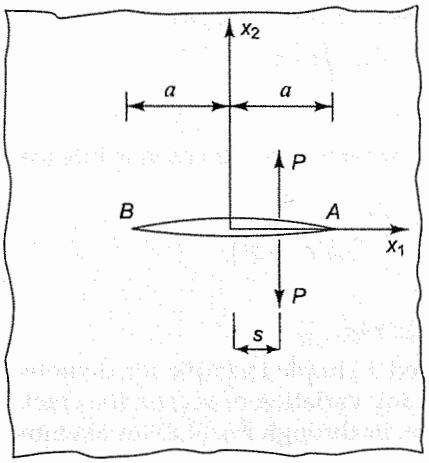

Fig. 4.2 A pair of wedge loads at distance s on the surfaces of a crack

These results are also found to be very useful in solving problems of distributed pressure on the crack surfaces by constructing Green's functions. To explore the approach of Green's function, we consider the problem of a triangular pressure distribution at the cracked surfaces as shown in Fig. 4.3 with maximum pressure p_0 acting at the centre. This problem is solved by invoking the solution to the symmetric line loads acting on the faces of the crack [Eq. (4.1)]. Consider two thin slices, each of width ds and at a distance s from the origin, as shown in the figure. Then, the load on one slice is given by

$$dP = \frac{(a-s)}{a}\, p_0 ds$$

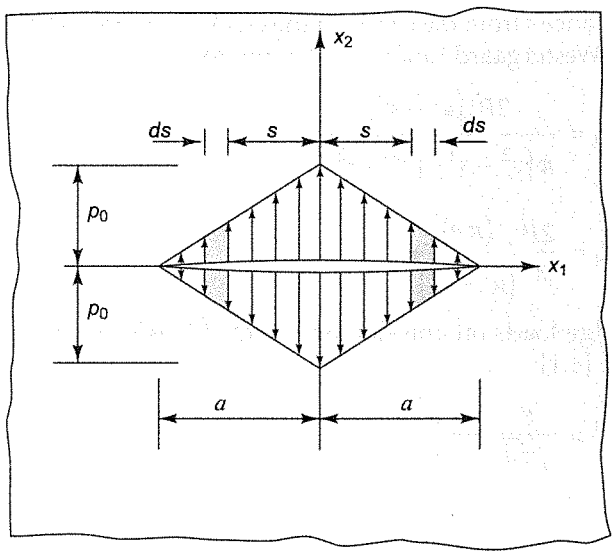

Fig. 4.3 Triangular pressure distribution acting at the surfaces of a crack

which contributes towards stress intensity factor as

$$dK_I = \frac{2(a-s)p_0\sqrt{\pi a}\,ds}{a\pi\left(a^2-s^2\right)^{1/2}}.$$

Now, to determine the effect of pressure, the equation is integrated to have the form

$$K_I = \frac{2}{\pi}p_0\sqrt{\pi a}\int_0^a \frac{(a-s)}{a\left(a^2-s^2\right)^{1/2}}ds$$

which on integration gives

$$K_I = (1-2/\pi)p_0\sqrt{\pi a}\,.$$

Note that we have considered a simple example for demonstrating the approach of Green's function; but problems having any variation of $p(x)$ on the crack surfaces can be solved through Eq. (4.1) for symmetric pressure, or through Eq. (4.2) for asymmetric pressure. If $p(x)$ is a simple distribution, one may be able to integrate to obtain a closed form solution; otherwise, one can always resort to numerical techniques to solve the problem.

4.1.2 Collinear Cracks in an Infinitely Long Strip

A classic problem in fracture mechanics is of collinear cracks in an infinitely long strip as shown in Fig. 4.4. Identical cracks, each of length $2a$, are separated by a distance W. The geometry of this problem is not usually encountered in practical cases and, therefore, one may think that the problem is solved just for the sake of academia. This is not the case, because the problem acts as a stepping stone to several real life problems dealing with finite size plates. In this section, we shall find the solution of this problem, but in subsequent sections of this chapter, appropriate portions will be cut out from this strip to solve problems encountered in several engineering applications of importance. The Westergaard function Z_I for the problem [4.2] is known to be

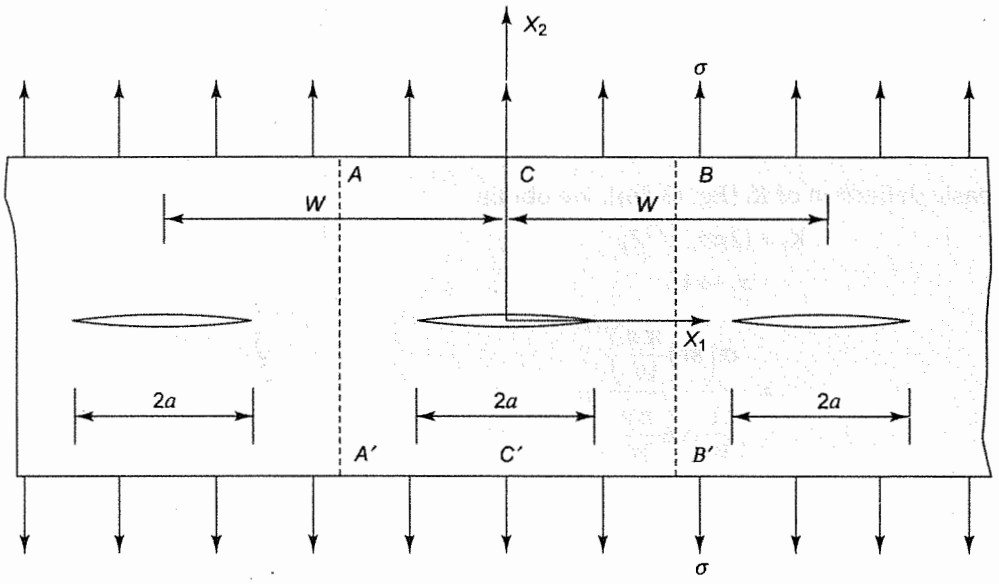

Fig. 4.4 Collinear cracks in an infinitely long strip

$$Z_I = \frac{\sigma \sin(\pi z/W)}{\left[\sin^2(\pi z/W) - \sin^2(\pi a/W)\right]^{1/2}} \tag{4.3}$$

where, the origin is at the center of a crack. Transforming axes to the tip of the crack by relation $z = a + z_o$ leads to

$$\sin\frac{\pi z}{W} = \sin\left(\frac{\pi z_o}{W}\right)\cos\frac{\pi a}{W} + \cos\left(\frac{\pi z_o}{W}\right)\sin\frac{\pi a}{W} \tag{4.4}$$

Since we have confined the analysis to the close proximity of the crack tip ($|z| << a$),

$$\sin\left(\frac{\pi z_o}{W}\right) \approx \frac{\pi z_o}{W}$$

$$\cos\frac{\pi z_o}{W} \approx 1$$

Simplifying Eq. (4.4) with the above approximations and substituting in Eq. (4.3), we obtain

$$Z_I = \frac{\sigma\left[\frac{\pi z_o}{W}\cos\frac{\pi a}{W} + \sin\frac{\pi a}{W}\right]}{\left[\frac{\pi^2 z_o^2}{W^2}\cos^2\frac{\pi a}{W} + \frac{2\pi z_o}{W}\cos\frac{\pi a}{W}\sin\frac{\pi a}{W}\right]^{1/2}}$$

Since z_o/W is a small number, the first term of the numerator as well as of the denominator are negligible, leading to

$$Z_I = \frac{\sigma\left(\sin\frac{\pi a}{W}\right)^{1/2}}{\left(\frac{2\pi z_o}{W}\cos\frac{\pi a}{W}\right)^{1/2}}$$

Using basic definition of K_I [Eq. (3.36)], we obtain

$$K_I = (2\pi z_0)^{1/2} Z_I$$

$$z_o \to 0$$

$$= \frac{\sigma\left(\sin\frac{\pi a}{W}\right)^{1/2}}{\left(\frac{1}{W}\cos\frac{\pi a}{W}\right)^{1/2}}$$

Manipulating the equation, so as to have the familiar $\sigma\sqrt{\pi a}$ in the numerator, we have

$$K_I = \sigma\sqrt{\pi a}\left(\frac{\tan\frac{\pi a}{W}}{\frac{\pi a}{W}}\right)^{1/2} . \tag{4.5}$$

It is worth noting that the expression of Eq. (4.5) is only an approximate relation. For $W >> a$, we obtain $K_I = \sigma\sqrt{\pi a}$, which is the same as that of an infinite plate with one crack.

4.2 Application of the Principle of Superposition

The principle of superposition can be applied to identical geometries for linear elastic bodies. Since only elastic bodies are considered in this chapter, the principle can be exploited to solve problems of fracture mechanics.

Take an example of a centre-cracked plate with two different loads, σ as a far field stress and line loads P at the cracked faces as shown in the Config. (s) of Fig. 4.5. Invoking the principle of superposition, stress at any point H in the vicinity of the crack tip is given by the sum of the stress of Config. (m) and Config. (n); that is,

$$\sigma_{22} = \sigma_{22}^m + \sigma_{22}^n$$

Substituting the values of σ_{22}^m and σ_{22}^n from Eq. (3.32b), we get

$$\sigma_{22} = \frac{K_I^m}{\sqrt{2\pi r}}\cos\frac{\theta}{2}\left(1+\sin\frac{\theta}{2}\sin\frac{3\theta}{2}\right) + \frac{K_I^n}{\sqrt{2\pi r}}\cos\frac{\theta}{2}\left(1+\sin\frac{\theta}{2}\sin\frac{3\theta}{2}\right)$$

$$= \frac{\left(K_I^m + K_I^n\right)}{\sqrt{2\pi r}}\cos\frac{\theta}{2}\left(1+\sin\frac{\theta}{2}\sin\frac{3\theta}{2}\right) \tag{4.6}$$

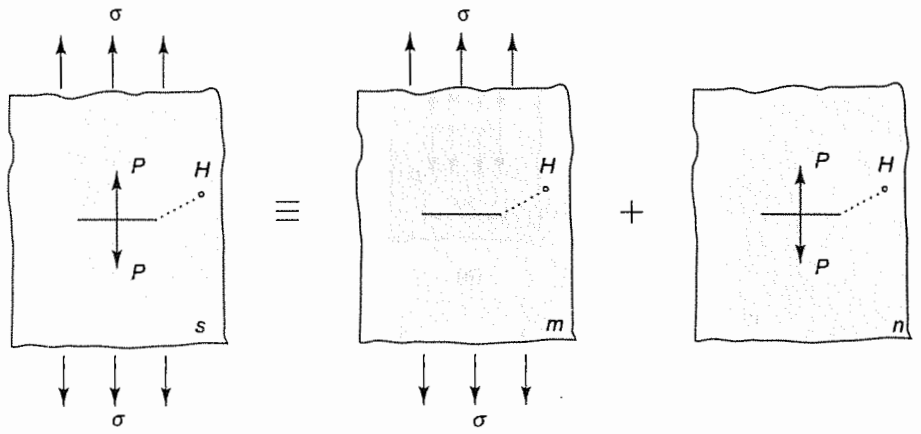

Fig. 4.5 Separating a complex problem into two simpler problems to exploit the principle of superposition

which means,

$$K_I = K_I^m + K_I^n \tag{4.7}$$

We thus conclude that when several external loads develop stress intensity factors of Mode I on a crack, the resulting stress intensity factor is the sum of individual stress intensity factor. However, it is clear from Eq. (4.6) that in the case of mixed modes, the stress intensity factors cannot be added to obtain the net stress intensity factor.

4.2.1 Internal Pressure on Cracked Faces

Consider the case of a large plate with an uniform pressure p applied on the crack faces (Fig. 4.6a). The pressure opens the crack faces and loads the specimen in Mode I. We would be determining the resulting stress intensity factor at the crack tips. The solution to this problem can be easily obtained through the Green's function approach using Eq. (4.1), as

$$K_I = p\sqrt{\pi a}$$

The same problem can also be solved using the principle of superposition. This method is different from the approach of Green's function. In fact, several interesting and powerful tricks are developed which can be used for solving more complex problems of fracture mechanics through the use of the principle of superposition.

Consider an infinite plate which has no crack but is loaded by a far field stress σ, shown through the starting Config. (*s*) in Fig. 4.6(b). Config. (*s*) is equivalent to Config. (*f*) with a centre-crack and the applied traction σ on the cracked faces, whose magnitude must be the same as that of the far field stress. This is because the neighboring atoms on the opposite side of the crack are no longer held together with the help of the interatomic bonding. In place of these bonds, external traction is applied on the cracked faces so that they do not open up under the far field stress and the stress in the entire plate remains uniform. Now, the Config. (*f*) has two external loads, the far field stress and the applied traction at the cracked faces. They are separated, keeping the geometry of the crack and the plate same, into Config. (*g*) and Config. (*h*). Thus, the superposition of Config. (*g*) and Config. (*h*) makes Config. (*f*), whose stress intensity factor is zero. Invoking the principle of superposition, we obtain:

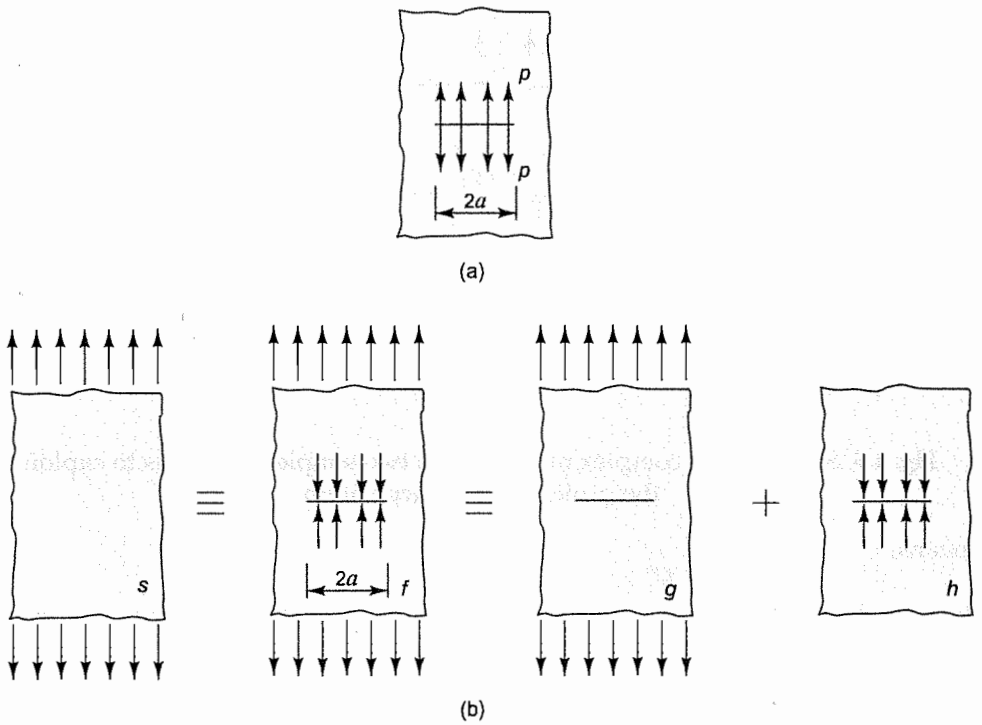

Fig. 4.6 (a) Internal pressure on the surfaces of a crack, and (b) determination of K_I by invoking the principle of superposition

$$K_I^g + K_I^h = 0$$

yielding $$K_I^h = -K_I^g = -\sigma\sqrt{\pi a}$$

If the direction of the externally applied traction in Config. (*h*) is reversed ($p = -\sigma$), we have the stress intensity factor of the centre-crack with internal pressure p, as

$$K_I = p\sqrt{\pi a}$$

4.2.2 Wedge Load at the Surface of a Crack Face

Consider the case of a line load P at one surface of the crack (Config. (*s*) of Fig. 4.7) and a far field stress σ on the side of the other crack face. Note that for maintaining equilibrium, $P = \sigma W$. Such a problem has practical applications in riveted joints. The Config. (*s*) can be separated into Config. (*h*) and Config. (*n*). As shown in the figure, Config. (*h*) is further separated into Config. (*l*) and Config. (*m*). The principle of superposition gives

$$\begin{aligned} K_I^s &= K_I^h - K_I^n \\ &= K_I^l + K_I^m - K_I^n \end{aligned} \tag{4.8}$$

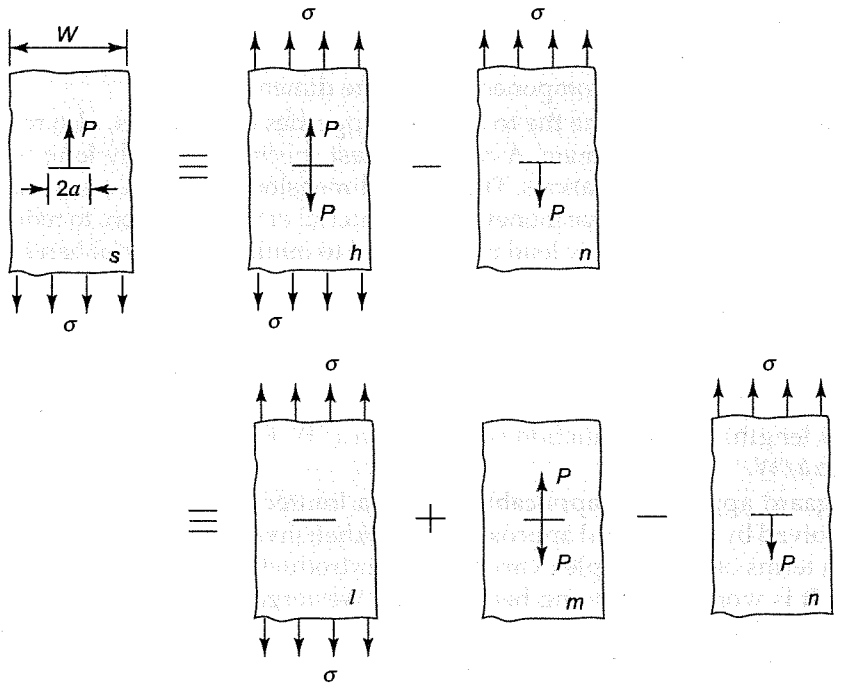

Fig. 4.7 A wedge load on one surface of a crack and a far field stress on the side of the other crack face

It is to be noted that loads on Config. (*n*) are the same as those on Config. (*s*), except with the difference in the direction of the loads. When the Config. (*n*) in Fig. 4.7 is taken to the left hand side of Eq. (4.8), it gets added to Config. (*s*), giving

$$2K_I^s = K_I^l + K_I^m$$

Using Eq. (4.2a) and substituting $P = \sigma W$, we have

$$K_I^M = \frac{P}{\sqrt{\pi a}} = \frac{\sigma W}{\sqrt{\pi a}}$$

The expression for K_I^l is well known as $\sigma\sqrt{\pi a}$ for the infinite plate. Thus, we have

$$K_I^s = \frac{\sigma\sqrt{\pi a}}{2} + \frac{\sigma W}{2\sqrt{\pi a}}$$

4.3 Crack in a Plate of Finite Dimensions

In practical applications, an edge (boundary) of a component may be close to the crack tip. Since the edge is traction free, it disturbs the stress field around the crack tip. The edge then may have a considerable influence on the stress field in the vicinity of the crack tip and on the stress intensity

factor. The situation may require an accurate determination of the SIF. When is an edge regarded close to the crack? If the distance of the edge from the crack tip is less than the crack length, or of the order of the crack length, the component is of finite dimensions.

Experimentalists, who determine the toughness properties of materials, also require accurate analysis of the SIF for a test specimen. A crack in a test specimen is fairly long (usually longer than 10 mm) for practical considerations. The lateral dimensions of the specimen cannot be made very large for reasons such as to save money on the material of the specimen, to reduce machining charges, to use a test-machine of low load capacity and to minimize material handling problems. Since free edges of a specimen have considerable influence on the stress field and the SIF, it becomes necessary to analyze the problem accurately. Usually, SIF is expressed in the form

$$K = \sigma\sqrt{\pi a} f(a/W)$$

where, W is the width of plate (dimension of the component from one edge to opposite edge along the crack length) and the function f depends on a/W. For most cases, $f(a/W)$ is written as a series of ratio a/W.

The Westergaard approach is applicable only to a limited cases of finite dimensions. More problems are solved by the general approach of Muskhelishvili, in which Airy's Stress Function is expressed in terms of two complex variables. An introduction to this method is discussed in Appendix 4A. It is worth mentioning here that the Westergaard approach is a special case of the general Muskhelishvili approach [4.3]. If a close form solution to a problem is not available, powerful numerical methods have been developed for determining stress intensity factor of a crack in a given component.

We now consider the case of a common problem—a centre-cracked plate of finite dimensions subjected to a tensile stress σ which acts normal to the crack plane. The SIF is estimated using the results of collinear cracks in an infinite strip (Fig. 4.4), by cutting a portion out at AA' and BB'. The separated portion is shown in Fig. 4.8, with traction on the cut faces. Since AA' and BB' are the planes of symmetry, shear stress on them is zero. The stress component σ_{11} has some distribution, shown qualitatively in the figure. In fact, the problem is somewhat similar to the biaxial loading (Fig. 3.6), where it is argued that σ_{11} does not change the SIF significantly. On the same lines, the effect of σ_{11} on cut faces may be ignored. Then, the SIF of a plate with a centre-crack is approximated to be same as that of the case of collinear cracks in an infinite strip, i.e.,

$$K_I = \sigma\sqrt{\pi a}\left[\frac{\tan\frac{\pi a}{W}}{\frac{\pi a}{W}}\right]^{1/2}$$

However, the Mode I problem of a finite plate with a centre crack is important and has been solved through advanced mathematical techniques and sophisticated numerical methods. It has been found that the exact solution is more close to the form

$$K_I = \sigma\sqrt{\pi a}\left[\sec\left(\frac{\pi a}{W}\right)\right]^{1/2}$$

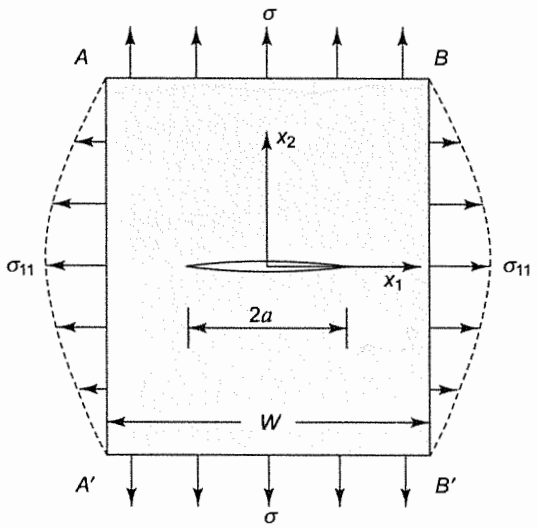

Fig. 4.8 Centre-cracked plate of finite dimensions

Note that for $a/W << 1$, K_I approaches $\sigma\sqrt{\pi a}$ which, as expected, is the solution of an infinite plate.

4.4 Edge Cracks

Edge cracks are more dangerous than interior cracks. We have already discussed in Sec. 4.3 that a free edge close to the crack influences the stress field near the crack tip. In the case of an edge crack, the free edge is not only close to the crack, but it intersects the crack (touches the surfaces of the crack). Edge cracks are very commonly encountered in day-to-day life. Since they are more dangerous, special attention is required to deal with them.

Consider an edge crack in a semi-infinite plate which is loaded by a far field stress σ, as shown in Fig. 4.9. The stress intensity factor for this case is known [4.2] to be equal to $1.12\,\sigma\sqrt{\pi a}$. When the edge crack is compared with one half of the overall length of an interior crack, the value of the SIF is about 12% more. We can justify the larger value by looking at the problem closely. The ends of cracked faces at the free edge tend to open up more easily. This is similar to the case of a cantilever beam whose deflection is more than the deflection of a beam supported at its two ends. SIF for a finite plate with an edge crack can be determined through the expression given in Appendix 4B.

The analysis for the case of edge crack is not straightforward, because the mouth of the crack lies on the free edge and the stress field is influenced considerably by the free edge. The problem can be solved by separating a portion $CBB'C'$ from the strip of collinear cracks (Fig. 4.4) and invoking the principle of superposition to make the traction zero on section . However, the solution is quite complex and is beyond the scope of this book.

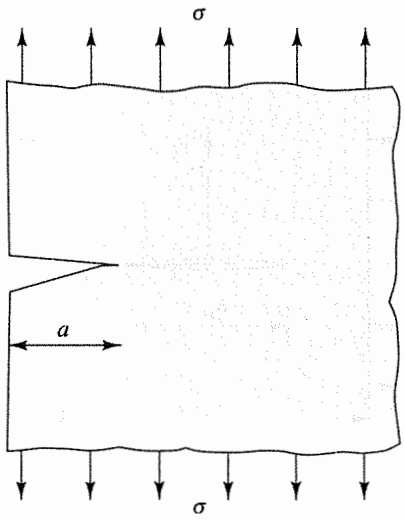

Fig. 4.9 Edge-crack in a large plate

4.5 Embedded Cracks

So far in this chapter, we have considered through-the-thickness cracks, i.e., the crack front runs from one face of the plate to another. But there are many cracks of practical importance where a crack initiates at one face of the plate, but does not go all the way to the other face. The front of such a crack is usually curved and embedded within the thickness of the plate. Embedded cracks are usually modeled as a semi-ellipse in the literature of fracture mechanics. Figure 4.10(a) shows an embedded crack, also known as surface crack. If the crack happens to be at the corner of the plate (Fig. 4.10(b)), it is usually modeled as a quarter-elliptical-crack.

When a semi-elliptical crack becomes critical, it may grow along the minor axis a, or major axis c, or along both. Later in this section, we would show that for $c > a$, the crack in most cases tends to grow more into the depth and less along the lateral direction.

Surface cracks are observed in boilers, compressor-chambers, pipelines, etc., which carry high pressure fluids or gases. Also, many structural components with embedded cracks are subjected to flexural loads. The SIF of some important cases may be obtained from handbooks [4.2, 4.4] or other reference books [4.1, 4.5, 4.6]. The SIF may also be determined using a FEM computer package.

It is worth noting that embedded cracks, such as those shown in Fig. 4.10a are exposed to a free surface of the plate. The free surface influences the stress field and the SIF considerably. This is similar to the case of the edge crack of through-the-thickness in which the free surface affects the stress field and makes the analysis difficult (Sec. 4.4). Therefore, the analysis of an embedded crack, with its crack face meeting the surface of the plate, is complex and one generally determines SIF through numerical techniques. However, one way to estimate the SIF of surface cracks is by considering the solution to an elliptical crack that is fully embedded in a plate, as shown in Fig. 4.11. Once the solution to this problem is obtained, the SIF of the semi-elliptical crack is approximated to be 12% higher, similar to the practice adopted for through-the-thickness edge cracks.

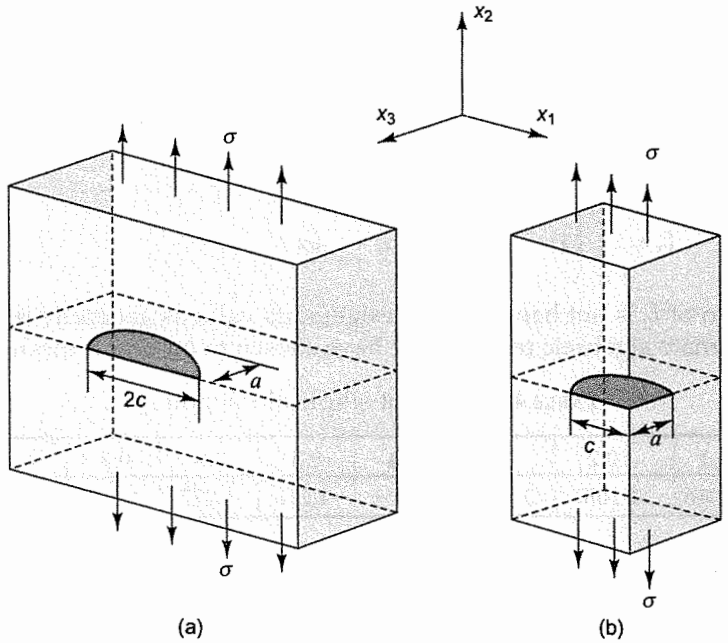

Fig. 4.10 (a) A semi-elliptical surface crack, and (b) a quarter-elliptical corner crack

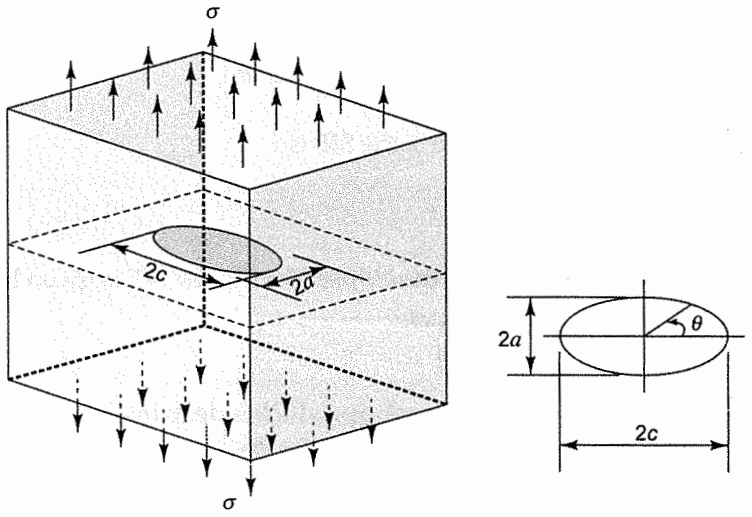

Fig. 4.11 A fully embedded elliptical crack

4.5.1 Elliptical Crack

The problem of the fully embedded elliptical crack was first presented in complete form by Irwin in 1962 for a large plate of infinite thickness [4.7]. The SIF at a point of the elliptical crack front is given by (Fig. 4.11)

$$K_I = \frac{\sigma(\pi a)^{1/2}}{I_2}\left[\sin^2\theta + \left(\frac{a}{c}\right)^2 \cos^2\theta\right]^{1/4} \tag{4.9}$$

where I_2 is the elliptical integral of a second kind that depends on a/c (ratio of minor to major axis) as defined in Fig. 4.11. I_2 is given by

$$I_2 = \int_0^{\pi/2}\left(1 - \frac{c^2 - a^2}{c^2}\sin^2\alpha\right)^{1/2} d\alpha \tag{4.10}$$

Since the evaluation of I_2 is not handy for a designer, its value is generally provided through a table or an approximate algebraic relation. We have chosen to present it through Table 4.1.

TABLE 4.1 Value of elliptical Integral I_2

a/c	0.0	0.1	0.2	0.3	0.4	0.5	0.6	0.7	0.8	0.9	1.0
I_2	1.000	1.016	1.1051	1.097	1.151	1.211	1.277	1.345	1.418	1.493	$\pi/2$

4.5.2 Semi-elliptical Cracks

As mentioned before, a surface crack is modeled as a half ellipse with its minor axis into the thickness direction. The SIF of the surface crack is then 12% higher over the corresponding SIF of the elliptical crack. Thus, the SIF at a point of the crack front of a semi-elliptical crack is

$$K_I = \frac{1.12\sigma(\pi a)^{1/2}}{I_2}\left[\sin^2\theta + \left(\frac{a}{c}\right)^2 \cos^2\theta\right]^{1/4} \tag{4.11}$$

At the extreme end of the minor axis ($\theta = 90°$), the SIF is

$$K_I^{90} = \frac{1.12\sigma(\pi a)^{1/2}}{I_2}$$

and at the extreme end of the major axis of the ellipse ($\theta = 0°$), the SIF is given by

$$K_I^{0} = \frac{1.12\sigma(\pi a)^{1/2}}{I_2}\left(\frac{a}{c}\right)^{1/2}$$

It is worth noting that the segment of the crack tip, which is deep inside the material, possesses a higher SIF. Thus, a crack tends to grow deeper into the thickness, rather than sideways on the surface, as shown in Fig. 4.12.

Also, for a very shallow crack ($a << c$), I_2 from Table 4.1 is close to unity and the SIF at $\theta = 90°$, becomes

$$K_I^{90} = 1.12\sigma(\pi a)^{1/2}$$

which is the same as the result of through-the-thickness edge crack of length a. In this case, the dimension of the major axis is no longer relevant. Therefore, a shallow crack is equivalent to a through-the-thickness edge crack of length a.

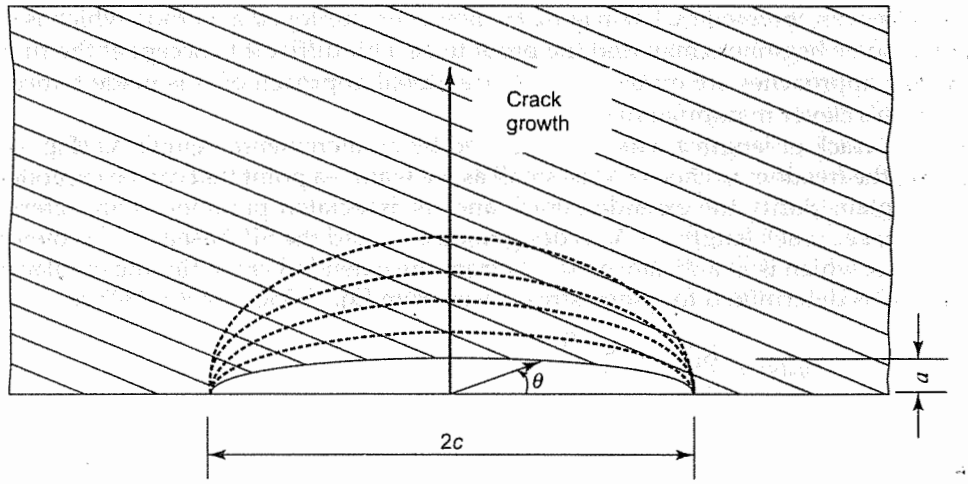

Fig. 4.12 The growth of a semi-elliptical surface-crack

The problem of the surface crack in a plate, where the crack depth a is comparable to thickness of the plate, has also been solved through finite element methods [4.4]. The SIF at the deepest segment of the crack front is expressed as

$$K_I = M\sigma\frac{(\pi a)^{1/2}}{I_2} \tag{4.12}$$

where the factor M is 1.12 for a very small a/t, t being the plate thickness. M increases with the increasing a/t, but it depends on two ratios, a/t and a/c. For further details, readers are referred to a handbook on stress intensity factors [4.4].

4.5.3 Quarter or Corner Cracks

A corner crack under tensile load [Fig. 4.10(b)] is exposed to two free surfaces, each one applying an additional correction factor on the SIF. The overall correction factor of such cracks in thick plates has found to be about 20% higher [4.1] i.e., the largest SIF on the crack front is

$$K_I = 1.2\sqrt{\pi a}$$

4.6 The Relation Between G_I and K_I

Energy release rate G_I is a global parameter and deals with energy. On the other hand, stress intensity factor K_I is a local parameter which deals with displacement and stress fields in the vicinity of the crack. Although the approaches are entirely different, the goal is same, i.e., to characterize a crack. It is like measuring edible oil through either mass or volume; both methods are employed in the Indian market. There is a relationship between the two methods. In fact, if the oil is sold by the liter, the relation should be prescribed on the container as per the law of the Government of India. Similarly, we should have a relation between G and K.

The relation was obtained by Irwin [4.8]. He however employed a method which is somewhat indirect and some beginners may find the proof to be a bit difficult to accept at the first reading. Since the two approaches are quite different, the global approach of G is made to become local through Irwin's clever manipulation.

Consider a crack of length a which is extended by an incremental length Δa (Fig. 4.13). Note that we have the freedom to choose Δa as small as we want—a point that can be exploited later. In order to maintain clarity the extended crack and its associated parameters are referred by the prime system; i.e., crack length $a + \Delta a$ is designated as a' and the SIF based on a' is denoted by K'. At a distance s, which is at a distance $(\Delta a - s)$ from the extended crack tip, the displacement of a crack face (u_2) is determined for plane stress cases from Eq. (3.33b) for $\theta = 180°$ as

$$u_2(s) = \frac{K_I'}{\mu}\left(\frac{\Delta a - s}{2\pi}\right)^{1/2} \frac{2}{(1+\nu)}$$

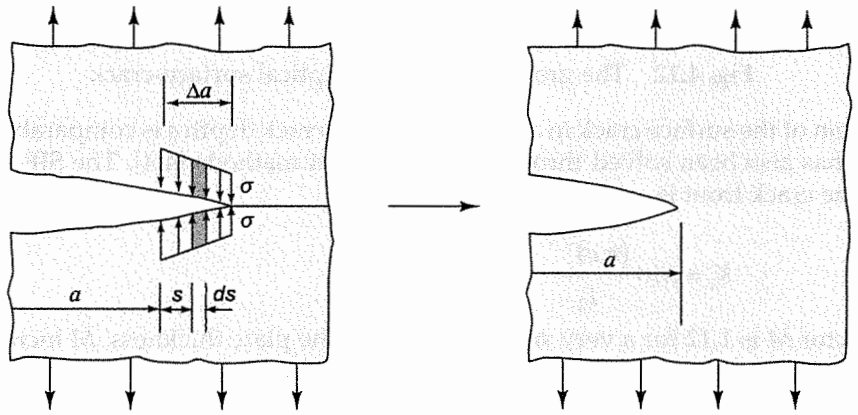

Fig. 4.13 Closure of the crack to find relation between G_I and K_I

Now, each crack face in the portion Δa is moved in through the distance $u_2(s)$ with the help of the traction σ_{22} so that the crack faces touch each other. The magnitude of stress σ_{22} is evaluated from the stress field of the unextended crack of length a, and therefore at a distance s, it is given by

$$\sigma_{22}(s) = \frac{K_I}{(2\pi s)^{1/2}}$$

Thus, the crack is closed by length Δa. Irwin argued that the total elastic work required by σ_{22} in closing the crack is equal to the energy released. Balancing the two energies, we have

$$G_I B\Delta a = 2\int_0^{\Delta a} \frac{B\sigma_{22}u_2}{2}\, ds \tag{4.13}$$

where B is the thickness of the plate; the integral is multiplied by 2 to account for strain energy in both cracked faces and divided by 2 to account for the linear relationship between σ_{22} and u_2. Substituting σ_{22} and u_2 in the equation and taking limit $\Delta a \to 0$, we have

$$G_I = \lim_{\Delta a \to 0} \frac{2}{(1+\nu)\mu\Delta a} \int_0^{\Delta a} \frac{K_I}{(2\pi s)^{1/2}} \frac{K_I'(\Delta a - s)^{1/2}}{(2\pi)^{1/2}} ds \tag{4.14}$$

We can express

$$K_I' = K_I + \Delta K_I$$

Since Δa can be chosen as small as we like, ΔK_I can be made small enough to be neglected in comparison to K_I. Then, Eq. (4.14) is simplified to

$$G_I = \lim_{\Delta a \to 0} \frac{K_I^2}{(1+\nu)\pi\mu\Delta a} \int_0^{\Delta a} \left(\frac{\Delta a - s}{s}\right)^{1/2} ds$$

To solve the equation, we substitute $s = \Delta a \sin^2\alpha$ to obtain

$$G_I = \frac{K_I^2}{(1+\nu)\pi\mu} \int_0^{\pi/2} 2\cos^2\alpha \, d\alpha$$

Solving the integral and realizing the shear modulus $\mu = E/2(1+\nu)$, we obtain

$$G_I = \frac{K_I^2}{E} \tag{4.15a}$$

The relation is simple, but is rigorous only for brittle materials in which the components remain elastic.

During the historical development of Fracture Mechanics, the relation of Eq. (4.15a) was made simple at the cost of making the expression of the SIF more complex than necessary. There is no need to have π under the square root in the expression $K_I = \sigma\sqrt{\pi a}$. It should have been $K_I = \sigma\sqrt{a}$ with $G_I = \pi K^2{}_1/E$. However, with so much work already carried out with $\sqrt{\pi}$ in the definition of K_I, it is extremely difficult to correct the historical mistakes. There are many similar compromises in the history of science and technology. For example, one hour has 60 minutes, or the angle around a point is 360° in place of a convenient decimal system just because a long time ago in Babylonia, there were sixty Gods leading to a sexagesimal number system (based on the number sixty).

In the case of a plane strain, the relationship becomes:

$$G_I = (1-\nu^2)\frac{K_I^2}{E} \tag{4.15b}$$

Similar relations for Mode II and Mode III can be obtained as:

$$G_{II} = \frac{K_{II}^2}{E} \qquad \text{for plane stress} \tag{4.15c}$$

$$G_{II} = (1-\nu^2)\frac{K_{II}^2}{E} \qquad \text{for plane strain} \tag{4.15d}$$

$$G_{III} = (1+\nu)\frac{K_{III}^2}{E} = \frac{K_{III}^2}{2\mu} \tag{4.15e}$$

In case all three modes are present, the energy of each mode is added up to G_{TOT}, as

$$G_{TOT} = G_I + G_{II} + G_{III}$$

4.7 Critical Stress Intensity Factor

Two Questions:

Why should we evaluate the SIF for a crack in a component?

How does it help a designer?

Recall that our prime goal of studying fracture mechanics is to predict whether a crack is likely to grow or not. If the SIF of a crack approaches or exceeds an upper limit of the stress intensity factor, the crack may grow. The upper limit is known as the critical stress intensity factor which is a material property and is usually denoted by the symbol K_{Ic} for Mode I cases (K_{IIc} and K_{IIIc} for Mode II and Mode III respectively). In order to provide a feel of stress intensity factor and the critical stress intensity factor, an analogy is made with stress and yield stress of a solid. Stress is a parameter which represents internal loading within the solid and yield stress is the limit on stress, beyond which the material is regarded to have failed by many designers. Similarly, stress intensity factor is a parameter to measure the severity of stress at the crack tip. But, critical stress intensity factor is the limit on the SIF, such that if the SIF exceeds the critical stress intensity factor, the crack may grow.

Thus, in order to predict the growth of a crack in a component, the designer should find two values: (i) the SIF determined through analysis for the geometry of the component, crack configuration and applied loads and (ii) the critical SIF determined through experiments for the material of the component. If the stress intensity factor exceeds the critical stress intensity factor, the designer should do something, such as reducing the loads on the component, modifying the geometry of the component, or choosing a material of higher toughness.

The SIF of some commonly encountered cases is listed in Appendix 4B. In addition, several handbooks [2.2, 2.4] are available and the designer may find the SIF of an application under consideration. Otherwise, he may have to determine the SIF for the problem usually through a numerical technique.

One difficulty, faced during the experimental determination of the critical SIF for the material of the component, is that critical SIF is found to be dependant on the thickness of a plate. In fact, the critical SIF is independent of the thickness only in the case of a thick plate, because the plate is then loaded in the plane strain. One question remains—what is the criterion of assuring that the plane strain conditions prevail? The size of the plastic zone in the vicinity of the crack tip decides it. If the plate thickness is significantly greater than the size of the plastic zone, then the conditions of plane strain exist. Determination of the plastic zone size is discussed in detail later in Chapter 5.

Thus, we find that the critical SIF becomes a property of the material only for plane strain cases. Therefore, in handbooks and literature, the values of critical SIFs of commonly used materials (steel, aluminum, titanium, brass, etc.) are given for plane strain conditions.

Critical stress intensity factor for thin plates depends on the plate thickness and its value is rarely provided as a function of thickness in literature. However, the critical SIF of a plane stress case is higher than the corresponding value in a plane strain. A designer may find that a component is subjected to plane stress, but critical SIF is available only for plane strain. He may safely use the critical SIF of the plane strain because it would provide a conservative design.

In certain design problems (e.g., components of airplanes, rockets and spaceships), using the critical SIF of a plane strain as material property may be too conservative, because structural plates are mostly used in plane stress. Adopting a too conservative approach is against the philosophy of engineering profession. Engineers should always strive to obtain numbers close to

reality. In aerospace applications, where the factor of safety is of the order of 1.1 for many components, using material toughness properties of plane strain is likely to make the machine heavy with poor payload. In such a situation, stress intensity factor is determined by preparing a test-specimen of same thickness as of plates used in the actual application.

However, for most down-to-earth problems (such as the designing components of automobiles, roof trusses, locomotive carriages, pipe lines, etc.) the conservative approach of using the critical SIF of the plane strain may be quite practical and useful.

Companies, specially dealing with aerospace parts, do generate data for in-house use. Unfortunately, the data is usually not placed in any open literature (handbooks, journals), so that competitors are not able to take any advantage. Looking through a bird's eye view, many of us think that there is unnecessary wastage of resources if the properties of a material are experimentally determined at several places in the world. An open policy is desirable where the companies share data freely. This will reduce the cost of testing and consequently the cost of their products.

Critical SIF of a material depends on many factors, such as

- Heat treatment which controls the yield stress of the material.
- Speed of the crack.
- Temperature of the specimen.
- Process of manufacturing (e.g., vacuum furnaced or air melted, as cast or rolled).
- Orientation of the crack with respect to the grains at the crack tip.
- Test method.

To provide a feel to the readers about the toughness of engineering materials, representative K_{Ic} is listed in Table 4.2 for quasi-static load conditions, at room temperature. In the table, the process of heat treatment of alloys has been accounted for by listing the yield stress of the material along with the K_{Ic}. For alloy steel or maraging steel, one can note from the table that K_{Ic} decreases substantially when the yield stress is increased by heat treatment. However, K_{Ic} of a material in Table 4.2 is only a representative value.

TABLE 4.2 Representative K_{Ic} of various materials

Material	*Yield stress, MPa*	K_{Ic}, *MPa* $\sqrt{m}$
Mild Steel	240	very high ($\simeq 220$)
Medium Carbon Steel	260	54
Alloy Steel*	860	99
	1070	77
	1515	60
	1850	47
Rotor Steel	626	50
Nuclear Reactor Steel	350	190
Maraging Steel	1770	93
	2000	47
	2240	38

(Contd.)

Material	*Yield stress, MPa*	K_{Ic}, *MPa* $\sqrt{m}$
Stainless Steel		80–150
Aluminum		
2014-T4	460	29
2014-T651	455	24
7075-T651	495	24
7178-T651	570	23
Titanium (Ti-6Al-4V)	910	55
Perspex (PMMA)		1.6
PVC		3.5
Nylon		3.0

* 40Ni2Cr1Mo28 (IS)/EN 24 (UK)/4340 USA

4.8 Bending and Twisting of Cracked Plates

In this chapter, so far, we have discussed cases where plates are subjected only to simple tensile or shear stress components. In such cases, stress components do not vary across the thickness of the plate. But in several engineering applications, a plate is subjected to bending and torsional moments and shear forces. Stress developed by a bending moment varies across the thickness, tension on one surface and compression on another. Similarly, twisting moments and shear forces develop stresses which vary across the thickness. Thus, the analysis is more complex.

4.8.1 Terminology of the Plate Theory

Consider a square element which has been sectioned out from a plate (Fig. 4.14). In the case of a thin plate, σ_{33} is negligible at all points of the plate. All the other five stress components are developed by three moments per unit length of the plate (M_1, M_2 and M_{12}) and two shear forces per unit length (V_1 and V_2). M_1 and M_2 are bending moments, whereas M_{12} is a twisting moment. If h is the thickness of the plate, all moments and shear forces can be expressed in terms of stress components, as follows:

$$
\begin{aligned}
M_1(x_1, x_2) &= \int_{-h/2}^{h/2} \sigma_{11}\, x_3 dx_3 \\
M_2(x_1, x_2) &= \int_{-h/2}^{h/2} \sigma_{22}\, x_3 dx_3 \\
M_{12}(x_1, x_2) &= \int_{-h/2}^{h/2} \sigma_{12}\, x_3 dx_3 \\
V_1(x_1, x_2) &= \int_{-h/2}^{h/2} \sigma_{13}\, dx_3
\end{aligned}
\tag{4.16}
$$

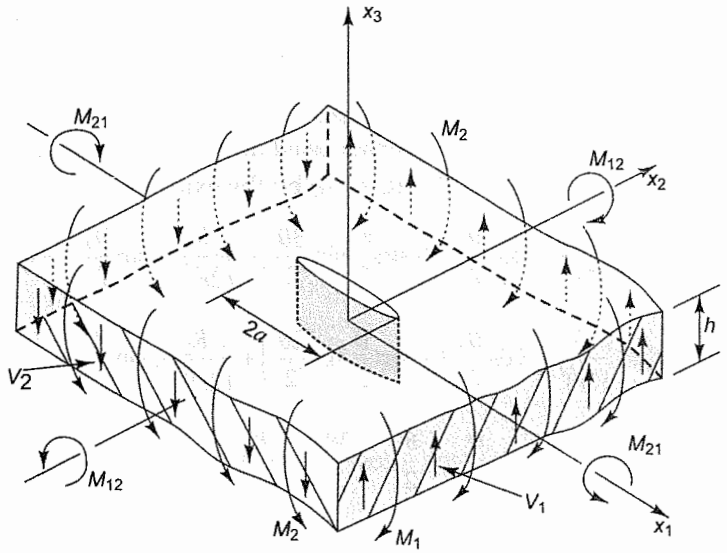

Fig. 4.14 A centre-cracked plate loaded with bending moments M_1 and M_2, twisting moment M_{12}, and shear forces V_1 and V_2

$$V_2(x_1, x_2) = \int_{-h/2}^{h/2} \sigma_{23}\, dx_3$$

For linear elastic materials in plane stress, components, σ_{11}, σ_{22}, σ_{12} vary linearly in x_3 directions and shear components σ_{13} and σ_{23} have parabolic distribution. In case moments and shear forces are known, the stress components can be determined by the following relations:

$$\sigma_{11} = \frac{12x_3M_1}{h^3}$$

$$\sigma_{22} = \frac{12x_3M_2}{h^3}$$

$$\sigma_{12} = \frac{12x_3M_{12}}{h^3}$$

$$\sigma_{13} = \frac{3}{2h}\left[1 - \left(\frac{2x_3}{h}\right)^2\right]V_1$$

$$\sigma_{23} = \frac{3}{2h}\left[1 - \left(\frac{2x_3}{h}\right)^2\right]V_2$$

4.8.2 Through-the-Thickness Crack in a Plate

For the crack shown in Fig. 4.14, surfaces of the crack are traction free ($\sigma_{22} = \sigma_{12} = \sigma_{23} = 0$). Invoking Eq. (4.16), we obtain the following boundary conditions on the crack surfaces:

$$M_2(x_1, 0) = 0\ ;\ M_{12}(x_1, 0) = 0\ ;\ V_2(x_1, 0) = 0$$

The solution to this problem is complex and only approximate or numerical results are available. It has been found convenient to express all the three moments and the two shear forces in the vicinity of the crack tip in terms of the three moment intensity factors K_1, K_2 and K_3. Note that these SIFs are different from K_I, K_{II} and K_{III} earlier used in this chapter. M_1^t, M_2^t, M_{12}^t, V_1^t and V_2^t, are evaluated in the vicinity of a crack tip (Fig. 4.14) by the expressions [4.9]

$$M_1^t = \frac{K_1}{(2r)^{1/2}} \cos\frac{\theta}{2}\left(1 - \sin\frac{\theta}{2}\sin\frac{3\theta}{2}\right) - \frac{K_2}{(2r)^{1/2}} \sin\frac{\theta}{2}\left(2 + \cos\frac{\theta}{2}\cos\frac{3\theta}{2}\right)$$

$$M_2^t = \frac{K_1}{(2r)^{1/2}} \cos\frac{\theta}{2}\left(1 + \sin\frac{\theta}{2}\sin\frac{3\theta}{2}\right) + \frac{K_2}{(2r)^{1/2}} \sin\frac{\theta}{2}\cos\frac{\theta}{2}\cos\frac{3\theta}{2}$$

$$M_{12}^t = \frac{K_1}{(2r)^{1/2}} \sin\frac{\theta}{2}\cos\frac{\theta}{2}\cos\frac{3\theta}{2} + \frac{K_2}{(2r)^{1/2}} \cos\frac{\theta}{2}\left(1 - \sin\frac{\theta}{2}\sin\frac{3\theta}{2}\right)$$

$$V_1^t = \frac{-K_3}{(2r)^{1/2}} \sin\frac{\theta}{2}$$

$$V_2^t = \frac{K_3}{(2r)^{1/2}} \cos\frac{\theta}{2}$$

Formal definitions of K_1, K_2 and K_3 can be stated as:

$$K_1 = \lim_{r\to 0} \sqrt{2r} M_2^t (r, \theta = 0)$$

$$K_2 = \lim_{r\to 0} \sqrt{2r} M_{12}^t (r, \theta = 0)$$

$$K_3 = \lim_{r\to 0} \sqrt{2r} V_2^t (r, \theta = 0)$$

4.8.3 Bending Moment on a Centre-Cracked Plate

Consider a large plate with far field moments, M_1^∞, M_2^∞, and M_{12}^∞, acting on it with a crack aligned with x_1 axis. The effect of M_1^∞ on the stress field near the crack tip is small. This is analogous to the small effect of σ_{11}^∞ on the plate considered under biaxial tension (Fig. 3.6). For design purposes, one can evaluate the SIFs from the following:

$$K_1 = \Phi M_2^\infty \sqrt{a}$$

$$K_2 = \psi M_{12}^\infty \sqrt{a}$$

$$K_3 = -\frac{\sqrt{10}\,\Omega}{(1+\nu)h} M_{12}^\infty \sqrt{a}$$

The large and thin plates Φ, Ψ, Ω, determined numerically, are shown in Figs 4.15–4.17.

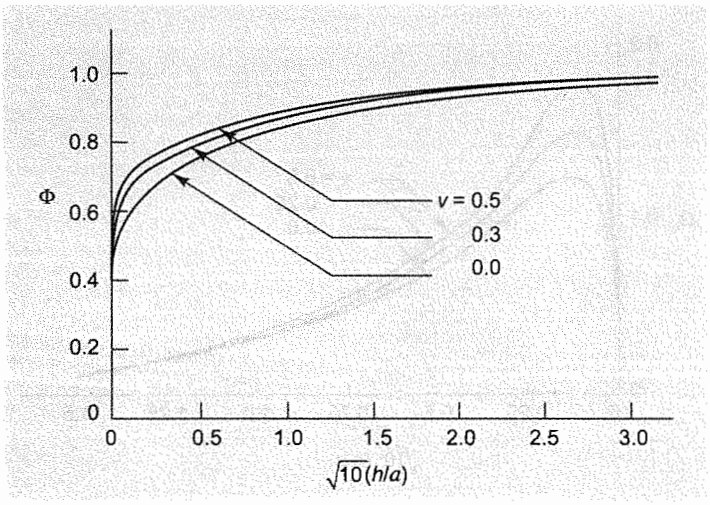

Fig. 4.15 Φ for a centre-crack in a thin plate [4.9]

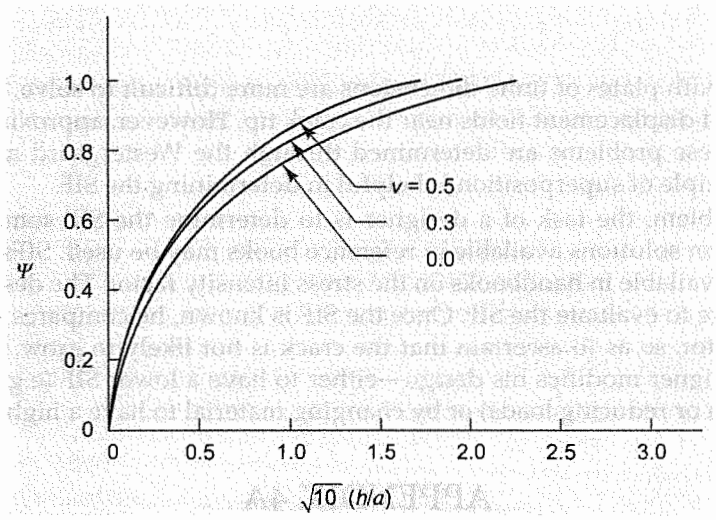

Fig. 4.16 Ψ for a centre-crack in a thin plate [4.9]

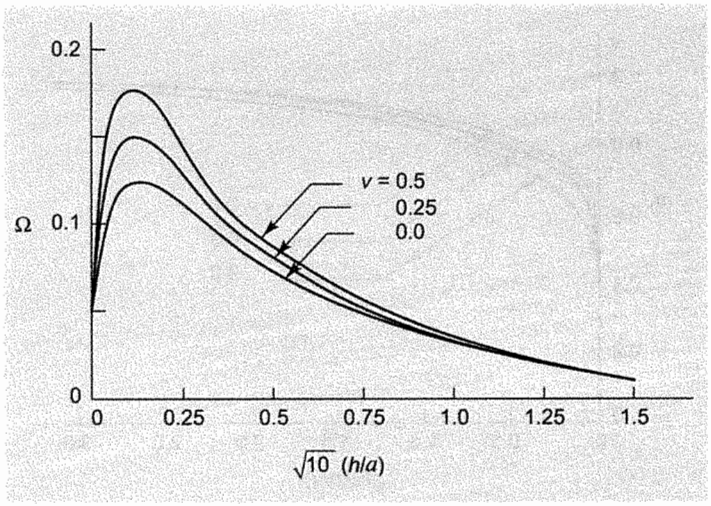

Fig. 4.17 Ω for a centre-crack in a thin plate [4.9]

4.9 Closure

Problems dealing with plates of finite dimensions are more difficult to solve, because the edges influence stress and displacement fields near the crack tip. However, approximate values of the SIFs of some of these problems are determined through the Westergaard approach. In some problems, the principle of superposition is helpful in determining the SIF.

For a given problem, the task of a designer is to determine the SIF somehow. For simple problems, close form solutions available in reference books may be used. SIFs of more complex problems may be available in handbooks on the stress intensity factor. The designer can also use a computer package to evaluate the SIF. Once the SIF is known, he compares it with the critical stress intensity factor, so as to ascertain that the crack is not likely to grow. If SIF exceeds the critical SIF, the designer modifies his design—either to have a lower SIF (e.g., by changing the crack configuration or reducing loads) or by changing material to have a higher critical SIF.

APPENDIX 4A

General Approach to Determine Stress and Displacement Fields

4A.1 Muskhelishvli Potentials

Solving the biharmonic equation through the Westergaard approach has its limitations, because they are restricted to a few simple cases. For the general approach, Airy's Stress Function is expressed in the form

$$\Phi(z) = \mathrm{Re}[\bar{z}\,\phi(z) + \int \psi(z)\,dz]$$

where $\phi(z)$ are $\psi(z)$ two analytic complex functions. They are chosen appropriately to satisfy the boundary conditions of the given problem.

Now, the goal is to express stress and displacement components in the terms of $\phi(z)$ and $\psi(z)$. For the development of expressions, one may refer to the monograph of Muskhelishvli [4.3] or other references [4.10]. The resulting stress field is given by

$$\sigma_{11} + \sigma_{22} = 4\text{Re}\,[\phi'(z)] = 2[\phi'(z) + \bar{\phi}'(z)] \tag{4.17a}$$

$$\sigma_{22} - \sigma_{11} + 2i\sigma_{12} = 2[\,\bar{z}\,\phi''(z) + \psi'(z)] \tag{4.17b}$$

where $\bar{z} = x_1 - ix_2$ and prime on a function corresponds to differentiation with z. Unlike in Chapter 3, the bar at the top of a complex number denotes complex conjugate. These two equations, in fact, represent the three equations for the three unknowns—σ_{11}, σ_{22} and σ_{12}. The first equation deals only with real numbers. The second equation is having both real and imaginary parts and thus represents two equations, because real and imaginary parts may be equated separately. Functions $\phi(z)$ and $\psi(z)$ are still unknown complex functions which, for a prescribed problem, are chosen to satisfy the boundary conditions. Alternatively, approximate solutions may be obtained by expressing each one of them in terms of a power series of z. Both approaches will be discussed subsequently in this section.

4A.2 Centre-cracked Plate

In Sec. 3.5.1, solution had been determined for a centre-cracked plate loaded by a biaxial field because the Westergaard function is not available for a uniaxial field. However, the problem of a uniaxial far field stress can be solved with the general approach. The expressions for $\phi(z)$ and $\psi(z)$ are available, which satisfy all the near and far field boundary conditions. They are:

$$\phi(z) = \frac{\sigma}{4}\,[2(z^2 - a^2)^{1/2} - z] \tag{4.18a}$$

$$\psi(z) = \frac{\sigma}{2}\,[z - a^2(z^2 - a^2)^{-1/2}] \tag{4.18b}$$

with its origin at the centre of the crack [Fig.3.2(a)]. To show that they satisfy the boundary conditions, we would be substituting $\phi(z)$ and $\psi(z)$ in Eqs (4.17). It is convenient to first evaluate differentials of $\phi(z)$ and $\psi(z)$ as

$$\phi'(z) = \frac{\sigma}{4}\left[\frac{2z}{(z^2 - a^2)^{1/2}} - 1\right]$$

$$\phi''(z) = -\frac{\sigma}{2}\left[\frac{a^2}{(z^2 - a^2)^{3/2}}\right]$$

$$\psi'(z) = \frac{\sigma}{2}\left[1 + \frac{a^2 z}{(z^2 - a^2)^{3/2}}\right]$$

To check the boundary conditions on the far field stress, we determine their values for $|z| >> a$ as

$$\phi'(z) \to \frac{\sigma}{4}; \quad \phi''(z) \to 0; \quad \psi'(z) \to \frac{\sigma}{2}$$

Substituting in Eqs (4.17a and b), we have

$$\sigma_{11} + \sigma_{22} = \sigma$$

$$\sigma_{22} - \sigma_{11} + 2i\sigma_{12} = \sigma$$

leading to $\sigma_{11} = 0; \quad \sigma_{22} = \sigma; \quad \sigma_{12} = 0$

They satisfy the far field stress boundary conditions of the uniaxial stress. In order to check the boundary conditions on traction free crack-faces, values of $\phi'(z)$, $\phi''(z)$ and $\psi'(z)$ are determined for $x_2 = 0$ and $-a < x_1 < a$ as

$$\phi'(z) = \frac{\sigma}{4}\left[\frac{2x_1}{(x_1^2 - a^2)^{1/2}} - 1\right]$$

$$\phi''(z) = -\frac{\sigma}{2}\left[\frac{a^2}{(x_1^2 - a^2)^{3/2}}\right]$$

$$\psi'(z) = \frac{\sigma}{2}\left[1 + \frac{a^2 x_1}{(x_1^2 - a^2)^{3/2}}\right]$$

Substituting them in Eqs (4.17a and b), for $-a < x_1 < a$, we have

$$\sigma_{11} + \sigma_{22} = -\sigma$$

$$\sigma_{22} - \sigma_{11} + 2i\sigma_{12} = \sigma$$

leading to $\sigma_{22} = 0; \quad$ and $\quad \sigma_{12} = 0$

Thus, the cracked surfaces are traction free.

For obtaining stress field in the vicinity of the crack tip, the origin may be moved to the crack tip, as done in Sec. 3.5, with the transformation $z = a + z_0$. It can be shown, by neglecting higher terms of r/a, that the stress field is same as obtained earlier through Eqs (3.32). Better accuracy in results can be achieved by retaining higher terms of r/a.

Many other problems can be solved by trying appropriate expressions for ϕ and ψ for a given problem. However, to arrive at such expressions, one relies on feel, experience or intuition.

4A.3 Solution Through Power Series

The general way is to express $\phi(z)$ and $\psi(z)$ in terms of a power series. For the symmetric case of a centre-cracked plate loaded in Mode I through a uniaxial stress, it has been shown [4.11] that the $\phi(z)$ and $\psi(z)$ can be expressed as

$$\phi(z_0) = A z_0^{\lambda+1} \tag{4.19a}$$

$$\psi(z_0) = B z_0^{\lambda+1} \tag{4.19b}$$

where the exponent λ is real but A and B may be complex; z_0 is measured from the crack tip. For solving the problem, $\phi(z)$ and $\psi(z)$ will be substituted in Eqs (4.17a and b) and the boundary conditions will be invoked. Boundary conditions on the cracked faces are:

$$\sigma_{22} = 0 \quad \text{for } -a < x < a \tag{4.20a}$$

$$\sigma_{12} = 0 \quad \text{for } -a < x < a \tag{4.20b}$$

Applying these boundary conditions, it can be shown that the problem be reduced to an eigenvalue problem with multiple roots of λ, each root having a solution. The overall solution would then be the sum total of all the individual solutions. Equation (4.17a) is added to Eq. (4.17b) to have:

$$\sigma_{22} + i\sigma_{12} = 2\text{Re}[\phi'(z_0)] + [\bar{z}_0 \phi''(z_0) + \psi'(z_0)] \tag{4.21}$$

For carrying out the details, we differentiate Eqs (4.19a and b) to obtain:

$$\phi'(z_0) = A(\lambda + 1)z_0^{\lambda} = A(\lambda + 1)r^{\lambda}(\cos\lambda\theta + i\sin\lambda\theta) \tag{4.22a}$$

$$\phi''(z_0) = A\lambda(\lambda + 1)z_0^{\lambda-1}$$

$$= A\lambda(\lambda + 1)r^{\lambda-1}[(\cos(\lambda - 1)\theta + i\sin(\lambda - 1)\theta] \tag{4.22b}$$

$$\psi'(z_0) = B(\lambda + 1)z_0^{\lambda} = B(\lambda + 1)r^{\lambda}(\cos\lambda\theta + i\sin\lambda\theta) \tag{4.22c}$$

Substituting in Eq. (4.21), we have

$$\sigma_{22} + i\sigma_{12} = 2A(\lambda + 1)r^{\lambda}\cos\lambda\theta + [r(\cos\theta - i\sin\theta)A\lambda(\lambda + 1)r^{\lambda-1}$$

$$\times \{\cos(\lambda - 1)\theta + i\sin(\lambda - 1)\theta\} + B(\lambda + 1)r^{\lambda}(\cos\lambda\theta + i\sin\lambda\theta)]$$

Equating real and imaginary parts and also by collecting terms, we obtain

$$\sigma_{22} = (\lambda + 1)r^{\lambda}[A\{2\cos\lambda\theta + \lambda\cos\theta\cos(\lambda - 1)\theta + \lambda\sin\theta\sin(\lambda - 1)\theta\} + B\cos\lambda\theta]$$

$$= (\lambda + 1)r^{\lambda}[A\{2\cos\lambda\theta + \lambda\cos(\lambda - 2)\theta\} + B\cos\lambda\theta] \tag{4.23a}$$

$$\sigma_{12} = (\lambda + 1)r^{\lambda}[A\lambda\{\cos\theta\sin(\lambda - 1)\theta - \sin\theta\cos(\lambda - 1)\theta\} + B\sin\lambda\theta]$$

$$= (\lambda + 1)r^{\lambda}[A\lambda\sin(\lambda - 2)\theta + B\sin\lambda\theta] \tag{4.23b}$$

On crack faces ($\theta = \pm\pi$) both σ_{22} and σ_{12} are zero, thus yielding

$$A\{2\cos\lambda\pi + \lambda\cos(\lambda - 2)\pi\} + B\cos\lambda\pi = 0 \tag{4.24a}$$

$$A\lambda\sin(\lambda - 2)\pi + B\sin\lambda\pi = 0 \tag{4.24b}$$

These equations represent an eigenvalue problem with λ representing the eigenvalues. Therefore, for having nontrivial solution,

$$\begin{vmatrix} (2\cos\lambda\pi + \lambda\cos(\lambda - 2)\pi) & \cos\lambda\pi \\ \lambda\sin(\lambda - 2)\pi & \sin\lambda\pi \end{vmatrix} = 0$$

leading to $\sin 2\lambda\pi = 0$. Consequently, for Mode I problems,

$$\lambda = -\frac{1}{2}, \frac{1}{2}, \frac{3}{2}, \frac{5}{2}, \ldots$$

Note that other negative possible values of λ(–3/2, –5/2...) are nor admissible, because they would give singular displacements at the vicinity of the crack tip. $\lambda = -1/2$ is the dominant mode and it gives singular stress and non-singular displacement. Other values of λ do not give singular stresses and therefore their contributions may be neglected if the analysis is carried out in a region which is very close to the crack tip, i.e., for a very small value of r/a.

The stress field near the crack tip corresponds to the dominant mode $\lambda = -1/2$. Eigenvector corresponding to this eigenvalue is determined through Eqs (4.24a and b), as

$$A = 2B$$

Substituting $\lambda = -1/2$ and $B = A/2$ in Eqs (4.23a and b) and manipulating trigonometric functions, we obtain

$$\sigma_{22} = \frac{A}{\sqrt{r}} \cos\frac{\theta}{2}\left[1 + \sin\frac{\theta}{2}\sin\frac{3\theta}{2}\right] \tag{4.25a}$$

$$\sigma_{12} = \frac{A}{\sqrt{r}} \cos\frac{3\theta}{2}\sin\frac{\theta}{2}\cos\frac{\theta}{2} \tag{4.25b}$$

Definition of K_I [Eq. (3.4)] leads to

$$K_I = \left(\sqrt{2\pi r}\,\frac{A}{\sqrt{r}}\right)$$

$$r \to 0$$

yielding, $$A = \frac{K_I}{\sqrt{2\pi}}$$

Substituting A in Eqs (4.25a and b), we obtain

$$\sigma_{22} = \frac{K_I}{\sqrt{2\pi r}} \cos\frac{\theta}{2}\left[1 + \sin\frac{\theta}{2}\sin\frac{3\theta}{2}\right]$$

$$\sigma_{12} = \frac{K_I}{\sqrt{2\pi r}} \sin\frac{\theta}{2}\cos\frac{\theta}{2}\cos\frac{3\theta}{2}$$

For determining the value of σ_{11}, we substitute $\lambda = -1/2$ in Eq. (4.22a) to evaluate $\phi'(z_0)$, which is then substituted in Eq. (4.17) to yield

$$\sigma_{11} + \sigma_{22} = \frac{2A}{\sqrt{r}} \cos\frac{\theta}{2} = \frac{2K_I}{\sqrt{2\pi r}} \cos\frac{\theta}{2}$$

leading to, $$\sigma_{11} = \frac{K_I}{\sqrt{2\pi r}} \cos\frac{\theta}{2}\left[1 - \sin\frac{\theta}{2}\sin\frac{3\theta}{2}\right]$$

The stress field thus obtained is same as that of Sec. 3.5.1. In order to predict more accurate results, similar analysis may be carried out for the next higher term ($\lambda = 1/2$) and be added to the results already obtained for $\lambda = -1/2$.

It is worth reviewing that the problem of a centre-cracked plate loaded in Mode I can been solved in three different ways (Sections 3.5, 4A.2 and 4A.3), giving the same stress field for a small value of distance r. The solution of Sec. 3.5 is always approximate because the problem was solved for a biaxial filed. However, the solution of Secs 4A.2 and 4A.3 can be obtained with a high accuracy if the contribution of higher terms is included in the solution.

A plate of finite dimensions is more difficult to solve because the stresses and displacements must also satisfy the prescribed conditions at the boundary of the component. One can refer to the work of Ramesh et al. [4.12] for the solution of a uniaxial field applied to a plate [4.12] of finite dimensions. For these problems, Muskhelishvili potentials $\phi(z)$ and $\psi(z)$ are represented through a series. The coefficients of the series can then be determined by matching the prescribed stresses at the boundary [4.13, 4.14].

APPENDIX 4B

SIF of Some Important Cases

In this appendix, the stress intensity factor for some important cases is listed, which are useful to (i) experimentalists for designing specimens and (ii) designers for determining the SIF for critical components. For other cases, readers can refer to handbooks like "*Stress Intensity Factor*" (2 volumes), edited by Y. Murakami, Pergamon Press, Oxford, 1987 [4.4].

1. Compact Tension (CT) Specimen, shown in Fig. 4.18(a) [4.15]

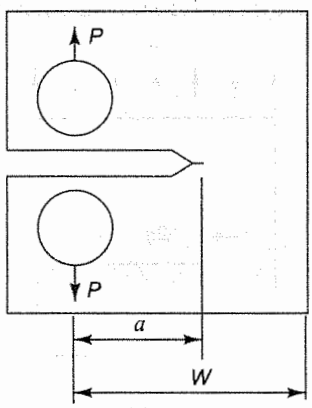

Fig. 4.18(a)

$$K_I = \frac{P}{BW^{1/2}} f(\alpha)$$

$$\alpha = \frac{a}{W}$$

B = Plate thickness

$$f(\alpha) = \frac{(2+\alpha)\left(0.886 + 4.64\alpha - 13.32\alpha^2 + 14.72\alpha^3 - 5.6\alpha^4\right)}{(1-\alpha)^{3/2}}$$

2. Single-Edge-Notch-Bend (SENB) Specimen, shown in Fig. 4.18(b) [4.15]

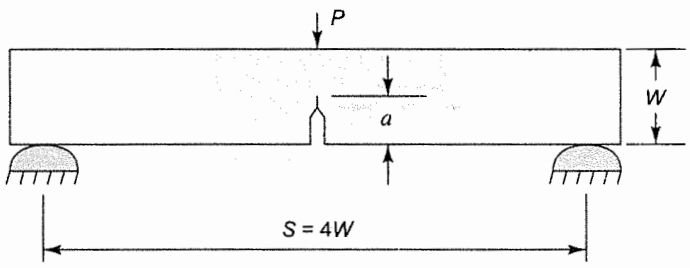

Fig. 4.18(b)

$$K_I = \frac{PS}{BW^{3/2}} f(\alpha)$$

$$\alpha = \frac{a}{W}$$

B = Plate thickness

$$f(\alpha) = \frac{3\alpha^{1/2}\left[1.99 - \alpha(1-\alpha)\left(2.15 - 3.93\alpha + 2.7\alpha^2\right)\right]}{2(1+2\alpha)\,(1-\alpha)^{3/2}}$$

3. Centre-Cracked Plate under Uniform Tension, shown in Fig. 4.18(c) [4.5]

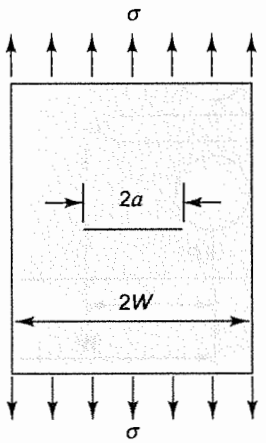

Fig. 4.18(c)

$$K_I = \sigma\sqrt{\pi a} f(\alpha)$$

$$\alpha = \frac{a}{W} \text{ for } 0 < \alpha < 0.7$$

$$f(\alpha) = 1.0 + 0.128\alpha - 0.288\alpha^2 + 1.523\alpha^3$$

4. Single-Edge-Cracked Plate under Uniform Tension, shown in Fig. 4.18(d) [4.5]

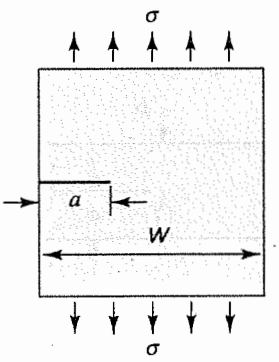

Fig. 4.18(d)

$$K_I = \sigma\sqrt{\pi a} f(\alpha)$$

$$\alpha = \frac{a}{W} \quad \text{for } 0 < \alpha < 0.6$$

$$f(\alpha) = 1.12 - 0.23\alpha + 10.55\alpha^2 - 21.72\alpha^3 + 30.39\alpha^4$$

5. Double-Edge-Cracked Plate under Uniform Tension, shown in Fig. 4.18(e) [4.5]

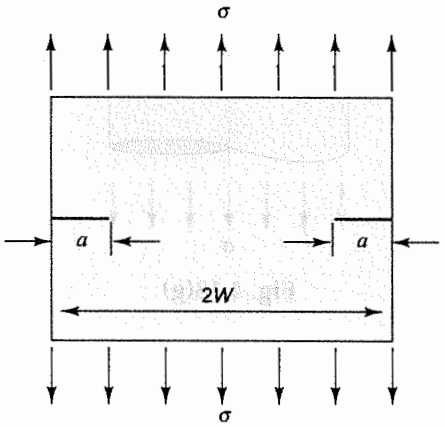

Fig. 4.18(e)

$$K_I = \sigma\sqrt{\pi a} f(\alpha)$$

$$\alpha = \frac{a}{W} \quad \text{for } 0 < \alpha < 0.7$$

$$f(\alpha) = 1.12 - 0.20\alpha - 1.20\alpha^2 + 1.93\alpha^3$$

6. Strip with Edge-Crack under bending, shown in Fig. 4.18(f) [4.5]

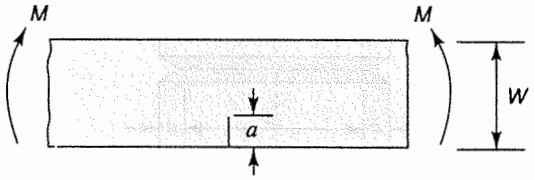

Fig. 4.18(f)

$$K_I = \frac{6M}{BW^2}\sqrt{\pi a}\, f(\alpha)$$

$$\alpha = \frac{a}{W}$$

B = Plate thickness

$$f(\alpha) = 1.12 - 1.40\alpha + 7.33\alpha^2 - 13.083\alpha^3 + 14\alpha^4$$

7. Circumferentially Cracked Round Bar under Tension, shown in Fig. 4.18(g) [4.6]

$$K_I = \sigma\sqrt{\pi a} f(\beta)$$

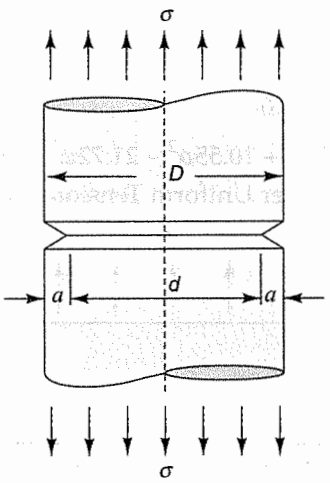

Fig. 4.18(g)

$$\beta = \frac{d}{D}$$

$$f(\beta) = \left(\frac{1}{\beta} + \frac{1}{2} + \frac{3}{8}\beta - 0.361\beta^2 + 7.33\beta^3\right)\frac{1}{2}\sqrt{\frac{1}{\beta}}$$

8. Circumferentially Cracked Round Bar under Torsion, shown in Fig. 4.18(h) [4.6]

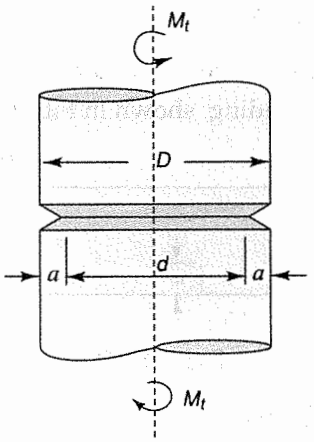

Fig. 4.18(h)

$$K_{III} = \frac{16M_t}{\pi D^3}\sqrt{\pi a} f(\beta)$$

$$\beta = \frac{d}{D}$$

$$f(\beta) = \left(\frac{1}{\beta^2} + \frac{0.5}{\beta} + \frac{3}{8} + \frac{5}{16}\beta + \frac{35}{128}\beta^2 + 0.21\beta^3\right)\frac{3}{8}\sqrt{\frac{1}{\beta}}$$

9. An Oblique Edge Crack in a Semi-Infinite Plane, shown in Fig. 4.18(i) [4.4]

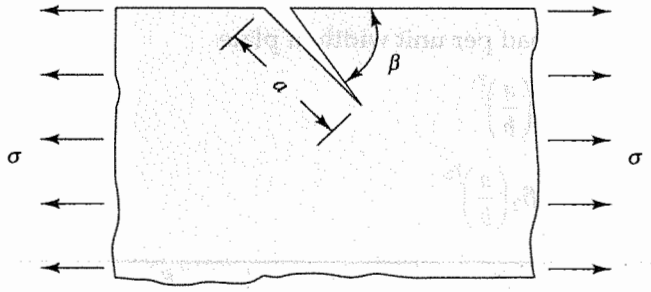

Fig. 4.18(i)

$$K_I = F_I \sigma \sqrt{\pi a}$$

$$K_{II} = F_{II} \sigma \sqrt{\pi a}$$

β	F_I	F_{II}
10°	0.162	0.174
20°	0.305	0.271
40°	0.625	0.365
60°	0.920	0.306
80°	1.098	0.119

10. Lapped Joint under Tension-Shear, shown in Fig. 4.18(j) [4.4]

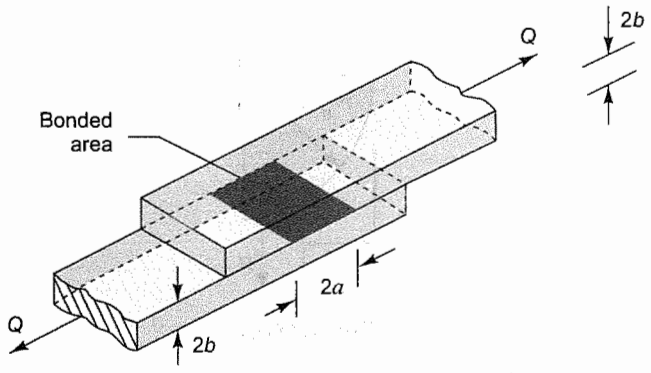

Fig. 4.18(j)

$$K_I = Q\sqrt{\frac{\pi}{a}}F_I\left(\frac{a}{b}, \kappa\right)$$

$$K_{II} = Q\sqrt{\frac{\pi}{a}}F_{II}\left(\frac{a}{b},\kappa\right)$$

$$\kappa = \sqrt{\frac{3(1-\nu^2)Q}{2bE}}$$

Q : Load per unit width of plate

$$F_I\left(\frac{a}{b},\kappa\right) = \beta_1\left(\frac{a}{b}\right)^{\gamma_1}$$

$$F_{II}\left(\frac{a}{b},\kappa\right) = \frac{2}{\pi} + \beta_2\left(\frac{a}{b}\right)^{\gamma_2}$$

κ	β_1	γ_1	β_2	γ_2
0	0.770	0.397	0.365	0.710
0.1	0.687	0.394	0.285	0.744
0.2	0.639	0.375	0.230	0.776
0.3	0.614	0.352	0.186	0.812
0.4	0.576	0.344	0.149	0.868
0.5	0.558	0.331	0.142	0.843

11. Arc-Shaped Tension (AT) Specimen, shown in Fig. 4.18(k) [4.15]

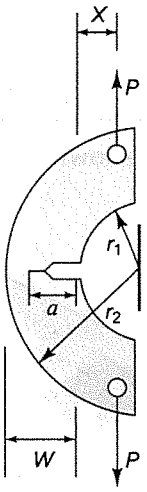

Fig. 4.18(k)

$$K_I = \frac{P}{BW^{1/2}}f(\alpha)$$

$$\alpha = \frac{a}{W}$$

B = Plate thickness

$$f(\alpha) = \left[\frac{3X}{W} + 1.9 + 1.1\alpha\right]\left[1 + 0.25(1-\alpha)^2\left(1 - \frac{r_1}{r_2}\right)\right] \times \left[\frac{\alpha^{1/2}}{(1-\alpha)^{3/2}}\right] \times$$
$$[3.74 - 6.3\alpha + 6.32\alpha^2 - 2.43\alpha^3]$$

12. Disc-Shaped Compact Tension (DCT) Specimen, shown in Fig. 4.18(l) [4.15]

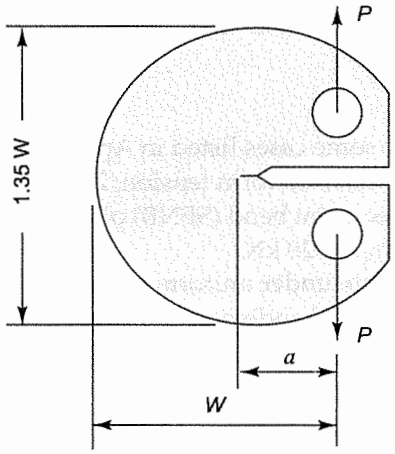

Fig. 4.18(l)

$$K_I = \frac{P}{BW^{1/2}} f(\alpha)$$

$$\alpha = \frac{a}{W}$$

B = Plate thickness

$$f(\alpha) = \frac{(2+\alpha) \times (0.76 + 4.8\alpha - 11.58\alpha^2 + 11.43\alpha^3 - 4.08\alpha^4)}{(1-\alpha)^{3/2}}$$

QUESTIONS

1. Why is the solution of collinear cracks in an infinitely long strip important?
2. Why is an edge crack more dangerous than a centre crack of the same length a?
3. In the case of a shallow elliptical edge crack, the SIF at the tip of the minor axis is higher than the SIF at the tip of the major axis. This may sound contrary to our intuition. Can you explain the results on physical grounds?
4. In a short fiber composite material, an embedded fiber does not act like a dangerous crack. Explain it by assuming the fiber has a shape of an ellipse.
5. Why does material property E appear in the expression that relates G_I with K_I?
6. Energy release rate of various modes can be summed, whereas the SIF cannot be. Why?

7. If a designer finds that a crack (e.g., slot) in a component gives $K_I > K_{Ic}$, discuss the different options available to avoid such a situation.
8. Why does K_{Ic} depend on the direction in a rolled plate?
9. Why do rolled or forged components have better toughness?
10. Name an application of bending and twisting a plate with a crack.
11. If we use a specimen with a large lateral dimension to find K_{Ic}, the accuracy of the experimental results is high. But, in experiments to determine the SIF, specimens with large lateral dimensions are not employed. Why not?

PROBLEMS

1. Determine value of K_I for some cases listed in Appendix 4B for the following values:
   (a) Centre-cracked plate under uniform tension; $2a = 60$ mm, $2W = 140$ mm, $\sigma = 150$ MPa.
   (b) Single-edge-notch three point bend (SENB) plate; $a = 20$ mm, $S = 150$ mm, $W = 50$ mm, $B = 25$ mm, $P = 20$ kN.
   (c) Single-edge-cracked plate under uniform tension; $a = 30$, $W = 70$ mm, $\sigma = 140$ MPa.
   (d) Strip with edge crack under bending; $a = 25$ mm, $W = 60$ mm, $B = 20$ mm, $M = 2000$ Nm.
2. A crack of 3 mm length is emanated from the surface of a 50 mm diameter hole in a large plate (Fig. 4.19). Compute the maximum stress σ that would not allow the crack to grow if $K_{Ic} = 55$ MPa $\sqrt{m}$, $\sigma_{ys} = 300$ MPa, $E = 207$ GPa. [**Hint:** Treat as single-edge-crack under tensile stress computed using Inglis solution Eq. (2.1)]

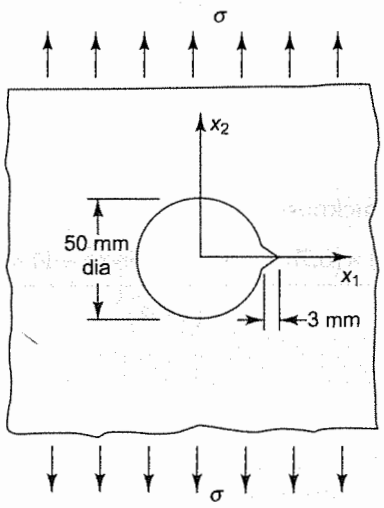

Fig. 4.19 The figure of Problem 2

3. A steel flat ($K_{Ic} = 90$ MPa $\sqrt{m}$, $\sigma_{ys} = 700$ MPa) is being considered as a structural member of a pedestrian bridge over a busy street. The flat is 100 mm high and 40 mm thick, and the main load on the flat is a bending moment. If there is an edge crack on the tension side, draw a curve for allowable bending moment vs crack length.

4. Determine K_I for the pressure distribution acting on the cracked faces of an infinite plate as shown in Fig. 4.20.

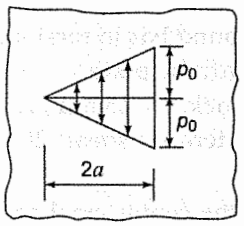

Fig. 4.20 The figure of Problem 4

5. The distribution of load per unit area on the cracked faces of a centre crack in a large plate is shown in Fig. 4.21. Determine the values of stress intensity factor.

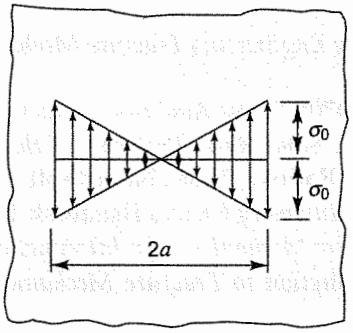

Fig. 4.21 The figure of Problem 5

6. Determine the values of K_I for a center crack of length $2a$ in a large plate, subjected to a triangular distribution of load per unit area, as shown in Fig. 4.22.

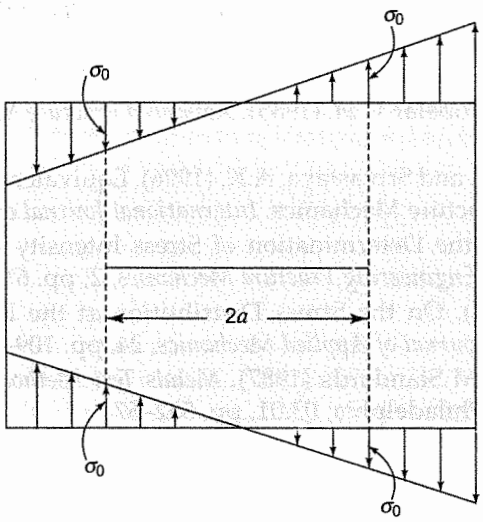

Fig. 4.22 The figure of Problem 6

7. Determine values of K_I in some cases (given in the text or listed in Appendix 4B) for the following values:
   (a) Circumferentially cracked round bar under tension; $a = 20$ mm, $D = 100$ mm, $P = 80$ kN.
   (b) Circumferentially cracked round bar in torsion; $a = 10$ mm, $D = 100$ mm, $M_t = 40$ kN.
   (c) An oblique crack in a semi-infinite plate; $a = 30$ mm, $\beta = 45°$, $\sigma = 200$ MPa.
   (d) Embedded semi-elliptical crack; $a = 15$ mm, $2c = 90$ mm, $t = 40$ mm, $\sigma = 160$ MPa.
   (e) Lapped bonded joint under tension shear; $2b = 8$ mm, $2a = 40$ mm, Width = 25 mm, $Q = 400$ N/mm, $\nu = 0.3$.
8. Determine G_I from the SIF of the center cracked infinite plate, subjected to a uniform tensile stress σ for both plane stress and plane strain. Check whether they agree with the expression used in Sec. 2.5.

REFERENCES

4.1 Broek, D. (1982). *Elementary Engineering Fracture Mechanics*, Martinus Nijhoff Publishers, The Hague.
4.2 Paris, P.C. and Sih, G.C. (1970). *Stress Analysis of Cracks*, ASTM STP 381, pp. 30–83.
4.3 Muskhelishvili, N.I. (1953). *Some Basic Problems of the Mathematical Theory of Elasticity*, translated from Russian by Radok, J.R.M., Noordhoff, Leyden.
4.4 Murakami, Y. (1987). *Stress Intensity Factors Handbook*, Pergamon Press, Oxford.
4.5 Gdoutos, E.E. (2005). *Fracture Mechanics—An Introduction*, Springer, The Netherland.
4.6 Hellan, Kare (1985). *Introduction to Fracture Mechanics*, McGraw-Hill Book Company, New York.
4.7 Irwin, G.R. (1962). The Crack Extension Force for a Part-Through Crack in a Plate, Transactions ASME, *Journal of Applied Mechanics*, 29, pp. 651–654.
4.8 Irwin, G.R. (1957). Analysis of Stresses and Strains near the End of a Crack Traversing a Plate, *Journal of Applied Mechanics*, 24, pp. 361–364.
4.9 Sih, G.C. (1977). *Mechanics of Fracture, Plates and Shells with Cracks*, Vol. 3, Noordhoff International Publishing, Leyden.
4.10 Meguid, S.A. (1989). *Engineering Fracture Mechanics*, Elsevier Applied Science, London.
4.11 Kanninen, M.F., and Popelar, C.H. (1985). *Advanced Fracture Mechanics*, Oxford University Press, New York.
4.12 Ramesh, K., Gupta, S., and Srivastava, A.K. (1996). Equivalence of Multi-parameter Stress Field Equations in Fracture Mechanics, *International Journal of Fracture*, 79, pp. R37–R41.
4.13 Isada, N. (1970). On the Determination of Stress Intensity Factors for Some Common Structural Problems, *Engineering Fracture Mechanics*, 2, pp. 61–79.
4.14 Williams, M.L. (1957). On the Stress Distribution at the Base of a Stationary Crack, Transactions ASME, *Journal of Applied Mechanics*, 24, pp. 109–114.
4.15 Annual Book of ASTM Standards (1987). *Metals Test Methods and Analytical Procedures*, ASTM Publications, Philadelphia, 03.01, pp. 552–57.

Chapter

5

Anelastic Deformation at the Crack Tip

Out of His eye the sun was born.

Rig Veda

5.1 Further Investigation at the Crack Tip

The material in the vicinity of a crack tip is most affected. We therefore attempted to place a magnifying lens at the crack tip in Chapter 4, and determined stress and displacement fields in its vicinity. We, of course, took the simple route of assuming that the material remains elastic even at the crack tip where the stresses are very large. The assumption is difficult to accept for most of the engineering materials because they do not remain elastic at high stresses. Under real conditions, the material in the vicinity of the crack tip deforms anelastically. In metallic components, the material yields and flows to decrease the stress. Anelastic deformation also occurs in the vicinity of the crack tip in components of other materials like plastics, composites, cardboards, etc.

Anelastic deformation has not been considered so far in the analysis of our models. Why is it so? We have observed in the previous chapters that even elastic solution to a problem is quite complex. The magnitude of complexity increases several folds if a plastic zone is included in the mathematical modeling. Therefore, if the size of the anelastic zone is small in comparison to the crack length, we assume, only for the sake of analysis, that the entire body remains elastic. Such analysis, as mentioned in the earlier chapters, is known as Linear Elastic Fracture Mechanics (LEFM). For a large plastic zone, more sophisticated analytical methods have been developed which would be discussed in the subsequent chapters.

Now, we will investigate what happens at the crack tip when loads are applied on a component. Similar to the behavior of a district magistrate who tries to diffuse a problem such as a communal tussle, the material in the neighborhood of the crack tip tries to reduce the danger of high stresses. In metals, plastic deformation occurs which is generally caused by nucleation and motion of dislocations. The material flows in such a manner that high stresses are reduced dramatically. Quite often the flow of material makes the crack tip blunt, which in turn decreases the magnitude of stress components. Thus, many potential catastrophic failures are avoided just by the local plastic deformation at the crack tip.

In highly extensible polymers, molecules may become oriented and can result in strain crystallization [5.1]. This blunts the crack tip. Often, the morphology of a material is found to change over a large area around the crack tip.

Those materials which are not able to release high stresses are usually found to have low toughness. Diamond is a good example of such materials. Its inter-atomic bonds are so strong that the material in the vicinity of a crack tip does not yield. Consequently, any plastic zone is not formed at the crack tip and the material toughness is very low. According to a Chinese proverb, trees which can bend under the blow of a high velocity cyclone survive better. To survive against the danger of high stresses near the crack tip, the material should be able to deform anelastically.

Discussions in this chapter would be confined mostly to metals. Since plastic zone plays a vital role in a fracture, we will investigate the shape of the plastic zone, yield planes, and the factors which control the size of the plastic zone. A designer who tries to avoid fracture failure in a component prefers that a large plastic zone is developed at the crack tip. This is contrary to the likings of a conventional designer who tries hard to avoid yielding at any portion of a component. In a way, the size of the plastic zone may be regarded as a parameter in representing the toughness of a material. This approach has not been adopted so far owing to problems in predicting the size accurately through analytic methods and also owing to difficulties involved in experimental determination of the size of the plastic zone.

5.2 Approximate Shape and Size of the Plastic Zone

The stress field in the vicinity of a crack tip has been determined in Sec. 3.5, assuming the material of the component remains elastic even at the crack tip. Knowing the stress field, we may invoke one of the two commonly accepted yield criteria, Mises or Tresca, for evaluating the size and shape of the plastic zone. Rigorous analysis becomes complex because two sets of constitutive equations should be used, one for plastic deformation inside the plastic zone, and another for elastic deformation outside the zone. The surface that separates the two zones is not known and the rigorous analysis may require iterative solutions to many problems.

A rigorous analysis is complex as closed form solutions are not available for most problems. We will determine only approximate solutions. The procedure adopted for finding the interface between a plastic and an elastic zone is as follows:

Consider that one moves on a radial line from a far away place (where the stress field is definitely elastic) towards the crack tip and a yield criterion is being applied continuously. As soon as the material is found to yield, we mark that point as the interface between the elastic and plastic fields. Similar consideration on other radial lines generates the shape and the size of the plastic zone. It is worth noting that the material in the plastic zone no longer takes high stresses predicted by elastic analysis. This, in fact, offsets the internal force balance, and therefore, the elastic field surrounding the plastic zone should be corrected or re-evaluated for a more rigorous analysis. To incorporate such a correction is quite complex and is beyond the scope of this book. The shape and size of the plastic zone thus obtained through the procedure can only be accepted as approximate figures.

Before we apply a yield criterion, it is useful to determine the principal stresses. Considering a case of Mode I, σ_{33} is a principal stress because $\sigma_{13} = \sigma_{23} = 0$ for plane problems. We need to rotate axes in $x_1 - x_2$ plane to determine the principal stresses σ_1 and σ_2. Figure 5.1 shows the Mohr circle, for which σ_{11}, σ_{22} and σ_{12} are known through Eq. (3.32). The centre σ_0 and the radius R of the Mohr circle are

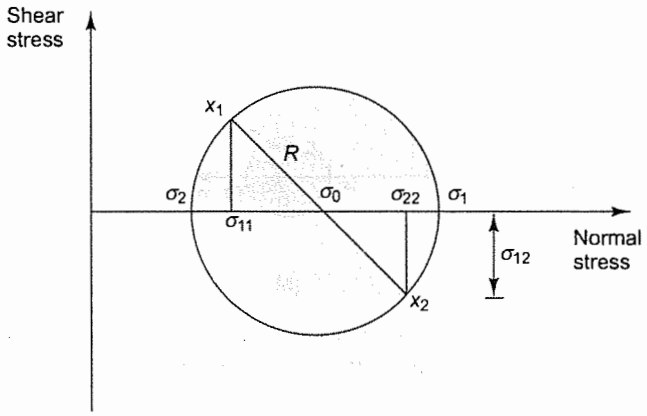

Fig. 5.1 Mohr circle to determine principal stresses

$$\sigma_0 = \frac{\sigma_{11} + \sigma_{22}}{2} = \frac{K_I}{\sqrt{2\pi r}} \cos\frac{\theta}{2}$$

$$R = \left[\left(\frac{\sigma_{22} - \sigma_{11}}{2}\right)^2 + \sigma_{12}^2\right]^{1/2} = \frac{K_I}{\sqrt{2\pi r}} \cos\frac{\theta}{2} \sin\frac{\theta}{2}$$

These equations determine principal stresses σ_1 and σ_2 as (defining the larger one as σ_1)

$$\sigma_1 = \sigma_0 + R = \frac{K_I}{\sqrt{2\pi r}} \cos\frac{\theta}{2}\left[1 + \sin\frac{\theta}{2}\right] \tag{5.1a}$$

$$\sigma_2 = \sigma_0 - R = \frac{K_I}{\sqrt{2\pi r}} \cos\frac{\theta}{2}\left[1 - \sin\frac{\theta}{2}\right] \tag{5.1b}$$

The third principal stress σ_3 becomes,

$$\sigma_3 = 0 \qquad \text{for plane stress} \tag{5.1c}$$

$$\sigma_3 = \nu(\sigma_1 + \sigma_2) = 2\nu \frac{K_I}{\sqrt{2\pi r}} \cos\frac{\theta}{2} \qquad \text{for plane strain} \tag{5.1d}$$

5.2.1 Plastic Zone Shape for Plane Stress

Two widely used yield criteria, Mises and Tresca, are applied to Mode I, so as to determine the plastic zone size for plane stress cases. All the three principal stresses and associated Mohr circles are shown in Fig. 5.2(a). To ensure the yielding of the material, the Mises criterion states [5.2] that:

$$(\sigma_1 - \sigma_2)^2 + (\sigma_2 - \sigma_3)^2 + (\sigma_3 - \sigma_1)^2 \geq 2\sigma_{ys}^2 \tag{5.2}$$

where σ_{ys} is the yield stress. Substituting σ_1, σ_2, and σ_3, in the equation and using the symbol r_{pz} in place of r for the equality sign of the Mises criterion, we obtain

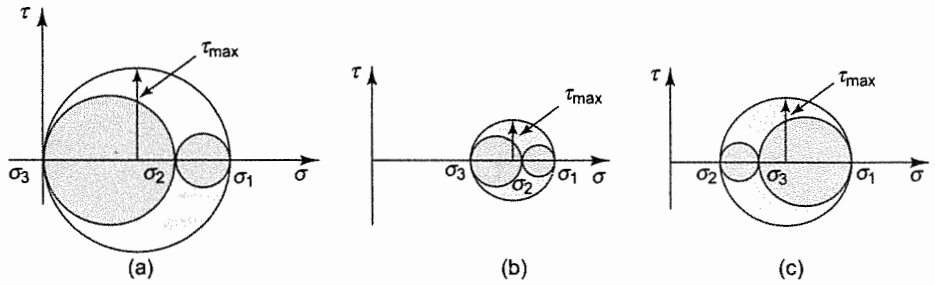

Fig. 5.2 Mohr circles for (a) plane stress, (b) plane strain for small θ, and (c) plane strain for large θ

$$\frac{K_I^2}{2\pi r_{pz}}\cos^2\frac{\theta}{2}\left[4\sin^2\frac{\theta}{2}+\left(1-\sin\frac{\theta}{2}\right)^2+\left(1+\sin\frac{\theta}{2}\right)^2\right]=2\sigma_{ys}^2$$

which is simplified to

$$r_{pz}=\frac{1}{4\pi}\frac{K_I^2}{\sigma_{ys}^2}\left(1+\frac{3}{2}\sin^2\theta+\cos\theta\right)$$

The resulting shape of the plastic zone size is plotted in Fig. 5.3(a) in terms of non-dimensional distance $r_{pz}/(K_I^2/(\pi\sigma_{ys}^2))$. The shape of the plastic zone size is slightly different if the Tresca yield criterion is invoked. In order to ensure yielding, the Tresca yield criterion [5.2] states that:

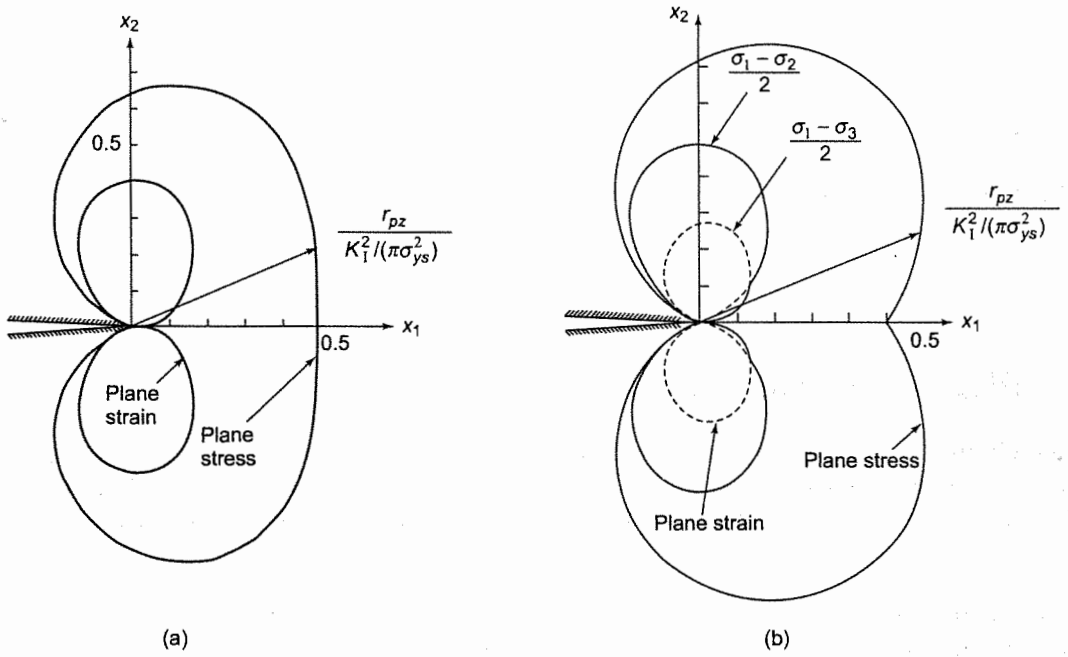

Fig. 5.3 Plastic zone shape and size for (a) Mises yield criterion, and (b) Tresca yield criterion

$$\tau_{max} \geq \frac{\sigma_{ys}}{2} \tag{5.3}$$

For plane stress, τ_{max} is given by the biggest Mohr circle [Fig. 5.2(a)] which is between σ_1 and σ_3. Thus, at $r = r_{pz}$

$$\frac{\sigma_1 - 0}{2} = \frac{\sigma_{ys}}{2}$$

Substituting σ_1 from Eq. (5.1a), we obtain the approximate shape of the plastic zone as [Fig. 5.3(b)]

$$r_{pz} = \frac{K_I^2}{2\pi\sigma_{ys}^2}\left[\cos\frac{\theta}{2}\left(1+\sin\frac{\theta}{2}\right)\right]^2$$

5.2.2 Plastic Zone Shape for Plane Strain

The third principal stress σ_3 is no longer zero [Eq. (5.1d)] and, therefore, it influences the yielding considerably. In fact, σ_3 is also a tensile stress, creating conditions of triaxiality of the tensile stresses. As a result, the plastic zone size is substantially smaller.

To find the shape of the plastic zone using the Mises yield criterion, σ_1, σ_2 and σ_3 are substituted in Eq. (5.2) and the resulting equation simplifies to

$$r_{pz} = \frac{K_I^2}{4\pi\sigma_{ys}^2}\left[\frac{3}{2}\sin^2\theta + (1-2\nu)^2(1+\cos\theta)\right]$$

If the Tresca yield criterion is applied, we should first find out which is the largest Mohr circle. Looking carefully into Eq. (5.1), we find σ_1 is always larger than σ_2 and σ_3. Subtracting Eq. (2.1d) from Eq. (2.1b), we obtain

$$\sigma_2 - \sigma_3 = \frac{K_I}{\sqrt{2\pi r}}\cos\frac{\theta}{2}\left[(1-2\nu) - \sin\frac{\theta}{2}\right]$$

Note that for small θ ($\leq 38.9°$ for $\nu = 1/3$), σ_3 is the smallest principal stress and the yielding is governed by σ_1 and σ_3 as shown in Fig. 5.2(b). Substituting σ_1 and σ_3 in Eq. (5.3), we have

$$\frac{K_I}{\sqrt{2\pi r_{pz}}}\cos\frac{\theta}{2}\left(1+\sin\frac{\theta}{2}-2\nu\right) = \sigma_{ys}$$

leading to

$$r_{pz} = \frac{K_I^2\cos^2\frac{\theta}{2}}{2\pi\sigma_{ys}^2}\left(1-2\nu+\sin\frac{\theta}{2}\right)^2$$

For a large value of θ ($\geq 38.9°$ for $\nu = 1/3$), σ_2 is the smallest principal stress and the yielding is governed by σ_1 and σ_2, as shown in Fig. 5.2(c). Then, r_{pz} is obtained by using Eq. (5.3) as

$$r_{pz} = \frac{K_I^2}{2\pi\sigma_{ys}^2}\sin^2\theta$$

Corresponding plastic zone shapes are shown in Fig. 5.3. As expected, the plastic zone size of plane strain is much smaller than that of plane stress. In fact, the difference between the two

plastic zones is so large that it should convince a designer to choose, as much as possible, thin plates or thin sections of a component.

It is worth noting here that the plastic zone size is proportional to the square of the stress intensity factor and inversely proportional to the square of the yield stress. Whenever yield stress of a metal is increased, say by an appropriate heat treatment, its plastic zone size decreases considerably; this in turn makes the material more prone to crack growth. The increase in yield stress may please a conventional designer, because he usually designs structural components based on a yield criterion. But as far as the toughness of a material is concerned, the designer is left with an inferior material. The designer should explore a happy compromise between yield stress and toughness, while choosing a material and its heat treatment.

5.3 Effective Crack Length

The appearance of the plastic zone at the tip does not allow its material to bear high stresses predicted by the elastic analysis. Looking from a different angle, one can argue that the material is soft in front of the crack tip and therefore the effective crack length is longer than the actual.

In fact, owing to the presence of the plastic zone, the stiffness of the component decreases or the compliance increases. Consequently, the crack is equivalent to a length that is longer than actual length. The size of the plastic zone in front of the crack tip determines the effective crack length. Therefore, considerable efforts have been made by many investigators to determine the plastic zone size accurately in front of the crack tip along the x_1-axis.

5.3.1 Approximate Approach

One of the simplest (but highly approximate) expressions for the plastic zone size is found from σ_{22} vs x_1 curve of Fig. 5.4 for Mode I. The length of the plastic zone r^* along x_1 direction is then obtained from the relation

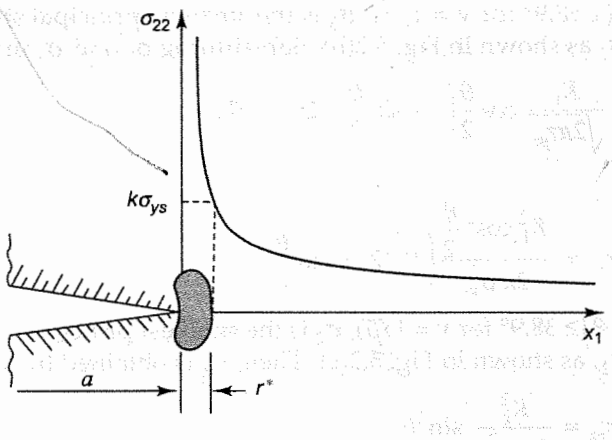

Fig. 5.4 Approximate plastic zone size r^*

$$\sigma_{22} = k\sigma_{ys} \tag{5.4}$$

where, k depends on whether the case is of plane stress or plane strain. Substituting $\sigma_{22} = K_I/(2\pi r^*)^{1/2}$ and solving for r^*, we obtain

$$r^* = \frac{K_I^2}{2\pi k^2 \sigma_{ys}^2} \tag{5.5}$$

We now evaluate k for both plane stress and plane strain. Due to the symmetry, σ_{12} vanishes on the $x_2 = 0$ plane. Also, on this plane $\sigma_{22} = \sigma_{11}$. Thus, we have principal stresses as

$$\sigma_1 = \sigma_{22}$$

$$\sigma_2 = \sigma_{22}$$

$$\sigma_3 = 0 \qquad \text{for plane stress}$$

$$\sigma_3 = \nu(\sigma_1 + \sigma_2) = 2\nu\sigma_{22} \qquad \text{for plane strain}$$

Substituting σ_1, σ_2 and σ_3 in Eq. (5.2), and then comparing the resulting expression with Eq. (5.4), we obtain

$$k = 1 \qquad \text{for plane stress}$$

$$k = 1/(1 - 2\nu) \qquad \text{for plane strain}$$

In fact, $k = 3$ for $\nu = 1/3$ in the case of plane strain. Substituting the value of k in Eq. (5.5), we obtain

$$r^* = \frac{1}{2\pi}\left(\frac{K_I}{\sigma_{ys}}\right)^2 \qquad \text{for plane stress, and} \tag{5.6a}$$

$$r^* = \frac{1}{18\pi}\left(\frac{K_I}{\sigma_{ys}}\right)^2 \qquad \text{for plane strain } (\nu = 1/3) \tag{5.6b}$$

These results are highly approximate; better expressions are obtained through the Irwin plastic zone correction, or the Dugdale approach.

5.3.2 The Irwin Plastic Zone Correction

Irwin [5.3] suggested a vastly improved expression for the plastic zone size along the x_1-axis through a model which accounts for the absence of high stresses within the yield zone. Consider a case of plane stress with $k = 1$. As shown in Fig. 5.5, the plastic zone size beyond the tip T of the actual crack is TL along x_1-axis. The tip of the effective crack is located somewhere inside the plastic zone. There should be an appropriate criterion to find the length of the effective crack. Note that if the tip of the effective crack is at point M, then the material beyond the tip will not be able to sustain $\sigma_{22} > \sigma_{ys}$. Moreover, the crack-faces of the effective crack are not actually separated between the points T and M and therefore tensile stress equal to σ_{ys} acts on the length δ for an elastic-perfectly plastic material. Irwin proposed that δ is so chosen such that the load not taken beyond the point M, given by the area P_c on length λ, is equal to the load sustained on length δ, given by area P_A. Then, the load not sustained on length λ becomes

$$P_c = B\left[\int_0^{\lambda} \sigma_{22} dx_1 - \sigma_{ys}\lambda\right]$$

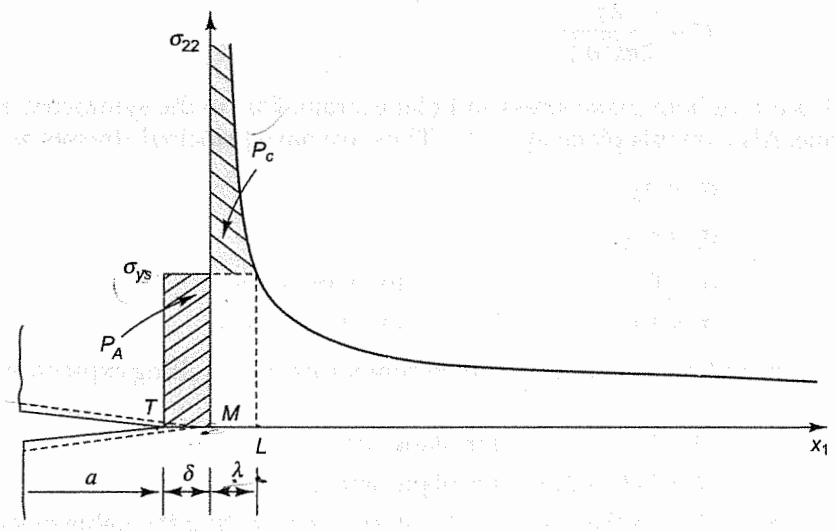

Fig. 5.5 Irwin plastic zone correction

where, B is the plate thickness. The load sustained (P_A) on length δ is

$$P_A = B\sigma_{ys}\,\delta$$

Irwin's correction ($P_A = P_c$) leads to

$$\sigma_{ys}\,\delta = \int_0^{\lambda} \sigma_{22} dx_1 - \sigma_{ys}\lambda = \int_0^{\lambda} \frac{K_I}{\sqrt{2\pi x_1}} dx_1 - \sigma_{ys}\lambda \tag{5.7}$$

where, K_I is based on the effective crack length ($a + \delta$). λ is determined by noting that at $x_1 = \lambda$, σ_{22} is equal to σ_{ys} for plane stress ($k = 1$), i.e.,

$$\sigma_{ys} = \frac{K_I}{\sqrt{2\pi\lambda}}$$

Rearranging, we have

$$K_I = (2\pi\lambda)^{1/2}\sigma_{ys}$$

Substituting in Eq. (5.7), we have

$$\sigma_{ys}\delta = \int_0^{\lambda} \frac{\sigma_{ys}(2\pi\lambda)^{1/2}}{\sqrt{2\pi x_1}} dx_1 - \sigma_{ys}\lambda$$

On solving, we obtain

$$\delta = \lambda$$

The overall plastic zone size becomes

$$r_p = 2\lambda = \frac{K_I^2}{\pi \sigma_{ys}^2} \tag{5.8}$$

The effective crack length a_{eff} is given by

$$a_{eff} = a + \delta = a + \lambda = a + \frac{K_I^2}{2\pi \sigma_{ys}^2} \tag{5.9}$$

Since K_I is based on the effective crack length, a_{eff} is still unknown. If the plastic zone is small in comparison to the crack length, K_I may be assumed to be equal to the SIF of crack length a. However, K_I can also be obtained in a closed form for the case of an infinite plate; the corrected SIF is expressed as

$$K_I = \sigma \left[\pi (a + \lambda)\right]^{1/2}$$

$$= \sigma \pi^{1/2} \left[a + \frac{K_I^2}{2\pi \sigma_{ys}^2}\right]^{1/2}$$

On solving, we obtain

$$K_I = \frac{\sigma \sqrt{\pi a}}{\left[1 - \frac{1}{2}\left(\sigma / \sigma_{ys}\right)^2\right]^{1/2}} \tag{5.10}$$

For a finite size specimen,

$$K_I = \sigma \left[\pi (a + \lambda)\right]^{1/2} f\left(\frac{a + \lambda}{W}\right)$$

or

$$K_I = \sigma \pi^{1/2} \left[a + \frac{K_I^2}{2\pi \sigma_{ys}^2}\right]^{1/2} f\left(\left(a + \frac{K_I^2}{2\pi \sigma_{ys}^2}\right) \Big/ W\right) \tag{5.11}$$

For certain geometries, function f is simple (e.g., $f = 1$ for a centre-cracked infinite plate and $f = 1.12$ for an edge-cracked infinite plate) and K_I can easily be obtained from the above equation. Otherwise, it can also be determined by an iterative procedure. For example, K_I on right hand side is taken based on the actual crack length a in the first round of iteration. The evaluated value K_I is then fed on the right hand side in the second round. The iterative procedure is repeated until two successive values of K_I are within a small percentage difference.

Irwin's correction to the plane strain case is useful to determine the plastic zone size. Due to the plastic deformation the crack tip becomes rounded. Since the rounded tip acts as a free surface, σ_{11} is released to zero. The effect of the release of σ_{11} is felt for some distance on the x_1-axis beyond the crack tip. Irwin [5.4] found that k is no longer 3 but is closer to $\sqrt{2\sqrt{2}}$ which may be taken as $\sqrt{3}$. Then, the plastic zone size for the plane strain becomes $(1/3\pi)K_I^2/\sigma_{ys}^2$. For an experimental determination of K_{Ic} of material, plane strain conditions are assured by taking plate

thickness to be much thicker than the plastic zone size. In fact, it is chosen to be more than 25 times of the plastic zone size and therefore, the ASME codes require

$$B \geq 2.5 \frac{K_I^2}{\sigma_{ys}^2}$$

The details of the experimental procedure to determine the critical SIF are presented in Chapter 8. To have an idea, the estimated plastic zone size (r_p) is listed in Table 5.1 for some commonly used materials for plane strain, corresponding to K_{Ic}.

TABLE 5.1 Estimated plastic zone size (r_p) at the critical stage of a crack for some common materials for plane strain in Mode I

Material	r_p *(mm)*
Nuclear Reactor Steel	93
Alloy Steel* (σ_{ys} = 1070 MPa)	1.8
High Strength Aluminum (7075-T651)	0.8
Titanium Alloy (Ti-6Al-4V)	1.3
Perspex (Plexiglass)	0.1

* 40 Ni2Cr1Mo28 (IS)/EN 24 (UK)/4340 (USA)

5.3.3 Plastic Zone Size through the Dugdale Approach

Dugdale [5.5] determined the plastic zone size through a different approach. He considered the effective crack to be of length $a + \rho$ where ρ is plastic zone size [Fig. 5.6(a)].

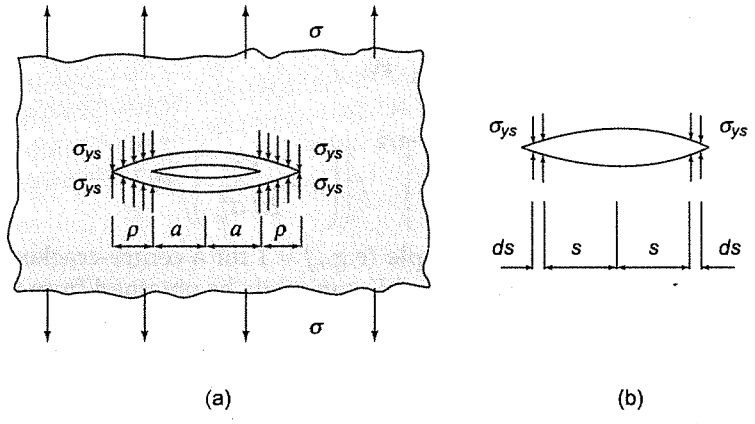

Fig. 5.6 (a) Plastic zone size through Dugdale's approach and (b) nullifying the singularity using Green's function approach

In the Dugdale approach, singularity at the tip of the effective crack is nullified by a uniform pressure equal to yield stress σ_{ys} (for plane stress cases with $k = 1$) on the portion ρ of the crack, as shown in the figure. In fact, to determine ρ we employ the criterion that ρ is the length on which pressure σ_{ys} exactly nullifies the singularity. If K_ρ is the singularity due to the pressure σ_{ys} and K_σ due to external load on the effective crack, we have

$$K_\sigma + K_\rho = 0 \tag{5.12}$$

K_σ is simple to evaluate and is given by

$$K_\sigma = \sigma\sqrt{\pi(a+\rho)}$$

To determine K_ρ, Green's function is used (as discussed in Sec. 4.1.1). Application of Eq. (4.1) to Fig. 5.6(a) gives

$$dK_\rho = -\frac{2}{\pi}\frac{\sigma_{ys}ds\sqrt{\pi(a+\rho)}}{\sqrt{(a+\rho)^2 - s^2}}$$

Integrating, we have

$$K_\rho = -\frac{2\sigma_{ys}\sqrt{\pi(a+\rho)}}{\pi}\int_a^{a+\rho}\frac{1}{\sqrt{(a+\rho)^2 - s^2}}ds$$

$$= -\frac{2\sigma_{ys}\sqrt{\pi(a+\rho)}}{\pi}\left[\cos^{-1}\frac{a}{a+\rho}\right]$$

Substituting K_ρ and K_σ in Eq. (5.12), we have

$$\sigma - \frac{2\sigma_{ys}}{\pi}\cos^{-1}\frac{a}{a+\rho} = 0$$

which is simplified to

$$\frac{a}{a+\rho} = \cos\left[\frac{\pi\sigma}{2\sigma_{ys}}\right]$$

An approximate, but simpler relation may be obtained for cases $\sigma << \sigma_{ys}$ and $\rho << a$ as

$$1 - \frac{\rho}{a} = 1 - \frac{\pi^2\sigma^2}{8\sigma_{ys}^2}$$

giving,

$$\rho = \frac{\pi\sigma^2\pi a}{8\sigma_{ys}^2} = \frac{\pi K_I^2}{8\sigma_{ys}^2} \tag{5.13}$$

We note that the plastic zone size of Dugdale's model is close to that of Irwin's correction [i.e., $K_I^2/(\pi\sigma_{ys}^2)$] for $\sigma << \sigma_{ys}$.

Example 5.1 A large plate of 5 mm thickness, made of medium carbon steel (σ_{ys} = 350 MPa) with a through-the-thickness centre-crack of $2a$ = 40 mm length, is subjected to a stress of 150 MPa. For Mode I loading, determine the effective crack length using Irwin's correction.

Solution: We start by assuming that the plate is loaded in plane stress.

$$K_I = \sigma\sqrt{\pi a} = (150\text{ MPa})\sqrt{\pi \times (0.020\text{ m})} = 37.6\text{ MPa}\sqrt{m}$$

$$r_p = \frac{K_I^2}{\pi\sigma_{ys}^2} = \frac{(37.6\text{ MPa}\sqrt{m})^2}{\pi(350\text{ MPa})^2} = 3.67\text{ mm}$$

Since r_p is not negligible in comparison to plate thickness, our assumption of plane stress conditions is justified. Invoking Eq. (5.10), we have:

$$K_I = \frac{\sigma\sqrt{\pi a}}{\left[1-\frac{1}{2}\left(\frac{\sigma}{\sigma_{ys}}\right)^2\right]^{1/2}} = \frac{(150\text{ MPa})\sqrt{\pi}\times(0.020\text{m})^{1/2}}{\left[1-\frac{1}{2}\left(\frac{150\text{MPa}}{350\text{MPa}}\right)^2\right]^{1/2}}$$

$$= 39.46\text{ MPa}\sqrt{m}$$

The plastic zone size is given by

$$r_p = \frac{K_I^2}{\pi\sigma_{ys}^2} = \frac{(39.46\text{MPa})^2}{\pi\times(350\text{MPa})^2} = 0.004046\text{ m} = 4.046\text{ mm}$$

And then the effective crack length becomes:

$$a_{\text{eff}} = a + \frac{r_p}{2} = 20\text{ mm} + 2.023\text{ mm} = 22.023\text{ mm}$$

Example 5.2 A steel plate (σ_{ys} = 350 MPa) of width 80 mm and thickness 5 mm has a centre-crack $2a$ = 40 mm length. If the far field stress is 150 MPa, determine the SIF and the length of the effective crack, using Irwin's correction.

Solution: We first check whether the plate is loaded in plane stress by finding r_p based on the actual crack length. Referring to Appendix 4B, we have

$$K_I = \sigma\sqrt{\pi a}\, f(\alpha);\quad \alpha = a/W = \frac{20\text{mm}}{40\text{mm}} = 0.5$$

$$f(\alpha) = 1.0 + 0.128\alpha - 0.288\alpha^2 + 1.523\alpha^3$$

$$= 1.182$$

$$K_I = \left(150\text{MPa}\sqrt{m}\right)\sqrt{\pi\times 0.02\text{m}}\times 1.182 = 44.44\text{ MPa}\sqrt{m}$$

$$r_p = \frac{K_I^2}{\pi\sigma_{ys}^2} = \frac{1}{\pi}\left(\frac{44.44\text{MPa}\sqrt{m}}{350\text{MPa}}\right)^2 = 5.13\text{ mm} \approx \text{Plate thickness}$$

Therefore, plane stress conditions do exist. Invoking Eq. (5.11), we have

$$K_I = \sigma\left[\pi\left(a+\frac{K_I^2}{2\pi\sigma_{ys}^2}\right)\right]^{1/2}\times f(\alpha') \tag{5.14}$$

where, $$\alpha' = \left(a+\frac{K_I^2}{2\pi\sigma_{ys}^2}\right)\Big/ W$$

This problem will now be solved through iteration. The general iterative procedure is that we guess a value of K_I and substitute it on the RHS of Eq. (5.14) to evaluate the variable K_I of LHS

and then compare the two values. In the second round of iteration, we guess another value of K_I on the RHS. The process continues till the two values converge. In this problem, we start the first round of iteration with $K_I = 44.44$ MPa $\sqrt{m}$ and substitute it in the RHS of Eq. (5.14) to have

$$\alpha' = 0.5641, \quad f(\alpha') = 1.2539$$

$$K_I = 50.08 \text{ MPa}\sqrt{m}$$

Since this K_I is quite different from the 44.44, we go for the second round of iteration by feeding K_I as 50.08 into RHS of Eq. (5.18) to have

$$\alpha' = 0.5815, \quad f(\alpha') = 1.2765$$

$$K_I = 51.758 \text{ MPa}\sqrt{m}$$

The third round gives

$$\alpha' = 0.587, \quad f(\alpha') = 1.2839$$

$$K_I = 52.306 \text{ MPa}\sqrt{m}$$

and the fourth round determines

$$\alpha' = 0.5889, \quad f(\alpha') = 1.2865$$

$$K_I = 52.48 \text{ MPa}\sqrt{m}$$

Since K_I is quite close to the value of the third round, we stop the iterative process. The plastic zone size is then given by

$$r_p = \frac{K_I^2}{\pi\sigma_{ys}^2} = \frac{(52.48 \text{ MPa}\sqrt{m})^2}{\pi \times (350 \text{ MPa})^2}$$

$$= 0.00716 \text{ m} = 7.16 \text{ mm}$$

and the effective crack length becomes,

$$a_{\text{eff}} = a + \frac{r_p}{2} = 0.02 \text{ m} + 0.00358 \text{ m} = 23.58 \text{ mm}$$

5.4 Effect of Plate Thickness

So far in this book, we have been using the terms plane stress and plane strain without having spelled out any formal quantitative criterion, which would help us identify whether a given case is of plane stress or plane strain. Such a criterion could not be given earlier because the parameter that differentiates between plane stress and plane strain is the size of the plastic zone. Only after quantitative models are developed, we can estimate the plastic zone.

In a thin plate, plane stress components σ_{33}, σ_{31} and σ_{32} and are able to relax to zero and the material deforms easily within the plastic zone. In the vicinity of the crack tip, both free surfaces of the plate move in forming a depression on each side, owing to in-plane tensile stresses and Poisson's effect. On the contrary, the material in a thick plate is constrained, giving rise to tensile stress σ_{33}.

There must be a limit on plate thickness under which a material is able to flow easily and the plate is deformed under plane stress. Similarly, there must be a limit on plate thickness over which the material is taken to be deformed under plane strain. Between the upper and lower limits of the plate thickness, the cases are known to have transitional behaviour, i.e., near a free surface, the material flows easily and deforms in plane stress and, in the interior, the material is constrained and is subjected to plane strain.

Now, the method to set the limits on the thickness for plane stress and plane strain will be explored. These limits are decided mainly on the basis of the long experiences of many investigators. It has been found that if the plastic zone size is about the thickness of the plate, the material within the plastic zone relieves 'out of plane stresses' and deforms easily. Therefore, for a plate with its thickness less than or equal to the size of the plastic zone, the crack is loaded in plane stress. Figure 5.7(a) shows the case of plane stress with a section through the plastic zone.

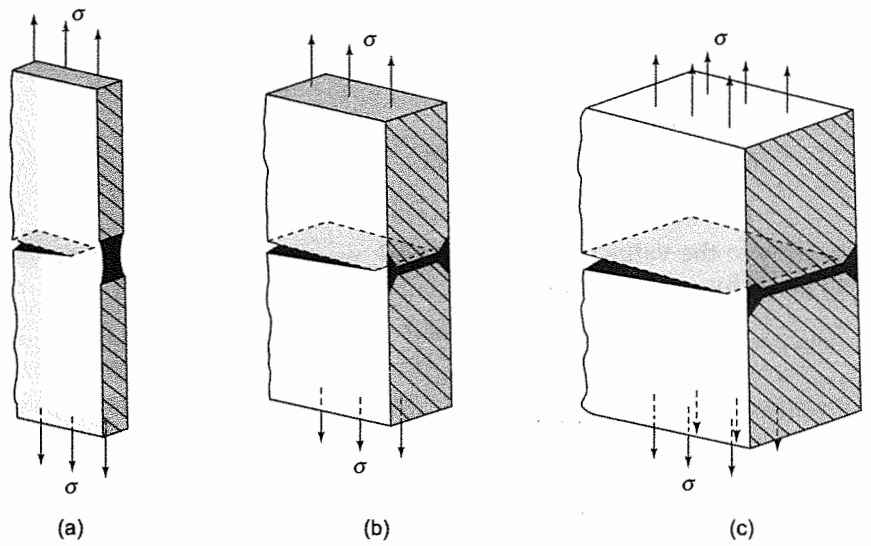

Fig. 5.7 Plastic zone size for (a) plane stress, (b) transitional case, and (c) plane strain

The thick plate [Fig. 5.7(c)] corresponds to plane strain, showing a smaller plastic zone. Even in this case, some effect of the free surface exists where the plastic zone is larger. However, the thick region of plane strain dominates and the surface effects can be neglected. A plate having thickness greater or equal to $2.5\, K_{Ic}^2/\sigma_{ys}^2$ is regarded as a case of plane strain. In transitional cases [Fig. 5.7(b)], the interior portion of the plate and the regions near its both surfaces have mixed effects on the plastic zone.

It is evident from Fig. 5.7 that the critical SIF of a plate depends upon its thickness. The nature of the critical SIF dependence on the plate thickness B is shown in Fig. 5.8 qualitatively. For $B \geq 2.5\, K_{Ic}^2/\sigma_{ys}^2$, the critical SIF remains constant and then we can regard the critical stress intensity factor as the material property. The value of K_{Ic} of commonly used materials is available. Representative K_{Ic} of some materials are presented in Table 4.2.

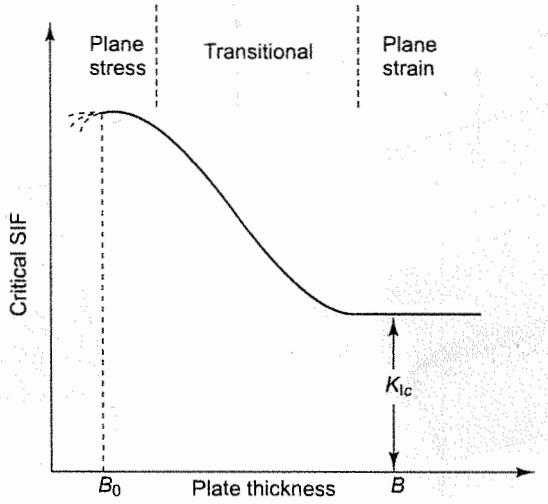

Fig. 5.8 Variation of critical SIF with plate thickness

For $B < 2.5\ K_{Ic}^2/\sigma_{ys}^2$ critical stress intensity factor depends on the thickness B. The relation between critical SIF and thickness should be provided to designers. However, this is not usually done, probably because experimental tests are expensive for tough materials. Users like aerospace-companies generate their own data base of critical SIF of plane stress or transitional cases, for commonly used thicknesses.

For plate thickness B_0 (Fig. 5.8), the plastic zone size is approximately equal to the thickness of the plate thickness and is considered to be the case of pure plane stress. For thinner plates, experimental determination of the critical SIF is difficult, because the plate tries to buckle close to the cracked surfaces and the specimen is then loaded in Mode III also.

Fractured planes of a plane stress case are different from those of a plane strain case. In case of Mode I, σ_{33} is always zero if conditions of plane stress prevail. Also on plane $x_2 = 0$, it is noted that $\sigma_{12} = 0$ and $\sigma_{22} = \sigma_{11}$. However, even at a point slightly away from the plane (θ is not equal to zero) σ_{22} is greater than σ_{11}. The maximum shear stress is dictated by σ_{22} and σ_{33} and therefore, a fracture is likely to occur on one of the two planes inclined at $\pm$ 45°, as shown in Fig 5.9(a). Note that the fractured surface is inclined to the free surfaces of the plate as shown in Fig. 5.9(b).

Under plane strain conditions in Mode I, yield planes are more complex. The crack growth is a combined effect of yielding due to the dislocation motion and the generation and nucleation of voids in front of the crack tip. In metals, the nucleation and the growth of voids are facilitated by the triaxiality of tensile stresses near the crack tip in case of plane strain. The voids coalesce (grow and join each other) during the crack growth. It has been observed that in plane strain cases, a crack usually grows on the plane of the original crack. Figure 5.10 shows the self similar growth on the crack-plane. This fact is exploited in designing experiments, so as to determine the critical SIF of a material.

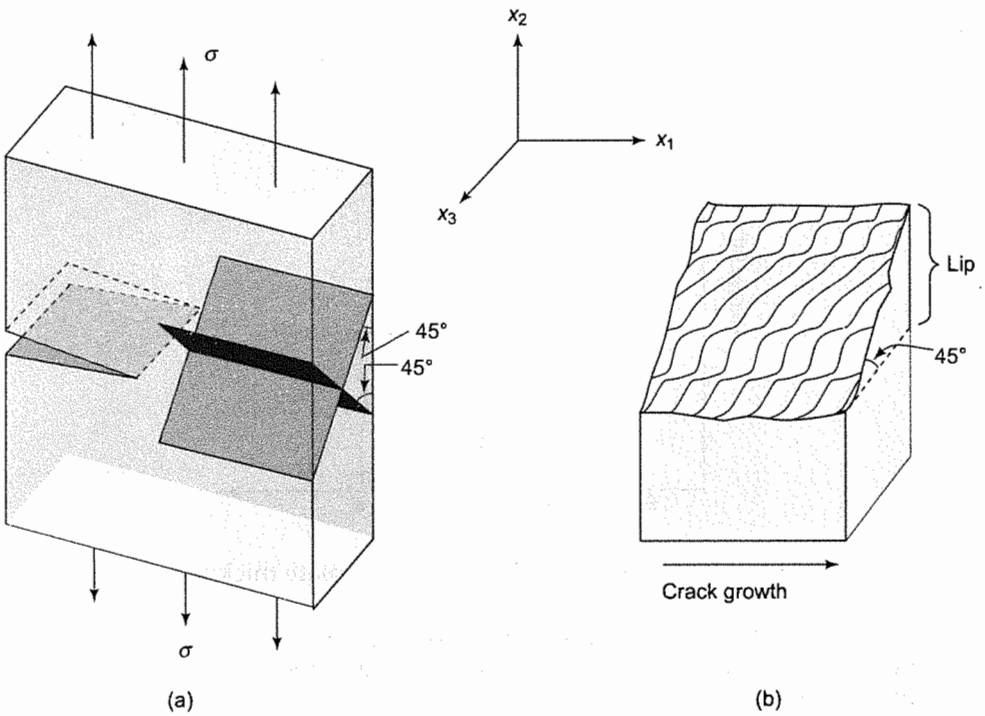

Fig. 5.9 Yield planes of plane stress, and (b) a cracked face

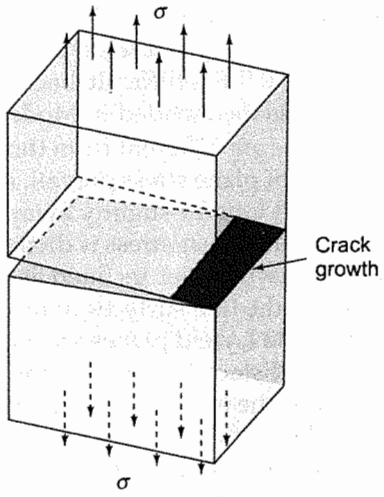

Fig. 5.10 Crack growth of plane strain cases

For the transitional behavior of a crack, the fracture is of mixed kinds (Fig. 5.11), flat in the interior, dominated by plane strain and slant close to the free surface. In fact, by looking at a fractured surface, one can conclude whether the fracture occurred prominently under plane stress or plane strain.

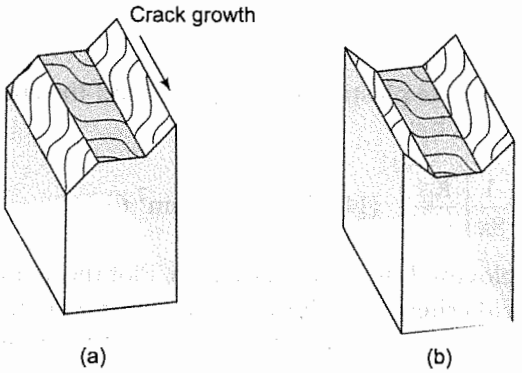

Fig. 5.11 Cracked faces of transitional cases

Cutting a material by conventional machines (lathe, milling, shaper and drill press) is a fracture phenomenon and the edges of a cut surface are found to have lips generally known as burrs. These burrs are regarded as a nuisance in a production shop and are removed through specially designed deburring machines.

5.5 Closure

The shape of the plastic zone has been obtained through a quantitative, but approximate method. This helps us in understanding the difference between plane stress and plane strain conditions. The critical stress intensity factor depends, in general, on the plate thickness. However, it does not depend on plate thickness, if the plates are thick enough to be loaded in plane strain. Thus, the critical stress intensity factor of plane strain (K_{Ic}) is treated as the property of a material.

Questions

1. The shape of the plastic zone, as determined in this chapter, is approximate. Why?
2. In comparison to a plane strain case, a plane stress loading gives much larger plastic zone for the same SIF? Why?
3. Looking at a fractured surface, can you distinguish whether the loading was in plane stress, plane strain or transitional?
4. Show the yield planes of plane stress cases through a clear diagram.
5. The plastic zone size obtained through Irwin's model is quite large in comparison to the plastic zone (r^*), obtained through the yield criterion applied to the elastic field. Why?
6. Can the effective crack length be used as a suitable parameter for formulating elastic plastic fracture mechanics?
7. Why is the fracture plane of plane strain case normal to the free surface and in the plane of the original crack surface for Mode I loading?
8. Why is burr developed during machining?
9. Does fracture mechanics recommend the enhancement of the yield stress of an alloy through a heat treatment? Justify your answer.

PROBLEMS

1. Show that the approximate plastic zone shape around the crack tip of a Mode II crack in an infinite plate is given by:

$$r_p(\theta) = \frac{1}{8\pi}\left(\frac{K_{II}}{\sigma_{ys}}\right)^2 (14 - 2\cos\theta - 9\sin^2\theta)$$

for plane stress employing Mises yield criterion. Plot the shape of the plastic zone.

2. Apply the Mises yield criterion to show that the approximate plastic zone shape around the crack tip of a Mode II crack in an infinite plate for plane strain loading is given by

$$r_p(\theta) = \frac{1}{8\pi}\left(\frac{K_{II}}{\sigma_{ys}}\right)^2 [12 + 2(1-2\nu)^2(1-\cos\theta) - 9\sin^2\theta)]$$

Plot the shape of the plastic zone.

3. Invoke the Mises yield criterion to show that the approximate plastic zone around the tip of a Mode III crack is a circle of radius

$$r_p = \frac{3}{2\pi}\left(\frac{K_{III}}{\sigma_{ys}}\right)^2$$

4. In a case of a mixed mode with loading in plane stress, find the approximate shape of the plastic zone, if $K_I = K_{II} = K$, and plot the shape represented by $r_p/(K^2/\pi\sigma^2_{ys})$ vs θ. Use of a computer is recommended.
5. Determine the plastic zone size r_p/a of an edge crack of length a in a thin infinite plate, loaded in Mode I with a far field stress σ using Irwin's correction.
6. Apply Irwin's correction to determine the SIF, the length of the effective crack and the plastic zone size for an edge crack of 15 mm length in a plate 80 mm width. The thickness of the plate is 5 mm and the far field stress is 150 MPa (σ_{ys} = 350 MPa).
7. A thin plate with an edge crack of 35 mm length is loaded in Mode I with a far field stress of 300 MPa. If the yield stress of the material is 900 MPa and the material is idealized as elastic-perfectly plastic, determine the plastic zone size on x_1-axis using Irwin's correction. What is the length of plastic zone size if the Dugdale Approach is applied?

REFERENCES

5.1 Atkins, A.G. and Mai, Y.W. (1985). *Elastic and Plastic Fracture: Metals, Polymers Ceramics,* Composites, Biological Materials, Ellis Horwood, Chichester.

5.2 Srinath, L.S. (1980). *Advance ' Mechanics of Solids,* Tata McGraw-Hill Publishing Co. Ltd, New Delhi.

5.3 Irwin, G.R. (1958). *Fracture, Handbuch der Physik,* Springer, Berlin, Vol. VI, pp. 551–590.

5.4 Irwin, G.R. (1968). Linear Fracture Mechanics, Fracture Transition and Fracture Control, *Engineering Fracture Mechanics,* I. pp. 241–257.

5.5 Dugdale, D.S. (1960). Yielding and Steel Sheets Containing Slits, *Journal of Mechanics and Physics of Solids*, 8, pp. 100–108.
5.6 Anderson, T.L. (2004). *Fracture Mechanics: Fundamentals and Applications*, CRC, Press-Book.
5.7 Sanford, R.J. (2003). *Principles of Fracture Mechanics*, Prentice Hall, Upper Saddle River.
5.8 Janssen, M., Zuidema, J. & Wanhill, R.J.H. (2004). *Fracture Mechanics*, Spon Press, Abingdon.
5.9 Ramesh, K. (2007). *e-Book on Engineering Fracture Mechanics*, IIT Madras, URL: http//apm.iitm.ac.in/smlab/kramesh/book_4.htm

Chapter

6

J-Integral

Siddharth said: "Is it not true my friend, that the river has very many voices? Has it not the voice of a king, of a warrior, of a bull, of a might bird, of a pregnant woman and a singing man, and a thousand other voices?"

Hermann Hesse

6.1 Relevance and Scope

A large plastic zone at the crack tip makes a material tough. However, in the early development of modern fracture mechanics, existence of the plastic zone was ignored in any analysis, because practical methods were not developed to account for the elastic-plastic behavior within the plastic zone. The LEFM assumes that the entire body, including the material very close to the crack tip, follows linear elastic relations.

The stress-strain behavior of an elastic-plastic deformation is not simple, as it is well known to be non-linear. With the availability of inexpensive computers, non-linear stress-strain behavior can now be accounted for. But, it is difficult to incorporate the non-uniqueness of the elastic-plastic behavior. That is, the loading behavior of an elastic-plastic material differs from the unloading behavior, as shown in Fig. 6.1. For a given value of strain (e.g., at $\varepsilon = \varepsilon_1$), there are always two stress values and therefore, one has to keep track of the specimen being loaded or unloaded. An analogy can be drawn with interaction with a person who is simple and straight forward like a linear elastic material. Non-linear elastic material corresponds to a man who is honest but rude. But elastic-plastic material is like dealing with a man who is not only rude but speaks truth sometimes and lies other times.

For many metals, the stress-strain relations get further complicated due to the Bauschinger's effect [6.1], which shows that the yield stress in unloading is different from that in loading. Such problems will not be elaborated here. But we realize that solving problems of an elastic-plastic material is quite difficult, even for a regular component with no voids or cuts. The magnitude of complexity increases further when the problem is solved in the vicinity of a crack tip.

Elastic-plastic behavior makes the analysis of fracture mechanics complex, because this implies the existence of two zones—the elastic-plastic zone, near the crack tip and the elastic zone surrounding it. The interface between the two zones is also not known and could be determined only by a complex analysis.

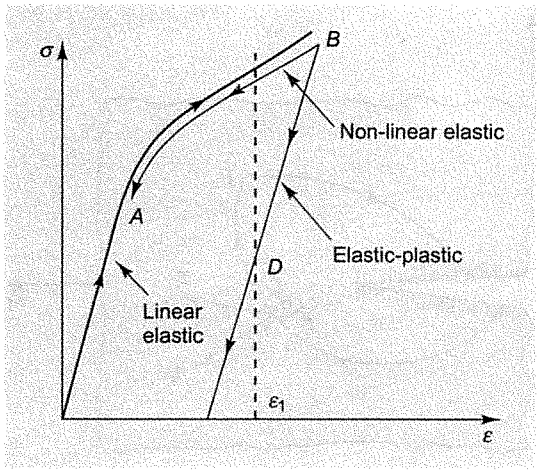

Fig. 6.1 Non-linear elastic and elastic-plastic material behavior

Because of these complex problems faced in any elastic-plastic analysis, it has, so far, not been possible to tackle the problem directly. In fact, we look for clever solutions which are improved over those of the LEFM, but are not too difficult for designers in field applications. The J-Integral is one such method which, in spite of some reservations, is the most accepted method to designers and researchers of elastic-plastic fracture mechanics (EPFM). In this chapter, we will discuss various aspects of the J-Integral.

6.2 Definition of the J-Integral

Like other parameters (G and K), the J-Integral is also a parameter to characterize a crack. In fact, G is a special case of the J-Integral, i.e., G is usually applied only to linear elastic materials, whereas the J-Integral is not only applicable to linear and non-linear elastic materials, but is considered to be very useful to characterize materials, exhibiting elastic-plastic behavior near the crack tip.

At first sight, the J-Integral looks like a strange term, but as we go along and develop it gradually, it would not look odd. For plane problems, consider a path Γ around a crack tip (Fig. 6.2) which starts from any point of a crack face and ends on any point on the other crack face. The path can be chosen arbitrarily within the material of the component. It may be smooth or may have corners, but should be continuous. J-Integral was first applied to fracture mechanics by Rice [6.2] in 1968 for plane problems. It is defined as:

$$J = \int_{\Gamma} \left(W dx_2 - T_i \frac{\partial u_i}{\partial x_1} ds \right) \tag{6.1}$$

where, $$W = \int \sigma_{ij} \, d\varepsilon_{ij}$$

The Einstein's summation convention is followed in defining the above expressions. For two dimensional plane cases W may be expressed in full form as:

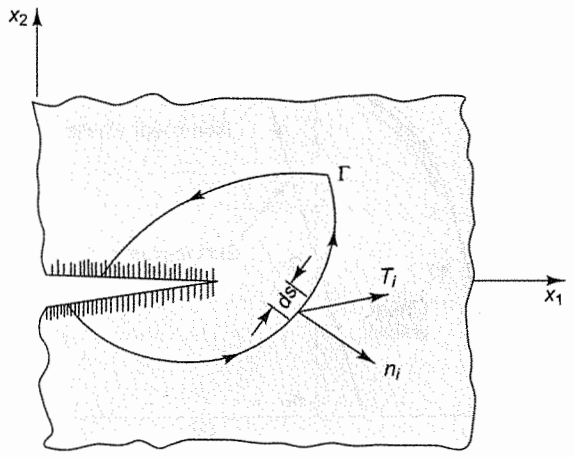

Fig. 6.2 Path Γ around the crack tip with outward normal n_i and traction T_i

$$W = \int_0^{\varepsilon_{11}} \sigma_{11}\, d\varepsilon_{11} + \int_0^{\varepsilon_{12}} \sigma_{12}\, d\varepsilon_{12} + \int_0^{\varepsilon_{21}} \sigma_{21}\, d\varepsilon_{21} + \int_0^{\varepsilon_{22}} \sigma_{22}\, d\varepsilon_{22}$$

Summing the middle terms, we have:

$$W = \int_0^{\varepsilon_{11}} \sigma_{11}\, d\varepsilon_{11} + 2\int_0^{\varepsilon_{12}} \sigma_{12}\, d\varepsilon_{12} + \int_0^{\varepsilon_{22}} \sigma_{22}\, d\varepsilon_{22}$$

Also, W which is strain energy per unit volume is a point function, i.e., it varies from point to point within the body of the component. Other parameters of Eq. (6.1) are:

T_i = traction vector at a point on the path Γ,

u_i = displacement vector at a point on the path.

In the expanded form, the second term of Eq. (6.1) for plane cases is:

$$\int_\Gamma \left(T_1 \frac{\partial u_1}{\partial x_1} + T_2 \frac{\partial u_2}{\partial x_1} \right) ds$$

Traction T_i at a point on path Γ is expressed through the well-known relation $T_i = \sigma_{ij} n_j$ (i.e., $T_1 = \sigma_{11} n_1 + \sigma_{12} n_2$ and $T_2 = \sigma_{21} n_1 + \sigma_{22} n_2$). Thus, by knowing the stress field and the direction of the normal at a point of path Γ, we can determine T_i. Later in this chapter, we will prove the following two important features of J-Integral:

(i) The J-Integral is path independent, i.e., Γ can be chosen arbitrarily within the body of a component.

(ii) For linear elastic bodies, the J-Integral represents energy release rate and is same as G.

Now, we will take up an example to show that the above mentioned features of the J-Integral are applicable to a practical case of the double beam cantilever solved in Sec. 2.7.

Example 6.1 Determine the J-Integral for a double cantilever beam (DCB) specimen, if each cantilever is pulled by a distributed load P, as shown in Fig. 6.3.

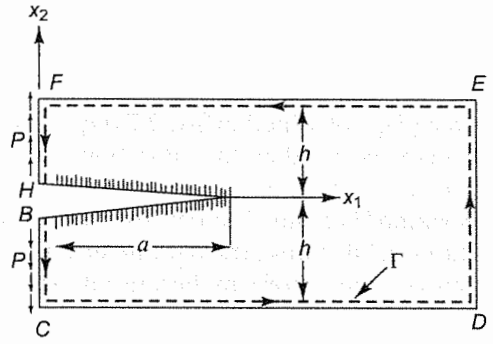

Fig. 6.3 Path Γ coinciding with outer edges of the DCB specimen

Solution: The chosen path Γ is *BCDEFH* and it coincides with the body contour. Segments *CD* and *EF* of the path Γ do not contribute to the J-Integral, because dx_2 is negligible and $T_i = 0$. The contribution of the segment *DE* towards the J-Integral is negligible, because stresses are very small, which in turn, make W and T_i negligible. On segments *BC* and *FH*, W is negligible, (no contribution of bending stress owing to zero bending moment and negligible contribution of shear stress) and the only non-trivial term is:

$$J = -2\int_0^h T_2 \frac{\partial u_2}{\partial x_1} dx_2 \tag{6.2}$$

where, the factor 2 accounts for the contribution from both cantilevers. Deflection u_2 of a cantilever at a distance x_1 is commonly evaluated by equating the bending moment with $EI\dfrac{\partial^2 u_2}{\partial x_1^2}$, leading to:

$$\frac{\partial^2 u_2}{\partial x_1^2} = \frac{Px_1}{EI}$$

Integrating it for the upper cantilever with the boundary condition $\partial u_2 / \partial x_1 = 0$ at $x_1 = a$, we obtain:

$$\frac{\partial u_2}{\partial x_1} = \frac{Px_1^2}{2EI} - \frac{Pa^2}{2EI}$$

Evaluating it at $x_1 = 0$ and using the relation $I = Bh^3/12$, we have:

$$\frac{\partial u_2}{\partial x_1} = -\frac{6Pa^2}{EBh^3}$$

Substituting in Eq. (6.2), we have:

$$J = \frac{12Pa^2}{EBh^3}\int_0^h T_2 dx_2$$

But $B\int_0^h T_2\, ds = P$ on face FH, leading to:

$$J_I = \frac{12P^2a^2}{EB^2h^3} \tag{6.3}$$

This expression is same as that of G_1, obtained in Sec. 2.7 [Eq. (2.20)]. One may note here that the definition of the J-Integral is more versatile than the definition of G, because the J-Integral can cut out a portion of the component at the will of an investigator and characterize the crack fully. Although the technique to determine J is quite different from that of G, both lead to the same result for linear elastic materials in the end. Of course, the parameter G is limited only to LEFM, whereas the J-Integral encompasses a much bigger domain, because it can deal with both non-linear and elastic-plastic materials.

6.3 Path Independence

The J-Integral is carried out along an arbitrary path Γ, which starts from one crack face and ends up on the other crack face, while going around the crack tip. It would be proved, in this section, that J is path independent for both linear and non-linear elastic materials. We first consider an area A of a plate not containing any cut or void and we surround it by a closed path S, as shown in Fig. 6.4(a). We will show that the value of integral I, containing the same integrand as that of the J-Integral, but evaluated along the closed path S, vanishes, i.e.

$$I = \int_S \left[W dx_2 - T_i \frac{\partial u_i}{\partial x_1} ds \right] \to 0 \tag{6.4}$$

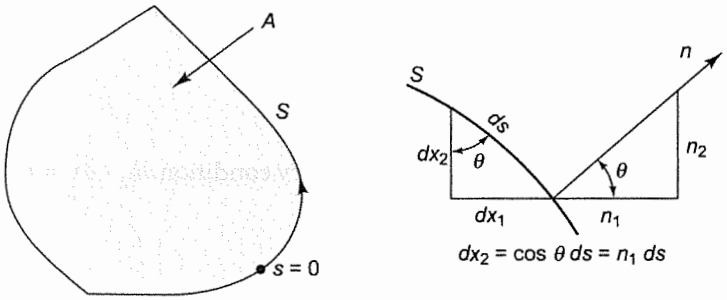

(a) (b)

Fig. 6.4 (a) Area A without any cut or void and enclosed by contour S, and (b) the relation between n_1 and dx_2

Substituting $dx_2 = n_1 ds$ [Fig. 6.4(b)] and $T_i = \sigma_{ij} n_j$ in the above equation, we have:

$$I = \int_S \left[W n_1 - \sigma_{ij} n_j \frac{\partial u_i}{\partial x_1} \right] ds$$

The integral will be converted from a line integral to an area integral using the Divergence Theorem, which is stated in general form as:

$$\int_S M n_i ds = \int_A \frac{\partial M}{\partial x_i} dA = \int_A M_i dA$$

where M is any variable. Invoking the Divergence Theorem, we have:

$$I = \int_A \left[\frac{\partial W}{\partial x_1} - \left(\sigma_{ij} \frac{\partial u_i}{\partial x_1} \right)_{,j} \right] dA$$

leading to

$$I = \int_A \left[\frac{\partial W}{\partial \varepsilon_{ij}} \frac{\partial \varepsilon_{ij}}{\partial x_1} - \sigma_{ij} \left(\frac{\partial u_i}{\partial x_1} \right)_{,j} - \sigma_{ij,j} \left(\frac{\partial u_i}{\partial x_1} \right) \right] dA \tag{6.5}$$

We simplify Eq. (6.5) by realizing that for an elastic material (linear or non-linear)

$$\sigma_{ij} = \frac{\partial W}{\partial \varepsilon_{ij}} \tag{6.6}$$

and the equilibrium equations gives $\sigma_{ij,j} = 0$. The equation is simplified to:

$$I = \int_A \left(\sigma_{ij} \frac{\partial \varepsilon_{ij}}{\partial x_1} - \sigma_{ij} \frac{\partial u_{i,j}}{\partial x_1} \right) dA \tag{6.7}$$

For further simplification, we note that:

$$\sigma_{ij} \frac{\partial \varepsilon_{ij}}{\partial x_1} = \frac{1}{2} \sigma_{ij} \frac{\partial \left(u_{i,j} + u_{j,i} \right)}{\partial x_1} \tag{6.8}$$

and owing to the symmetry of σ_{ij}

$$\sigma_{ij} \frac{\partial u_{j,i}}{\partial x_1} = \sigma_{ji} \frac{\partial u_{j,i}}{\partial x_1} = \sigma_{ij} \frac{\partial u_{i,j}}{\partial x_1}$$

Then, Eq. (6.8) is simplified to:

$$\sigma_{ij} \frac{\partial \varepsilon_{ij}}{\partial x_1} = \sigma_{ij} \frac{\partial u_{i,j}}{\partial x_1}$$

Substituting in Eq. (6.7), we have:

$$I = \int_A \left[\sigma_{ij} \frac{\partial u_{i,j}}{\partial x_1} - \sigma_{ij} \frac{\partial u_{i,j}}{\partial x_1} \right] dA \rightarrow 0$$

This proves that the left hand side of Eq. (6.4) is zero for a closed curve and is valid for all materials whose constitutive equation can be defined through the relation of Eq. (6.6). This result will now be

used to prove the path independence of the J-Integral. Consider an area A, shown in Fig. 6.5, which is closed by four segments, BCD, DE, EFG and GB. Note that the segments DE and GB coincide with the crack surfaces. Segments BCD and EFG can be chosen arbitrarily within the material as long as they do not cross each other. We now split the integral of Eq. (6.4) into four parts, as:

$$\int_{BCD} + \int_{DE} + \int_{EFG} + \int_{GB} = 0$$

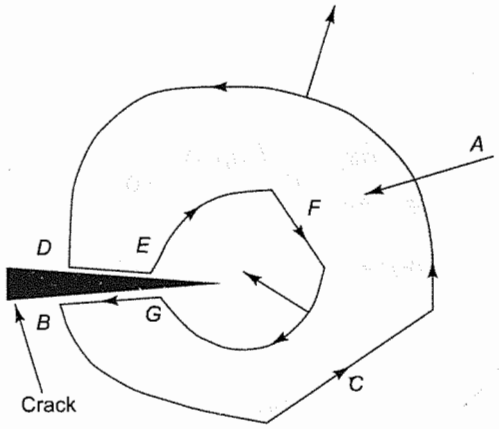

Fig. 6.5 Area A enclosed by two curves around the crack tip and two segments along the crack surfaces

Integrations along DE and GB do not contribute because $dx_2 \simeq 0$ and $T_i = 0$ for the traction free crack surfaces considered here. Two surviving integrals are:

$$\int_{BCD} + \int_{EFG} = 0 \tag{6.9}$$

The integral along BCD is counter-clockwise with its normal pointing into the external region and the integral along EFG is clockwise, with its normal pointing towards the interior. We can reverse the direction of the path of the inside curve from clockwise to counter-clockwise direction by introducing a negative sign. We then have:

$$\int_{BCD} = \int_{GFE}$$

Alternatively,

$$\int_{\Gamma_1} = \int_{\Gamma_2}$$

as shown in Fig. 6.6. Thus, we conclude that path Γ of the J-Integral can be chosen anywhere within the material.

We should note here that path independence of the J-Integral is valid only for cases in which $\sigma_{ij} = \partial W / \partial \varepsilon_{ij}$ is applicable. In fact, this is a constitutive relation and thus the property of the material plays an important role. This constitutive relation is valid for an elastic material, i.e., as the load is decreased, the strain retraces the path of loading (it goes from B to A as shown in Fig. 6.1). However, this is not true for an elastic-plastic material because unloading follows a different path from B to D. In fact, the relation between stress and strain for elastic materials is

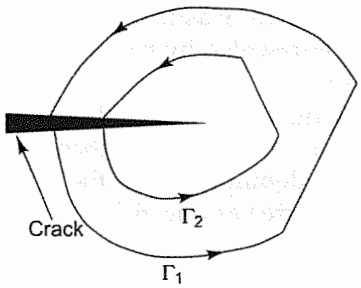

Fig. 6.6 Path independence of J-integral

unique, but it is not so for an elastic-plastic material. However, if the loads on a component are increased monotonically (with no unloading), the mathematical behavior of an elastic-plastic material is the same as that of any non-linear elastic material. Thus, even if a component is deformed plastically under a monotonic loading, the equations of non-linear elasticity can be used. Under these conditions, the J-Integral is taken as path independent for plastic deformation also. The elastic-plastic fracture mechanics is based on this idea.

The integration path Γ can be chosen far away from the crack tip to avoid the plastic zone or it may be taken very close to the crack tip so that it passes through the plastic zone. In any case, the J-Integral remains the same, provided there is no unloading. This suggests that the J-Integral is fully capable of characterizing a crack. Depending upon the conditions of a given problem, one can choose the path to minimize complexities in the evaluation of the J-Integral.

For linear elastic materials the J-Integral, represents the potentiality for release of energy from the system per unit area extension of the crack growth, and is the same as G. The proof showing that they are same [6.3] is given in Appendix 6A, presented at the end of this chapter.

6.4 Stress-Strain Relation

We shall now replace the elastic-plastic behavior of a material by a non-linear elastic behaviour for cases where the load on a component increases monotonically. It would be convenient if we have only one smooth curve, such that it behaves essentially as a linear elastic material within the elastic limit and elastic-plastic at high stresses. Note that stress-strain relations of all material are empirical. We should choose an appropriate form of a constitutive relation.

One of the most convenient constitutive relations has been formulated by Ramberg and Osgood. It is appropriate to describe the behavior of most engineering materials. However, there are some materials whose behaviour cannot be modeled by the Ramberg and Osgood relation. The relation is used in several different forms, but a convenient equation describing Ramberg–Osgood materials [6.4] for the one-dimensional case is:

$$\varepsilon = \frac{\sigma}{E} + \frac{\sigma^n}{F} \tag{6.10}$$

where E is the Young's Modulus of the material. Also, n and F are the other two material constants which are determined empirically by fitting the Ramberg–Osgood equation to an experimental stress-strain curve. In fact, n is known as the hardening exponent and its value is unity for linear

elastic materials. It is greater than one for elastic-plastic materials (monotonically loaded). An elastic-perfectly plastic material is represented by $n = \infty$. For most of the commonly used metals, the value of n is in the range of 5–15.

The material constant F is much larger than E, and therefore the second term in the Ramberg–Osgood relation is negligible for small values of σ and then Eq. (6.10) behaves as a linear relation. As σ increases, the second term starts dominating, but the first term still contributes to the elastic strain. In fact, Eq. (6.10) can also be written as (Fig. 6.7):

$$\varepsilon = \varepsilon_e + \varepsilon_p$$

where

$$\varepsilon_e = \frac{\sigma}{E} \quad \text{and} \quad \varepsilon_p = \frac{\sigma^n}{F}$$

For large values of σ, the first term in Eq. (6.10) becomes small and can be neglected.

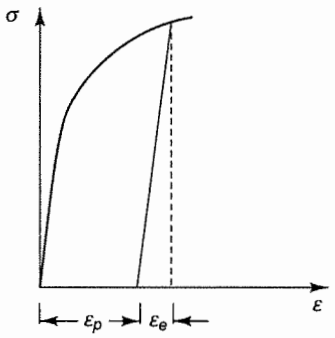

Fig. 6.7 Elastic strain ε_e and plastic strain ε_p

We should note that n which is an exponent is a dimensionless number, but F has the dimension of stress to the power n. Some countries still do not follow SI unit system. In fact, an advanced country where extensive experimental data are generated still follows FPS unit system. We should modify Eq. (6.10) from one system of units to another.

Example 6.2 An alloy steel is represented by the equation

$$\varepsilon = \frac{\sigma}{30,000} + \frac{\sigma^{6.8}}{2 \times 10^{12}}$$

where σ is given in ksi. Modify the equation for σ given in MPa.

Solution: In the given Ramberg–Osgood equation, the units of E and F are ksi and $\text{ksi}^{6.8}$ respectively. Using the equivalence relation of 1 ksi = 6.895 MPa , we modify E and F to:

$$E = 30,000 \times (6.895)^1 = 206.8 \times 10^3 \text{ MPa}$$

$$F = 2 \times 10^{12} \times (6.895)^{6.8} = 1.0 \times 10^{18} (\text{MPa})^{6.8}$$

Thus, the Ramberg–Osgood equation in SI units becomes:

$$\varepsilon = \frac{\sigma}{206.8 \times 10^3} + \frac{(\sigma)^{6.8}}{1.0 \times 10^{18}}$$

where σ is in MPa.

The material constants n and F are determined from an experimental stress-strain curve by first converting it into a relation between stress and plastic strain and then taking its logarithm. A straight line is fitted to the data, whose slope becomes n. If a straight line cannot be fitted to the experimental data, the material is not represented by a Ramberg–Osgood relation.

6.5 Further Discussion on J-Integral

6.5.1 From a Designer's Point of View

In the previous three sections, we have introduced the definition of the J-Integral and have discussed about some of its useful features, such as its path independence and its physical interpretation as an energy release rate for elastic materials. We also hinted that with a clever methodology, the J-Integral can be applied to elastic-plastic materials keeping the complexity of the problem under control; so much so, that it can be used by a practising engineer or a designer. How is this achieved?

Once a crack becomes critical and starts growing, most designers and engineers are not too much concerned about its further growth. To them, as soon as a crack starts propagating, the material is assumed to have failed. This is analogous to designers' attitude towards yielding. It is well known that most of the engineering materials (e.g., mild steel) deform considerably beyond yield stress before the final rupture takes place. Still a designer regards a component as failed as soon as any yielding initiates. Similarly, a designer looks at any kind of crack growth with panic feelings and he would try his best to avoid it. Thus, the designer is interested in predicting loads which are just about to propagate a crack; i.e., if the loads are increased by small amounts, the crack is likely to grow.

The fact remains that a designer is only interested in knowing the condition of *"onset of the crack growth"*. This condition is exploited when the J-Integral is applied to elastic-plastic materials. If we do not allow the growth of a crack, then we need not account for unloading. This simplifies the analysis considerably; elastic-plastic behavior is no longer different from the non-linear elastic behavior, as far as mathematical equations are concerned.

This idea sounds logical and rigorous, but there is a snag or a catch. Until we allow a crack to grow by a small distance, we would never know whether we are close to the condition at which the crack is just about to grow. In fact, while performing experiments to determine the critical value of the J-Integral, we do allow a small growth of the crack. And as soon as we allow the growth of the crack, the unloading is initiated and then the J-Integral approach is not rigorous anymore. Since better techniques are not available we compromise at this point. Initially, in the 1970s many investigators were very skeptical about the approach of the J-Integral. But based on further investigations and many experiments, we have realized that the compromise is acceptable.

6.5.2 Experiments to Determine the Critical J-Integral

Experiments to determine the critical J are designed in such a manner that a large amount of plastic deformation is allowed to occur near the crack tip. In fact, the plastic zone size may be as large as the crack length. This is in sharp contrast to experiments designed to find K_{Ic} or G_{Ic}, where the plastic zone size is controlled to remain small in comparison to the crack length.

Details of the experiments are presented in Chapter 8. However, it would be useful to discuss some salient features of the commonly used 3-point bend specimen, as shown in Fig. 6.8. The

uncracked ligament b is chosen to be approximately the same as the crack length a. The bending moment is maximum at the centre of the span, where the depth of the beam is considerably smaller than W. Consequently, stresses are very high in front of the crack tip, forming a plastic hinge and the rotation of the beam, as shown in the figure. It is to be noted here that in the rest of the beam, elastic deformation is small, owing to combined effect of larger depth and lower bending moment. Consequently, the deflection u is caused mainly by the plastic deformation at the crack tip. Thus, clever experimental techniques have been developed which account for the large plastic zone in the vicinity of the crack tip.

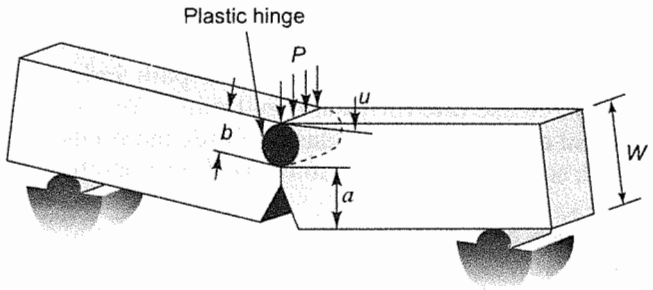

Fig. 6.8 Plastic hinge formed in the uncracked ligament b

6.5.3 Comments on the Numerical Evaluation of J-Integral

As stated earlier, the primary goal of a designer is to predict whether a crack in a component is likely to grow under the given loading conditions. He can either obtain the critical J value from literatures or he can conduct an experiment to determine it. Stress-strain relations, such as the Ramberg–Osgood relation describing the elastic-plastic material (only for monotonically increasing load) are also available to the designer. His task is to evaluate the J-Integral in an application knowing the constitutive relations, the loading conditions and, of course, the geometry of the component.

The J-Integral is generally evaluated through a numerical programme, most probably using a finite element method. With the availability of sophisticated computers, the task is not difficult. The designer may take the help of an expert in the field of FEM. These days standard packages are also available, which makes it simpler for a designer to determine the value of J. This is because the J-Integral is evaluated by integrating on an arbitrary path around the crack tip and we need not evaluate the strain or stress field very accurately near the crack tip. In fact, we can choose the integration path which is far away from the crack, thus avoiding the use of singular elements in the vicinity of the crack tip. Also, we do not require choosing a fine grid close to the crack tip and still maintain the calculations reasonably accurate. With the increasing acceptance of finite element methods and the availability of standard packages, the determination of J is no longer a prohibitively difficult task in research and development work of many industries.

6.5.4 Predicting Safety or Failure

The J-Integral may be determined through a numerical method, or it may also be obtained from a handbook. In an application, if the J value of a crack is less than the critical J-Integral (J_c), the design

is safe against any fracture failure. On the other hand, whenever J exceeds J_c the designer must modify his design, either by choosing a tougher material or changing the geometry of the component. For example, if the failure is predicted for a slot in a component, the length of the slot may be reduced. In other cases, the stress on the component may be decreased by changing the geometry, such as increasing the moment of inertia of the component. In some cases, the designer may not have the freedom to change the geometry and he may settle for lower limits on the external loads.

6.5.5 Comments on the Experimental Determination of the Toughness of Ductile Materials

The usage of the SIF method is mostly restricted to the LEFM, where the plastic zone is considerably smaller than the crack length. Experiments to determine the critical SIF are carefully designed to restrict the size of the plastic zone. This is done by making the specimen thick, so as to achieve plane strain conditions. Also, the lateral dimensions of the specimen are chosen reasonably large, so that a large portion of the specimen is under elastic deformation. Because the plastic zone of some tough materials is fairly large, the specimen size becomes accordingly larger, so much so that in certain cases the specimen size should be made of a plate as thick as 200 mm or more. A specimen of such thickness may also create many problems. First of all, the loads required to deform such a large specimen are enormously high and the test would require a machine of an extremely high capacity and also a high cost. Secondly, large amounts of the material will be required, which may have to be made specially of such thickness. Thirdly, the machining and handling cost of specimen will become rather steep. Because of these practical problems, Begley and Landes looked for alternative techniques in determining material toughness and suggested that the J-Integral provides more feasible and economical test-techniques for determining the toughness of ductile materials [6.5].

The J-Integral approach, on the other hand, allows the analysis of any elastic-plastic behavior of the material in the vicinity of the crack tip. Unlike the SIF methods, this approach does not limit the size of the plastic zone during the analysis, as the non-linear material behavior is incorporated. To determine the critical J-Integral, the specimens are designed in such a manner that there results a large amount of plastic deformation near the crack tip, so much so that the elastic deformation in the rest of the specimen may be neglected in many experiments. There is no need to make the specimen very large and the critical J value can be determined in a laboratory equipped with a normal loading machine, such as a 10 ton tensile machine.

In spite of several strong points in favor of the J-Integral approach, the SIF method is still surviving. Unlike the critical K whose values are listed in literature for commonly used engineering materials, the critical J is still not widely available in literature and handbooks. If a designer is adopting the J-Integral approach, he may have to pay for the experimental tests, which usually turn out to be rather expensive.

Moreover, it has been found that there is a large variation in the critical J value for ductile materials, due to its non-linear stress-strain behavior. For a small variation in the critical load, the corresponding variation in J_c is much larger. However, the large variation in J_c should not disturb us, because whenever a designer predicts loads for a maximum allowable J, the variation in the failure-load will be accordingly smaller. For example, two tests on the same material may give the critical J value with a large variation of 40% or so. When these results are used by a designer, maximum allowable load may vary only by 5%. There is nothing wrong in such an analysis, provided we realize that the large variation in the value of the critical J is normal.

6.6 Engineer Approach—A Short Cut

6.6.1 A Simplified Relation for the J-Integral

To minimize errors designers like to avoid making lengthy calculations and complex analysis. They would rather make use of the formulae available in handbook and plug numbers to get the answer. Therefore, natural question arises—can we prepare tables or handbooks that would avoid numerical analysis to determine J value of a crack?

The energy release rate in a linear elastic case can be expressed as:

$$G = \frac{\beta^2 K^2}{E} = \frac{\beta^2 \pi \sigma^2 a}{E} \tag{6.11}$$

where β accounts for the geometry of the crack and the component. For example, $\beta^2 = 1$ in a centre-cracked infinite plate, but for an edge crack, β^2 becomes 1.12. For other cases, β^2 may be taken from a handbook. Substituting $\varepsilon = \sigma / E$ in Eq. (6.11), we obtain:

$$G = \beta^2 \pi \sigma \varepsilon a \tag{6.12}$$

For materials following the Ramberg–Osgood relation, it has been realized that an expression [6.4] analogous to elastic cases [Eq. (6.12)] can be developed as:

$$J_p = H \sigma \varepsilon_p a \tag{6.13}$$

where ε_p is the plastic strain and H is a dimensionless factor that depends on geometry. Taking the plastic strain from Eq. (6.10) as $\varepsilon_p = \sigma^n / F$ and substituting the same in Eq. (6.13), we obtain:

$$J_p = \frac{H \sigma^{n+1} a}{F} \tag{6.14}$$

Then overall the J-Integral becomes:

$$J = \frac{\pi \beta^2 \sigma^2 a}{E} + \frac{H \sigma^{n+1} a}{F} \tag{6.15}$$

If handbooks/tables listing β^2 and H values are made available to a designer and material constants E, n and F are known, the designer can easily determine the values of J, thus minimizing the chances of making errors in computing J through a numerical analysis. In case, the value of σ is large, the second term in Eq. (6.15) dominates and we may ignore the effect of the elastic deformation.

Example 6.3 Determine the J-Integral for a component loaded in Mode I, with a far field stress of 200 MPa and an edge crack of 40 mm length. The geometrical factors are $\beta^2 = 1.12$ and $H = 7$; the material follows the Ramberg–Osgood relation with the material constants given as:

$$E = 207 \text{ GPa}, \; n = 6.8, \text{ and } F = 1 \times 10^{18} \text{ (MPa)}^{6.8}$$

Solution: Substituting the data in Eq. (6.15), we obtain:

$$J = \frac{\pi \times 1.12 \times (200 \times 10^6 \text{ Pa})^2 \times (0.04 \text{ m})}{(207 \times 10^9 \text{ Pa})} + \frac{7 \times [(200^{7.8} (\text{MPa})^{7.8}] \times (0.04 \text{ m})}{[1 \times 10^{18} (\text{MPa})^{6.8}]}$$

$$= 27.2 + 248.4 = 275.6 \text{ kJ/m}^2$$

Knowing the critical J-Integral (J_c) through experiments and using Eq. (6.15), a designer may like to determine the maximum allowable stress σ. The equation can be solved for σ through an iterative procedure by guessing its value in the first trial. The problem can be solved easily with the help of a digital computer. In case the elastic contribution is negligible, σ is directly obtained as:

$$\sigma_{max} = \left[\frac{EJ_c}{Ha}\right]^{1/(n+1)} \tag{6.16}$$

To study how $\Delta\sigma_{max}$ varies with ΔJ_c, we differentiate the equation and then divide it by σ_{max} to have:

$$\frac{\Delta\sigma_{max}}{\sigma_{max}} = \left(\frac{1}{n+1}\right)\frac{\Delta J_c}{J_c}$$

We note that usually n is significantly larger than one and therefore the percentage variation in σ_{max} is much less than the percentage variation in J_c.The above relation justifies the discussion presented in Sec. 6.5.6. We may look at the problem from a different angle. If J_c is to be determined experimentally, σ_{max} may easily vary by 5–10% from specimen to specimen. The variation in J_c will be about eight times larger if n is close to 7. Therefore, we conclude that large variation in the experimental values of J_c should not be seen with contempt; the variation in the predicted σ_{max} values would still be small.

6.6.2 Applications to Engineering Problems

For any application of the J-Integral to practical problems, the Ramberg–Osgood relation is written in a slightly different form [6.3] as:

$$\frac{\varepsilon}{\varepsilon_0} = \frac{\sigma}{\sigma_0} + \alpha\left[\frac{\sigma}{\sigma_o}\right]^n \tag{6.17}$$

This relation has four material constants (n, α, σ_0 and ε_0) in place of the three constants of Eq. (6.10). However, this form of the relation is better, because α is a dimensionless number. Since an equation expressed in another form cannot have more independent constants, there should be some relation between the four constants. In fact, σ_0 can be chosen anywhere on the elastic portion of the $\sigma - \varepsilon$ curve and the corresponding ε_0 is evaluated by the relation:

$$\sigma_0 = E\varepsilon_0 \tag{6.18}$$

Many investigators prefer to choose σ_0 as the yield stress (σ_{ys}) of the material. Realizing a relation exists between σ_0 and ε_0, we can compare Eq. (6.17) to Eq. (6.10) and obtain $F = \sigma_0^n / \varepsilon_0\alpha$.

Corresponding to Eq. (6.17), J_p is usually expressed as [6.6]:

$$J_p = \alpha\sigma_0\varepsilon_0 b g_1 h_1 \left(\frac{P}{P_0}\right)^{n+1} \tag{6.19}$$

where P is the applied load per unit thickness of plate, P_0 is the limit or collapsed load of the plate based on yield stress σ_{ys} ($=\sigma_0$), b is the uncracked ligament; and g_1 and h_1 are geometric factors which depend on a/W and n. Values of g_1 and h_1 are listed for some common practical applications in Appendix 6B, presented at the end of this chapter [6.3, 6.7].

For a centre-cracked plate shown in Fig. 6.9, P_0 depends on the collapse-load for the material yielding in the uncracked ligament b on each side, and is given by:

$$P_0 = 2b\sigma_0 \qquad \text{for plane stress}$$

$$P_0 = \frac{4}{\sqrt{3}} b\sigma_0 \qquad \text{for plane strain.}$$

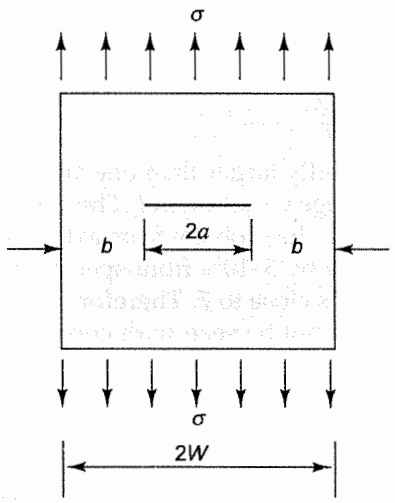

Fig. 6.9 Centre-cracked plate

Example 6.4 A centre-cracked panel of width $2W = 500$ mm and thickness $B = 20$ mm is pulled normal to the crack length ($2a = 100$ mm), with a far field stress σ. Estimate the maximum σ that can be applied without causing the growth of the crack if, $J_p = 400$ kJ/m^2. The material constants of the Ramberg–Osgood equation are known to be $n = 5$, $\alpha = 5.4$, σ_{ys} ($= \sigma_0$) = 520 MPa and $\varepsilon_0 = 0.00251$.

Solution: We would use the equation:

$$J_p = \alpha\, \sigma_0\, \varepsilon_0\, b\, g_1\, h_1 \left(\frac{P}{P_0}\right)^{n+1}$$

where,
$$b = \frac{(500 \text{ mm} - 100 \text{ mm})}{2} = 200 \text{ mm}$$

To find P_0, g_1 and h_1 through the tables of Appendix 6B, we should know whether the plate is subjected to plane strain or plane stress. At this stage, we start solving the problem, assuming that the plane strain conditions prevail. Once the maximum σ is determined, we can evaluate the plastic zone size and check the justification of our assumption.

From Appendix 6B, we obtain:

$$P_0 = \frac{4b\sigma_0}{\sqrt{3}} = \frac{4 \times (0.2 \text{ m}) \times (520 \times 10^6 \text{ Pa})}{\sqrt{3}} = 240 \times 10^6 \text{ N/m}$$

$$g_1 = \frac{a}{W} = \frac{50\,\text{mm}}{250\,\text{mm}} = 0.2$$

$$h_1 = 3.71$$

Substituting these values, we obtain:

$$\frac{P}{P_0} = \left[\frac{J_p}{\alpha\,\sigma_0\,\varepsilon_0\,b g_1\,h_1}\right]^{1/(n+1)}$$

$$= \left[\frac{(400\times10^3\,\text{J/m}^2)}{5.4\times(520\times10^6\,\text{Pa})\times0.00251\times(0.2\,\text{m})\times0.2\times3.71}\right]^{1/6}$$

$$= 0.852$$

which gives, $P = 0.852 \times (240 \times 10^6\ \text{N/m}) = 204.5 \times 10^6\ \text{N/m}$

$$\sigma = \frac{P}{2W} = \frac{204\times10^6\,\text{N/m}}{(0.5\,\text{m})} = 408\ \text{MPa}$$

We should now explore whether our initial assumptions regarding this problem as a case of plane strain were justified. Therefore, an estimate should be made on the plastic zone size. Earlier in Chapter 5, the Dugdale Approach was found to be handy, but in that case the material was taken to be elastic-perfectly plastic. With a hardening material, the plastic zone size (r_p) is obviously smaller, but the estimation of r_p is difficult. However, analysis of Mode III is simpler and r_p has been determined for a work-hardening material with the hardening exponent n. Based on its results, r_p of Mode I is estimated to be:

$$r_p = \frac{1}{\lambda\pi}\frac{(n-1)}{((n+1)}\frac{K_I^2}{\sigma_{ys}^2}$$

where, $\lambda = 1$ for plane stress, and $\lambda = 3$ for plane strain. K_I is evaluated on the basis of the actual crack length to keep the calculations simple, using the relation:

$$K_I = \sigma\sqrt{\pi a}\,f(\alpha)$$

where, $$\alpha = \frac{a}{W} = \frac{50\,\text{mm}}{250\,\text{mm}} = 0.2$$

$$f(\alpha) = 1.0 + 0.128\alpha - 0.288\alpha^2 + 1.523\alpha^3 = 1.026$$

Then, we have:

$$K_I = (408\ \text{MPa}) \times \pi^{1/2} \times (0.05\ \text{m})^{1/2} \times 1.026$$

$$= 165.9\ \text{MPa}\sqrt{m}$$

The plastic zone size for a plane strain is:

$$r_p \approx \frac{1}{3\pi}\times\frac{4}{6}\left(\frac{165.9\,\text{MPa}\sqrt{m}}{520\,\text{MPa}}\right)^2 = 7.20\,\text{mm}$$

The plastic zone size is only slightly smaller than the thickness of the plate. We should now redo the entire problem for the case of a plane stress:

$$P_0 = 2b\sigma_{ys}$$
$$= 2 \times (0.2 \text{ m}) \times (520 \times 10^6 \text{ Pa}) = 208 \times 10^6 \text{ N/m}$$
$$h_1 = 3.71$$
$$\frac{P}{P_0} = \left[\frac{400 \times 10^3 \text{ J/m}^2}{5.4 \times (520 \times 10^6 \text{ Pa}) \times 0.00251 \times 0.2 \times (0.2\text{m}) \times 3.71}\right]^{1/6} = 0.852$$
$$P = 0.852 \times 208 \times 10^6 = 177.2 \times 10^6 \text{ N/m}$$
$$\sigma = \frac{P}{2W} = \frac{177.2 \times 10^6}{0.5} = 354.4 \text{ MPa}$$

which gives the SIF as:

$$K_I = 354.4 \times \pi^{1/2} \times (0.05)^{1/2} \times 1.026 = 144 \text{ MPa}\sqrt{m}$$

The plastic zone size for plane stress is estimated to be:

$$r_p = \frac{1}{\pi}\frac{(n-1)}{(n+1)}\frac{K_I^2}{\sigma_{ys}^2} = \frac{1}{\pi} \times \frac{4}{6} \times \left(\frac{144 \text{ MPa}\sqrt{m}}{520 \text{ MPa}}\right)^2 = 16.27 \text{ mm}$$

This is close to the plate thickness (= 20 mm) and therefore the plane stress analysis is applicable.

Example 6.5 Consider an axially cracked pressured cylinder of steel (E = 207 GPa) with internal radius of 80 mm and wall thickness of 16 mm (Fig. 6.10). An axial crack of 3 mm depth has been identified on the inner surface of the cylinder. If the yield stress σ_0 of the material is 700 MPa, the hardening exponent $n = 7$, the material constant of Ramberg–Osgood relation $\alpha = 6.2$ and $J_p = 280$ J/m^2, determine the maximum pressure that the cylinder can resist against the crack growth.

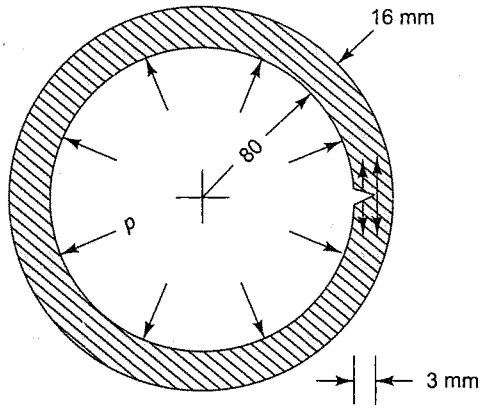

Fig. 6.10 Axially cracked pressurized cylinder

Solution:

$R_i = 80$ mm, $W = 16$ mm, $a = 3$ mm, $b = 13$ mm,

$R_c = 83$ mm, $a/W = 0.188$, $W/R_i = 1/5$ (Appendix 6B, Fig. 6.17)

$n = 7$, $\alpha = 6.2$

$$\sigma_{ys} = \sigma_0 = 700 \text{ MPa}, J_p = 280 \text{ kJ/m}^2$$

$$\varepsilon_0 = \sigma_0 / E = \frac{700}{207 \times 10^3} = 0.00338$$

From Appendix 6B, we obtain:

$$g_1 = \frac{a}{W} = 0.188$$

$$h_1 = 11.4$$

$$p_0 = \frac{2b\sigma_{ys}}{\sqrt{3}\, R_c} = \frac{2 \times (0.013\text{m} \times 700\text{MPa})}{\sqrt{3} \times (0.083\text{ m})} = 126.6\text{MPa}$$

Then, we have:

$$\frac{p}{p_0} = \left(\frac{J_p}{\alpha\, \sigma_0\, \varepsilon_0\, b g_1\, h_1} \right)^{1/(n+1)}$$

$$= \left(\frac{280 \times 10^3 \text{ J/m}^2}{6.2 \times (700 \times 10^6 \text{ Pa}) \times 0.00338 \times (0.013\text{m}) \times 0.188 \times 11.4} \right)^{1/8}$$

$$= 0.953$$

leading to $p = 0.953 \times 126.6 = 120.6$ MPa

6.7 Closure

The plastic zone size near the tip of a crack is large for tough materials, and parameters G and K of LEFM may not be suitable. Therefore, another parameter, the J-Integral has been developed that can also account for non-linear stress-strain behaviour of the plastic zone. Such analysis is known as (EPFM).

The J-Integral is an expression which remains path independent when integrated along a path from any point of a crack surface to any point of the other crack surface. When the J-Integral is applied to a linear elastic material, it is same as the energy release rate G.

To account for the elastic-plastic behavior, only a single constitutive relation is generally adopted. It has been found that the Ramberg–Osgood stress-strain relation can be employed for most engineering materials. At low stresses, the equation is almost linear, representing elastic deformation; at high stresses, the non-linear behavior dominates.

For checking whether a load is safe on a component, the J-Integral can be evaluated either through numerical analyses or by using tables from a handbook. If the value of J of a crack is less than the critical J_c, the material is safe against any crack growth.

The experimental procedure to determine the value of J_{Ic} is described in Chapter 8. It is worth mentioning that the plate thickness of a specimen for finding K_{Ic} is large and impractical for materials with the large plastic zone, because plane strain conditions must be created. On the contrary, a test specimen to determine J_{Ic} allows a large plastic zone at the crack tip and the specimen thickness does not necessarily have to be large.

APPENDIX 6A

Equivalence of G and J for Elastic Materials

It would be proved that for plane bodies, made of linear elastic materials, the expression of the J-Integral is equivalent to G. Consider the general case of a plane body of area A with no body forces. The contour of this body is represented with a curve Γ_0, which is split into two parts: Γ_T, where traction is prescribed and Γ_u, on which displacement conditions are given (Fig. 6.11). Note that the free surface belongs to Γ_T. Potential energy Φ is then given by:

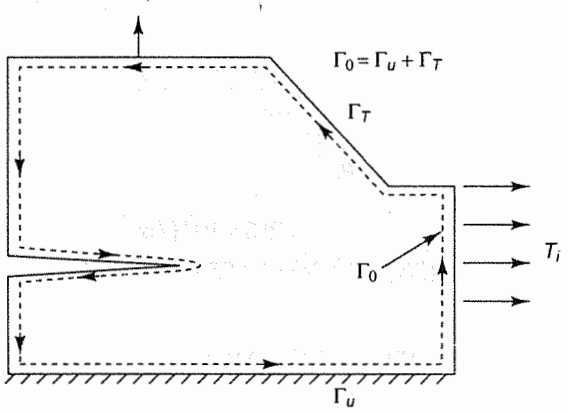

Fig. 6.11 Path Γ_0 chosen to coincide with the body contour and cracked surfaces

$$\Phi = \int_A W dA - \int_{\Gamma_T} T_i u_i \, ds$$

Leading to,

$$G = -\frac{d\Phi}{da} = -\int_A \frac{dW}{da} dA + \int_{\Gamma_T} T_i \frac{du_i}{da} ds \tag{6.20}$$

Transforming the origin to the crack tip by the relation,

$$X_1 = x_1 - a \tag{6.21}$$

we obtain:

$$\frac{d}{da} = \frac{\partial}{\partial a} + \frac{\partial X_1}{\partial a} \frac{\partial}{\partial X_1}$$

From Eq. (6.21), we have:

$$\frac{\partial X_1}{\partial a} = -1; \text{and } \frac{\partial}{\partial X_1} = \frac{\partial}{\partial x_1}$$

Then, the differentiation relation simplifies to:

$$\frac{d}{da} = \frac{\partial}{\partial a} - \frac{\partial}{\partial x_1}$$

Operating it on Eq. (6.20), we obtain:

$$G = -\int_A \frac{\partial W}{\partial a} dA + \int_A \frac{\partial W}{\partial x_1} dA + \int_{\Gamma_T} T_i \frac{\partial u_i}{\partial a} ds - \int_{\Gamma_T} T_i \frac{\partial u_i}{\partial x_1} ds \tag{6.22a}$$

But the integrand of the first term is modified as follows:

$$\frac{\partial W}{\partial a} = \frac{\partial W}{\partial \varepsilon_{ij}} \frac{\partial \varepsilon_{ij}}{\partial a} = \frac{1}{2} \sigma_{ij} \frac{\partial (u_{i,j} + u_{j,i})}{\partial a}$$

Making use of the symmetry of stress tensor $(\sigma_{ij} = \sigma_{ji})$, we obtain:

$$\frac{\partial W}{\partial a} = \sigma_{ij} \frac{\partial (u_{i,j})}{\partial a} = \sigma_{ij} \left(\frac{\partial u_i}{\partial a} \right)_{i,j} \tag{6.22b}$$

Invoking the principle of virtual work, we have:

$$\int_{\Gamma_T} T_i \frac{\partial u_i}{\partial a} ds = \int_A \sigma_{ij} \left[\frac{\partial u_i}{\partial a} \right]_{i,j} dA \tag{6.22c}$$

Substituting Eqs (6.22b) and (6.22c) in Eq. (6.22a), we obtain (note $\partial u_i = 0$ *on* Γ_u and therefore $\Gamma_T \to \Gamma_0$)

$$G = \int_A \frac{\partial W}{\partial x_1} dA - \int_{\Gamma_0} T_i \frac{\partial u}{\partial x_1} ds \tag{6.23}$$

The first term can now be converted into the line integral by invoking the Divergence Theorem, for which closed contour Γ_0 is chosen to coincide with the body contour and the crack faces as shown with the dashed line in Fig. 6.11. Although the singularity of the crack tip lies on the path Γ_0, it is not serious for the first term of Eq. (6.23). For small values of r, strain energy density W varies, as $1/r$ because it is a product of stress and strain, each varying as $1/\sqrt{r}$. Therefore, dW/dx_1 varies as $1/r$, but dA varies a r^2 and thus the singularity is nullified when $r \to 0$. Then, the divergence theorem modifies Eq. (6.23) to:

$$G = \int_{\Gamma_0} W n_1 ds - \int_{\Gamma_0} T_i \frac{\partial u_i}{\partial x_1} ds$$

The contour Γ_0 can be split into two parts,

$$\Gamma_0 = \Gamma + \Gamma_c$$

where Γ_c is the portion on the crack surfaces and Γ is the usual integration path of the J-Integral (from one crack surface to another). Also, it is worth noting that on Γ_c path $dx_2 \approx 0$ and $T_i = 0$. By noting $n_1 ds = dx_2$ [Fig. 6.4(b)], the above equation is thus simplified to:

$$G = \int_\Gamma W dx_2 - \int_\Gamma T_i \frac{\partial u_i}{\partial x_1} ds$$

The right hand side has the expression of J, which is path independent, and therefore,

$$G = J$$

Thus, for linear elastic materials, the expression of the J-Integral is equivalent to G.

APPENDIX 6B

The J-Integral of Some Common Cases through Engineering Approach

For the engineering approach (Sec. 6.6), J_p is defined as $J_p = \alpha\sigma_0\varepsilon_0 b g_1 h_1 (P/P_0)^{n+1}$. In this appendix, the expressions for the geometric factor g_1 and collapse load P_0 are given, and the geometric factor h_1 is listed for plane stress ($p - \sigma$) and plane strain ($p - \varepsilon$) for some commonly encountered cases. Usually, σ_0 is chosen to be same as yield stress (σ_{ys}).

6B.1 Three-Point Bend Specimen

The specimen is loaded with force P per unit thickness, as shown in Fig. 6.12.

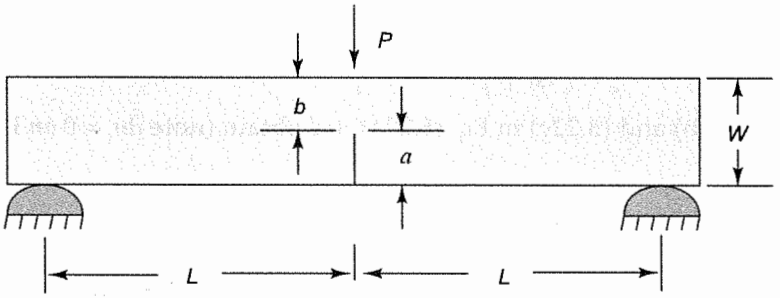

Fig. 6.12 Three-point bend specimen

$P_0 = 0.728\ \sigma_{ys}\ b^2/L$ for plane strain
$P_0 = 0.536\ \sigma_{ys}\ b^2/L$ for plane stress
$g_1 = 1$, and h_1 = listed in Table 6.1 for $L/W = 2$.

Table 6.1 h_1 for three-point bend specimen

a/W	Type	n								
		1	2	3	5	7	10	13	16	20
1/8	p-ε	0.937	0.869	0.805	0.687	0.580	0.437	0.329	0.245	0.165
	p-σ	0.676	0.600	0.548	0.459	0.383	0.297	0.238	0.192	0.148
1/4	p-ε	1.20	1.034	0.930	0.762	0.633	0.523	0.396	0.304	0.215
	p-σ	0.869	0.731	0.629	0.479	0.370	0.246	0.174	0.117	0.0593
3/8	p-ε	1.33	1.15	1.02	0.846	0.695	0.556	0.442	0.360	0.265
	p-σ	0.963	0.797	0.680	0.527	0.418	0.307	0.232	0.174	0.105
1/2	p-ε	1.41	1.09	0.922	0.675	0.495	0.331	0.211	0.135	0.0741
	p-σ	1 .02	0.767	0.621	0.453	0.324	0.202	0.128	0.0813	0.0298
5/8	p-ε	1.46	1.07	0.896	0.631	0.436	0.255	0.142	0.084	0.411
	p-σ	1.05	0.786	0.649	0.494	0.357	0.235	0.173	0.105	0.471
3/4	p-ε	1.48	1.15	0.974	0.693	0.500	0.348	0.223	0.140	0.0745
	p-σ	1.07	0.786	0.643	0.474	0.343	0.230	0.167	0.110	0.0442

6B.2 Centre-Cracked Plate

The plate is pulled by the load P per unit thickness, as shown in Fig. 6.13.

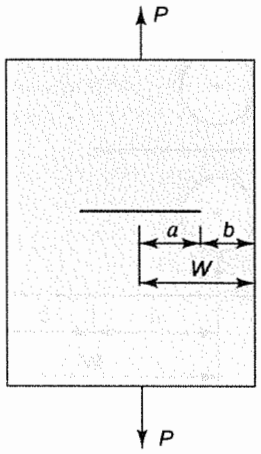

Fig. 6.13 A centre-cracked plate

$P_0 = 4b\ \sigma_{ys} / \sqrt{3}$ for plane strain

$P = 2b\ \sigma_{ys}$ for plane stress

$g_1 = a/W$

h_1 = (Listed in Table 6.2)

Table 6.2 h_1 for centre cracked plate

a/W	Type	n								
		1	2	3	5	7	10	13	16	20
1/8	p-ε	2.80	3.61	4.06	4.35	4.33	4.02	3.56	3.06	2.46
	p-σ	2.80	3.58	4.01	4.47	4.65	4.62	4.41	4.13	3.72
1/4	p-ε	2.54	3.01	3.21	3.29	3.18	2.92	2.63	2.34	2.03
	p-σ	2.54	2.97	3.14	3.20	3.11	2.86	2.65	2.47	2.20
3/8	p-ε	2.34	2.62	2.65	2.51	2.28	1.97	1.71	1.46	1.19
	p-σ	2.34	2.53	2.52	2.35	2.17	1.95	1.77	1.61	1.43
1/2	p-ε	2.21	2.29	2.20	1.97	1.76	1.52	1.32	1.16	0.978
	p-σ	2.21	2.20	2.06	1.81	1.63	1.43	1.30	1.17	1.00
5/8	p-ε	2.12	1.96	1.76	1.43	1.17	0.863	0.628	0.458	0.300
	p-σ	2.12	1.91	1.69	1.41	1.22	1.01	0.853	0.712	0.573
3/4	p-ε	2.07	1.73	1.47	1.11	0.895	0.642	0.461	0.337	0.216
	p-σ	2.07	1.71	1.46	1.21	1.08	0.867	0.745	0.647	0.532

6B.3 Compact Tension Specimen

The standard compact tension specimen is pulled by the force P, as shown in Fig. 6.14.

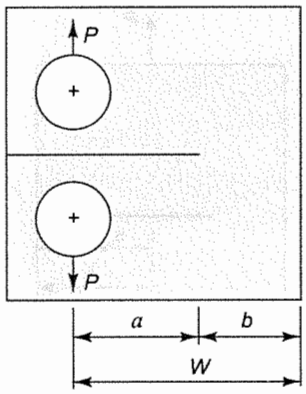

Fig. 6.14 Compact tension specimen

$P_0 = 1.455\ \beta\, b\ \sigma_{ys}$ for plane strain

$P_0 = 1.071\ \beta\, b\ \sigma_{ys}$ for plane stress

$g_1 = 1$

h_1 = (Listed in Table 6.3)

$\beta = [(2a/b)^2 + 4a/b + 2]^{1/2} - 2a/b - 1$.

Table 6.3 h_1 for compact tension specimen

a/W	Type	n								
		1	2	3	5	7	10	13	16	20
1/4	p-ε	2.23	2.05	1.78	1.48	1.33	1.26	1.25	1.32	1.57
	p-σ	1.61	1.47	1.28	1.06	0.903	0.729	0.601	0.511	0.395
3/8	p-ε	2.15	1.72	1.39	0.970	0.693	0.443	0.276	0.176	0.098
	p-σ	1.55	1.25	1.05	0.801	0.647	0.484	0.377	0.284	0.220
1/2	p-ε	1.94	1.51	1.24	0.919	0.685	0.461	0.314	0.216	0.132
	p-σ	1.40	1.08	0.901	0.686	0.558	0.436	0.356	0.298	0.239
5/8	p-ε	1.76	1.45	1.24	0.974	0.752	0.602	0.459	0.347	0.248
	p-σ	1 .27	1.03	0.875	0.695	0.593	0.494	0.423	0.370	0.310
3/4	p-ε	1.71	1.42	1.26	1.03	0.864	0.717	0.575	0.448	0.345
	p-σ	1.23	0.977	0.833	0.683	0.598	0.506	0.431	0.373	0.314

6B.4 Single-edge Notched Plate

The plate with an edge crack is pulled by far field stress $\sigma (= P/W)$ as shown in Fig. 6.15.

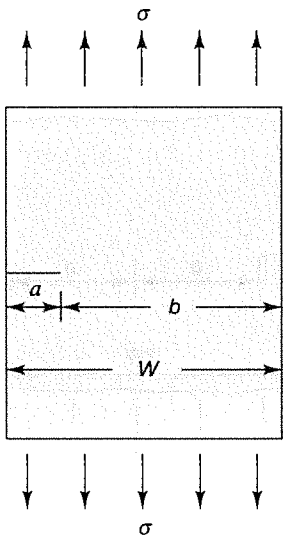

Fig. 6.15 Single-edge-notched plate

$P_0 = 1.455\ \beta b\ \sigma_{ys}$ for plane strain

$P_0 = 1.072\ \beta b\ \sigma_{ys}$ for plane stress

$g_1 = a/W$

h_1 = (Listed in Table 6.4)

$\beta = [\ 1+(a/b)^2]^{1/2} - a/b$

Table 6.4 h_1 for single-edge-notched plate

a/W	Type	n								
		1	2	3	5	7	10	13	16	20
1/8	p-ε	4.95	6.93	8.57	11.5	13.5	16.1	18.1	19.9	21.2
	p-σ	3.58	4.55	5.06	5.30	4.96	4.14	3.29	2.60	1.92
1/4	p-ε	4.34	4.77	4.64	3.82	3.06	2.17	1.55	1.11	0.712
	p-σ	3.14	3.26	2.92	2.12	1.53	0.960	0.615	0.400	0.230
3/8	p-ε	3.88	3.25	2.63	1.68	1.08	0.539	0.276	0.142	0.0595
	p-σ	2.81	2.37	1.94	1.37	1.01	0.677	0.474	0.342	0.226
1/2	p-ε	3.40	2.30	1.69	0.928	0.514	0.213	0.090	0.0385	0.0119
	p-σ	2.46	1.67	1.25	0.776	0.510	0.286	0.164	0.0956	0.0469
5/8	p-ε	2.86	1.80	1.30	0.697	0.378	0.153	0.0625	0.0256	0.0078
	p-σ	2.07	1.41	1.106	0.755	0.551	0.363	0.248	0.172	0.107
3/4	p-ε	2.34	1.61	1.25	0.769	0.477	0.233	0.116	0.059	0.0215
	p-σ	1.70	1.14	0.910	0.624	0.447	0.280	0.181	0.118	0.0670

6B.5 Double-Edge Notched Plate

The double-edge notched plate is pulled by far field stress σ (= $P/2W$), as shown in Fig. 6.16.

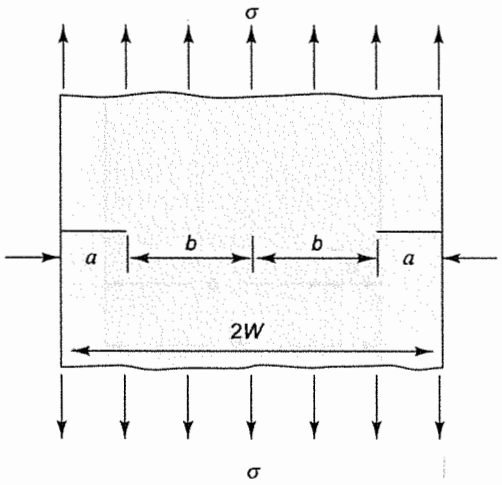

Fig. 6.16 Double-edge-notched plate

$P_0 = (0.72W + 1.82b)\ \sigma_{ys}$ for plane strain

$P_0 = 4b\ \sigma_{ys}/\sqrt{3}$ for plane stress

$g_1 = 1$

h_1 = (Listed in Table 6.5)

Table 6.5 h_1 for double-edge-notched plate

a/W	Type	n								
		1	2	3	5	7	10	13	16	20
1/8	p-ε	0.572	0.772	0.922	1.13	1.35	1.61	1.86	2.08	2.44
	p-σ	0.583	0.825	1.02	1.37	1.71	2.24	2.84	3.54	4.62
1/4	p-ε	1.10	1.32	1.38	1.65	1.75	1.82	1.86	1.89	1.92
	p-σ	1.01	1.23	1.36	1.48	1.54	1.58	1.59	1.59	1.59
3/8	p-ε	1.61	1.83	1.92	1.92	1.84	1.68	1.49	1.32	1.12
	p-σ	1.29	1.42	1.43	1.34	1.24	1.09	0.970	0.873	0.674
1/2	p-ε	2.22	2.43	2.48	2.43	2.32	2.12	1.91	1.60	1.51
	p-σ	1.48	1.47	1.38	1.17	1.01	0.845	0.732	0.625	0.208
5/8	p-ε	3.16	3.38	3.45	3.42	3.28	3.00	2.54	2.36	2.27
	p-σ	1.59	1.45	1.29	1.04	0.882	0.737	0.649	0.466	0.020
3/4	p-ε	5.24	6.29	7.17	8.44	9.46	10.9	11.9	11.3	17.4
	p-σ	1.65	1.43	1.22	0.979	0.834	0.701	0.630	0.297	

6B.6 Axially Cracked Pressurized Cylinder

Pressurized cylinders are commonly used in industries; a crack along the axial direction may grow under pressure p_o, as shown in Fig. 6.17.

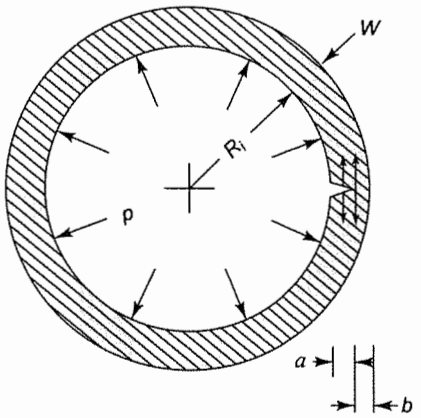

Fig. 6.17 Axial crack in a pressurized cylinder

$p_0 = 2b\,\sigma_{ys}\,/(\sqrt{3}\;R_c)$

$g_1 = a/W$

h_1 = (Listed in Table 6.6)

$R_c = (R_i + a)$.

Table 6.6 h_1 for internally pressurized cylinder with axial crack

a/W	W/R_i	n					
		1	2	3	5	7	10
1/8	1/5	6.32	7.93	9.32	11.5	13.1	14.9
	1/10	5.22	6.64	7.59	8.76	9.34	9.55
	1/20	4.50	5.79	6.62	7.65	8.07	7.75
1/4	1/5	7.00	8.34	9.03	9.59	9.71	9.45
	1/10	6.16	7.49	7.96	8.08	7.78	6.98
	1/20	5.57	6.91	7.37	7.47	7.21	6.53
1/2	1/5	9.79	10.4	9.07	5.61	3.52	2.11
	1/10	10.5	11.6	10.7	6.47	3.95	2.27
	1/20	10.8	12.8	12.8	8.16	4.88	2.62
3/4	1/5	11.00	5.54	2.84	1.24	0.83	0.493
	1/10	16.1	8.19	3.87	1.46	1.05	0.787
	1/20	23.1	13.1	5.87	1.90	1.23	0.883

6B.7 Circumferentially Cracked Cylinder

Figure 6.18 shows the cylinder subjected to an axial load P, with a circumferential crack on the inside surface of depth a. The far field axial stress for this case is $\sigma = P/(\pi(R_0^2 - R_i^2))$.

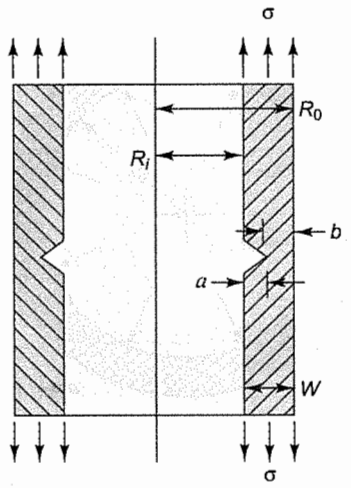

Fig. 6.18 Circumferentially cracked cylinder

$P_0 = 2\,\pi\,\sigma_{ys}\,(R_0^2 - R_c^2)/\sqrt{3}$

$g_1 = a/W$

h_1 = (Listed in Table 6.7)

$R_c = R_i + a$

Table 6.7 Value of h_1 for circumferentially cracked cylinder

a/W	W/R_i	n					
		1	2	3	5	7	10
1/8	1/5	3.78	5.00	5.94	7.54	8.99	11.1
	1/10	4.00	5.13	6.09	7.69	9.09	11.1
	1/20	4.04	5.23	6.62	7.82	9.19	11.1
1/4	1/5	3.88	4.95	5.64	6.49	6.94	7.22
	1/10	4.17	5.35	6.09	6.93	7.30	7.41
	1/20	4.38	5.68	6.45	7.29	7.62	7.65
1/2	1/5	4.40	4.78	4.59	3.79	3.07	2.34
	1/10	5.40	5.90	5.63	4.51	3.49	2.47
	1/20	6.55	7.17	6.89	5.46	4.13	2.77
3/4	1/5	4.12	3.03	2.23	1.55	1.30	1.11
	1/10	5.18	3.78	2.57	1.59	1.31	1.10
	1/20	6.64	4.87	3.08	1.68	1.30	1.07

QUESTIONS

1. Why is the numerical evaluation of J_I usually simpler than the evaluation of G_I or K_I, in the case of the LEFM?
2. Path independence of the J-Integral is not valid for elastic-plastic materials. Why?
3. If path independence is not valid for elastic-plastic materials, how can we apply it to real life cases dealing with large plastic zone in the vicinity of the crack tip?
4. Although a variation is found to be large in an experimentally determined J_{Ic}, it is acceptable for design purposes. Justify.
5. Why is the Ramberg-Osgood relation convenient for determining the J-Integral for elastic-plastic materials?
6. Why are the specimens very thick to determine the value of K_{Ic} of ductile materials?
7. Unlike the case of K_{Ic}-test, the specimen recommended for finding the critical J-Integral need not be thick for ductile materials. Why?

PROBLEMS

1. Consider an infinitely long strip with an edge-crack of length a. The lower surface of the strip is bonded to a rigid surface and the upper surface to a rigid rail as shown in Fig. 6.19.

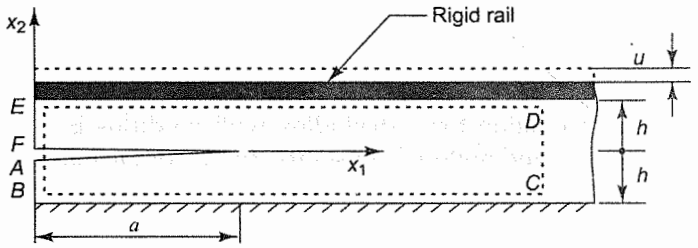

Fig. 6.19 The figure of Problem 1

If the rail is displaced in the x_2 direction by distance u, determine J_I (and then K_I) by choosing a convenient path. Consider plane stress and plane strain cases separately. Note that:
(a) Path *ABCDEF* is so chosen that points *C* and *D* are quite far away from the crack tip,
(b) The variation of the displacement field with x_1 is zero, and
(c) On segment *CD*,

Plane stress: $\sigma_{11} \neq 0,\ \sigma_{22} \neq 0,\ \sigma_{33} = 0,\ \varepsilon_{11} = 0,\ \varepsilon_{22} \neq 0,\ \varepsilon_{33} \neq 0;$

Plane strain: $\varepsilon_{11} = 0,\ \varepsilon_{22} \neq 0,\ \varepsilon_{33} = 0,\ \sigma_{11} \neq 0,\ \sigma_{22} \neq 0,\ \sigma_{33} \neq 0$

2. Consider two infinitely long strips of thickness h_1 and h_2 with material properties as shown in Fig. 6.20. These strips are bonded together with an edge-crack of length a. The strips are wide enough to assume plane strain conditions. The lower face of the bottom strip is bonded to a rigid surface, while the top surface of the upper strip is bonded to a rigid rail. Determine the J-Integral, if the rail is pulled up by distance u. (Note: At the interface $(\sigma_{22}^{(1)} = \sigma_{22}^{(2)}$ but $\varepsilon_{22}^{(1)} \neq \varepsilon_{22}^{(2)}.)$

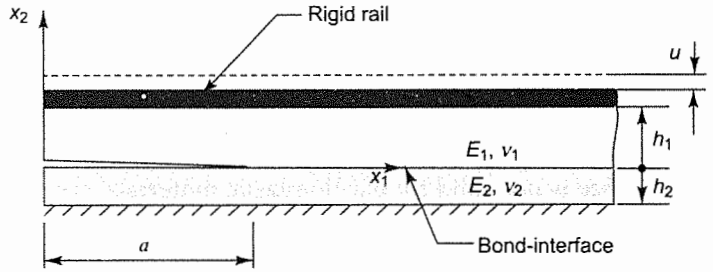

Fig. 6.20 The figure of Problem 2

3. Same as Problem 1, with a difference that the top rail is moved by a distance w in the x_3 direction.
4. Consider a *DCB* specimen made by bonding two infinitely long strips as shown in Fig. 6.21. Determine J_1 if the ends of cantilevers are loaded with moments M.

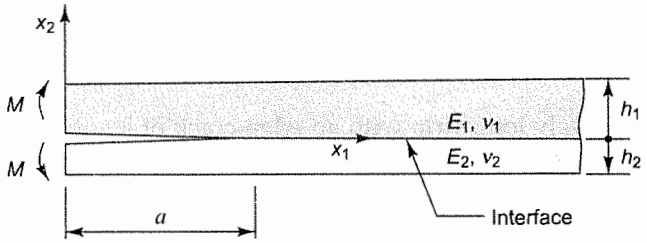

Fig. 6.21 The figure of Problem 4

5. Stress-strain relation for a steel alloy with modulus E = 207 GPa is shown in Fig. 6.22. Determine σ_{ys}, and material constants α and n of the Ramberg–Osgood equation.

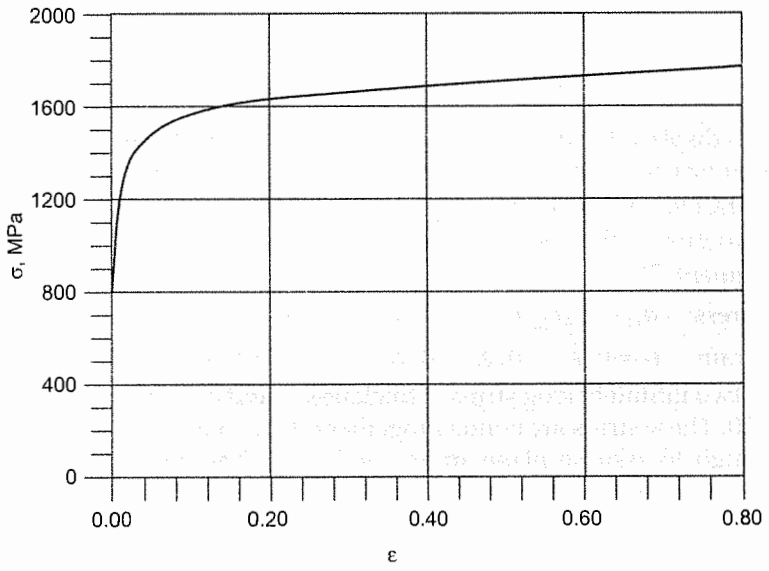

Fig. 6.22 The figure of Problem 5

6. Consider a three-point bend specimen with a centre load as shown in Fig. 6.23. The material properties for the Ramberg-Osgood relation are:

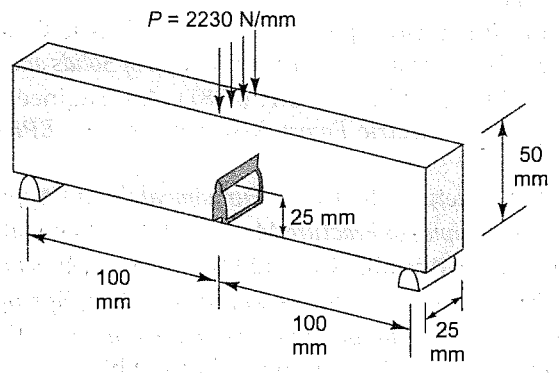

Fig. 6.23 The figure of Problem 6

$$\sigma_{ys} = \sigma_0 = 700 \text{ MPa}, \varepsilon_0 = \sigma_0/E$$
$$E = 207 \text{ GPa}, \alpha = 8.2, n = 6$$

(a) Determine K_I
(b) Estimate the plastic zone size
(c) Determine G_I based on the LEFM
(d) Determine J_p using the engineering approach.

7. Consider a circumferentially cracked cylinder of 240 mm internal radius, 24 mm wall thickness and 3 mm long crack all around the circumference (Fig. 6.18). The material follows the Ramberg-Osgood equation with the following material constants:

$$\sigma_{ys} = \sigma_0 = 800 \text{ MPa}, \varepsilon_0 = \sigma_0/E$$
$$E = 207 \text{ GPa}, \alpha = 8.6, n = 3.$$

The cylinder is subjected to axial tension. If $J_p = 150$ kJ/m^2, determine the maximum axial tensile stress. Neglect J_e.

8. Determine the maximum tensile stress for the cylinder of Problem No. 7 when the wall thickness and crack length are changed to 8 mm and 2 mm respectively. All other dimensions and material properties remain the same.

REFERENCES

6.1 Chakrabarty, J. (1987). *Theory of Plasticity*, McGraw-Hill Book Company, New York.
6.2 Rice, J.R. (1968). A Path Independent Integral and Approximate Analysis of Strain Concentrations by Notches and Cracks, *Journal of Applied Mechanics*, 35, pp. 379–386.
6.3 Kanninen M.F. and Popelar, C.H. (1985), *Advanced Fracture Mechanics*, Oxford University Press, New York.
6.4 Broek, David (1988). *The Practical Use of Fracture Mechanics*, Kluwer Academic Publishers, Dordrecht.

6.5 Begley, J.A. and Landes, J.D. (1972). The J-Integral as a Fracture Criterion, Fracture Toughness, p1. Part II, ASTM STP 514, *American Society for Testing and Materials*, Philadelphia, pp. 1–20.

6.6 Goldman, N.L. and Hutchinson, J.W. (1975), Fully Plastic Crack Problems: The Centre-Cracked Strip under Plane Strain, *International Journal of Solids and Structures*, 11, pp. 575–591.

6.7 Kumar, V., German, M.D., and Shih, C.F. (1981). An Engineering Approach for Elastic-Plastic Fracture Analysis, *Electric Power Research Institute EPRI NP-1931, Project 1287-1, Topical Report.*

6.8 Anderson, T.L. (2004). *Fracture Mechanics: Fundamentals and Applications*, CRC, Press-Book.

6.9 Sanford, R.J. (2003). *Principles of Fracture Mechanics*, Prentice Hall, Upper Saddle River.

6.10 Janssen, M., Zuidema, J. & Wanhill, R.J.H. (2004). *Fracture Mechanics*, Spon Press, Abingdon.

6.11 Gdoutos, E.E. (2005). *Fracture Mechanics—An Introduction*, Springer, The Netherland.

6.12 Ramesh, K. (2007). *e-Book on Engineering Fracture Mechanics*, IIT Madras, URL: http//apm.iitm.ac.in/smlab/kramesh/book_4.htm

Chapter

7

Crack Tip Opening Displacement

If I don't get there headed straight, may be I get there by zig zagging or jumping over the problem.

Dr Nathan Kline

7.1 Introduction

Crack tip opening displacement (*CTOD*) is another parameter suitable to characterize a crack. Unlike parameters G and K, it can be used for both linear elastic fracture mechanics (LEFM) and elastic-plastic fracture mechanics (EPFM). It was formulated by Wells [7.1, 7.2] and Cottrell [7.3] and became more popular in Europe, at least in the initial stages. In fact, the parameter was formulated about a decade before it was realized that the J-Integral could be used for EPFM. How is *CTOD* defined?

The material cannot withstand very high stresses within the plastic zone, and the usual stress field of the square root singularity no longer exists. However, rigorous analysis is complex and we would like to explore a simple model. The yielding of the material and resulting rearrangement of the stresses around the crack tip can be accounted by an effective crack, which is longer than the actual crack as discussed in Chapter 5. The tip of the effective crack is located inside the plastic zone (Fig. 7.1). Now, the linear equations of elasticity can be applied to the effective crack. One can

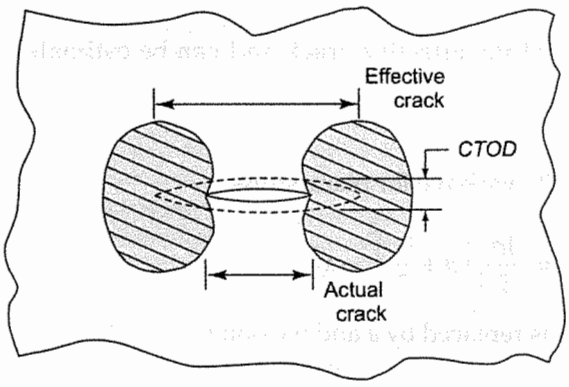

Fig. 7.1 The effective crack and *CTOD*

then visualize that the effective crack has some finite opening at the location of the actual crack tip. The opening is defined as the crack tip opening displacement as shown in Fig. 7.1.

In reality, there is hardly any opening of the crack tip; only the tip may become more rounded as the plastic deformation increases. Thus, the definition of the *CTOD* is based on a model that a beginner may find a bit difficult to accept. Further, the symbol for a crack tip opening displacement is still not standardized. Some people use the symbol δ, while others call it *COD* (crack opening displacement). However, the term '*COD*' is found ambiguous, because at any location of the crack, the opening is called a crack opening displacement. Therefore, we will be using *CTOD* as the parameter and $CTOD_c$, as its critical value.

The *CTOD* parameter has been found more useful for cracks having large plastic zones. Like the J-Integral, the *CTOD* is another approach to deal with elastic-plastic fracture mechanics (EPFM). However, in the next section, we will explore equivalent relations between *K*, *G* and *CTOD* for cracks with small plastic zone (LEFM).

7.2 Relationship Between CTOD, K_I and G_I for Small Scale Yielding

In this section, we will prove that for small scale yielding in the vicinity of the crack tip

$$CTOD = \frac{K_I^2}{\lambda E \sigma_{ys}} \tag{7.1}$$

where λ is a constant and its value is close to unity. In fact, its value depends on the plastic zone and, therefore, λ is influenced by the model chosen for determining the plastic zone size. Since $G_I = K_I^2/E$ for plane stress, we can express *CTOD* in terms of the relation

$$CTOD = \frac{G}{\lambda \sigma_{ys}}. \tag{7.2}$$

For deriving Eq. (7.1), we will use the expression of crack opening displacement of Mode I, developed in Chapter 3 [Eq. (3.35)]. Thus, at distance of x_1, *COD* becomes:

$$COD = \frac{4\sigma}{E}\sqrt{a_{\text{eff}}^2 - x_1^2} \quad \text{for plane stress} \tag{7.3}$$

$$COD = \frac{4\sigma(1-\nu^2)}{E}\sqrt{a_{\text{eff}}^2 - x_1^2} \quad \text{for plane strain}$$

where, a_{eff} is the length of the effective crack and can be estimated using Irwin's correction [Eq. (5.9)] as

$$a_{\text{eff}} = a + \frac{r_p}{2}. \tag{7.4}$$

Substituting a_{eff} in Eq. (7.3), we have for plane stress

$$COD = \frac{4\sigma}{E}\left[\left(a + \frac{r_p}{2}\right)^2 - x_1^2\right]^{1/2}$$

For evaluating *CTOD*, x_1 is replaced by a and we obtain

$$CTOD = \frac{4\sigma}{E}\left[\frac{r_p}{4}\left(4a + r_p\right)\right]^{1/2}$$

For LEFM, r_p may be neglected in comparison to $4a$ and the expression simplifies to

$$CTOD = \frac{4\sigma}{E}\sqrt{ar_p}$$

where r_p is given by Eq. (5.8)

$$r_p = \frac{K_I^2}{\pi\sigma_{ys}^2}.$$

K_I in this expression is based on a_{eff}. In the case of small scale yielding considered in this section, the approximate relation is used by determining K_I on the actual crack length a. Then, the *CTOD* is expressed as

$$CTOD = \frac{4\sigma}{E}\sqrt{a\left(\frac{\sigma^2\pi\, a}{\pi\,\sigma_{ys}^2}\right)} = \frac{4\sigma^2 a}{E\sigma_{ys}}.$$

This expression can be restated by using $K_I = \sigma\sqrt{\pi a}$ as

$$CTOD = \frac{4K_I^2}{\pi\, E\sigma_{ys}}.$$

If the Dugdale approach is used, it can be shown that

$$CTOD = \frac{K_I^2}{E\sigma_{ys}} = \frac{G_I}{\sigma_{ys}}.$$

Thus, the equivalence relations depend upon the model adopted for finding the effective crack length. Also, the relations depend upon the hardening parameter of work hardening materials. The value of λ in Eq. (7.1) can vary between and $\pi/4$ and 2.2. However, direct experimental methods find that λ is closer to unity (through optical methods [7.4] and the metallographic sectioning of the crack tip filled with a plastic [7.5]).

7.3 Equivalence Between *CTOD* and J

Both the *CTOD* and the J-Integral characterize elastic-plastic fracture and, therefore, a relation should exist between them. Consider a crack of actual length a and an effective crack of length a_{eff} (Fig. 7.2), whose crack tip is located at point B. Figure 7.2 shows *CTOD* as the distance AC. An appropriate integration path *ABC* is chosen for determining the J-Integral which is restated as

$$J = \int_{\Gamma}\left(Wdx_2 - T_i\frac{\partial u_i}{\partial x_1}ds\right).$$

Along the integration path, dx_2 is negligibly small, making the first term of J negligible. If the material is considered to be elastic-perfectly plastic, $T_2 = \sigma_{ys}$ on the integration path Γ, then, J simplifies to

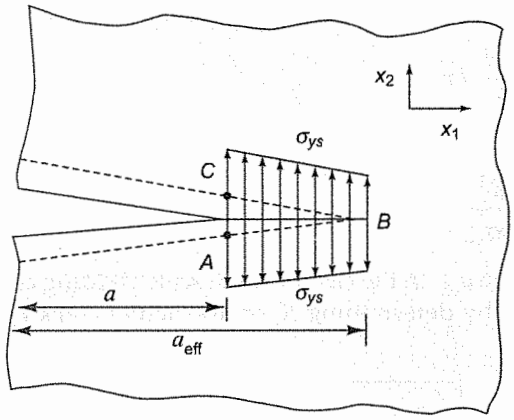

Fig. 7.2 Finding J-integral along path ABC

$$J = -\int_{\Gamma} T_i \frac{\partial u_2}{\partial x_1} ds$$

$$= \int \sigma_{ys} d\left(u_2^{BC} - u_2^{AB}\right)$$

$$= \sigma_{ys}\, CTOD$$

leading to $$CTOD = \frac{J}{\sigma_{ys}} \tag{7.5}$$

However, the material within the plastic zone may deform with work hardening, as characterized by the factor n. The relation is then written in more general form as

$$CTOD = \frac{J}{\alpha \sigma_{ys}} \tag{7.6}$$

where α is a dimensionless factor that depends on n. Test methods to determine $CTOD_c$ are described in Chapter 8.

7.4 Closure

Crack tip opening displacement parameter can characterize materials for both LEFM and EPFM. This approach is not well-developed to give simple relations between field stresses (or loads) and *CTOD* and therefore the parameter is not convenient to predict crack growth in practical situations. The *CTOD* approach may be useful to compare toughness of materials. In certain cases, J_{Ic} or K_{Ic} may be determined by finding $CTOD_c$ and then using equivalence relations. However, some uncertainty exists in using the equivalence relations because they depend on the elastic-plastic material behavior and the model adopted to find the effective crack length.

QUESTIONS

1. What are other symbols used in the literature for *CTOD*?
2. Through a clear sketch, show the distance that depicts *CTOD*.
3. Why are direct relations not available between *CTOD* and a load applied on the component?
4. *CTOD* was developed about a decade earlier than the application of the J-Integral to fracture problems began. Still, the *CTOD* remains unpopular. Why so?
5. The *CTOD* is a virtual displacement, which is determined through a model. Do you think that the model is based on a sound approach? Justify your answer.

PROBLEMS

1. Determine G_{Ic}, J_{Ic} and $CTOD_c$ for a hardened steel if material properties are: σ_{ys} = 700 MPa, E = 207 GPa, K_{Ic} = 48 MPa $\sqrt{m}$ and ν = 0.3.
2. A cylindrical vessel with closed ends is made of steel with yield stress 350 MPa and modulus 207 GPa. The diameter of the pressure vessel is 1.6 m and the wall-thickness is 18 mm. The critical *CTOD* is known to be 0.08 mm. Use the small scale yielding model to determine the maximum pressure the vessel can withstand if a through-the-thickness crack of length $2a$ = 20 mm is detected, parallel to the axis of the cylinder.

REFERENCES

7.1 Wells, A.A. (1961). "Unstable Crack Propagation in Metals: Cleavage and Fast Fracture," *Proceedings of Crack Propagation Symposium*, Cranfield, 1, pp. 210–230.

7.2 Wells, A.A. (1963). "Application of Fracture Mechanics at and beyond General Yielding," *British Welding Journal*, 10, pp. 563–570.

7.3 Cottrell, A.H. (1961). "Theoretical Aspects of Radiation Damage and Brittle Fracture in Steel Pressure Vessels," *Iron Steel Institute Special Report*, No. 69, pp 281–296.

7.4 Rooke, D.D. and Bradshaw, F.J. (1969). "A Study of Crack Tip Deformation and a Derivation of Fracture Energy," *Fracture*, 1969, pp. 46–57.

7.5 Bowles, C.Q. (1970). *Strain Distribution and Deformation at the Crack Tip in Low Cycle Fatigue*, Army Mat. and Mech. Res. Center, Watertown, Mass. Rept. AMMRC CR 70–73.

Chapter

8

Test Methods

It is said that in old days when an armourer fulfilled an order for iron shirt of mail, he first put it on himself and his client dealt him a few blows with his sword. If the craftsman survived, his 'product' was considered satisfactory... But if the armour's work was not good enough, there was no one to pay the money to.

S. Venestky

8.1 Introduction

A material is selected to have adequate toughness for a given application. We, therefore avoid using materials of low toughness like glass, carbides and ceramics for most of the daily structural applications except in some special cases. One of the main reasons for widespread popularity of mild steel is that its toughness is very high. Toughness is a material property as yield stress. Proper test methods should be developed to determine material toughness.

For a long time, people understood toughness of materials intuitively. People could value it but could not measure it. One crude measure, still sometimes used today, is to find how much a material elongates before it fails. In the field of engineering, this property is known as elongation. A material with 10% elongation is much tougher than another material having 2% elongation. However, the modern fracture mechanics has shown that elongation alone cannot measure the toughness of a material.

A better estimate of toughness can be realized by finding the area under the stress-strain curve up to the ultimate tensile strength. Larger area corresponds to higher toughness. Keeping track of the area under the curve may not be practical for the field engineers. However, the field engineers adopt a simple method. They keep track of the elongation as well as the ultimate strength of a material. These two properties give a reasonable estimate of the area under the stress-strain curve. However, this method does give some feel of the toughness of the material but is not rigorous. It is used only when modern techniques are not available.

The first method developed for measuring toughness is known as Charpy or Izod notch sensitivity test. In these tests, a specimen with a notch is impacted by a very large pendulum mass,

and the energy absorbed in failing the specimen either through bending or breaking at the notch is measured. A tougher material absorbs more energy. These test machines became popular rather quickly and are still used all over. In fact, this kind of notch sensitivity test explained the failure of ships in the cold waters of the Northern Atlantic Ocean during the Second World War. The steel used in making the structure of these ships changed its behavior from ductile to brittle below a certain temperature and, then, even a small flaw in the hull would grow and break the ship into two parts.

Notch sensitivity impact tests are simple to conduct and not very expensive. However, they are not based on rigorous analysis. It is difficult to use the results of these tests to predict whether a crack is likely to grow under given loading conditions. In these tests, the thickness of the specimen chosen is not based on the toughness of the material and thus considerations of plane stress and plane strain are not accounted for. In fact, unlike in the rigorous tests of finding K_{Ic} and J_{Ic}, there is hardly any consideration in choosing the size of the specimen of Charpy or Izod test based on the material toughness. Further, notch sensitivity tests are always conducted under dynamic impact which is generally not the case in many engineering applications. For less ductile materials, the sharpness of the crack tip is important but rigorous considerations regarding the crack tip sharpness are not undertaken in the specimen of the Izod or Charpy test. As a postgraduate student in early seventies at the Brown University, I was surprised to find that the existing impact test machine was taken out of the test facility area because test methods for J-Integral were being developed and it would be disgrace to Brown University if some one found out that Charpy tests were being conducted at the side of J-Integral tests.

However, we will soon realize that evaluation of K_{Ic} or J_{Ic} is so sophisticated a process that many field engineers fail to understand the theories and their applications. Even if they understand the modern test methods, the tests are so expensive that they are out of the reach of many engineering companies. Consequently, crude methods are still widely used to estimate the toughness of a material; Charpy and Izod test machines are still popular.

One of the ironies is that research and development resources are mostly used up for theoretical developments and analysis. These days not much importance and respect is given to experimental development. Consequently, experimental methods have not been developed and simplified at a similar pace and whatever have been developed are still out of means of many engineering companies. To develop new materials, to improve properties of existing materials or to assure proper material selection of machine components, it is essential to have effective test methods. At the same time, it is desirable that the test methods are made simple enough for a semi-technical person to conduct them routinely. Unfortunately, test methods developed so far are quite sophisticated and beyond the reach of many small and medium size companies.

It is important to emphasize that fracture toughness is a material property. It cannot be derived from other material properties like modulus, yield stress, etc. However, other properties may influence toughness of a material. For example, when an alloy steel is given heat treatment to obtain higher yield stress, its toughness decreases. We cannot calculate or determine toughness just by knowing the yield stress of the material. A separate experimental test is required to determine material toughness.

In the previous chapters, four commonly used parameters *G*, *K*, *J* and *CTOD* have been discussed. Which parameter is adopted by a designer depends upon the application. *K* is widely used for LEFM and *J* for EPFM. *G* is generally used for brittle materials and finds its application in special cases such as interlaminar toughness of fiber composite laminates. *CTOD* is an alternative

approach to deal with EPFM. Depending upon the extent of usage, we have chosen to present test methods in the order *K*, *J*, *G* and *CTOD* in this chapter.

Before we start discussing the details of the various test methods, we would like to comment that, in general, a crack propagates in a mixed mode, that is, a propagating crack has components of all three Modes, I, II and III. However, it has been found that Mode I dominates in most of the real life cases. Therefore, a greater emphasis has been placed on test techniques of mode I. In fact, test techniques and codes are already available for Mode I, whereas test methods for Mode II and Mode III have not yet been investigated adequately. Therefore, in this chapter, we will confine our discussion mostly to Mode I cracks.

8.2 K_{Ic}-Test Technique

Experimental determination of the critical stress intensity factor (K_{Ic}) is most widely studied and developed. Code on K_{Ic} test was made for the first time in 1965–66 but since then the code has been revised several times. In this section, we will be discussing the salient features from the ASTM Code Designation E 399-83 to determine K_{Ic} of a material [8.1].

We discussed in Chapter 4 that the critical stress intensity factor of a material depends on the thickness of the plate. However, for a thick plate it is independent of thickness because the material in front of crack tip deforms in plane strain. Then, critical stress intensity factor can be treated as the property of the material. Thus, the experiment should be controlled so as to have its loading in plane strain only; that is, the plastic zone size in front of the crack tip is quite small in comparison to the specimen thickness. Then the Linear Elastic Fracture Mechanics (LEFM) can be applied to do the analysis. The entire body of the specimen is assumed to be deformed elastically and small strain theory having linear stress-strain relations is invoked.

Before presenting the details of K_{Ic}-test, it is summarized as follows. To begin with, K_{Ic} of the specimen is guessed. Then, the specimen is prepared following several dimensional constraints which are based on the guessed value of K_{Ic}. The crack tip is made very sharp with a fatigue growth. The specimen is pulled in a tensile machine to obtain a relation between the load and the crack mouth opening displacement. This relation provides the critical load P_Q. Accounting for the crack length and geometry of specimen, the stress intensity factor K_Q corresponding to P_Q is determined using LEFM. If K_Q satisfies all the constraints on the geometry of the specimen and of fatigue growth, it becomes K_{Ic}. The remaining portion of this section describes the method in detail.

8.2.1 Various Test Specimens

Four kinds of test specimens are shown in Figs 8.1 and 8.2—Compact Tension (CT), Single Edge Notch Bend (SENB), Arc-shaped Tension (AT) and Disc-shaped Compact Tension (DCT). However, CT and SENB specimens are the ones widely used. AT specimen is convenient for cylindrical geometries such as pressure vessels or pipings and DCT specimen is suitable for circular blanks, round bars, cores, etc. Also, there are two recommended geometries for AT specimen, one with $X/W = 0.5$ and another $X/W = 0$. For introducing a crack in a specimen, a notch is cut by a machine usually of length $0.45W$. The tip of the crack is then sharpened by growing the machined crack further so as to have crack length a close to $0.5W$ through a controlled fatigue loading.

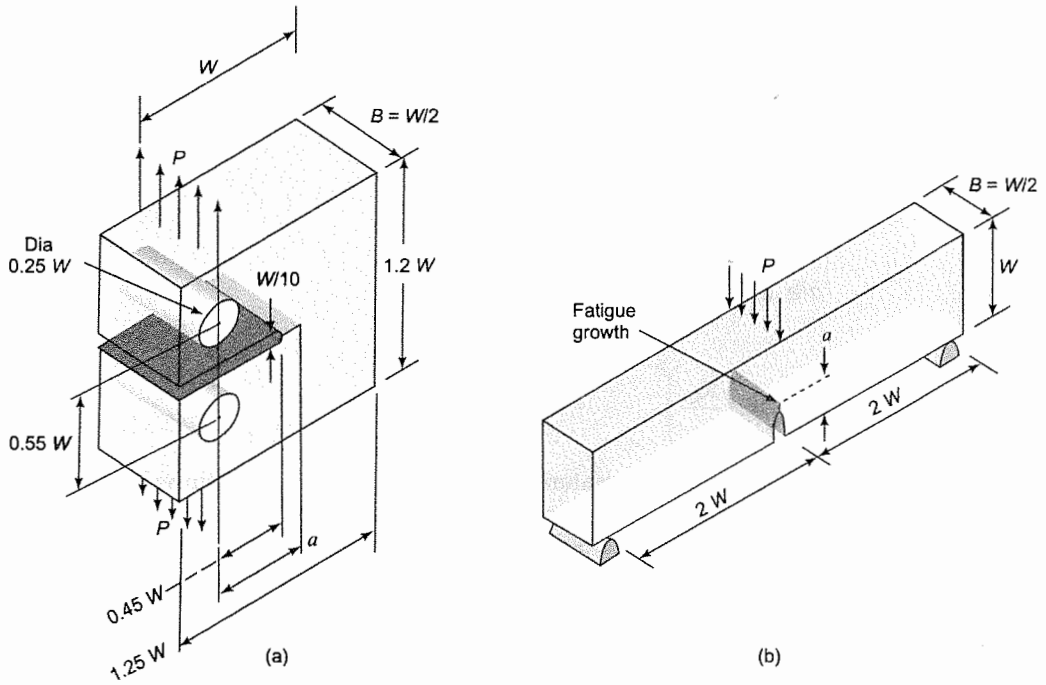

Fig. 8.1 (a) CT specimen, and (b) SENB specimen

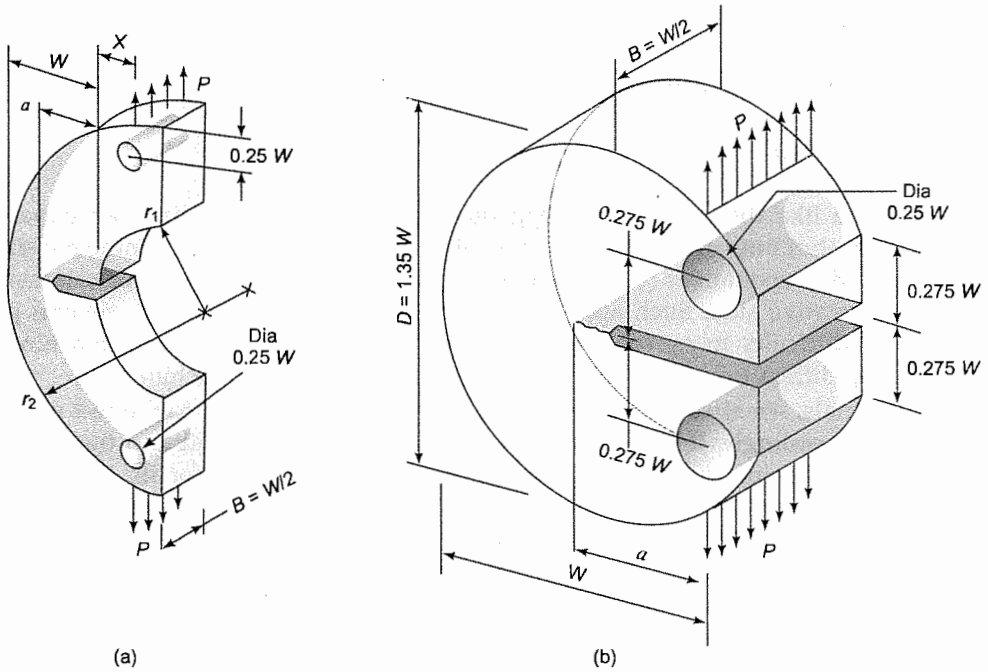

Fig 8.2 (a) AT specimen, and (b) DCT specimen

8.2.2 Constraints on Specimen-Dimensions

Specimen plate thickness B, crack length a and width W must satisfy the following requirements:

$$B \geq 2.5\left(\frac{K_{Ic}}{\sigma_{ys}}\right)^2 \tag{8.1a}$$

$$a \geq 2.5\left(\frac{K_{Ic}}{\sigma_{ys}}\right)^2 \tag{8.1b}$$

$$W \geq 5.0\left(\frac{K_{Ic}}{\sigma_{ys}}\right)^2 \tag{8.1c}$$

where σ_{ys} is the usual yield stress of the material. Why should these conditions be imposed? The first condition is required to meet the foremost requirement—the specimen must be loaded in plane strain. The plastic zone size, based on Irwin's correction, is close to 0.1 $(K_{Ic}/\sigma_{ys})^2$ for plane strain. When the inequality 8.1(a) is invoked, the thickness of specimen is much larger (about 25 times) than the plastic zone size, assuring plane strain conditions at the crack tip.

The constraint on the crack length can also be justified. If the specimen is designed to have a small crack length, the far field stress has to be high to develop large enough SIF at the tip for the crack to grow. But the large far field stress is undesirable because the analysis would not be accurate.

The third inequality is also justified because the free surface of lateral faces should be reasonably away from the crack tip. Although the effect of free surfaces is accounted for in the analysis, the accuracy improves if the free surfaces are far away from the crack tip.

8.2.3 A Dilemma

Inequalities 8.1 are like the chicken and egg problem. The goal is to have an experimental determination of K_{Ic} but until and unless we know its value, how can we determine the size of the specimen through the inequalities (8.1a)? One way out is that we take a very thick specimen and stay on the conservative side. Such approach is not recommended owing to several practical problems such as difficulty in purchasing a thick plate for the specimen, high machining cost, specimen handling difficulties and requirement of a high capacity test machine.

For many materials, we already have an idea of the range of K_{Ic} prior to the test and one can design specimen accordingly. If K_{Ic} of a new material is to be determined and there is no prior information about the expected K_{Ic}, one would have to guess a value for its K_{Ic} , design new specimens accordingly and perform the test (the details of the test will be presented shortly). The fracture toughness of the material thus obtained is given a tentative name K_Q. Once the value of K_Q is known, specimen dimensions (a, B and W) are evaluated through Inequality 8.1. The test is a valid test if all the three inequalities are satisfied and then K_Q becomes K_{Ic}. Otherwise, another guess on K_{Ic} is required and the experiment is conducted again with modified dimensions of the specimen.

8.2.4 Fatigue Crack Growth to Sharpen the Tip

An ideal crack should have a zero radius curvature at the tip because it is the worst case scenario; the stresses near the tip are highest and the material is weakest against fracture failure. A crack is generally prepared in a two-step procedure, (i) making a machined slot, and (ii) extending its tip by fatigue loading. It is worth noting that a cutting tool cannot make a very sharp notch. There is always a finite radius of curvature of the cutting edge of the tool, and also cutting of an engineering material is associated with some plastic flow. As stated earlier, the slot is machined cut to a length which is close to $0.45W$ and then the tip is extended by at least $0.05W$ with the help of an appropriate fatigue load.

The tip of the machined slot should be prepared carefully to guide the fatigue-growth. Two kinds of notches are recommended—(i) V-notch, and (ii) Chevron notch, as shown in Fig. 8.3. V-notch is relatively simple to prepare but the crack front after the fatigue-growth may get inclined; the crack front may have a shorter crack length on one face of the specimen in comparison to that on the opposite face. Specimen having more than 10% difference in the two crack lengths should be rejected. Further, in some specimen fatigue crack emanating from the V-notch may not even grow in the plane of the machined slot, and such specimen should be rejected.

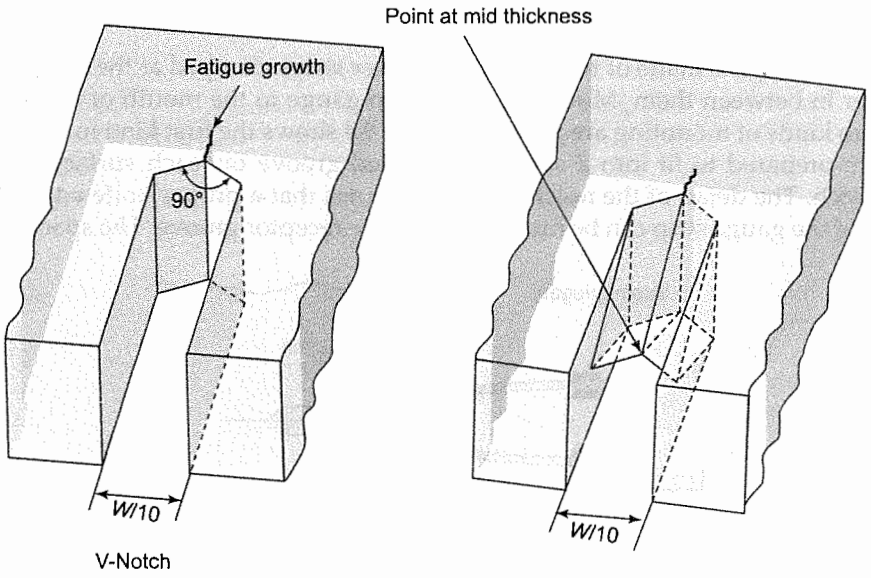

Fig. 8.3 V-notch and Chevron notch

The Chevron notch minimizes the problems of the V-notch but it is relatively difficult to prepare. The notch is prepared with an angle tool forming four inclined faces near the tip. In fact, a valley is formed on each side of the specimen. The bottom line of the valley is inclined having one end at the mid thickness. The Chevron notch works well because the thickness at the crack tip is very small (tending to be zero) and the fatigue crack nucleates with a small number of load cycles. The nucleated crack front is guided on the self-similar plane because the thickness is smallest as long as the crack tip is with in the Chevron notch. Once a crack tip moves for a certain distance on the

self-similar plane, it is expected that it would continue to grow on the same plane when the crack tip comes out of the notch. If the growing crack deviates away from the plane of the crack, the specimen should be rejected.

The maximum load of the fatigue loading should not be large because it would then develop a plastic zone of the significant size. The crack growth will no longer be sharp then. On the other hand, a low fatigue load is not practical as it would take a large number of load cycles to prepare a specimen. The following constraint should be followed for fatigue crack growth:

$$K_{f(\max)} \geq 0.6\, K_Q \tag{8.2}$$

where $K_{f(\max)}$ corresponds to the maximum value of the fatigue load. Like the previous inequalities, this inequality also poses difficulties as K_Q is not known a priori; Inequality (8.2) should be checked after K_Q is determined. If $K_{f(\max)}$ employed is more than $0.6\, K_Q$, the experiment is rejected and a new specimen is fatigued at a lower maximum load.

8.2.5 Clip Gauge

A clip gauge measures the Crack Mouth Opening Displacement (*CMOD*) accurately. It is also known as *COD* gauge. The measurement of the displacement should be highly linear and very sensitive with an accuracy better than 1%.

A typical clip gauge is made of two elastic cantilever strips clamped at the far end of the gauge with a spacer in between them. Mounting of the clip gauge to the mouth of a crack is designed carefully. Two kinds of mounting are popular. Figure 8.4 shows the first kind in which free ends of the strips are prepared to fit into a suitably designed groove on each surface receptor of the machined notch. The detail of the notched surface shows that a proper knife edge is prepared so that the end of the gauge strip can be fitted well into the receptor groove. The spacing between the

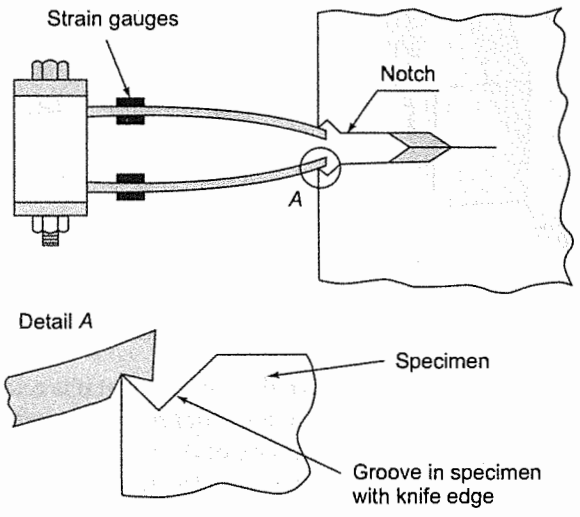

Fig. 8.4 (a) Clip gauge mounted on specially prepared receptor grooves, and (b) details of the receptor groove

strips is designed to accommodate substantial bending of the cantilever strips at the time of mounting the gauge into the notch. When a load is applied to the specimen and the mouth of the crack opens, the strips strive to become straight. This ensures a good positive contact between the ends of the gauge-strips and grooved surfaces of the crack-notch. Figure 8.5 shows the other kind of mounting. The free ends of the thin strips are designed such that they bend outward as shown in the figure. The bent portions are fastened using screws to the side face of the specimen. Tapped holes, two on each side of the notch of the specimen, are made on the side face such that they match with the clear holes in the clip gauge and substantial bending of the strips is achieved at the time of mounting. Electrical strain gauges are mounted on both sides of each strip as shown in Figs 8.4 and 8.5. A full Wheatstone-Bridge is used to monitor strains in the strips. The gauge is calibrated to determine distance between the ends of cantilever strips.

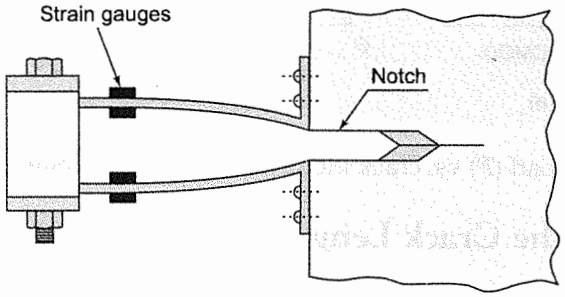

Fig. 8.5 Clip gauge screwed to the side face of a specimen

8.2.6 Load-Displacement Test

A specimen is loaded to obtain load vs. crack mouth opening displacement (*CMOD*) using a clip gauge. CT, AT and DCT specimen are pulled in a tensile machine to record load vs. *CMOD* relation; SENB specimen is loaded in a 3-point loading set up with span $S = 4W$ as shown in Fig. 8.1.

Depending upon the material, three types of response are observed between load P and crack mouth opening displacement as shown in Fig. 8.6. In all three cases *P-CMOD* curves are linear at low loads. In the case (a) the curve starts becoming nonlinear with increasing load owing to growing plastic zone at the crack tip and the stable crack growth. In the case (b) the crack grows with a pop-in sound and the load drops for a while before it starts increasing again. The case (c) is the response of an ideal brittle material.

Now we should define a criterion to determine fracture load P_Q from these experimental records. The criterion should guarantee that either the crack tip has already moved by a small distance or it is definite to move if load is increased by a small amount.

For the case (a) of Fig. 8.6, a 5% secant offset line *OS* is drawn and its intersection with *P-CMOD* curve gives fracture load P_Q. The 5% secant line is drawn by having its slope 5% less than the initial slope of *P-CMOD* curve. It has been found that 5% secant line corresponds to about 2% increase in crack length in CT and SENB specimens. Note that 5% is judicially chosen in the code and is similar to 0.2% offset used in determining yield stress of a material. For finding accurate value of P_Q the *P-CMOD* curve should be recorded with proper scales such that the initial slope

lies between 0.7 and 1.5. For case (b), the load which initiates pop-in crack growth is taken to be fracture load P_Q. In the case (c) of the brittle growth, the maximum load is P_Q.

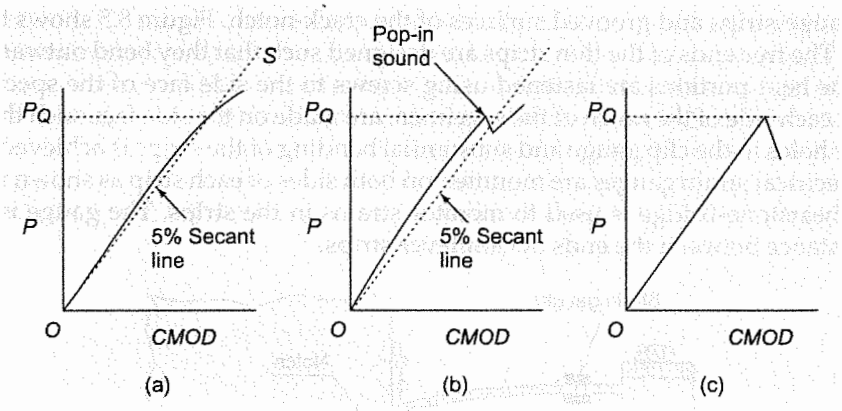

Fig. 8.6 Load (P) vs. crack mouth opening displacement ($CMOD$)

8.2.7 Measuring the Crack Length

For accurate measurement of the crack length, it is recommended that the specimen is split into two halves by letting the crack run all the way. Looking into a split surface, three kinds of surface-zones can be observed—(i) machine cut (ii) fatigue grown and (iii) surface produced through fracture during the loading. The texture and reflectivity of an incident light from the fatigue-area are much different from those of the fractured surface and, therefore, three surface zones can be easily identified. Figure 8.7 shows all the three surface-zones and the commonly observed shape of the fatigue crack front developed from a Chevron notch. The front of the fatigue grown crack is generally found to be curved as shown in the figure. The crack length is taken as $a = 1/3\,(a_1 + a_2 + a_3)$. The test is rejected if anyone of the three crack lengths differs more than by 5% from a. The test is also rejected if any part of the crack front of fatigue growth is close to the machined notch within $0.005\,a$ or 1.3 mm.

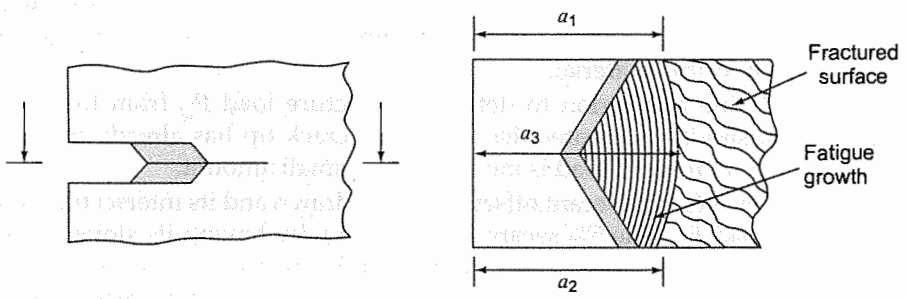

Fig. 8.7 Measurement of crack length

8.2.8 Data Analysis

Knowing critical load P_Q, crack length a and specimen dimensions, LEFM is invoked to determine K_{Ic}. Specimens are made of finite dimensions and therefore effect of the size must be incorporated in the data analysis. Appendix 4A gives relevant formulae for each case. For SENB specimen, K_I has the following form:

$$K_I = \frac{PS}{BW^{3/2}} f(a/W) \tag{8.3}$$

and for CT, AT and DCT specimen,

$$K_I = \frac{P}{BW^{1/2}} f(a/W). \tag{8.4}$$

Form of $f(a/W)$ is quite involved and one may make a mistake in calculating its value for a given a/W. Table 8.1, therefore, lists its values for SENB, CT and DCT specimen for various a/W.

TABLE 8.1 Value of $f(a/W)$ for determining K_{Ic}

	$f(a/W)$		
a/W	*SENB*	*CT*	*DCT*
0.450	2.286	8.340	8.705
0.455	2.320	8.458	8.838
0.460	2.354	8.580	8.974
0.465	2.390	8.704	9.112
0.470	2.426	8.830	9.254
0.475	2.463	8.960	9.399
0.480	2.501	9.093	9.547
0.485	2.540	9.230	9.698
0.490	2.580	9.369	9.853
0.495	2.621	9.512	10.01
0.500	2.663	9.659	10.17
0.505	2.705	9.807	10.33
0.510	2.749	9.964	10.51
0.515	2.794	10.12	10.68
0.520	2.840	10.29	10.86
0.525	2.887	10.45	11.04
0.530	2.936	10.63	11.23
0.535	2.985	10.82	11.42
0.540	3.036	10.93	11.62
0.545	3.089	11.17	11.83
0.550	3.142	11.36	12.04

Equations (8.3) and (8.4) enable us to find K_Q corresponding to P_Q. If K_Q satisfies all dimensional Inequalities 8.1 and fatigue Inequality 8.2, it becomes the material property K_{Ic}. If not, another guess for K_Q is made, next specimen is prepared with modified dimensions, and the entire test is repeated. Note that it is a trial and error method.

8.2.9 Comments on Plane Strain K_{Ic}-Test

For tough materials with low yield stress, thickness required for K_{Ic}-test specimen is high and it would not be practical to do K_{Ic} test. Thus, it is difficult to make specimens for tough materials like mild steel, nuclear reactor steel, commercially available aluminum, etc. In fact, the difficulty encountered in testing of these materials motivated researchers to formulate J-Integral test which will be discussed in detail in the next section. However, even if we determine plane strain K_{Ic} of tough material like mild steel, the result may not be useful to us because in most of the practical applications, sheet thickness falls in the category of plane stress.

Alloy steels are now being increasingly used in engineering applications. Their properties are altered considerably through heat treatment. One can practically choose almost any yield stress he wants in his steel alloys. If the yield stress is increased, K_{Ic} changes considerably to a lower value. There are innumerable combinations of K_{Ic} and yield stress σ_{ys} and there are many different kinds of alloys available in the market. Characterization of K_{Ic} for all materials is a voluminous task because considerable time, care and expenses are required for each test. Consequently, it becomes difficult for a designer to obtain sufficient data on K_{Ic}.

Most of the plates or standard sections such as angle, channel, tube, I-Beam, etc., are made through rolling with elongated grains in the direction of the rolling. Thus, toughness depends also on the direction of crack front. For example, a through-the-thickness crack growing in rolling direction is less tough in comparison to a crack advancing in the direction of the width of the plate.

A K_{Ic} test is costly. It needs a well trained person to design specimens. Growing a crack through a fatigue load is expensive and time consuming. As a result, not many laboratories are equipped to conduct K_{Ic} test. Even after progressing so much in analytical field, a designer faces problems in selecting a material in the absence of an adequate data bank. In many cases, engineering companies are not able to afford the K_{Ic} test. Designers are forced to somehow manage by taking K_{Ic} of a similar looking material and modifying it with some correction factors based on the yield stress.

8.3 Test Methods to Determine J_{Ic}

The J-Integral has been developed to account for elastic-plastic behavior of the material in the plastic zone near the crack tip. Methods to find J_{Ic} are quite different from the procedure of finding K_{Ic}. In K_{Ic}-test method, specimen is chosen to be of a large thickness so that the plastic zone size near the crack tip is small and nonlinear stress strain relations in the plastic-zone do not affect the linear elastic analysis significantly. On the other hand, a specimen of much smaller thickness for J_{Ic}-test can be chosen with a large plastic zone size at the vicinity of the crack tip.

8.3.1 Graphical Interpretation

For test methods, the energy interpretation of J-Integral is found to be more convenient. Figure 8.8 shows the energy interpretation for G_I for linear elastic material and J_I for elastic-plastic material. Linear load-displacement relations (P vs. u) are shown in Fig. 8.8 (a) for two cracks with length a and $a+\Delta a$. It has already been shown in Section 2.6 that area between the two linear lines is equal to $G_I\, B\Delta a$ where B is the thickness of the plate.

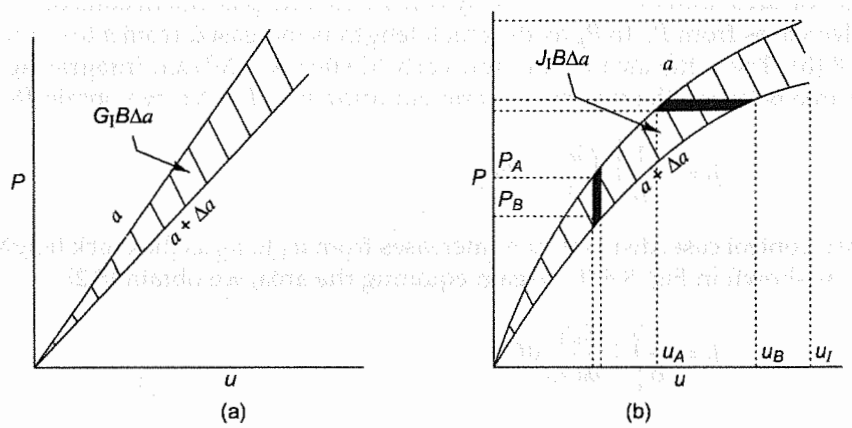

Fig. 8.8 (a) G_I through linear P-u relations, and (b) J_I through elastic-plastic P-u relations

For elastic-plastic case shown in Fig. 8.8 (b), think in terms of two specimens identical in all respects except with the slight change in crack length. The area between the two curves corresponds to $J_I\, B\Delta a$. The area can be determined from P-u relations in several different ways:

(i) Area under a P-u curve of elastic-plastic deformation (Fig. 8.9) is defined as:

$$U_{EP} = \int P du$$

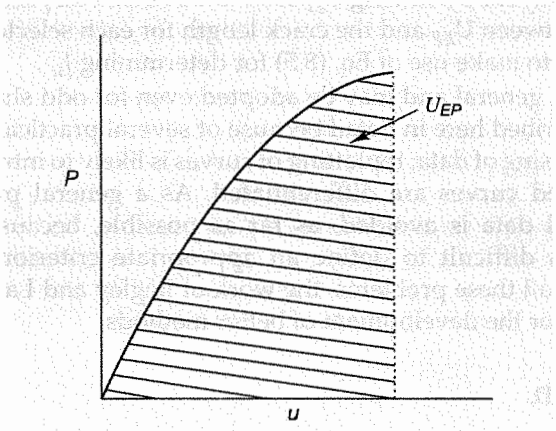

Fig. 8.9 Area under P-u curve (U_{EP})

Now, consider the case of Fig. 8.8 (b) for two cracks of length a and $a+\Delta a$. Both specimens are deformed to the displacement u_1. Analogous to definition of G in Chapter 2, we can express J in terms of U_{EP}. However, for the case of constant u, external work W_{ext} is zero and expression of J_I becomes:

$$J_I = -\frac{1}{B}\left(\frac{\partial U_{EP}}{\partial a}\right)_{u_1} \tag{8.5}$$

(ii) We find the area under the P-u curve by considering displacement controlled case in which load decreases from P_A to P_B as the crack length is increased from a to $a + \Delta a$ as shown in Fig. 8.8 (b). Then, the area of the thin vertical slice is $(-\Delta P)\Delta u$. Integrating to obtain the entire area between the two curves and equating it to $B J_I \Delta a$, we obtain [8.2].

$$J_I = -\frac{1}{B}\int_0^{u_1}\left(\frac{\partial P}{\partial a}\right)_u du \tag{8.6}$$

(iii) In a load control case, displacement increases from u_A to u_B as the crack length is increased by Δa, as shown in Fig. 8.8 (b). Again equating the area, we obtain [8.2]:

$$J_I = \frac{1}{B}\int_0^{P_1}\left(\frac{\partial u}{\partial a}\right)_P dP \tag{8.7}$$

8.3.2 Historical Development

For tough materials such as those used in nuclear reactors, the thickness of K_I-test specimen should be very high so as to meet plane strain requirements and therefore specimen becomes very large as discussed earlier; determination of K_{Ic} is prohibitively expensive. Begley and Landes [8.3] developed an experimental technique which was based on J-Integral. They made use of Eq. (8.5). In the method developed, CT specimens of identical geometry with different initial crack length are prepared, and load-displacement relation for each specimen is obtained on a tensile test machine. The data are analyzed by finding U_{EP} for a few selected displacements (u_1, u_2, u_3) and then the curves are plotted between U_{EP} and the crack length for each selected displacement. U_{EP} vs. a curves are differentiated to make use of Eq. (8.5) for determining J_{Ic}.

The technique is quite general and may be adopted even for odd shaped specimen. However, the technique is not described here in detail because of several practical problems. The technique requires extensive processing of data; replotting of curves is likely to introduce large errors in some cases. Then the replotted curves are differentiated. As a general practice, differentiation of experimentally obtained data is avoided, as far as possible, because a small error may get amplified. Further, it is difficult to define an appropriate criterion for 'the onset of crack propagation'. In spite of all these problems, the work of Begley and Landes played an important role as a stepping stone for the development of better methods.

8.3.3 Formulation

For more convenient techniques to determine J_{Ic}, Eq. (8.6) is further exploited. Consider a SENB specimen (Fig. 8.10) for which some discussion has been presented in Section 6.5. A crack of length

a is introduced in a specimen with thickness B and width W. The uncracked ligament b is about 50% of width W. The ligament b is subjected to vigorous plastic deformation when load P is applied at the centre. Deflection of the load point is u and rotation of two segments of the specimen is 2Ψ.

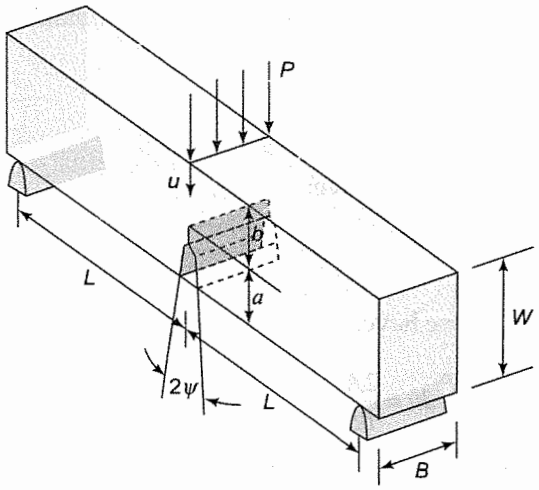

Fig. 8.10 SENB specimen with a deep crack

The critical J-Integral, denoted by J_{Ic}, is the value of J_I which would grow the crack if there is an incremental increase in J_I. However, it is not possible to tell when a crack is at 'the onset of crack growth'. We should allow a small crack growth to make sure that 'the onset of crack growth' has already been achieved. Based on experience, it has been found that unloading caused by the small crack growth, does not change the value of J_I significantly. Therefore, a small crack growth may be permitted in experimental determination of J_{Ic}.

If area under the P-u record of the bend-specimen is A, we will show that J-Integral is given by [8.4]

$$J_I = \frac{2A}{Bb} \tag{8.8}$$

This expression can be proved using dimensional analysis applied to the specimen of Fig. 8.10. The rotation Ψ is made of two parts: (i) Ψ_p caused by intense plastic deformation of the uncracked ligament, and (ii) Ψ_e due to elastic deformation in the specimen. It is worth noting that Ψ_p dominates specially in the case of a deep crack. The effect of elastic deformation thus may be neglected. Ψ_p depends on the following parameters: bending moment at the crack plane (M), uncracked ligament (b), specimen thickness (B), flow stress (σ_f), modulus (E) and hardening parameter (n). The dimensionless group $M/(\sigma_f Bb^2)$ depends upon Ψ_p, σ_f/E and n. It can be expressed as:

$$\frac{M}{\sigma_f Bb^2} = f\left(\psi_p, \sigma_f / E, n\right)$$

Since $\Psi_p = u/L$ and $M = \alpha PL$, where α is a factor, the equation is modified to:

$$P = \frac{\sigma_f B b^2}{\alpha L} f\left(\frac{u}{L}, \frac{\sigma_f}{E}, n\right) \tag{8.9}$$

Differentiating with crack length a and realizing $\frac{\partial}{\partial a} = -\frac{\partial}{\partial b}$ we obtain:

$$\left(\frac{\partial P}{\partial a}\right)_u = -\frac{2\sigma_f B b}{\alpha L} f\left(\frac{u}{L}, \frac{\sigma_f}{E}, n\right) \tag{8.10}$$

Substituting Eq. (8.9) into Eq. (8.10), we have:

$$\left(\frac{\partial P}{\partial a}\right)_u = -\frac{2P}{b}$$

Now, substituting it in Eq. (8.6), we have:

$$J_I = \frac{1}{B}\int_0^{u_1} \frac{2P}{b} du = \frac{2A}{Bb} \tag{8.11}$$

In case CT specimen is used, Eq (8.11) is modified to [8.5]

$$J_I = \frac{A}{Bb} g(a_o / W) \tag{8.12}$$

where a_o is the initial crack length and

$$g(a_o / W) = 2\left[(1+\alpha)/\left(1+\alpha^2\right)\right]$$

with α defined as:

$$\alpha = \left[(2a_o / b)^2 + 2(2a_o / b)^{1/2} - (2a_o / b) + 1\right]$$

8.3.4 Details of J_{Ic} Test Method

Our objective is to determine J_{Ic} corresponding to the initiation of a crack growth. This section describes the salient features of ASTM Code 813 [8.5]. Similar to K_{Ic}-test, two kinds of specimen are recommended—Single Edge Notch Bend (SENB) and Compact tension (CT). Following constraints are required on the specimen:

$$a \geq 0.5\,W \tag{8.13a}$$

$$b \geq 25 J_{Ic} / \sigma_f \tag{8.13b}$$

$$B \geq 25 J_{Ic} / \sigma_f \tag{8.13c}$$

where flow stress σ_f is defined in terms of yield stress σ_{ys} and ultimate tensile strength σ_{uts} as:

$$\sigma_f = \left(\sigma_{ys} + \sigma_{uts}\right)/2$$

The definition of flow stress accounts for work hardening of the material. Justification of the constraints on the specimen size will be discussed subsequently. The code requires that the crack tip should be sharpened by growing a machined notch with a fatigue load. Like in the case of K_{Ic}-test, the specimen size of J_{Ic}-test is linked with the value of J_{Ic} which is not known a priori. Therefore, specimen size is based on a guessed J_{Ic} and the resulting value of J-Integral is called J_Q. If J_Q satisfies Inequalities (8.13), it is a valid test, otherwise specimen dimensions should be modified for the next test.

For evaluating J_{Ic}, several specimens of identical size and almost of same initial crack length are prepared. Each specimen is loaded in a tensile machine to obtain load vs. displacement $(P - u)$ curve as shown in (Fig. 8.9). The crack is allowed to extend by a small length and the crack extension is varied from specimen to specimen. The crack extension should be measured accurately. Before the specimen is broken apart, the extension should be marked or frozen. This can be achieved through several techniques. The specimen can be heat-tinted. Heat tinting for steel is carried out for 10 minutes at 800°C. After the heat tinting, which chahnges the color of the cracked surface due to oxidation, the specimen is broken apart for measuring Δa. Another technique is to use a dye penetrant which would color the cracked surfaces. Dye penetrants are easily available in the market as they are widely used to detect surface cracks.

Nature of the cracked surface of a specimen is shown in Fig. 8.11. The crack front is generally curved as shown and it is important to measure Δa very accurately. In a thick specimen, it is recommended that the crack length should be determined by taking average of nine measurements across the thickness of the specimen.

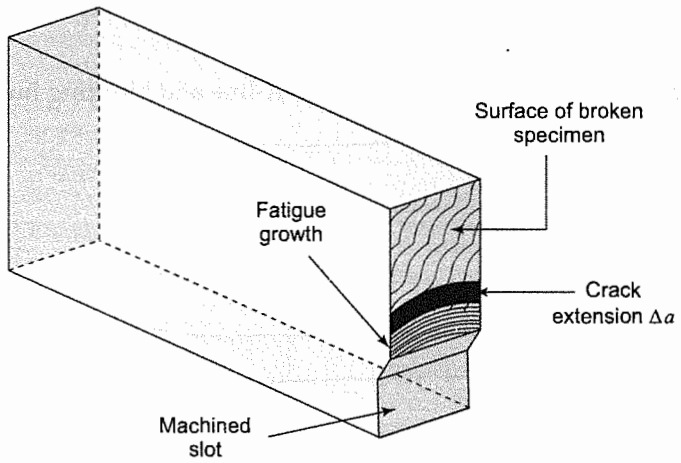

Fig. 8.11 Crack extension

J_I is determined from each specimen using Eq. (8.8) and is plotted against crack extension as shown in (Fig. 8.12). A straight line, known as R-line, is best fitted through the J_I points. A blunting line, $J_I = (\sigma_{ys} + \sigma_{uts})\Delta a$, is drawn whose intersection with R-line gives J_Q as shown in the figure. It is now worthwhile to justify the form of blunting line and the constraints on the specimen. Because of the intense plastic deformation the crack-tip blunts before stable crack

growth initiates. The blunting can be considered as a small crack growth as shown in Fig. 8.13. For estimating the small crack growth, the blunt crack can be modeled as a semicircle with its radius $CTOD/2$. Since $CTOD = J_I/\sigma_f$, the small crack growth due to blunting is $J_I/2\sigma_f$ and therefore the 'on-set of crack propagation' corresponds to:

$$\begin{aligned} J_I &= 2\sigma_f \Delta a \\ &= \left(\sigma_{ys} + \sigma_{uts}\right)\Delta a \end{aligned} \tag{8.14}$$

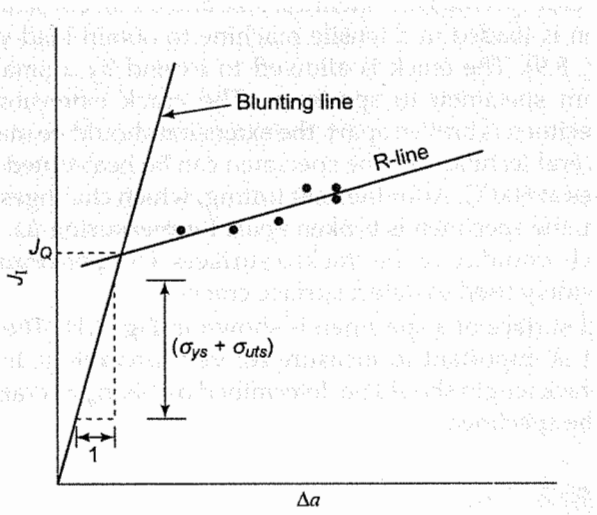

Fig. 8.12 Determining J_Q through R-line and blunting line

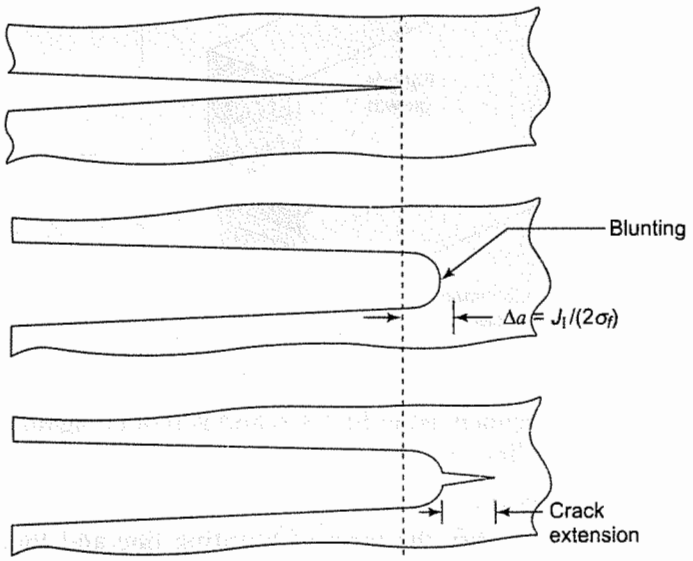

Fig. 8.13 Blunting of crack tip and crack extension

Thus, stable crack growth is beyond the blunting line. The nearest experimental point can never be at the blunting line owing to practical considerations; there has to be a small but finite crack extension for accurate measurements. Since R-line is extrapolated to find J_Q, it is prone to data processing error. To minimize the error, the nearest experimental point should be close to the intersection of blunting line and R-line.

J_{Ic} measurements require that the plate thickness B should be much larger than the size of the intense plastic deformation which is given by $J_1/2\sigma_f$. Thus, Inequality (8.13c) assures that B is much bigger than the intense plastic deformation. Similarly, Inequality (8.13b) assures that the uncracked ligament is much larger than the intense plastic zone. Inequality (8.13a) is required to enhance plastic deformation in front of the crack tip .

8.3.5 Comments on J_{Ic}-Test

J_{Ic} corresponds to the onset of crack extension because stable growth is not admissible as it involves unloading. In most of the real life materials, a crack goes through a fairly large stable growth before it becomes unstable. Thus, J_{Ic} is conservative in comparison to K_{Ic} which admits some stable crack growth. However, in sensitive applications, like in a nuclear reactor, even a small extension of a crack is considered as failure and J_{Ic} is found to be more suitable.

Conducting J_{Ic}-tests is expensive because several specimens should be used to draw the R-line. Further each experiment should be prepared carefully with the expensive fatigue crack growth. Measurement of crack extension, Δa, involves further expense in marking the crack front (e.g., heat tinting) and making accurate measurements. Consequently, data on J_{Ic} are not readily available. Further, a large but natural scatter in J_{Ic} discussed in Secs 6.5 and 6.6, discourages tabulation of material properties.

Now, we would explore how J_{Ic}-test helps in reducing the size of a test specimen. Minimum recommended thickness B_K of K_{Ic}-test specimen is:

$$B_K = 2.5\left(\frac{K_{Ic}^2}{\sigma_{ys}^2}\right)$$

and minimum thickness B_J for J_{Ic}-test specimen is:

$$B_J = 25\left(J_{Ic}/\sigma_f\right)$$

For the sake of comparing the thickness in the two kinds of tests, we take $\sigma_f = \sigma_{ys}$ to have:

$$B_K/B_J \approx \left(K_{Ic}\right)^2/\left(10J_{Ic}\sigma_{ys}\right)$$

Taking $J_{Ic} \approx K_{Ic}^2/E$

$$B_K/B_J \approx \frac{E}{10\sigma_{ys}}$$

For most of the engineering materials, we know that modulus is much larger than yield stress. For reactor steel with E close to 207×10^3 MPa and yield stress of 350 MPa, the ratio of thickness is

about 60—a dramatic reduction in specimen size. J_{Ic}-test enables us to determine toughness of a ductile material accurately by using a reasonable sized specimen. This has made the test popular within a short duration especially with critical industries like nuclear plants.

8.4 Test Methods to Determine G_{Ic} and G_{IIc}

Critical energy release rate of commonly used isotropic materials (metal, plastics) is not usually determined. However, in certain special cases, parameter G is found to be more appropriate. A laminate of fiber composite material is known to possess poor interlaminar toughness. Similarly, when two sheets made of metals are adhesively bonded together, the bond is usually weak against interlaminar crack growth. Thus appropriate techniques should be developed to measure interlaminar toughness of small magnitude. It is worth noting that stresses around the tip of an interlaminar crack are low and anelastic deformation is small. Therefore, LEFM is appropriate for such cases and determination of G_{Ic} is usually preferred.

In this section, test techniques for determination of critical energy release rate of interlaminar crack are discussed for Mode I and Mode II.

8.4.1 Determination of Interlaminar G_{Ic}

A Double Cantilever Beam (DCB) specimen of thickness B and height of each cantilever h is employed to determine critical energy release rate. The end of each cantilever is pulled in a tensile test machine and the loads are applied through hinges as shown in Fig. 8.14. The hinges release any bending moment which may otherwise get developed due to the rotation of the cantilever end. The other end of the specimen tends to move downwards due to its dead weight. This inclination is eliminated by a small counter weight tied to specimen through a thread as shown in the figure.

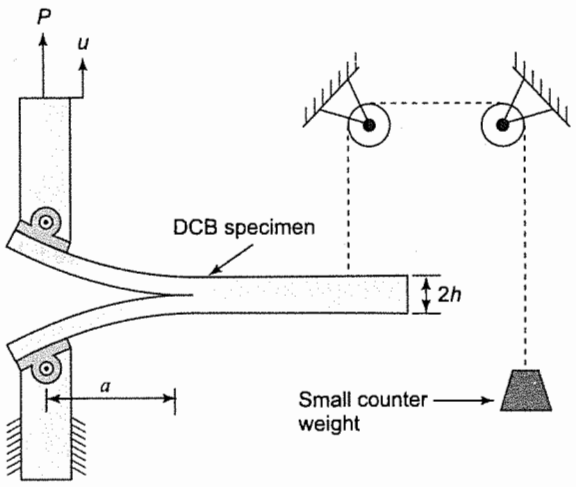

Fig. 8.14 The cantilevers of a DCB specimen pulled through hinges and a counter weight to balance the dead weight of the specimen

The overview of the test techniques is as follows: (i) experiments are conducted to determine compliance of the DCB specimen for several crack lengths, (ii) critical load is determined for each crack length, and (iii) G_{Ic} is obtained with a suitable data reduction scheme [8.6].

The DCB specimen is pulled in a tensile test machine on displacement control with a low pulling speed and the crack is allowed to grow by a small distance usually in the range of 5-15 mm. The machine is stopped for some time (till the crack tip becomes stationary) and then the length of the extended crack is measured. The load carried by the specimen decreases from point A to point D (Fig. 8.15) because the stiffness of the specimen decreases with crack growth. The slope of the u - P curve up to point A gives the compliance; the load at point A is the critical load P_c for the crack length.

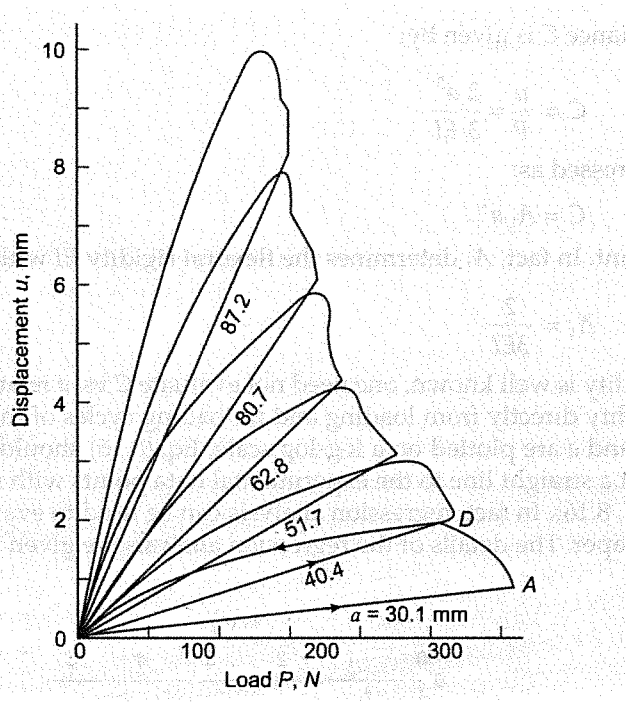

Fig. 8.15 Loading-unloading cycles to determine compliance and P_c for several crack length

Now, our aim is to find compliance for the increased crack length. To achieve it, the load on the specimen is decreased by moving the jaw of the tensile machine in the opposite direction till the load becomes zero. The unloading curve is usually not linear and is ignored. The specimen is loaded again to have further crack growth by a small distance. The loading curve gives the compliance of the increased crack length with critical load at point D. Compliance and critical load are determined by repeating the process several times as shown in Fig. 8.15. G_I of DCB specimen is given by (Sec. 2.7)

$$G_I = \frac{P^2 a^2}{EIB} \tag{8.15}$$

It is worth noting that modulus E and moment of inertia I may not be known to the investigator because composite material is not a standard material like steel. The modulus may vary from one laminate to another. We would not determine E and I through separate tests. Further, composite materials or bonded sheets do remain elastic during interlaminar growth and therefore we can use elastic solution for the deformation of DCB specimen. Usually, one specimen grip of the tensile machine remains stationary; the force and the displacement of the other specimen grip are recorded accurately. Accounting for the deflection of both cantilevers, displacement u is given by:

$$u = \frac{2}{3}\frac{Pa^3}{EI}$$

and then the compliance C is given by:

$$C = \frac{u}{P} = \frac{2}{3}\frac{a^3}{EI}$$

The equation is expressed as:

$$C = A_1 a^3 \tag{8.16}$$

where A_1 is a constant. In fact, A_1 determines the flexural rigidity EI with the relation:

$$A_1 = \frac{2}{3EI} \tag{8.17}$$

In case flexural rigidity is well known, one need not evaluate C vs. a relation. However, we would obtain flexural rigidity directly from loading and unloading cycles of the experiment for most of the cases. When C and a are plotted on a log-log scale, Eq. (8.16) should give a straight line with slope 3. Thus, we fit a straight line to the experimental data points with slope 3 and $ln(A_1)$ is read from the graph (Fig. 8.16). In fact, regression analysis can be used to evaluate A_1 without plotting points on a graph paper. The details of the regression analysis are given in Appendix 8A.

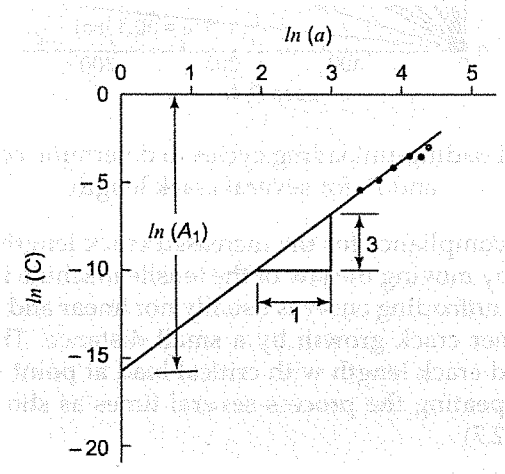

Fig. 8.16 Fitting a straight line of slope 3 to determine A_1

Corresponding to critical load P_c, Eq. (8.15) gives critical release energy rate as

$$G_{Ic} = \frac{P_c^2 a^2}{EIB}$$

Note that G_{Ic} is a material property and P_c and a are the only two variables in the above expression. Defining the product of these variables as:

$$A_2 = P_c a$$

we obtain:

$$G_{Ic} = \frac{A_2^2}{EIB} \tag{8.18}$$

In order to evaluate A_2 we note that

$$P_c = \frac{A_2}{a} \tag{8.19}$$

Figure 8.17 shows the plotted values of P_c and a on a log-log scale with best fitted line of slope-1; the intercept of the line with $ln(P_c)$ axis yields the value of A_2. Substituting for EI from Eq. (8.17) into Eq. (8.18) we obtain:

$$G_{Ic} = \frac{3}{2}\frac{A_1 A_2^2}{B} \tag{8.20}$$

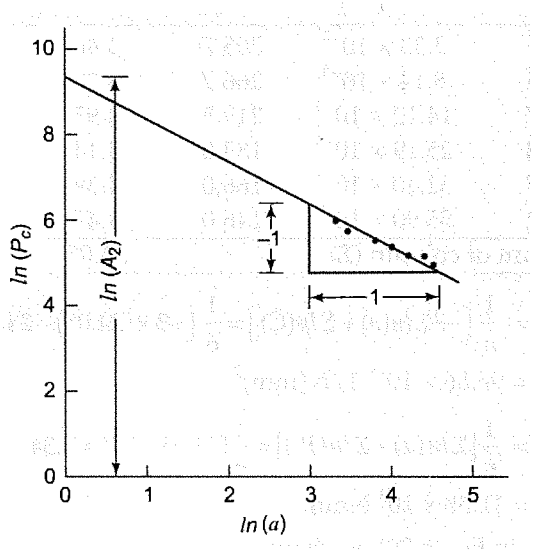

Fig. 8.17 Fitting a straight line of slope –1 to determine A_2

Example 8.1 Consider a DCB specimen made of fiber composite laminate whose cantilevers are pulled in a tensile machine for several crack lengths as shown in Fig. 8.15.
Determine G_{Ic} if the specimen thickness is B = 25 mm.

Solution: Crack length a, compliance C and critical load P_c are determined in Fig. 8.15 and tabulated in Table 8.2 along with the logarithmic values. Plots of $ln\ (C)$ vs $ln(a)$ and $ln(P_c)$ vs $ln(a)$ are shown in Fig. 8.18 along with the best fit lines of slopes 3 and -1. Through regression analysis (Appendix 8A), we have:

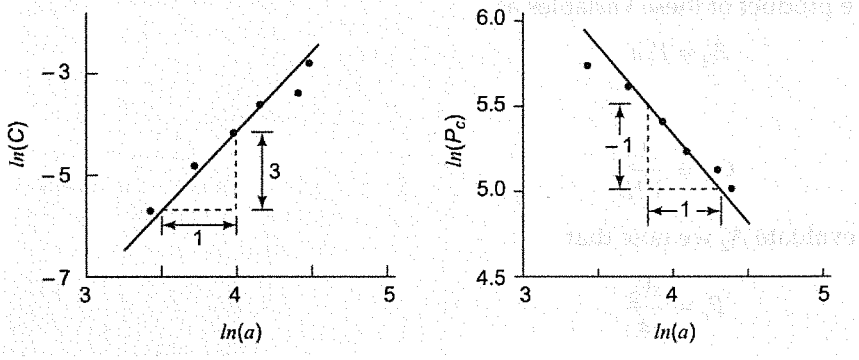

Fig. 8.18 (a) Variation of $ln(C)$ with $ln(a)$, and (b) variation of $ln(P_c)$ with $ln(a)$

Table 8.2 Logarithmic values of a, C and P_c of Example 8.1

S.No.	a (mm)	C (mm/N)	P_c (N)	$ln(a)$	$ln(C)$	$ln(P_c)$
1	30.1	3.33×10^{-3}	305.7	3.40	– 5.70	5.72
2	40.4	8.14×10^{-3}	266.7	3.70	– 4.81	5.59
3	51.7	14.12×10^{-3}	219.5	3.95	– 4.26	5.39
4	62.8	25.19×10^{-3}	183.0	4.14	– 3.68	5.21
5	80.7	32.40×10^{-3}	166.0	4.39	– 3.43	5.11
6	87.2	55.90×10^{-3}	146.0	4.47	– 2.88	4.98
Sum of column (Σ)				24.05	– 24.76	32.00

$$ln\ (A_1) = \frac{1}{n}\left[-3\Sigma ln(a) + \Sigma ln(C)\right] = \frac{1}{6}\left[-3\times(24.05) - 24.76\right] = -16.15$$

yielding $A_1 = 96.86 \times 10^{-9}\ 1/\text{N(mm)}^2$

and $$ln\ (A_2) = \frac{1}{n}\left[\Sigma ln(a) + \Sigma ln(P_c)\right] = \frac{1}{6}[24.05 + 32] = 9.34$$

yielding $A_2 = 11.38 \times 10^3$ Nmm

Substituting A_1 and A_2 in Eq. (8.20), we have

$$G_{Ic} = \frac{3}{2}\frac{A_1 A_2^2}{B} = \frac{3}{2} \times \frac{\left(96.86\times10^{-9}\ /\text{Nmm}^2\right)\times\left(11.38\times10^3\text{Nmm}\right)^2}{25\ \text{mm}}$$

$$= 0.753\ \text{N/mm} = 753\ J/\text{m}^2$$

8.4.2 Determination of Interlaminar G_{IIc}

Interlaminar critical energy release rate for Mode II is determined by employing an end notched flexure specimen shown in Fig. 8.19. The edge crack is on the midplane where the shear stress is the highest. The initial crack length is approximately equal to 0.5 L but it should not exceed 0.69 L. The specimen is loaded in a 3-point bend fixture as shown in Fig. 8.19. For this system it has been shown [8.7] that:

$$G_{II} = \frac{9P^2Ca^2}{2B\left(2L^3+3a^3\right)} \tag{8.21}$$

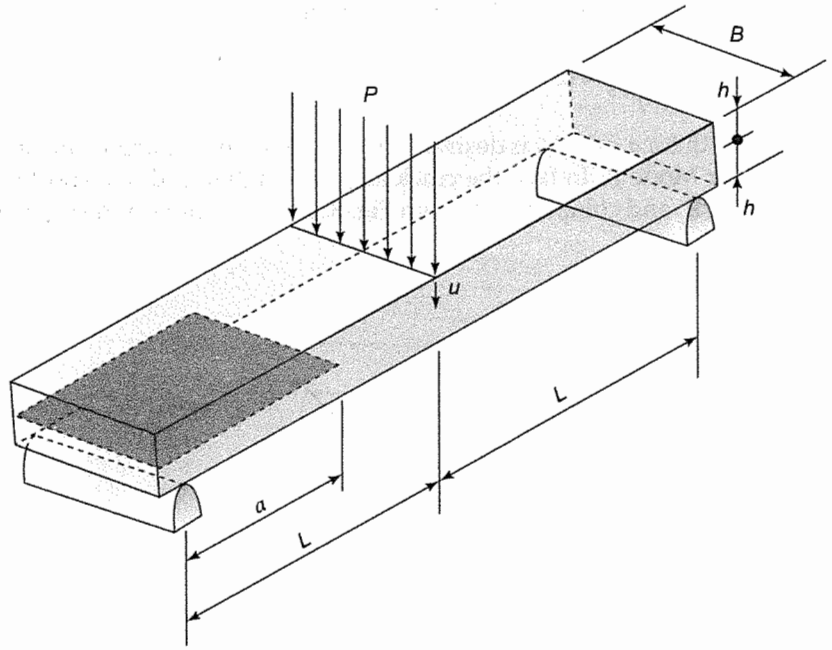

Fig. 8.19 Edge-notched flexure specimen loaded in 3-point bend fixture

where C is the compliance. The compliance can be found using the beam theory as:

$$C = \frac{2L^3+3a^3}{8EBh^3}$$

However, C is not evaluated using this formula due to uncertainty in the modulus of a laminate. It is determined directly from the P-u record.

We would now check the stability of crack growth. Substituting C in Eq. (8.21) and differentiating the resulting expression with respect to a we have:

$$\frac{dG_{II}}{da} = \frac{9P^2a}{8EB^2h^3}$$

Note that dG_{II}/da is always positive in load control testing and once the crack becomes critical, its growth is unstable. The case of displacement control is more interesting. Substitution of $P = u/C$ in Eq. (8.21) yields:

$$G_{II} = \frac{9u^2a^2}{2CB\left(2L^3 + 3a^3\right)}$$

Substituting the expression of C in this equation and differentiating with respect to a, we obtain:

$$\frac{dG_{II}}{da} = \frac{72u^2Eh^3a}{\left(2L^3+3a^3\right)^2}\left[1 - \frac{9a^3}{2L^3+3a^3}\right]$$

For unstable crack growth, dG_{II}/da should be positive, giving:

$$a \leq \frac{L}{(3)^{1/3}} = 0.693\,L$$

The unstable crack growth for $a < 0.69\,L$ is desirable because it gives a sharp value of critical load P_c as shown in Fig. 8.20 for Mode II. In fact, the crack acquires high speed in a short duration at the critical load P_c. Knowing P_c and compliance C from Fig. 8.20 we can determine G_{IIc} using Eq. (8.21).

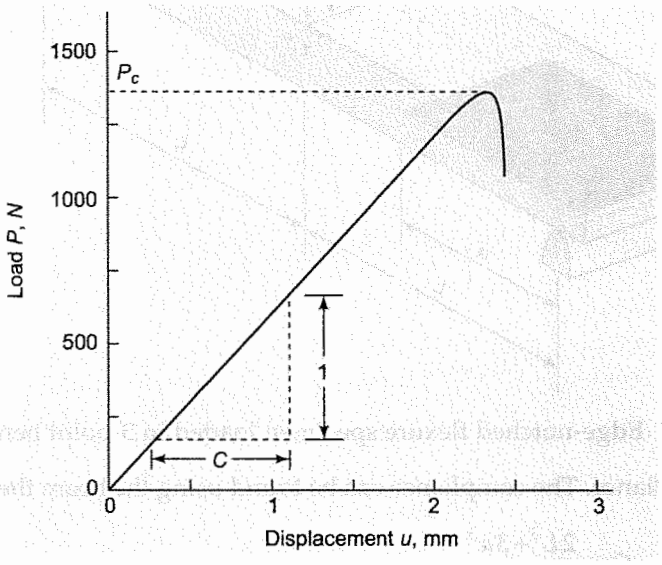

Fig. 8.20 *P-u* record to determine compliance and critical load

Example 8.2 An end-notched specimen is made of height $2h = 2.8$ mm, initial crack length $a = 26$ mm, total length between the support $2L = 100$ mm and thickness $B = 25$ mm. The load-displacement relation under 3-point loading is shown in Fig. 8.20. Determine the critical energy release rate G_{IIc}.

Solution: From Fig. 8.20 compliance C is evaluated in the linear portion of *P-u* record as:

$$C = 1.67 \times 10^{-3}\ \text{mm/N} = 1.67 \times 10^{-6}\ \text{m/N}$$

and the critical load is:

$$P_c = 1361 \text{ N}$$

Then, we have:

$$G_{IIc} = \frac{9P_c^2Ca^2}{2B\left(2L^3+3a^3\right)}$$

$$= \frac{9\times(1361\text{ N})^2\times\left(1.67\times10^{-6}\text{ m/N}\right)\times(0.026\text{ m})^2}{2\times(0.025\text{ m})\times\left[2\times(0.05\text{ m})^3+3\times(0.026\text{ m})^3\right]} = 1243\ J/\text{m}^2$$

To sum up, in this section experimental techniques have been presented for determining interlaminar toughness of fiber composite laminates or two strips bonded together for both Mode I and Mode II cases. Energy release rate parameter has been found to be the most convenient. G_{Ic} is determined by employing a DCB specimen with repeated load cycles for different crack lengths. The relations between compliance and crack length, and critical load and crack length then yield G_{Ic}. To find G_{IIc}, an end notched specimen is used which is loaded under a 3-point bend test. The compliance and the critical load for unstable crack growth determine G_{IIc}.

8.5 Determination of Critical *CTOD*

The definition and the formulation of crack tip opening displacement are presented in Chapter 7. In this section, an experimental technique to determine the critical crack tip opening displacement ($CTOD_c$ or δ_c) will be discussed.

We would present the salient features of the test technique discussed in the British Standard BS 5762 [8.8]. The code recommends the use of SENB (single-edge-notched bend) specimen to be loaded under a 3-point bend fixture. The geometry of the specimen is similar to one adopted for K_{Ic}-test. However, the V-notch, rather than the Chevron notch, is recommended. The specimen should be pre-fatigued as prescribed for K_{Ic}-test. Crack mouth opening displacement (*CMOD*) is measured when load P is applied at the centre of the SENB specimen.

The general criterion is that load and *CMOD* are determined when the crack is at the onset of an unstable crack growth. With an appropriate data reduction scheme, $CTOD_c$ is determined. However, the character of *P-CMOD* record varies from material to material. Often, it is difficult to determine when exactly the unstable growth initiates.

We will now discuss the various kinds of experimental measurement of *P-CMOD* relations. The simplest case deals with initiation of unstable crack growth with pop-in. In Fig 8.21 (a), there is no stable crack growth prior to pop-in whereas stable growth occurs in the case (b) prior to pop-in. The load at which pop-in initiates is taken as the critical load. For this critical load, plastic component u_p of measured *CMOD* is found by drawing a line parallel to the initial *P-CMOD* record as shown in Fig. 8.21.

We would now consider the cases when pop-in response is not observed. Figure 8.22 (a) deals with the case of no stable growth and unstable crack growth is initiated at the maximum load P_{max}. In case (b), stable growth occurs prior to unstable crack growth and unstable crack is initiated at the maximum load P_{max}. In case (c), stable growth occurs but unstable growth is initiated prior to the maximum load. However, it is difficult to identify the load that initiates the unstable crack

growth in routine testing. Therefore, maximum load is taken to be critical load. Thus, in all three cases of Fig. 8.22, maximum load is treated as the critical load of unstable crack growth. Plastic component u_p is also shown for these cases in the figure.

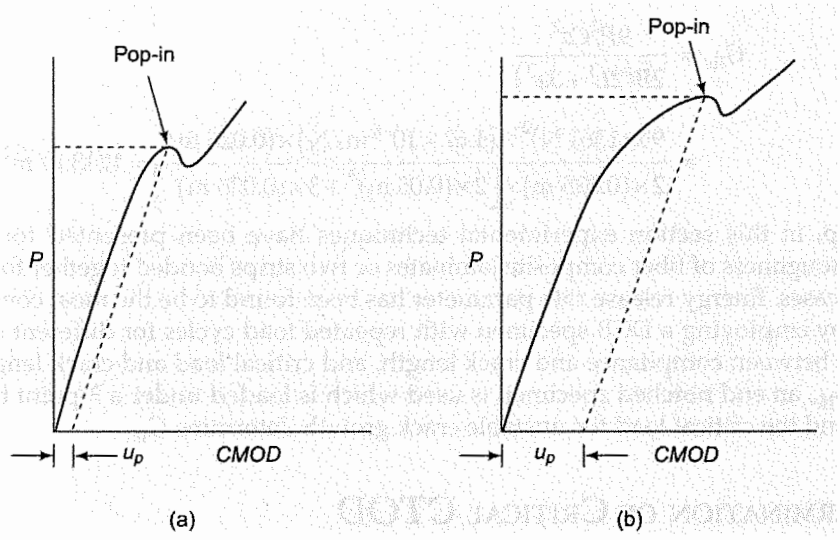

Fig. 8.21 (a) *P-CMOD* record with pop-in and no stable crack, and (b) with stable growth before pop-in

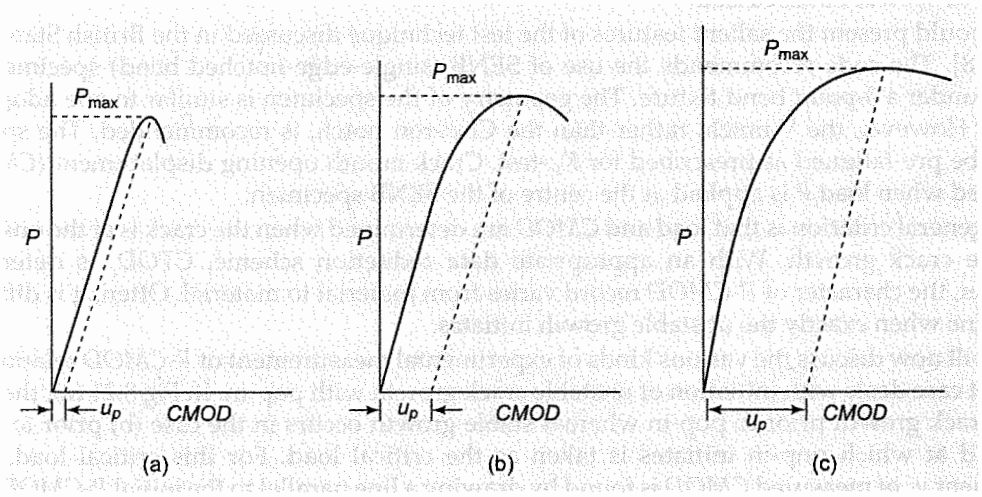

Fig. 8.22 *P-CMOD* record for (a) no stable growth, (b) stable growth prior to unstable growth initiating at P_{max} and (c) stable growth but unstable growth is initiated before P_{max}

The $CTOD_c$ is made of elastic and plastic parts given as:

$$CTOD_c = (CTOD_c)_e + (CTOD_c)_p$$

The elastic part $(CTOD_c)_e$ is calculated by finding K_{Ic} from *P-CMOD* records using secant line as described in Sec. 8.2. Then, the Dugdale model is invoked to find $(CTOD_c)_e$. For plane strain, the result of Dugdale model is modified by a factor of ½ to account for constraints on plastic deformation. Thus, the elastic portion of $(CTOD_c)_e$ is given by the expression:

$$(CTOD_c)_e = \frac{K_{Ic}^2(1-\nu^2)}{2\sigma_{ys}E} \tag{8.22}$$

The plastic portion of $(CTOD_c)_p$ is determined by assuming that the uncracked ligament works like a plastic hinge with its centre at a distance rb from the crack tip as shown in Fig. 8.23(a). Knowing u_p, rb and a, we determine $(CTOD_c)_p$ through simple analysis of similar triangles [Fig. 8.23(b)] as:

$$(CTOD_c)_p = \frac{u_p rb}{a+rb} \tag{8.23}$$

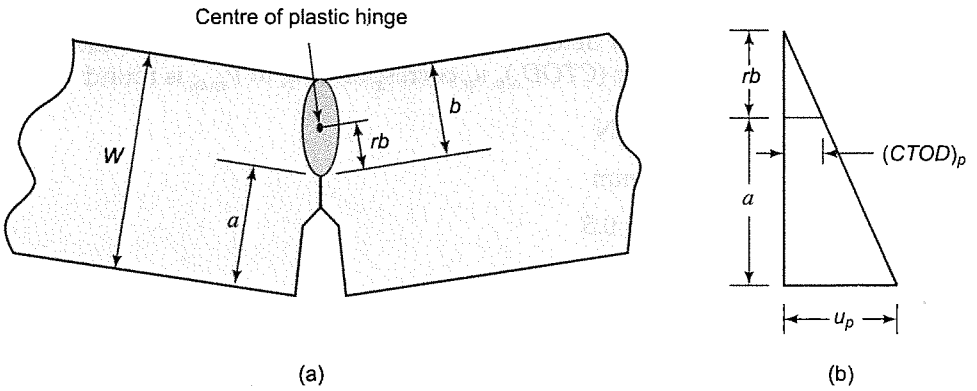

Fig. 8.23 (a) Plastic hinge with its centre at distance rb from the crack tip and (b) obtaining $(CTOD_c)_p$ through similar triangles

The factor r is determined through experimentation, and it is found to lie between 0.33 and 0.48. However, experimental determination of r is difficult on a routine test basis; therefore, a nominal value of $r = 0.4$ is used for standard testing of $CTOD_c$ giving

$$(CTOD_c)_p = \frac{0.4u_p(W-a)}{0.6a+0.4W} \tag{8.24}$$

Example 8.3 A single-edge-cracked bend specimen is loaded in a 3-point bend fixture (Fig. 8.1) and variation of centre load with *CMOD* is recorded. The span of the bend fixture is s =200 mm for the specimen of width W = 50 mm, thickness B = 25 mm, and crack length a = 25 mm. *P-CMOD* record of the test is shown in Fig. 8.24. Determine $CTOD_c$ following British Standard BS 5762 if E = 207 GPa, ν = 0.29, and σ_{ys} = 600 MPa.

Solution: S = 0.2 m, W = 0.05 m, B = 0.025 m, a = 0.025 m, $E = 207 \times 10^3$ MPa, ν = 0.29. From Fig. 8.24,

P_c = 26600 N (through 5% secant line)

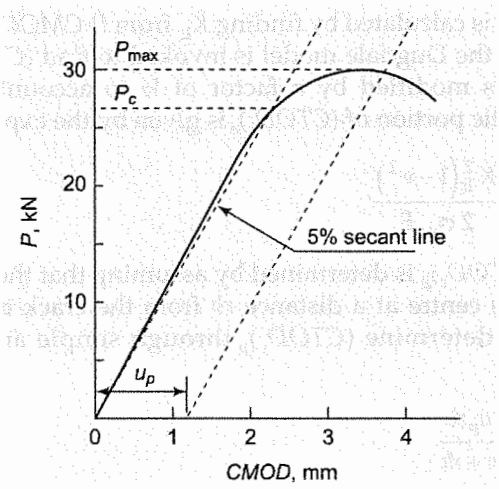

Fig. 8.24 *P-CMOD* record. For determining $(CTOD_c)_e$, 5% secant line is drawn to find K_{Ic}. For evaluating $(CTOD_c)_p$ u_p corresponding to P_{max} is found

$$P_{max} = 29800 \text{ N}$$

$$u_p = 1.14 \text{ mm}$$

$$\alpha = a/W = 0.5$$

Through Table 8.1 we find $f(\alpha)$ as:

$$f(\alpha) = 2.663$$

$$K_{Ic} = f(\alpha)\frac{P_c S}{BW^{3/2}} = \frac{2.663 \times (26600 \text{ N})(0.2 \text{ m})}{(0.025 \text{ m}) \times (0.05 \text{ m})^{3/2}}$$

$$= 50.7 \text{ MPa}\sqrt{\text{m}}.$$

Substituting in Eq. (8.22), we have:

$$(CTOD_c)_e = \frac{K_{Ic}^2(1-\nu^2)}{2\sigma_{ys}E} = \frac{\left(50.7 \text{ MPa}\sqrt{\text{m}}\right)^2\left(1-0.29^2\right)}{2(600 \text{ MPa}) \times \left(207 \times 10^3 \text{ MPa}\right)}$$

$$= 0.0095 \text{ mm}$$

Through Eq. (8.24), we have:

$$(CTOD_c)_p = \frac{0.4u_p(W-a)}{0.6a+0.4W} = \frac{0.4 \times (1.14 \text{ mm}) \times (0.05 \text{ m} - 0.025 \text{ m})}{0.6 \times 0.025 \text{ m} + (0.4 \times 0.05 \text{ m})}$$

$$= 0.325 \text{ mm}$$

The overall $CTOD_c$ becomes:

$$CTOD_c = 0.0095 + 0.325 = 0.335 \text{ mm}$$

Note that the elastic part of *CTOD* is negligible.

8.6 Closure

In this chapter test techniques are presented with reasonable details for finding K_{Ic}, J_{Ic}, G_{Ic}, G_{IIc}, and $CTOD_c$. Out of all these, K_{Ic} is the most widely used and its values are listed in literature for commonly used engineering materials. Determination of K_{Ic} is a relatively simple technique but a good quality *CMOD* gauge is required. Designs based on plane strain K_{Ic} are too conservative for high toughness materials. Also, determination of K_{Ic} for these materials is very difficult and expensive due to large thickness of the specimen. Therefore, EPFM should be used for which J_{Ic} or $CTOD_c$ are required. In comparison to $CTOD_c$ it is found that J_{Ic} is more convenient for designers. However, methods to find J_{Ic} are still complex, expensive and time consuming. It is hoped that simpler test-technique will be developed in future. G_{Ic} and G_{IIc} are found convenient for determining interlaminar toughness of composite materials. The test method for finding G_{Ic} is better developed and more widely used.

APPENDIX 8A

Regression Analysis to Fit a Line of Known Slope

Data analysis for finding G_{Ic} requires fitting a straight line of a known slope to experimentally recorded data. The line is $y = mx + c$ for which slope m is known and c is to be determined. The line is best fitted so as to minimize sum of square of the distance from data points to the line. Consider a point (x_i, y_i) and if the distance of the point from the line is d_i, the sum D of the square of the distance for n points is:

$$D = \sum_{i=1}^{n} d_i^2 = \sum \frac{(mx_i - y_i + c)^2}{m^2 + 1}$$

For minimum D, $\dfrac{dD}{dc} = 0$

leading to $$c = \frac{(-\Sigma m x_i + \Sigma y_i)}{n}$$

For $m = 3$, $$c = \frac{(-3\Sigma x_i + \Sigma y_i)}{n}$$

and for $m = -1$, $$c = \frac{(\Sigma x_i + \Sigma y_i)}{n}$$

Questions

1. Why are results of Charpy or Izod impact tests not useful in predicting loads that would grow an existing crack in a component with known geometry and boundary conditions?
2. Why are Charpy or Izod tests still popular in industries?
3. Why are the dimensions of specimen for plane strain K_{Ic}-test based on material toughness K_{Ic}?

4. Why is it difficult to find plane strain K_{Ic} of ductile materials?
5. Why is it required to extend a machined notch by fatigue for K_{Ic}-test?
6. There is a constraint on the maximum stress of fatigue load. Why so?
7. Why is Chevron notch better than V-notch for K_{Ic}-test?
8. In comparison to V-notched specimen, it is observed that fatigue crack initiation occurs at less number of cycles in Chevron notched specimen. Why so?
9. What does 5% secant line assure in K_{Ic}-test?
10. Why is texture of fatigue growth different from the texture of fractured surface?
11. Use of K_{Ic} by a designer is on conservative side. Comment on the statement.
12. K_{Ic} can be determined through one specimen, whereas to determine J_{Ic} several specimens are required. Why so?
13. Why do dimensions of specimens for J_{Ic}-test depend on J_{Ic}?
14. How do we implement the requirement of 'onset of crack initiation' in J_{Ic}-test?
15. Determination of critical SIF for plane stress is less rigorous because plastic zone size is large, and linear elastic analysis deviates considerably from the actual stresses and strains. However, J_{Ic} can be obtained quite accurately for plane stress cases. Why so?
16. G_{Ic}-test is found to be best suited for experimental determination of low toughness of certain cases such as interlaminar crack growth in fiber composite laminates. Why is K_{Ic}-test not suitable?
17. In G_{Ic}-test of interlaminar cracks, flexural rigidity (EI) is evaluated through the experiment on a DCB specimen and not through a separate experiment such as a tensile test. State the reasons.
18. In processing the data of G_{Ic}-test, how are the theoretical results exploited in the regression analysis?
19. Why do we like to have unstable crack growth in interlaminar G_{IIc}-test?
20. What are important requirements of a clip gauge?

PROBLEMS

1. The machined Chevron notch of SENB specimen is extended by a fatigue load with $P_{max} = 40$ kN and $P_{min} = 5$ kN. The dimensions of the specimen are:

   Thickness $B = 25$ mm
   Width $W = 50$ mm
   Span $S = 100$ mm
   Average crack length $a = 24.1$ mm.

   The critical load determined through 5 % secant line is 80 kN and the yield stress of the material is 800 MPa. Determine K_Q and check whether the dimensions of the specimen and fatigue load were proper.
2. A compact test specimen is employed to find plane strain K_{Ic}. The dimensions of the specimen are:

   Thickness $B = 30$ mm
   Width $W = 100$ mm
   Average crack length $a = 49.8$ mm

The experimental record of *P-CMOD* is shown in Fig. 8.25. Determine K_Q and check whether the experiment is valid if the yield stress of the specimen material is 600 MPa.

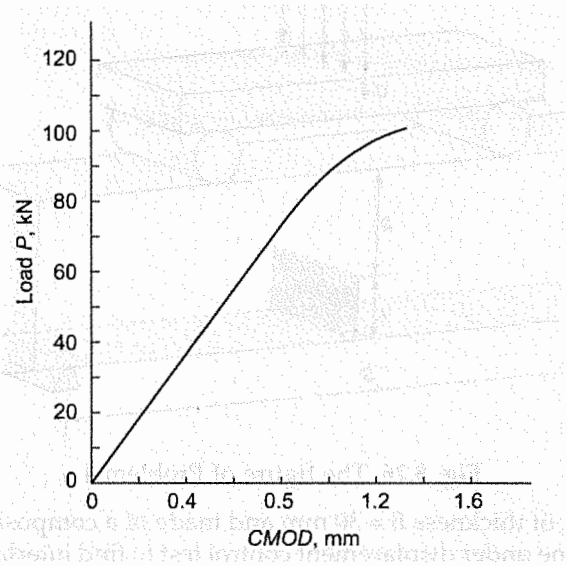

Fig. 8.25 The figure of Problem 2

3. Four SENB specimens of an unknown steel material were prepared to find J_{Ic} of the following dimensions:

   Thickness B = 20 mm
   Width W = 40 mm
   Span S = 160 mm

   The machined notch is fatigue grown till overall crack length is close to 0.5 W.
   Area (A) under the load displacement curve for a small crack growth is determined. The details of uncracked ligament b, crack extension Δa, and area A are:

Expt. No	b	Δa	A
	(mm)	(mm)	(Nm)
1	19.2	0.36	22.46
2	19.6	0.82	25.08
3	18.7	1.22	26.93
4	20.1	2.70	38.19

   The yield stress and ultimate tensile strength of the material are 350 MPa and 550 MPa respectively. Determine J_{Ic} and then find whether dimensions of the specimen were valid for finding J_{Ic}.

4. A bend specimen is loaded under four-point bending as shown in Fig. 8.26. Develop the expression for J if load displacement ($P - u$) record is known.

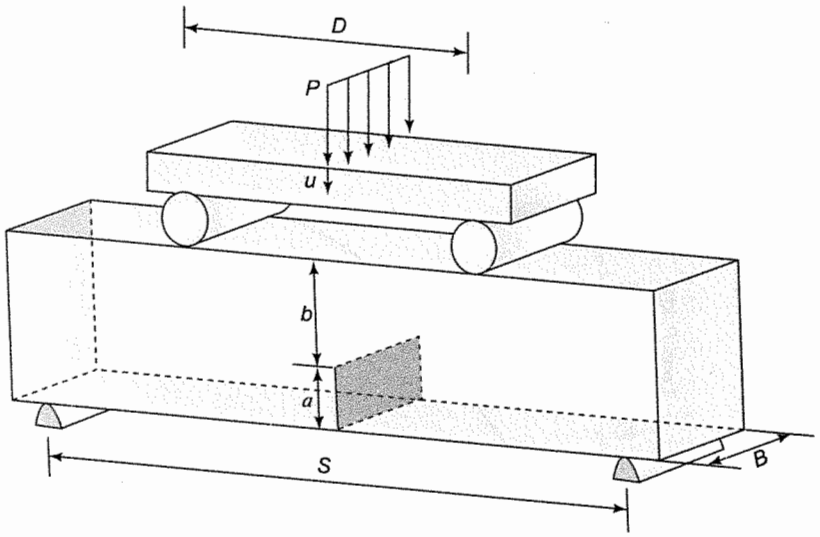

Fig. 8.26 The figure of Problem 4

5. A DCB specimen of thickness $B = 30$ mm and made of a composite material is pulled in a tensile test machine under displacement control test to find interlaminar toughness. Figure 8.27 shows the load-displacement record of loading and unloading cycles. The crack length

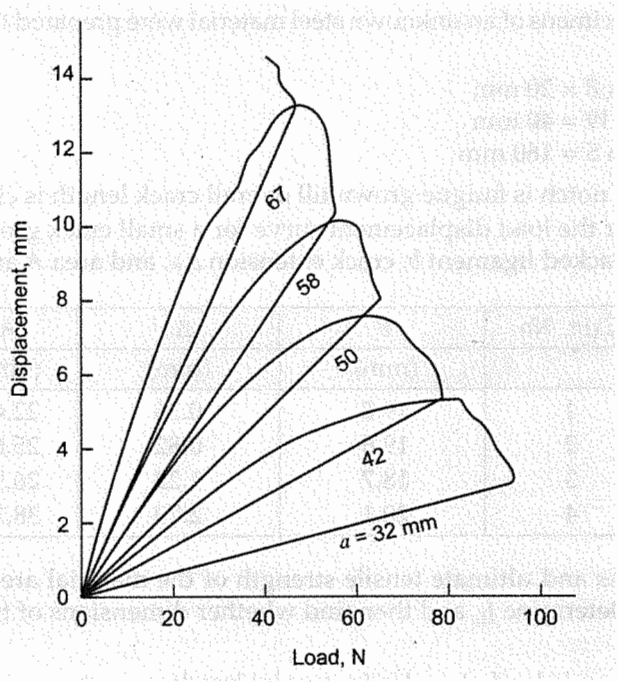

Fig. 8.27 The figure of Problem 5

of each loading is also shown in the figure. Determine critical energy release rate of interlaminar crack. Also, determine G_{Ic} through individual triangles; find the average and then compare it with G_{Ic} obtained by evaluation of A_1 and A_2.

6. An end-notched flexure specimen of a polymer composite is of length $2L$ = 160 mm, thickness B = 22 mm and overall height $2h$ = 3.2 mm (Fig. 8.19). A precrack of length a = 40 mm is introduced at a midplane of the specimen. Estimate the critical load if the estimated G_{IIc} is 1200 J/m^2 and modulus in the direction of specimen length is 110 GPa.

References

8.1 Annual book of ASTM Standards (1987). *Metals Test Methods and Analytical Procedures*, ASTM Publications, Philadelphia, 03.01, pp. 522–557.

8.2 Hertzberg, R.W (1989). *Deformation and Fracture Mechanics of Engineering Materials*, John Wiley and Sons, New York.

8.3 Begley, J.A. and Landes, J.D. (1972). The J-integral as a Fracture Criterion, *Fracture Toughness Part II*, ASTM STP 514, American Society for Testing and Materials, Philadelphia, pp. 1–20.

8.4 Broek, D. (1982). *Elementary Engineering Fracture Mechanics*, Martinus Nijhoff Publishers, The Hague.

8.5 Annual Book of ASTM Standards (1986). *Metals Test Methods and Analytical Procedures*, ASTM Publications, Philadelphia, 03.01, pp. 772–786.

8.6 Carlsson, L.A. and Pipes, R.B. (1987). *Experimental Characterization of Advanced Composite Materials*, Prentice-Hall Inc., New Jersey.

8.7 Carlsson, L.A., Gillespie Jr., J.W. and Pipes, R.B. (1986). On the Design and Analysis of the End Notched Flexure (ENF) Specimen for Mode II Testing, *Journal of Composite Materials*, 20, pp. 594–604.

8.8 BS 5762 (1979). *Methods for Crack Opening Displacement COD Testing*, British Standards Institution, London.

8.9 Ramesh, K. (2007). *e-Book on Engineering Fracture Mechanics*, IIT Madras, 2007. URL: http//apm.iitm.ac.in/smlab/kramesh/book_4_htm

Chapter

9

Fatigue Failure and Environment-assisted Fracture

Fatigue is a process that is capable of selecting the weakest link in strength...

V. Finkel

9.1 Introduction

The performance of a machine or structural component is usually tested in a laboratory where conditions are controlled. In real life conditions, the component is subjected to several harsh conditions. Fluctuating loads, known as fatigue loads, quite often cause failure of components. In addition, the combined effect of stresses and a corrosive environment may cause a premature failure of a component. It is now well-known that both of them cause the growth of subcritical cracks to their critical length, followed by the rapid crack growth and eventual failure of the component. It is difficult to protect the component from various fluctuating loads as we live with many machines which either rotate or have back and forth motions. Also it is difficult to control the service environment of a component. Even abundant materials like water or its vapors, various salts, oils, edible items are known to cause the growth of subcritical cracks to their critical length. Thus the designer of a component should identify its service conditions and if required, he should carry out an appropriate analysis to avoid its premature failure.

In this chapter, various aspects of fatigue failure and environment-assisted fracture are presented. In addition, a brief discussion on the combined effect of a fluctuating load and a corrosive environment is included.

9.2 Fatigue Failure

A component, which fails through yielding at a high constant (unfluctuating) load, may fail under a substantially smaller fatigue load. To consider an analogy, our muscles are not strong enough to make a tree fall. We can chip off the trunk bit by bit with an axe until the groove becomes so large that the tree can be pulled down easily with a rope. The process is slow but repeated action makes it fall.

Innumerable examples of fatigue loads can be observed in our nearby environment. Many machines use rotating shafts. Shafts are designed to carry torque, but lateral loads, which generate bending moments, cannot be avoided. Consequently, a fiber on the shaft surface which is aligned parallel to the axis is subjected to tensile and compressive stresses in every rotation. Consequently, the axles of railway wagons, automobiles, and gear boxes are subjected to fluctuating loads. Failure of a locomotive axle should be avoided as it can stall the entire train suddenly with the wagons tumbling and climbing over each other. One serious accident took place only two kilometers away from IIT Kanpur as late as in 1980s. One axle of a goods train failed and, consequently, most of the wagons were derailed and deshaped. It was a huge financial loss only due to fatigue failure in one of the axles of the train.

The wings of an airplane are subjected to fluctuating loads of wind gusts during the flights and therefore, the wings are carefully designed. In fact, before the flight test of a newly developed airplane, the entire wing is experimentally tested to fluctuating wind loads, simulated in the laboratory, till it fails. In another example, the fuselage of a plane is subjected to one cycle of pressure per flight because at high altitude the air pressure is increased inside to make it comfortable for the passengers. The fuselage of the ill-fated commercial Comet Jet airplanes failed in 1950s owing to a fatigue crack growth nucleated near an opening in its fuselage.

In sophisticated way of modern living, many automated machines and gadgets have been developed which involve some kind of rotation, reciprocating motions or vibrations, and, therefore, some crucial components are subject to fatigue loads. One cannot really avoid fatigue loads; they are as natural to machines as breath is to a human body. Therefore, we should learn more about them so as to avoid surprise failures. It has been observed that most fracture failures are initiated by fatigue loads. Initially, the crack length is subcritical and the crack is not dangerous. With subsequent load cycles, the crack grows to acquire length close to the critical length and then only conventional fracture mechanics (K_{Ic}, J_{Ic}, etc.) come into picture [9.1–9.3]. Mechanisms of crack initiation, especially quantitative models, are still not known well. However, once a crack has nucleated and has grown to the stage where it can be detected, some empirical or semi-empirical formulations are available for its subsequent growth.

9.2.1 Terminology

There are two kinds of fatigue loads, (i) constant amplitude load and, (ii) variable amplitude load. The loads on locomotive axles are of constant amplitude whereas fluctuating wind load on a wing of an airplane is of variable amplitude. In certain cases, both types of loads may be superposed on a component.

Figure 9.1 shows the constant amplitude loading with maximum stress σ_{max} and minimum stress σ_{min} with the stress range $\Delta\sigma$ given by:

$$\Delta\sigma = \sigma_{max} - \sigma_{min}$$

We define mean stress σ_m as:

$$\sigma_m = \frac{\sigma_{max} + \sigma_{min}}{2}$$

Corresponding to σ_{max} and σ_{min}, we can determine K_{max} and K_{min} as

$$K_{max} = f(a/W)\, \sigma_{max} \sqrt{\pi a} \tag{9.1}$$

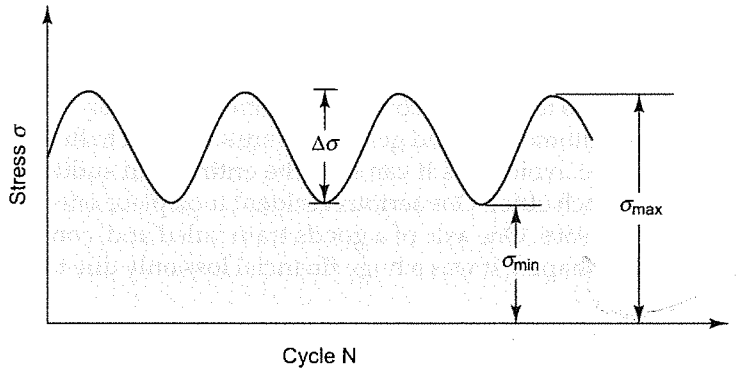

Fig. 9.1 Constant amplitude loading

$$K_{min} = f(a/W)\,\sigma_{min}\sqrt{\pi a}$$

where $f(a/W)$ is the geometric factor for crack length a and component width W.

In most cases, dependence of $f(a/W)$ on crack length a is secondary in comparison to $\sqrt{a}$ dependence. In order to keep the calculations simple, some designers prefer not to consider variation of $f(a/W)$. The difference of K_{max} and K_{min} is an important parameter for determining crack growth and is expressed as:

$$\Delta K = K_{max} - K_{min}$$

Another parameter, stress ratio R, is also used and defined as:

$$R = \frac{\sigma_{min}}{\sigma_{max}} = \frac{K_{min}}{K_{max}}$$

There are three categories of R — positive, zero and negative, as shown in Fig. 9.2. Positive R is tension-tension fatigue whereas negative R is tension-compression fatigue. For negative stress ratio, compressive stress loading is not likely to grow the crack and, therefore, some investigators treat this case same as the one having $R = 0$. However, in sophisticated analysis, $R = 0$ and $R < 0$ may be treated differently; some introductory discussion is included in Sec. 9.7.

A fatigue crack may be initiated at an existing notch, an inclusion or a surface. It has been observed that initiation requires a large number of load cycles. Once a crack is initiated, it grows by some distance in every cycle, initially with extremely small growth per cycle. As the crack becomes longer, the rate of propagation per load cycle, da/dN, also increases. Obviously, cracks of very small lengths cannot be detected by available non-destructive test-techniques. The number of cycles required to initiate a crack and then make it grow to a detectable length is known as initiation life N_i. Detectable crack in most cases is still sub-critical and needs to grow further under the fatigue load. The number of cycles required to grow the smallest detectable crack to a critical size is known as propagation life N_p. Thus, the total life N becomes

$$N = N_i + N_p$$

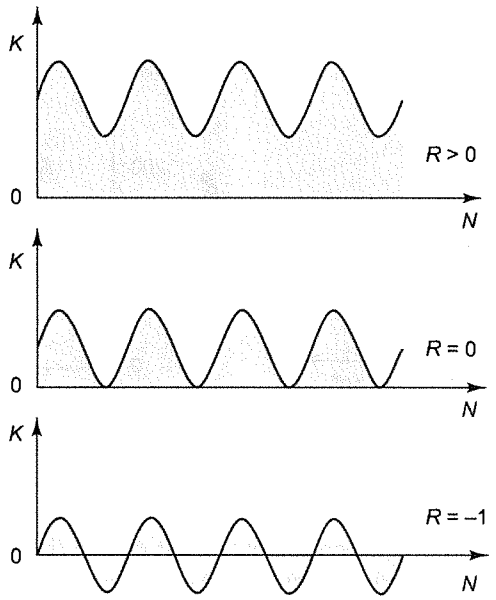

Fig. 9.2 Three categories of stress ratio

9.2.2 S-N Curve

In the nineteenth century, many structural bridges collapsed and the axles of locomotives failed owing to fatigue loads. It was then realized that a structure could fail even if the applied stress was much smaller than the yield stress. Fatigue test-machines were then developed. A test-machine applies a constant amplitude loading on a rotating shaft with bending stress ($R = -1$). Using the machine an empirical relation is determined between applied stress (peak value of the fluctuating load) and number of cycles N required to cause the failure. The relation is generally known as S-N curve shown in Fig. 9.3 (a) for steel and Fig. 9.3 (b) for nonferrous metals. At a higher stress, of course, the component has a shorter fatigue life. For steel, it is found that below the endurance limit σ_e the material does not fail. However, distinct endurance limit is not observed for nonferrous metals. It has been a common practice to design a steel component such that the critical stress does not exceed σ_e. Now, more sophisticated models are being developed based on the concepts of fracture mechanics. For nonferrous metals, conventional design approach has been to determine allowable stress σ_a for a reasonable number of cycles, say 10^8 cycles, as shown in S-N curve of Fig. 9.3 (b).

S-N curves have been in use for more than a century, and are still being used by conventional designers. S-N curves have certain limitations. An S-N curve adopts a black-box approach and it does not explore the mechanisms of failure. It does not even distinguish between initiation life and propagation life; only overall fatigue life is taken into account. There is hardly any consideration of the specimen size; that is, data generated on small size specimen may not be applicable on large size components. Also, the data on an S-N curve has a large scatter suggesting that the formulation

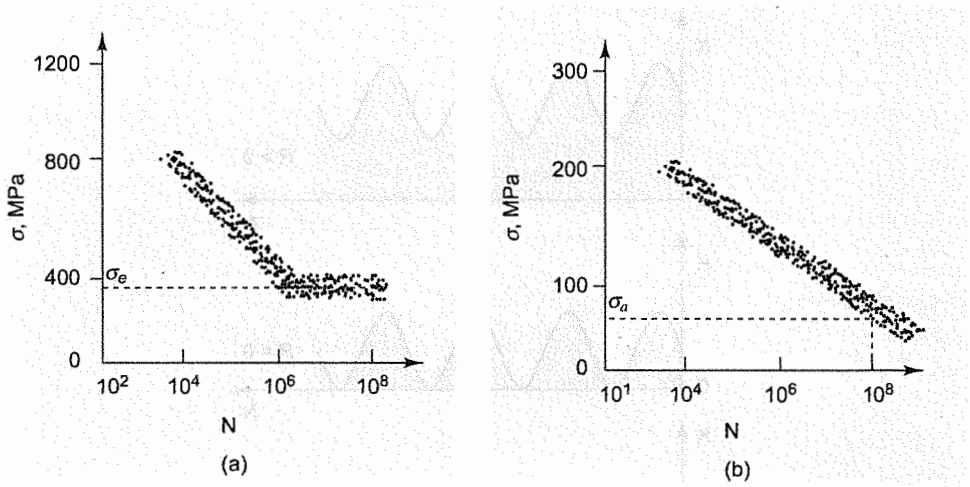

Fig. 9.3 (a) S-N curve for steel with endurance limit σ_e and (b) S-N curve for non-ferrous metals with no clear cut endurance limit

needs to be more rigorous. A component, designed on the basis of endurance limit, may still fail during its use. Locomotive wheel-axles are checked frequently for fatigue crack growth because S-N curve does not impart sufficient confidence for a fool proof performance.

The field of damage tolerance is being developed these days. Certain defects in a component can be tolerated with a reasonable assurance on quality. Number of defects may increase or existing defects may become longer with time. A non-destructive test is conducted to assess if the component is still safe for further usage. However, designs based on S-N curve approach do not entertain damage tolerance.

9.2.3 Crack Initiation

Crack initiation is observed to occur at the tip of an existing crack or at some point of a free surface.

A fatigue crack grows with each applied load cycle and therefore, crack growth per unit cycle, da/dN, is an important parameter. Initially, da/dN is extremely small, may be as small as 10^{-10} m/cycle which is of the order of one lattice parameter. Such a small crack growth rate cannot be detected easily and, therefore, it is included in crack initiation.

As the crack grows ΔK increases and da/dN eventually becomes quite large. When a fatigue crack is about to become critical, da/dN may become as large as several millimeters per load cycle. The crack growth is divided into three regions as shown in Fig. 9.4 on log-log scale. The crack growth curve is known as Sigmoidal Curve. In the region I, da/dN is very small. In fact, there is no initiation of crack growth if ΔK is smaller than a threshold ΔK_{th}. Even for ΔK exceeding ΔK_{th}, crack

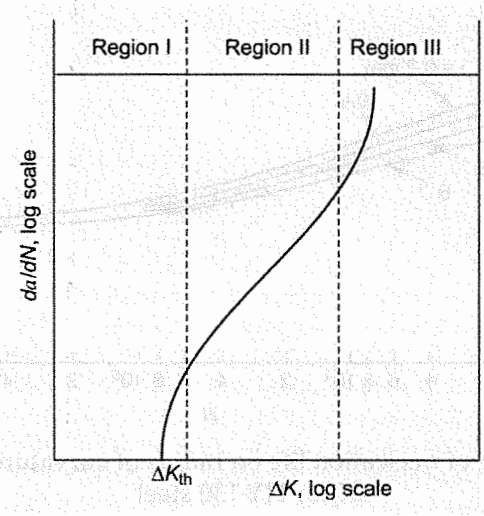

Fig. 9.4 Characteristic growth curve of a fatigue crack

TABLE 9.1 Representative value of ΔK_{th} and its dependence on stress ratio R

Material	$\sigma_{uts}(MPa)$	*R-ratio*	$\Delta K_{th}(MPa\sqrt{m})$
Mild Steel	430	–1.00	6.4
		0.50	4.3
		0.75	3.8
Austenitic Steel	685	–1.00	6.0
Maraging Steel	2010	0.67	2.7

growth per cycle cannot be easily detected. Threshold ΔK_{th} depends on material properties and stress ratio R; Table 9.1 shows representative values for some commonly used materials [9.4].

Initiation at the Tip of an Existing Defect

In case of a structural component, a crack may initiate at the tip of an existing defect, a reentrant corner, a slot, a void or an inclusion. In these cases, there exists some ΔK that helps in the nucleation of the fatigue crack. The initiation is influenced significantly by the radius of curvature of the defect. An inclusion with sharp notch is likely to nucleate the fatigue crack easily. Some investigators [9.4] have tried to investigate the effect of the radius of curvature on the initiation life N_i. Figure 9.5 shows the variation for initiation life with $\Delta K_I/\sqrt{\rho}$ where ρ is the radius of curvature of the crack tip [9.5]. Clearly, N_i is high for blunt crack tips.

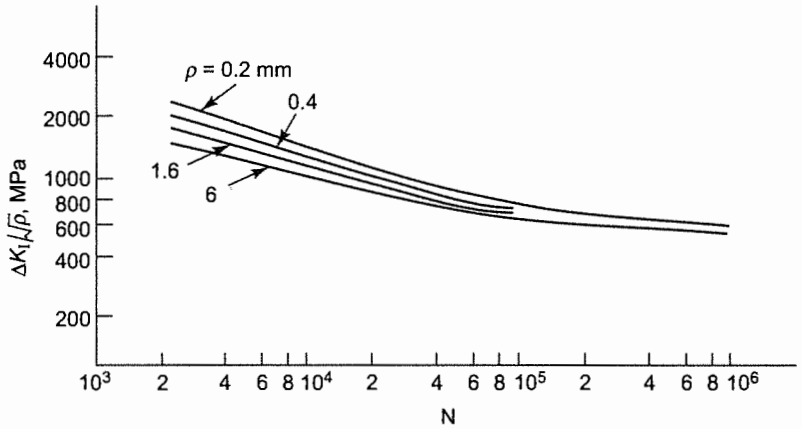

Fig. 9.5 Dependence of nucleation life on radius of curvature of the defect and ΔK_I for HY-130 steel

Initiation on a Surface

It is commonly observed that a fatigue crack initiates on a surface where no crack was existing before the cyclic load was applied. In fact, fatigue load, being a powerful force, tries to first initiate a crack on the surface of an existing inclusion, a hole or a reentrant corner. If any such initiation is not favorable, the fatigue load initiates a crack on a free surface. What causes the initiation?

When a metal specimen is subjected to a cyclic load, it is observed that dislocation glide bands initiate on the specimen surface. With increasing load cycles, these glide bands multiply laterally and become denser. As a result, the surface no longer remains smooth. The dislocations transport material from or to the surface, creating extrusions and intrusions on the surface as shown in Fig. 9.6. An intrusion acts like a crack with a finite ΔK. If the initial surface is not very smooth it encourages nucleation and growth of these intruded cracks. In fact, the surface of critical load bearing shafts is polished to have a very low roughness. It pays to make the surface very smooth as it delays the nucleation of surface cracks and enhances N_i. It is difficult to predict initiation life from the free surface of a component because the micro-mechanism of crack nucleation is still not well understood and quantitative formulations are difficult.

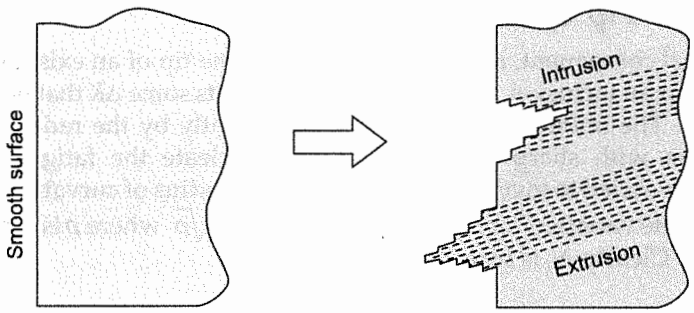

Fig. 9.6 Extrusion and intrusion created by glide bands

9.2.4 Crack Propagation

The crack propagation rate, da/dN, depends on ΔK and stress ratio R and it can be expressed in as

$$\frac{da}{dN} = f(\Delta K, R)$$

Many attempts have been made to find the nature of this relation. The results are empirical or semiempirical. For many materials, dependence of da/dN on R is not very significant, especially in Region II as shown in Fig. 9.7. Most designers are contented with the simple form:

$$\frac{da}{dN} = f(\Delta K)$$

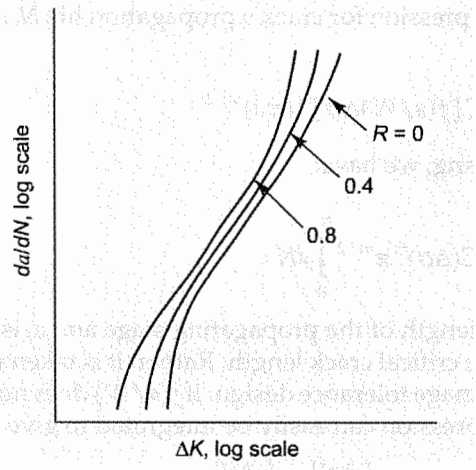

Fig. 9.7 Effect of stress ratio on Sigmoidal curve

Paris law is most widely used and is stated as:

$$\frac{da}{dN} = C(\Delta K)^m \tag{9.2}$$

where C and m are material constants to be evaluated through experiments for a material under consideration. To have a feel of the material constants, representative relations for some materials are:

- Ferrite-Pearlite steel [9.3]

$$\frac{da}{dN} = 6.8 \times 10^{-12} (\Delta K)^{3.0} \tag{9.3}$$

- Martensitic steel [9.3]

$$\frac{da}{dN} = 1.33 \times 10^{-10} (\Delta K)^{2.25} \tag{9.4}$$

- Austenitic stainless steel [9.3]

$$\frac{da}{dN} = 5.5 \times 10^{-12} (\Delta K)^{3.25} \tag{9.5}$$

- Cast iron [9.6]

$$\frac{da}{dN} = 4.3 \times 10^{-8} (\Delta K)^{4} \tag{9.6}$$

- Aluminum alloy (7075-T6) [9.6]

$$\frac{da}{dN} = 1.1 \times 10^{-11} (\Delta K)^{3.89} \tag{9.7}$$

In these relations, crack length a is in meter and ΔK in MPa$\sqrt{m}$. It is worthwhile to discuss the Paris law further and obtain an expression for crack's propagation life N_p. Substituting ΔK into the Paris law, we obtain:

$$\frac{da}{dN} = C[f(a/W)\Delta\sigma]^m (\pi a)^{m/2}$$

Rearranging and integrating, we have:

$$\int_{a_0}^{a_f} \frac{a^{-\frac{m}{2}} da}{f^m(a/W)} = C(\Delta\sigma)^m \pi^{m/2} \int_0^{N_p} dN \tag{9.8}$$

where a_0 is the initial crack length of the propagating stage and a_f is final crack length. It is worth noting that a_f need not be the critical crack length. Rather, it is taken usually to be the longest crack length permissible in the damage tolerance design. If $f(a/W)$ does not vary strongly, it can be taken as constant and then the expression can easily be integrated to give:

$$N_p = \frac{a_0^{\left(-\frac{m}{2}+1\right)} - a_f^{\left(-\frac{m}{2}+1\right)}}{(m/2-1)C\, f^m(a_0/W)(\Delta\sigma)^m \pi^{\frac{m}{2}}} \tag{9.9}$$

Note that this expression is not valid for $m = 2$ and one should go back to Eq. (9.8), which is simplified to:

$$\int_{a_0}^{a_f} \frac{a^{-1} da}{f^2(a/W)} = C(\Delta\sigma)^2 \pi \int_0^{N_p} dN$$

On integration,

$$N_p = \frac{\ln\left(\frac{a_f}{a_0}\right)}{C f^2(a_0/W)(\Delta\sigma)^2 \pi} \tag{9.10}$$

Example 9.1 An edge crack, detected on a large plate, is of length 3.1 mm under a constant amplitude cyclic load having $\sigma_{max} = 310$ MPa and $\sigma_{min} = 172$ MPa. If the plate is made of a ferrite-pearlite steel and $K_{Ic} = 165$ MPa $\sqrt{m}$, determine (a) propagation life up to failure and (b) propagation life if the crack length a is not allowed to exceed 25 mm.

Solution: For this large plate with the edge crack

$$f(a/W) = 1.12$$

$$\Delta\sigma = 138 \text{ MPa and } a_0 = 0.0031 \text{ m}$$

(a) The critical length $a_c = a_f = K_{Ic}^2/[\pi(1.12\ \sigma_{max})^2] = 0.0719$ m
Taking value of C and m from Eq. (9.3) we obtain propagation life up to fracture using Eq. (9.9) as

$$N_p = \frac{(0.0031)^{\left(-\frac{3}{2}+1\right)} - (0.0719)^{\left(-\frac{3}{2}+1\right)}}{\left(\frac{3}{2}-1\right)} \left[\frac{1}{6.8\times10^{-12}\times(1.12)^3(138)^3\times\pi^{3/2}}\right]$$

$$= \frac{17.96-3.729}{0.5} \times 7153 = 203.6\times10^3 \text{ cycles}$$

(b) Replacing $a_f = 0.0719$ by $a_f = 0.025$ in the solution of Part (a), we have

$$= \frac{17.96-6.325}{0.5} \times 7153 = 166.4\times10^3 \text{ cycles}$$

It is worth noting that difference in propagation life of two cases is small, only 37200 cycles. This is so because the crack propagates faster at a higher crack length.

The S-N curve approach has been used for a very long time and to a certain extent it works. It is worth exploring whether S-N curve is a subset of the Paris law. Focusing again on Eq. (9.9), we may argue that a_f is governed by K_{Ic} and if the material is not changed from one experiment to another, it remains constant. Similarly, a_0 is the initial crack length which can again be taken constant if specimen geometry is not altered during experimentation. We have then,

$$N_p = \frac{\text{constant}}{(\Delta\sigma)^m}$$

leading to $\log N_p = -m \log \Delta\sigma + \text{constant}.$

This is a familiar linear S-N curve on log-log plot.

If the effect of stress ratio R is to be included, the Paris law has been modified by several investigators. One such law, proposed by Forman et al. [9.7], is stated as

$$\frac{da}{dN} = \frac{C(\Delta K)^m}{(1-R)K_c - \Delta K}$$

where K_c is the critical stress intensity factor. If K_{min} is negative, the crack tip closes for compressive portion of a stress cycle and therefore K_{min} is taken as zero ($R = 0$).

The complete Sigmoidal curve of crack propagation can also be expressed through one equation. Erdogan and Ratwani [9.8] have suggested the following expression:

$$\frac{da}{dN} = \frac{C(1+\beta)^m(\Delta K - \Delta K_{th})^n}{K_c - (1+\beta)\Delta K}$$

where c, m, n, ΔK_{th} and K_c are material constants, and

$$\beta = \frac{K_{max} + K_{min}}{K_{max} - K_{min}}$$

Some investigators argue that the plastic zone size plays an important role in actual crack propagation, and in such a case elastic-plastic fracture mechanics should be used. One such form of crack propagation law is

$$\frac{da}{dN} = C(\Delta J)^m$$

where J is J-Integral. A similar analysis may be carried out with CTOD parameter or effective crack length.

9.2.5 Effect of an Overload

An overload is a pulse (or a set of pulses) of higher amplitude on a constant amplitude fatigue load as shown in Fig. 9.8. The crack propagation rate retards considerably after the overload pulse [9.9, 9.10].

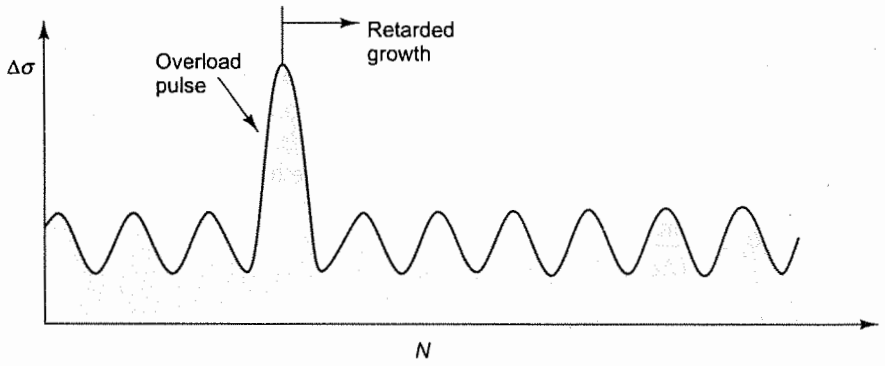

Fig. 9.8 An overload pulse on the constant amplitude fatigue load

Why does the propagation rate decrease after the overload pulse? To understand it, we look into the behavior of the plastic zone near the crack tip. The overload forms a much larger plastic zone. During the unloading portion of the overload pulse, the surrounding elastic material tries to regain its original state. However, the plastic zone cannot regain the original state and, therefore, compressive residual stresses are developed in the vicinity of the crack tip. In the follow-up pulses of the constant amplitude load, the tensile loading at the crack tip is suppressed by the residual compressive stresses. Consequently, da/dN is lowered appreciably. The crack tip may remain within the enclave of residual compressive stress for many subsequent pulses of the constant amplitude load as shown in Fig. 9.9.

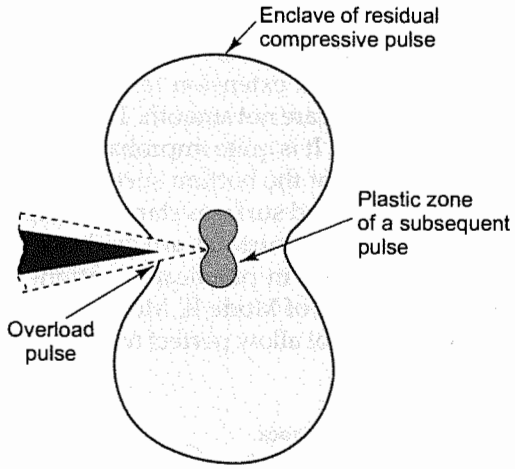

Fig. 9.9 Enclave of residual compressive stress developed by the overload and plastic zone of subsequent pulses

It, therefore, takes some load cycles for the crack tip to come out of the enclave and then only da/dN regains its value based on the length of the crack and ΔK at that location. The effect of overload on crack growth is shown in Fig. 9.10.

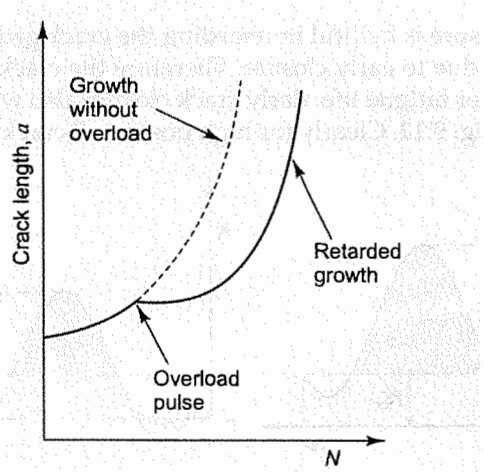

Fig. 9.10 Retarded growth of the crack owing to the overload pulse

9.2.6 Crack Closure

We will first consider the cases when K_{min} is zero ($R = 0$). During the unloading portion of a load cycle, it has been observed that crack faces start touching each other for some finite tensile stress. Figure 9.11 shows that the crack closes at a point A. When the stress is reduced further to zero,

compressive stress at the crack tip is developed [9.11]. Why does a crack close at point A and not at point B? To understand it, we should study the nature of cracked surfaces developed through the fatigue load. Each cycle produces some crack extension forming a ridge and a valley, known as striation. Furthermore, surfaces of a striation are not smooth. They are rough owing to non-uniform local plastic deformation during separation. It is quite improbable to expect that all the peaks of the top surface will fit exactly into the valleys of the bottom surface on unloading. Therefore, as K is reduced below point A of Fig. 9.11, the touched surfaces start exerting compressive load. The early crack closure is facilitated if the newly created surfaces are oxidized or have some other chemical reaction with the atmospheric air. Moreover, in practical situations it is rare to have only pure Mode I acting on a crack. Some contribution of Mode II, Mode III is generally present that causes lateral shift of cracked surfaces and would not allow perfect matching of the surfaces on unloading.

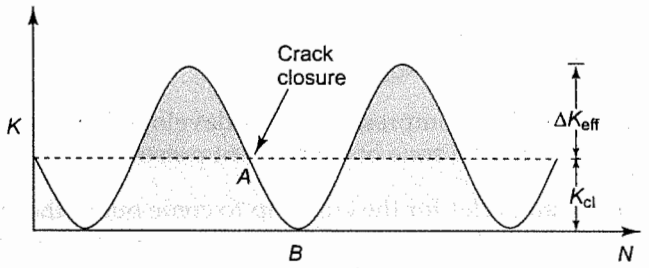

Fig. 9.11 Early closure of a crack and reduction in ΔK to ΔK_{eff}

Fortunately, the crack closure is helpful in retarding the crack growth. It is clear from Fig. 9.11 that effective ΔK is reduced due to early closure. Therefore the crack propagation rate is reduced and a component has a longer fatigue life. Early crack closure also works for $R < 1$ and may work for positive R as shown in Fig. 9.12. Clearly for high positive R crack closure is less.

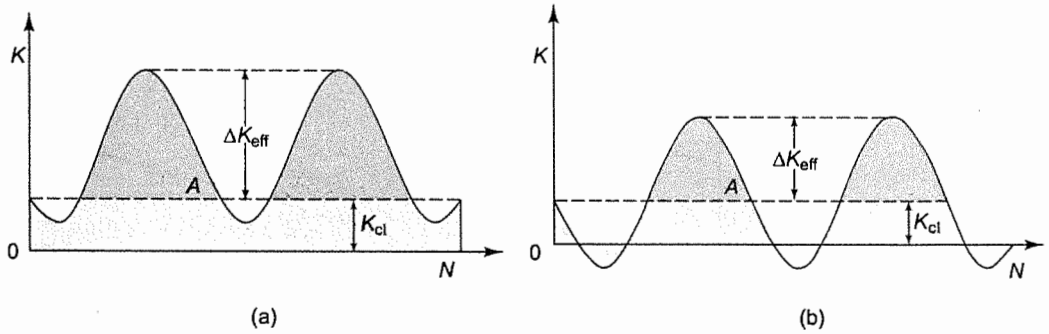

Fig. 9.12 (a) Crack closure for $R > 0$, and (b) for $R < 0$

How to find the effective ΔK? One can perform experiments to find K at which the crack closes. However, it is not possible to do experiments every time a component is designed. We would rather have some models to determine it. The effective ΔK is expressed as

$$(\Delta K)_{eff} = K_{max} - K_{cl}$$

where K_{cl} is the stress intensity factor at the time of closure of crack faces [9.12, 9.13]. However, K_{cl} is generally not determined. An alternative procedure is adopted by modifying the Paris law by associating a factor U with ΔK. The Paris law is then written as:

$$\frac{da}{dN} = C\,(U\Delta K)^m \tag{9.11}$$

where

$$U = \frac{K_{max} - K_{cl}}{K_{max} - K_{min}}$$

Several empirical models have been suggested for finding U. Elber [9.12] proposed the formula for 2024-T3 aluminum as

$$U = 0.5 + 0.4\,R \tag{9.12}$$

and Schijve [9.13] suggested the formula for 2024-T3 aluminum, as

$$U = 0.55 + 0.33\,R + 0.12\,R^2 \tag{9.13}$$

Crack closure has already been accepted by industry and some computer packages do make necessary correction on crack propagation rate.

9.2.7 Variable Amplitude Fatigue Load

Constant amplitude fatigue load is simpler to study but is not as common as variable amplitude load in many applications. Machines and structures like pumps, vehicles, earth moving equipments, rolling mills, ball and cylindrical bearings, airplanes, bridges, ships and off-shore structures are subject to variable amplitude fatigue loads.

Can the Paris law or some other law for crack propagation rate still be used? Yes, but with some reservations. The data of the variable amplitude load should be processed before invoking the Paris law [9.3, 9.8]. However, there exists a problem of fundamental nature. We have already noted in Sec. 9.6 that a high stress pulse retards the propagation rate of some subsequent load cycles significantly. The number of retarded load cycles depends upon the relative magnitude of stresses. In case of variable amplitude loads there are many overload pulses, each having associated load cycles with retarded crack growth. It is difficult to keep track of the extent of retardation and predict the crack growth. However, if the variable amplitude is limited to a narrow band, the retardation of the crack growth may be ignored. This simplification is on the conservative side and a designer may not mind it.

To predict the life or the crack growth of a component, one should know the expected load history based on previous experiences. It is worth noting that the nature of load varies considerably from one kind of application to another [9.14]. For example, variable amplitude load on aircraft wing is quite different from the load on a lifting crane. Moreover, the load fluctuations generally do not follow the Gaussian distribution. Based on the application, a suitable statistical procedure is adopted to determine root mean square value of ΔK. If Paris law is chosen, the propagation equation becomes:

$$\frac{da}{dN} = C(\Delta K_{rms})^m$$

Example 9.2 Fluctuating load on a critical component of an offshore structure is shown by a histogram in Fig. 9.13. During a routine check-up, an edge crack of length 1.5 mm is detected. If the crack length is not allowed to exceed 25 mm, determine the remaining life of the component. Use Paris law with material constants as $C = 6.0 \times 10^{-12}$ (MPa)$^{-3.2}$ m$^{-0.6}$ and $m = 3.2$.

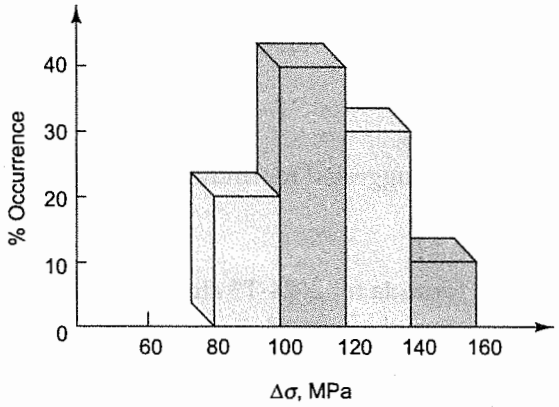

Fig. 9.13 Percentage occurrence of load pulses of the variable amplitude load

Solution: $(\Delta\sigma)_{rms}$ is evaluated as

$$(\Delta\sigma)_{rms} = \sqrt{0.2\times 90^2 + 0.4\times 110^2 + 0.3\times 130^2 + 0.1\times 150^2} = 117.4 \text{ MPa}$$

$$\frac{da}{dN} = C(\Delta K_{rms})^m$$

Using Eq. (9.9),

$$N_p = \frac{0.0015^{\left(\frac{-3.2}{2}+1\right)} - 0.025^{\left(\frac{-3.2}{2}+1\right)}}{\left(\frac{3.2}{2}-1\right)\times 6.0\times 10^{-12}\times (1.12)^{3.2}\times (117.4)^{3.2}\times \pi^{\frac{3.2}{2}}}$$

$$= \frac{49.47 - 9.146}{135.6\times 10^{-6}} = 297\times 10^3 \text{ cycles}$$

9.3 Environment-Assisted Fracture

9.3.1 Introduction

Man makes various machines, structures, and other mechanical systems, which deteriorate slowly in their service environment. In fact, all kinds of atmosphere, most kinds of water, oils, chemicals, gases, and food corrode structural components. The corrosion is known to be high in the vicinity of a crack tip where stresses are large and the plastic deformation is intense. In metal components, slip bands with innumerous dislocations facilitate the dissolution of material and thus the crack length increases slowly. This process may also be facilitated by the anodic dissolution at the crack tip. For example, when a component of mild steel is submerged in water, it loses its metallic ions close to the crack tip.

The loss of metallic ions leaves extra electrons on the surface, thus making the crack tip behave as an anode. The dissolution through such an electrolytic cell (galvanic cell) is known to be accelerated under a stressed field. Also, owing to the tensile field at the crack tip, small sized hydrogen atoms may diffuse into the component's material, causing hydrogen embrittlement and easy growth of the crack. Thus, the environment–assisted corrosion gradually increases the length of a subcritical crack. The growth of a crack length, in turn, increases the Stress Intensity Factor (SIF) and a stage reaches when the SIF becomes critical, causing rapid failure of the component. A designer should choose the material of the component or the working environment carefully to limit the environment-assisted crack growth.

It is difficult to formulate the environment-assisted fracture mechanics. It is an interdisciplinary field involving chemistry of materials, electrical aspects of current flow, and various mechanical and materials aspects such as diffusion, plastic deformation, grain boundaries, impurity content, voids, etc. Many different kinds of corrosion mechanisms act on the tip of a crack. Some mechanisms are known and backed by experimental findings. Models for some other mechanisms are available in literature but they have not been verified still by experimental. The complexity of the formulation increases further as there are many different kinds of materials and a variety of corrosive environments. The corrosion of a material is often found to be affected considerably by a slight change in a material parameter such as impurity content, percentages of alloying elements, heat treatment, work-hardening, etc. Also a slight change in environment may influence the corrosion substantially. For example, atmospheric humidity plays a crucial role in the rusting of steel components. Consequently, a comprehensive coverage on environment-assisted cracking is beyond the scope of this book and only an overview is presented in this chapter.

A corrosive environment affects all surfaces of a component. Even a smooth surface develops roughness under the combined effect of high stresses and environment. The micro-crevices thus generated grow with time. Some of them become cracks of finite length and grow further to cause component's failure. Similar to the fatigue failure from a smooth surface, there is an incubation time for an environment-assisted crack to nucleate. In this chapter, owing to the complexity involved we will not discuss nucleation of cracks on smooth surfaces. We would be confining our attention only to an already existing crack in a metal component to study how a corrosion crack nucleates on the tip of the existing crack and how it grows to cause the eventual failure of the component.

9.3.2 Micromechanisms

Most structural metals like aluminum, titanium, steel, copper, etc. are naturally protected from a thin oxide layer on their external surfaces. The thin layer, being passive in most metals, protects the interior material from rapid corrosion. For example, if an aluminum component is cut in air, a thin layer of aluminum oxide is immediately developed on the new surfaces and protects the component. For stress corrosive cracking, the passive layer should be broken. As discussed in the earlier chapters, the stresses at the crack tip are high, which cause intensive plastic deformation in the plastic zone. In metals, slip bands consisting of innumerous dislocations make the surface near a crack tip rough with micro-cracks. Consequently, the passive thin layer is broken, exposing the material to the corrosive atmosphere. In fact, the size of the plastic zone is not important because only the plastic deformation near the crack tip is influenced by the corrosion. Thus, the rate of crack growth does not depend much on increasing stress intensity factor with the advancement of the crack length. This aspect will be discussed further in the next section.

The crack surface in the vicinity of a crack-tip, as stated in the previous section, becomes the anode of the electrolytic cell formed. If the crack surface of steel component is wet with water, the iron ions in the vicinity of the crack tip dissolve, leaving excess electron on the surface. Thus the crack surface near the tip starts acting as the anode of the electrolytic cell as modeled in Fig. 9.14. Far away from the crack tip, the passive layer works as the cathode of the cell. The excess electrons on the anode pass through the conducting body of the component to the cathode surfaces. These electrons then reduce the hydrogen ions of the surrounding water, resulting into the evolution of hydrogen gas. Some of these hydrogen atoms may diffuse into the component to cause hydrogen embrittlement which is discussed subsequently in this section. The current density of the electrolytic cell regulates the rate of material loss at the crack-tip. Since the metal is in direct contact with the corrosive environment near the tip, the current density can be high. However, the resistance of the cathode oxide layer is quite high and thus it restricts the current density of the electrolytic cell and the dissolution rate to low levels. It is worth noting that the crack growth through anodic dissolution is continuous.

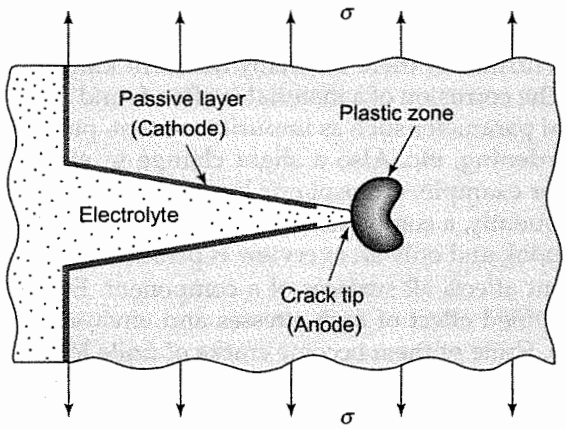

Fig. 9.14 The electrolytic cell formed near the crack tip

It is also observed that in comparison to the interior crystalline material the grain boundaries of most metals are more anodic. This causes higher dissolution rate at the grain boundaries, resulting into intergranular crack growth.

Owing to the tensile stresses in the vicinity of the crack tip of a component, the hydrogen atoms, being small in size, diffuse into the grain boundaries, the voids, the inclusions and highly strained slip-bands. The diffused hydrogen atoms make the material brittle and the process is known as hydrogen embrittlement. The diffusion is usually slow but makes the material in the vicinity of the crack tip brittle and the crack is no longer able to withstand the SIF. Consequently, the crack grows to the point where the effect of hydrogen embrittlement is diminished. The crack thus moves by a small step. Usually the failure is intergranular as grain boundaries are more susceptible to hydrogen embrittlement. It again takes some time for hydrogen atom to diffuse beyond the extended crack tip. Thus, unlike the continuous anodic dissolution the crack, the growth through hydrogen embrittlement is in short steps.

In some cases, the anodic dissolution facilitates the diffusion of hydrogen. For example, anodic dissolution grows a crack tip within a grain till it reaches a grain boundary, thus exposing the grain boundary for hydrogen diffusion. Thus the environment-assisted crack growth is often caused by the simultaneous actions of several mechanisms.

9.3.3 Test Methods

Tests on environment-assisted cracking fall into two categories: (i) the constant load method and (ii) the constant displacement method. In both categories, specimens with a precrack are employed whose notch is sharpened with a fatigue growth. The constant load test setup requires multiple specimens and thus the testing expenses are on higher side. On the other hand, only one specimen can suffice in the constant displacement test, but the crack does not grow to become critical to cause the failure and therefore the experiment yields less number of results. Details of strengths and limitations of each method will be discussed subsequently in this chapter.

Constant Load Method

In the constant load test, a cantilever specimen with a sharp notch is commonly used as shown in Fig. 9.15. A lever arm is bolted to the far end of the specimen so as to generate high bending moment using a dead load P. The bending moment remains constant throughout the duration of an experiment. But the Stress Intensity Factor (SIF) increases with the advancing crack. The crack tip is surrounded within a corrosion chamber where corrosive environment is controlled as per the requirements.

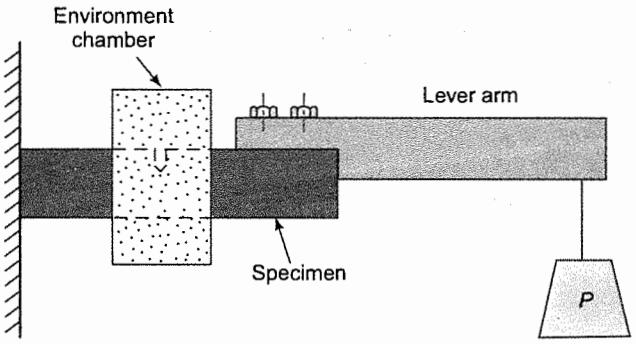

Fig. 9.15 A schematic test setup of the constant load method

The crack tip is prepared following the same procedure as used for making specimens for K_{Ic}-test (Sec. 8.2.4). A machine crack is prepared, preferably with a Chevron notch to initiate the fatigue crack at small number of cycles. The fatigue load is carefully chosen to have the SIF at the crack tip substantially smaller than the SIF developed by the constant load during environment-assisted testing.

A standard test machine such as a universal testing machine may be employed but corrosion test are long duration tests and therefore use of a costly machine may be avoided. A simple setup as shown in Fig. 9.15 can be easily designed and developed in a test laboratory. The constant load test yields several results such as:

- Determination of time-to-failure for an initial SIF, K_{Ii}
- Determination of threshold SIF, K_{Ith}, below which the precrack would not grow
- Determination of the rate of crack growth, da/dt.

It is worth noting here that most real life structures of aerospace, automobile, nuclear plants, etc. are not thick enough to qualify for plane strain conditions. Also the results are required for a

specific set of material-environment interface. Since there are many combinations of materials and environments, it is practically very difficult to have data for all cases in the open literature. Thus a user is expected to determine results for the combination of material and environment to which the component would be subjected in service conditions. In such a circumstance, the user may get the testing done under the conditions which simulate the actual application of the component. Thus, he need not make specimens which satisfy stringent conditions of plane strain. Thinner specimens corresponding to plane stress or transitional cases (Fig. 5.8) may be used which will fail at the maximum value of SIF, K_{max}. Of course, in case a specimen meets the requirements of plane strain, the specimen will fail at K_{Ic}.

A set of multiple specimens, usually 5 to 10, are employed to conduct the constant load test. The specimens are loaded with varying initial stress intensity factor, K_{Ii}. During the experimentation the crack length of a specimen is continuously monitored. To determine the length of a crack it is not recommended to use the usual method of monitoring the change of electrical resistance with the increasing crack length. The resistance method applies a voltage on the specimen which may affect the voltage of the electrolytic cell formed at the crack tip. Thus the resistance method is likely to introduce errors in experimentation. One usually adopts the method of monitoring the change in compliance by recording the crack mouth opening displacement and then calculating the crack length.

It usually takes a fairly long time for the precrack to start growing once a specimen is placed in a corrosive environment. This time is known as incubation time, t_{inc}. After the incubation time, it takes an additional time t_g for the crack to grow till failure. Thus the total time-to-failure t_f becomes:

$$t_f = t_{inc} + t_g$$

The characteristic relation between time log(t) and K_{Ii} is shown in Fig. 9.16. If such a relation is available to a designer and the initial crack length of a crack is known, he can estimate the life of a component.

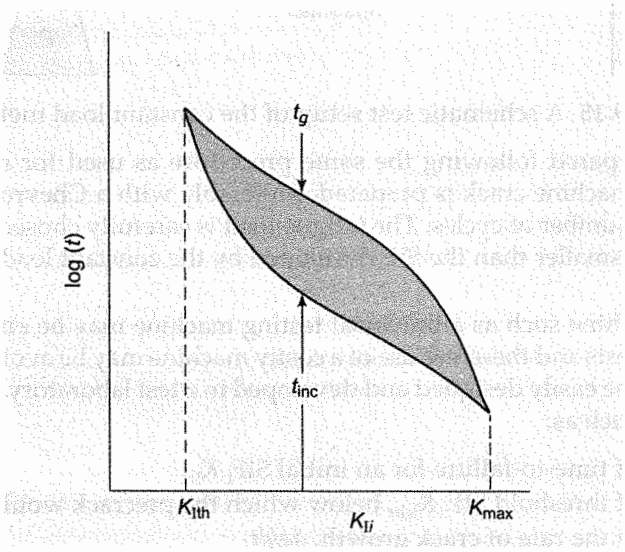

Fig. 9.16 Characteristic relation of incubation time t_{inc} and growth time t_g versus initial SIF, K_{Ii}

A relation between K_{Ii} and time-to-failure t_f is also explored through constant load tests to determine threshold K_{Ith}, below which no crack extension takes place due to the stress-assisted corrosion. Figure 9.17 shows a characteristic relation between K_{Ii} and time to failure. It is, in fact, difficult to determine K_{Ith} as tests have to be performed for very long durations. Some experiments are conducted by applying a load which develops SIF just above the K_{Ith}. Then load is reduced to have no crack growth even when the specimen is exposed for a long time. What should be the adequate test duration to determine K_{Ith}? For some material-environment combinations, 1000 hours of test time is adequate to assume that the crack would not grow if the specimen is exposed for longer time. But for other combinations it may require testing for longer duration. In fact, the adequate duration of a test depends on the material-environment interface. Therefore for testing an altogether new combination, preliminary testing is required to determine the adequate test duration.

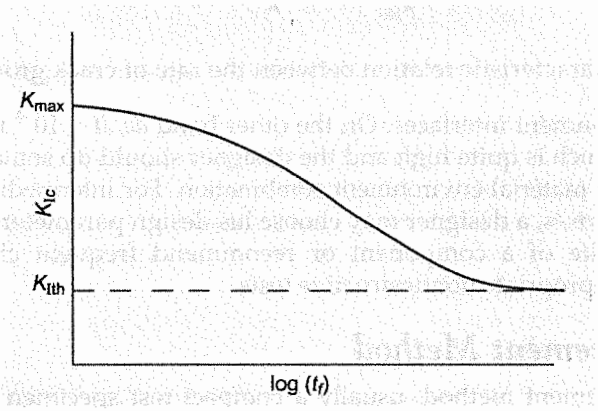

Fig. 9.17 Characteristic relation between initial SIF and time-to-failure, t_f

The constant load tests also leads to another useful relation between the rate of crack growth and the instantaneous SIF that increases with the crack growth. Figure 9.18 shows the schematic diagram of log(da/dt) versus K_I where a is the crack length. In most combinations of materials and environments, three regions are observed. An initial crack having its SIF less than K_{Ith} does not grow at all. In Region I, there is a steep rise in da/dt with K_I. In the Region II, da/dt shows a plateau; that is, there is no increase in the crack growth rate with the increasing SIF. As mentioned in the previous section, the corrosion depends only on the material in the vicinity of the crack tip. At a higher SIF the plastic zone size increases, but the flow stress at the crack tip is not affected much. Thus stress corrosion cracking in the Region II continues to grow at the constant rate till the SIF starts approaching K_{max}. The rate of crack growth increases at a much faster rate in the Region III and causes the failure of the specimen. The rate of increase in da/dt is so high in certain materials that the Region III is not even recorded. However, the Region III is not of much use to us and we need not make special arrangement to monitor it. We thus note that in the Region I a stress induced corrosion crack is nucleated at the tip of the existing precrack. The Region II signifies the growth period of the crack. The Region III is not important as the crack propagates rapidly to cause the failure of the component.

The crack growth rate in the Region II is usually in the range of 10^{-8} mm/s to 10^{-4} mm/s for most material-environment interfaces. It is worth noting that $da/dt \approx 10^{-8}$ mm/s corresponds to about 0.3 mm crack growth per year which is negligible for most applications. There is no need to do analysis

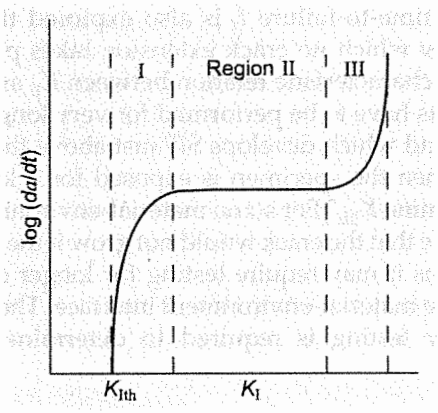

Fig. 9.18 Characteristic relation between the rate of crack growth and SIF

on such material-environment interfaces. On the other hand $da/dt \approx 10^{-4}$ mm/s corresponds to 9 mm growth in a day which is quite high and the designer should do some major design changes such as exploring other material-environment combination. For intermediate cases of da/dt in the range of 10^{-6} and 10^{-7} mm/s, a designer may choose his design parameters to either avoid failure within the designed life of a component or recommend frequent checking of the crucial components through appropriate nondestructive tests.

Constant Displacement Method

In the constant displacement method, usually a compact test specimen is modified. An initial displacement is given between the two ends of the cantilevers of the specimen and then the displacement is maintained (fixed grip loading). Initially the SIF is high but it decreases as the environment-assisted crack grows. A universal test machine can be used to conduct this test but usually a simple configuration is incorporated within the specimen. Figure 9.19 shows the schematic diagram of the configuration in which a tapped hole is made in the top cantilever. In the bottom

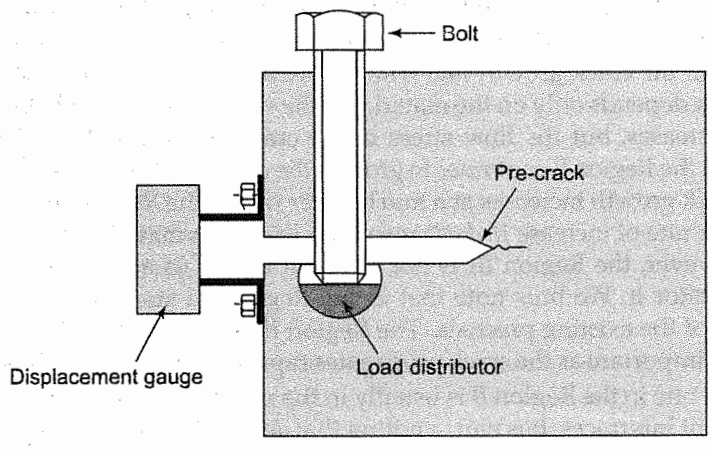

Fig. 9.19 A schematic test setup of the constant displacement method

cantilever a through-the-thickness hole is made within which a rod with its top flattened is slipped in. In fact, this hole is made before the machine crack is introduced in the specimen so as to facilitate its fabrication. This rod distributes the point load applied by the bolt that is screwed into the tapped hole in the top cantilever. By rotating the bolt the bottom cantilever is pushed out to develop the required initial gap between the two ends of the cantilevers. The specimen is placed within an environmental chamber or it can be taken to an outdoor field to simulate the conditions of the actual application.

The crack length is monitored to determine the crack growth rate. The length at which the crack stops growing corresponding to K_{Ith} and thus one single experiment yields K_{Ith} unambiguously. Recall that in case of the constant load method, several tests are required at K_{Ii} slightly above and slightly below the K_{Ith}. Even after running an experiment for a long duration, there is still a doubt that the crack would have grown if the experiment had been conducted for a longer duration. However, there is a major difference between the two kinds of experiments. In the constant load method the SIF increases till failure. On the other hand, the SIF decreases in the constant displacement test to K_{Ith} and thus the test does not evaluate the time-to-failure and the incubation time.

9.3.4 Major Factors Influencing Environment-assisted Fracture

There are many factors which influence the crack growth in a component under the combined action of the stresses and environment. Some of the important parameters are:

***Alloy chemistry*:** The environment-assisted cracking in materials often depends on the percentage of the alloying elements. In certain materials even minor changes in the alloying elements drastically alters the environment-assisted cracking. For example, the rate of crack extension in aluminum 7079-T651 is about 1000 times greater than that of Aluminum 7178-T651 when tested in 3.5 % sodium chloride water [9.15].

***Heat treatment*:** The yield stress of many alloys is enhanced by proper heat treatments, but the increase in the yield stress may deteriorate the corrosion resistant. For example, in a study the alloy steel 4340 was tested under the flowing sea water conditions [9.15]. When the heat treatment was changed to increase its yield stress from 900 to 1400 MPa, decrease in K_{Ic} was not much, 95 to 66 MPa $\sqrt{m}$ only. However, the threshold SIF, K_{Ith}, dropped drastically from 76 to 10 MPa $\sqrt{m}$. In another study [9.15] on over-aging of the aluminum alloy 7079-T651, it was found that the rate of crack growth decreased by a factor of 100 when the over-aging was increased from 1 hour to 15 hours at 160° C.

Humidity: The humidity of environment has pronounced effect on environment-assisted fracture of certain materials. In the aluminum alloy 7075-T651, it was found that the crack growth rate increased 24 times when the relative humidity of the surrounding air was increased from 5% to 67% [9.15].

Salt concentration: Service components are often immersed in a liquid with a salt whose concentration may have marked influence on the corrosion behaviour. For example, an increase in the concentration of potassium iodide enhances the crack growth rate (da/dt) in aluminum alloy 7079-T651 as shown in Table 9.2 [9.16].

TABLE 9.2 Variation of crack growth rate with the concentration of potassium iodide

Concentration of K_I *(Mole)*	*da/dt (mm/s)*
0.002	3×10^{-5}
0.020	7×10^{-5}
0.200	80×10^{-5}
2.000	600×10^{-5}

Temperature: For some combinations of materials and environments, there is a considerable influence of the temperature on the stress assisted cracking. If the influence is considerable, a relation may be explored to do accelerated tests at higher temperatures and predict the behavior on a longer time span at lower temperatures of components in service.

Work-hardening: Plastic deformation in a metal generates a large number of dislocations which in turn enhance the corrosion. It is a common observation that a steel wire corrodes first at bends where material is work-hardened. Some designers like to choose cold rolled sections and sheets as materials of their components because their yield stress is significantly higher over that of hot-rolled sections, about 20 % in mild steels. However, higher susceptibility to environment-corrosion of work-hardened materials offsets the advantage of the higher yield stress.

9.3.5 Liquid Metal Embrittlement

Liquid Metal Embrittlement (LME) is another mechanism of environment-assisted crack growth. On the surface of a metal component, a thin layer of some other liquid metal may cause the rapid growth of a crack. In some cases the growth rate may be as high as 5000 mm/s. The exact mechanism is not known but some investigators believe that the layer of a liquid metal around the crack tip reduces the cohesive strength of the molecules of a ductile material, causing rapid growth of the crack. Not all combinations of metals exhibit liquid metal embrittlement. Table 9.3 shows which combinations of liquid metals and common structural materials are sensitive to LME.

TABLE 9.3 LME of a liquid metal layer on structural materials

	Mercury	*Zinc*	*Lead*	*Tin*
Aluminum	yes	yes	no	yes
Copper	yes	no	yes	yes
Iron	yes	yes	yes	no
Titanium	yes	no	no	no

9.3.6 Design Considerations

In the design of structural and machine components, designers often do not give serious consideration to fracture failure due to combined effect of stress and environment. In many cases,

environment-assisted crack growth may be so slow that the crack may not become critical during the life span of the component and thus need not be considered. It is worth noting here that not all kinds of failures (strength, buckling, fatigue, creep, deflection beyond a certain stage, wear, etc.) are analyzed in detail during the design of a component and only the relevant parameters are identified and pursued. There are significant numbers of real life situations in which environment-assisted cracking may cause the failure of components in service conditions. These cases should be analyzed carefully for stress-assisted corrosion.

Threshold stress intensity factor K_{Ith} seems to be attractive property for safe design. However for most combinations of environment and material, K_{Ith} is small, of the order of 5–15 MPa $\sqrt{m}$. If a component is designed to limit the SIF of its cracks to K_{Ith}, the design will be very conservative and thus expensive and impractical. For practical and economical designs, crucial components should be checked at a regular interval through nondestructive techniques (Chapter 12) to identify cracks which may become critical and cause the failure. In the modern industrial world, long pipelines carrying various liquids or gases, railway tracks, axle of railway coaches and wagons, piping of chemicals plants, etc. are routinely checked during the service conditions to identify potentially dangerous cracks, which might have developed during the usage. Since these cracks may grow and fail the components, necessary remedial actions are taken.

9.4 Environment-Assisted Fatigue Failure

The formulation of fatigue failure in an inert environment is still not well developed as well as the environment-assisted growth of a stationary crack is also not formulated well due to many parameters involved. The combination of the two makes the formulation still more complex and causes the failure of a service component earlier than expected. Furthermore, often a synergy effect exists between fatigue crack growth and environment-assisted cracking. For example, the formation of a passive layer on the newly created surfaces of an advancing crack may get affected by the fatigue load. In fact, the fluctuating load may break the new passive layer or delay its formulation, resulting into higher crack growth.

A designer faces difficulties in predicting the life of a component loaded with combined effect of stress, cyclic load and corrosive environment as reliable models are not available to him. He may get tests conducted in simulated service conditions of the component. The tests are not only expensive but takes very long time, weeks, months or years depending on the application. The accelerated tests are still in the preliminary stages as it is difficult to correlate their results with actual conditions of outdoors usages. The fatigue failure of most commonly used metals like steel, aluminum and titanium is even enhanced considerably by the presence of water molecules in air. And it is not practical, for most cases, to limit the humidity of surrounding air of structural components. In fact, a certain minimum humidity is necessary for the comfort of people and thus it is not justified to create the environment of dry air around a machine or a structure. Figure 9.20 shows the dependence of the crack extension per cycle in 7075-T6 aluminum alloy on the water content in the environment [9.15]. There is a marked influence of water molecules on the crack growth rate. When water content was increased from 2×10 to 2×10^4 ppm, the crack growth rate increased from 2.6×10^{-5} to 18×10^{-5} mm/s—a substantial increase of seven times.

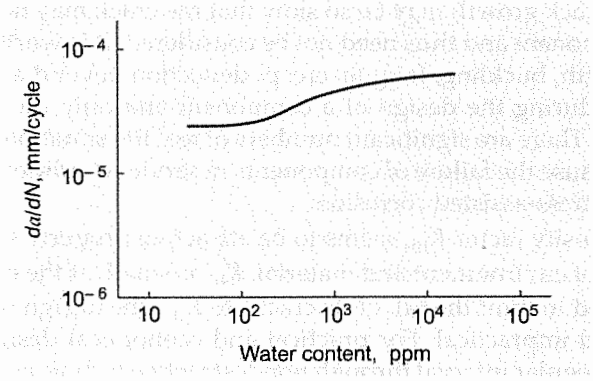

Fig. 9.20 Dependence of the crack extension per cycle in the aluminum alloy 7075-T6 on the water content in the environment for $K_{max} = 13.75$ MPa$\sqrt{m}$

Many variables which have significant effect on environment-assisted cracking have already been discussed in Sec. 9.3.4. However environment-assisted cyclic load adds two more variables to the list of large number of variables, the frequency and the mean stress. The frequency is found to have a considerable effect in many cases. Often a low frequency loading causes more environmental corrosion, probably because it gives more time to the corrosive medium to work on the crack tip. Experiments on 12Ni-5Cr-3Mo steel showed no dependence of crack growth rate per cycle (*da/dN*) on frequency when the specimens were tested in air between slow rate of 0.1 and fast rate of 10 cycles per second (Fig. 9.21). However when specimens were tested in the medium of 3% NaCl at the high frequency load of 10 cps the relation between *da/dN* and ΔK was not too different from the results of testing in air. As the frequency was reduced to 0.1 cps, there was a considerable shift in the relation towards higher rate of crack growth [9.15].

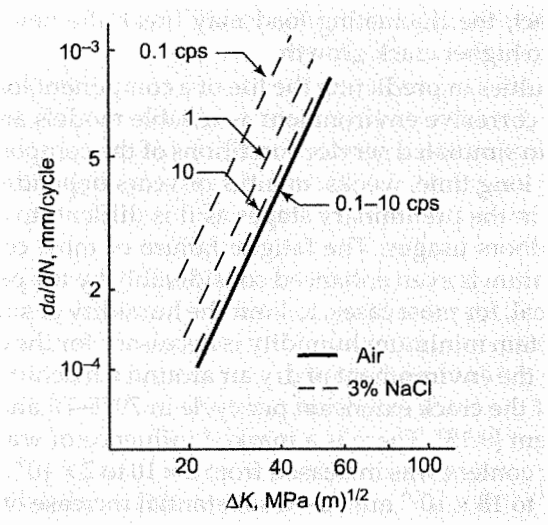

Fig. 9.21 Variation in the crack extension per cycle with frequency in steel alloy 12Ni-5Cr-3Mo tested in 3% NaCl solution

In short, the combined effect of a cyclic load and a corrosive environment hastens the crack growth rate in many materials. A designer is recommended to look into the chances of environment-assisted fatigue failure. Furthermore, one should be careful in generating the data on fatigue failure. May be, the environment is also playing a significant role in the results as even the atmospheric humidity may have a considerable effect on the crack growth. This raises a doubt that probably early investigators, say before the year 1990, were not conscious of the contribution of environment while generating data on fatigue crack growth and we may reevaluate some of the important data.

9.5 Closure

Fatigue loads and corrosive environment are two harsh service conditions on a structural component. A subcritical crack, which would not grow under the controlled and ideal test conditions of a laboratory, may grow under these harsh conditions. The crack length eventually will increase to its critical length, followed by its rapid growth to the failure of the component. The formulation of crack nucleation and growth is quite complex because many micro-parameters are involved. Only a limited success has been achieved so far.

It takes a large number of cycles to nucleate a fatigue crack at the tip of an existing crack. Similarly it takes a fairly long incubation time for an environment-assisted crack to appear at the tip of an existing crack. In fact, satisfactory analyses have not been so far developed to predict the nucleation of cracks under a fatigue load or in a corrosive environment or both. The irony is that the time required to nucleate a crack is quite long and is comparable to the duration a nucleated crack takes to propagate to the final failure of the component. Thus it is difficult to predict the total time to fracture and therefore a crucial structural component should be checked through non-destructive techniques on a regular interval to detect nucleated cracks. The propagation time is handy to give us some convenient breathing space between the two consecutive checks.

In case of a fatigue load, the crack proportion rate per cycle is determined through an empirical law such as the Paris law. The propagation rate depends on ΔK and the stress ratio but experiments show that ΔK plays a dominant role. An overload pulse develops compressive residual stresses in the vicinity of the crack tip and therefore it retards the crack propagation rate significantly of some load cycles following the overload pulse. Further, crack closure is another phenomenon that reduces ΔK because the crack closes prior to complete unloading.

In environment-assisted fracture, several kinds of mechanisms act on a crack tip. In metals, an electrolytic cell may develop with the crack tip acting as the anode. The metals near the crack tip dissolves as metal ions leave the component to the electrolytic solution and thus the crack length increases slowly. Another mechanism is the hydrogen embrittlement. The hydrogen atoms, being small in size, may diffuse into the metal near the crack tip because the stresses are tensile in the plastic zone. Consequently, the metal becomes brittle in the vicinity of the crack tip and the crack grows easily. Unlike the fatigue crack growth rate which depends on the increasing ΔK with an advancing crack, the environment-assisted crack growth is found not to depend on the increasing SIF of a growing crack.

Environment-assisted fatigue deals with the combined action of fatigue loading and environment corrosion, resulting into the faster growth of a crack. In some cases, there exists a synergy effect between the fatigue loading and the environment-assisted cracking, increasing the crack growth rate further.

QUESTIONS

1. Give three applications each of constant amplitude fatigue load and variable amplitude fatigue load.
2. What are the shortcomings/limitations of S-N curve approach?
3. Why is it difficult to formulate crack initiation of a fatigue crack?
4. How does a fatigue crack get initiated on a smooth surface?
5. In case of negative stress ratio, σ_{min} is usually taken to be zero. Why so?
6. Propagation rate of a fatigue crack, in general, depends on ΔK and R but the Paris law, which ignores the effect of R, is very popular. Why so?
7. Some investigators claim that ΔJ should be used in place of ΔK in a crack propagation law for a fatigue crack. Is the claim justified?
8. How does an overload retard the growth of a fatigue crack?
9. What is crack closure? Why does it happen?
10. How is crack propagation rate determined for variable amplitude fluctuating load?
11. How do we account for retardation of a fatigue crack growth owing to overloads in variable amplitude fatigue load?
12. Are predictions of crack growth accurate enough for engineering applications considering the present know-how?
13. Why does the environment-assisted cracking occur mostly through inter-granular growth?
14. What is anodic dissolution?
15. Why does the rate of anodic dissolution depend on the resistance of the passive layer?
16. Why is it difficult to determine K_{Ith} through the constant load testing?
17. Why does work-hardening cause higher rate of crack extension of environment-assited cracks?
18. Does the rate of crack growth of a corrosion crack not depend on the SIF for most materials?
19. It is difficult to design components which would not fail due to fatigue loads or stress induced environment-cracking or both. Therefore a crucial component should be routinely checked to identify whether cracks, which have potential to grow and cause the failure of the component, have developed since the last check-up. Comment on these statements.

PROBLEMS

1. Determine nucleation life if a slot is made in a large plate (HY-130 steel) having a tip-radius of 2 mm and a length of 40 mm from one edge to another. The plate is subjected to a fatigue load of σ_{max} = 140 MPa and σ_{min} = 0.0 MPa.
2. An inclusion is detected in a plate of HY-130 steel through X-ray. It is modeled as a through-the-thickness crack of length 22 mm, with the radius of curvature of the tip as 0.2 mm. If the plate is subjected to a fatigue load of constant amplitude with σ_{max} = 140 MPa and σ_{min} = 0.0 MPa, determine the number of cycles required to nucleate a crack at the tip of the inclusion.
3. Determine the propagation life for the case of Problem 1 if the crack is not allowed to exceed 60% of the critical length corresponding to K_{Ic} = 150 MPa$\sqrt{m}$. Use the Paris law with $C = 7.2 \times 10^{-12}$ MPa^{-3} m$^{-1/2}$ and $m = 3.0$. Also determine the total fatigue life (take slot length as initial crack length).

4. The Paris law of fatigue growth of a crack is known to have the form

$$\frac{da}{dN} = C(\Delta K_I)^3$$

where a is in meter and ΔK_I in MPa$\sqrt{m}$. The centre crack in a large plate, initially of length $2a = 8$ mm, grows to $2a = 10$ mm in 2000 load cycles when a constant amplitude fluctuating load is applied with $\sigma_{max} = 180$ MPa and $\sigma_{min} = 100$ MPa. Determine the life of the component beyond $2a = 10$ mm if the same amplitude load continues on the component and the maximum allowable crack length in the damage tolerant design is $2a = 50$ mm.

5. To find material constants for Paris law, it was found that an already nucleated centre crack grows from $2a = 5.6$ mm to $2a = 7$ mm in 10,000 cycles of a constant amplitude load. When the same load is continued, the crack grows from $2a = 32$ mm to $2a = 36.8$ mm in 1400 cycles. If $\sigma_{max} = 180$ MPa and $\sigma_{min} = 90$ MPa, find the constants C and m.
6. A centre-crack in a large plate is detected at $2a = 5.0$ mm when the plate is subjected to fluctuating load of $\sigma_{max} = 180$ MPa and $\sigma_{min} = 80$ MPa. After 360×10^3 cycles it grows to $2a = 14.2$ mm. Additional 180×10^3 cycles are required to increase the crack length to $2a = 37.4$ mm. Determine elastic constants of the Paris law. (From the two equations, eliminate C and determine m by trial and error.)
7. An edge crack in a large plate is subjected to a constant amplitude fatigue load with $\sigma_{max} = 150$ MPa and $\sigma_{min} = 10$ MPa. Calculate the life of the component if initial crack length is 2.4 mm and $K_{Ic} = 80$ MPa$\sqrt{m}$. Also, find the life if correction for crack closure is made and $U = 0.5 + 0.4R$. (The material constants of the Paris law are $C = 6.0 \times 10^{-12}$ (MPa)$^{-3}$ (m)$^{-1/2}$, and $m = 3$.)
8. On a large plate, used as a critical component of a machine, amplitude of the fatigue load shifts several times in a sequence of every 1000 cycles as shown in Fig. 9.22. The material

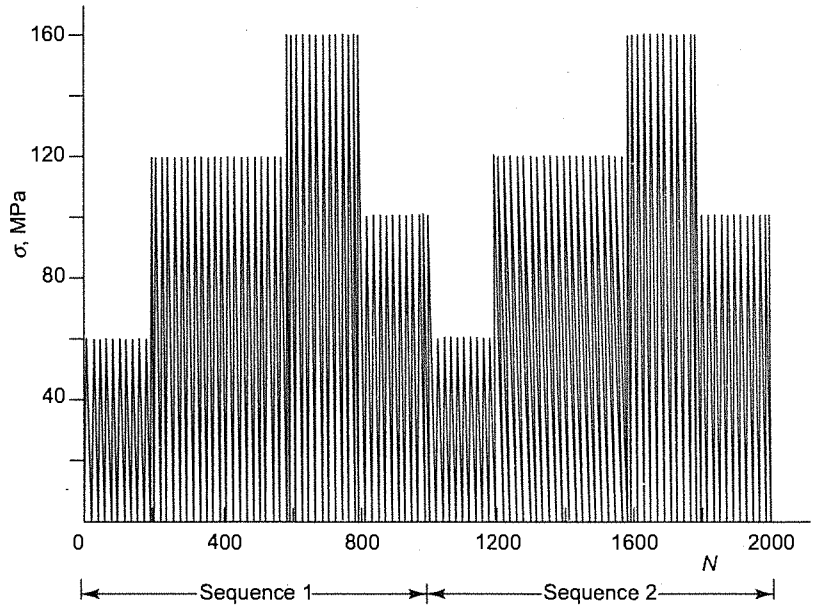

Fig. 9.22 The figure of Problem 8

follows the Paris law with $C = 2.2 \times 10^{-12}$ (MPa)$^{3.4}$ (m)$^{-0.7}$, $m = 3.4$. Determine how many load sequences are needed to cause the failure if the initial crack of $2a = 7.2$ mm is detected near the centre of the plate and $K_{Ic} = 80$ MPa.

9. A machine is used only for the first five days of a year and it is stored in an open ground in the rest of the year where it is subjected to a corrosive atmosphere. A crucial component of the machine is made of an alloy steel and its critical SIF is known as 60 MPa$\sqrt{\text{m}}$. Just before using the machine, a centre crack of length $2a = 4$ mm has been detected in the component. During the operation of the machine the component is subjected to a fatigue load of frequency 24 cycles per minute with its maximum stress of 120 MPa and minimum stress zero. The material of the component follows the Paris law of fatigue growth given by Eq. (9.3). Make an estimate of the remaining life of the component if the crack growth rate under the corrosive conditions is 1.5×10^{-7} mm/s. For the estimate to be conservative, neglect the nucleation time for both fatigue and corrosive growth. Also, estimate the life of the component if the machine is stored in a non-corrosive environment.

References

9.1 Ellyin, Fernard (1997), *Fatigue Damage, Crack Growth and Life Prediction*. Chapman and Hall, London.

9.2 Suresh, S. (1991). *Fatigue of Materials*, Cambridge University Press. Cambridge.

9.3 Barsom, J.M. and Rolfe, S.T. (1987). *Fracture and Fatigue Control in Structures–Applications of Fracture Mechanics*, Prentice-Hall, Inc., Englewood Cliffs, New Jersey.

9.4 Pook, L.P. and Smith, R.A. (1979). *Fracture Mechanics: Current Status, Future Prospect*, Proceeding of Conference, Cambridge. Editor: Smith, R.A. pp. 29–67.

9.5 Barsom, J.M. and McNicol, R.C. (1974). *Effect of Stress Concentration on Fatigue Crack Initiation in HY-130 Steel, ASTM STP 559*. American Society for Testing and Materials, Philadelphia, pp. 183–204.

9.6 Ashby, M.F. and Jones D.R.H (1980). *Engineering Materials: An Introduction to Properties and Applications*, Pergamon Press, Oxford.

9.7 Forman, R.G., Kearney, V.E. and Engle, R.M. (1967). "Numerical Analysis of Crack Propagation in Cyclic-Loaded Structure", *Journal of Basic Engineering, Transactions of ASME 89*, pp. 459–464.

9.8 Erdogan, F. and Ratwani, M. (1970). "Fatigue and Fracture of Cylindrical Shells Containing a Circumferential Crack", *International Journal of Fracture Mechanics*, 6, pp. 379–392.

9.9 Gdoutos, E.E. (2005). *Fracture Mechanics– An Introduction*, Springer.

9.10 Broek, D. (1982). *Elementary Engineering Fracture Mechanics*, Martinus Nijhoff Publishers, The Hague.

9.11 Meguid, S.A. (1989). *Engineering Fracture Mechanics*, Elsevier Applied Science, London.

9.12 Elber. W. (1976). "Equivalent Constant-Amplitude Concept for Crack Growth under Spectrum Loading", *Fatigue Crack Growth under Spectrum Loads, ASTM STP 595*, American Society for Testing and Materials, Philadelphia, pp. 236–250.

9.13 Schijve, J. (1981). "Some Formulae for the Crack Opening Stress Level", *Engineering Fracture Mechanics*, 14, pp. 461–465.

9.14 Broek, David (1988). *The Practical Use of Fracture Mechanics*, Kluwer Academic Publishers, Dordrecht.
9.15 Hertzberg, Richard W. (1989). *Deformation and Fracture Mechanics of Engineering Materials*, John Wiley & Sons, New York.
9.16 Kaesche, Helmut (2003). *Corrosion of Metals: Physicochemical Principles and Current Problems*, Springer Verlag.
9.17 Janssen, M., Zuidema, J. and Wanhill,R. J. H. (2004), Spon Press, London.
9.18 Knott, J. F. (1973), *Fundamentals of Fracture Mechanics*, John Wiley & Sons, New York.
9.19 Raghavan, V. (1988), *Material Science and Engineering*, Prentice-Hall of India Pvt. Ltd., New Delhi.
9.20 Ramesh, K. (2007). *e-Book on Engineering Fracture Mechanics*, IIT Madras, URL: http//apm.iitm.ac.in/smlab/kramesh/book_4.htm

Chapter

10

Finite Element Analysis of Cracks in Solids*

Science studies what is, engineering creates what never has been.

von Karman

10.1 Finite Element Method

Finite Element Method (FEM) is one of the numerical methods to obtain an approximate solution to many of the fracture mechanics problems. This method has become very popular with the availability of powerful computers. In the finite element method the domain of the problems is discretized into a number of subdomains, called finite elements which are connected with one another at points known as nodes. The variables of the problem, such as displacements, temperature, velocity, etc., are approximated piecewise, so that they are represented in each element by simple polynomials. The coefficients of the polynomial equivalently expressed as nodal values of the variable are determined such that the governing equations and boundary conditions are satisfied in the best possible manner. The approximation procedure may be a variational method (such as minimization of potential energy) or a weighted residual approach [10.1, 10.2, 10.3]. In general, the solution becomes more and more accurate by choosing smaller elements and more number of nodal variables. The necessary and sufficient conditions on the nodal variables and the shape functions to assure the convergence are well laid out in FEM theory.

To briefly explain the methodology let us consider a two-dimensional stress analysis problem in which the domain is divided into elements as shown in Fig. 10.1. Here the displacement variable $\phi^{(e)}(x,y)$ in each element domain $\Omega^{(e)}$ may be defined as a polynomial,

$$\phi^{(e)}(x,y) = a_1 + a_2 x + a_3 y + \cdots + a_n y^n$$

Equivalently, it can be expressed in terms of nodal values as

$$\phi^{(e)}(x,y) = N_1(x,y)\phi_1 + N_2(x,y)\phi_2 + \cdots + N_n(x,y)\phi_n$$

* Contributed by Prof. N.N. Kishore, Department of Mechanical Engineering, IIT Kanpur.

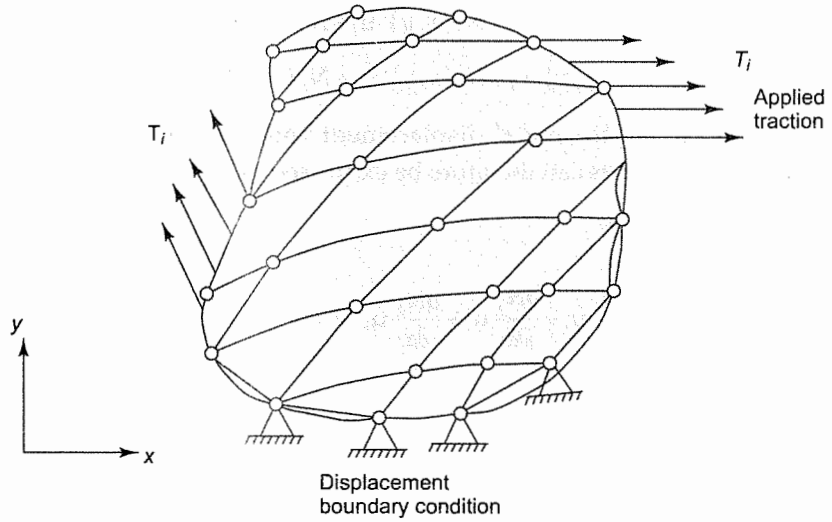

Fig. 10.1 Two-dimensional body and finite element discretization

where $\phi_1, \phi_2, \ldots, \phi_n$, are the values of the function ϕ at the n-nodes in the element, and $N_1(x, y)$, $N_2(x, y)$ ..., $N_n(x, y)$ are known as interpolation functions, trial functions or shape functions. This recasting of $\phi^{(e)}(x, y)$ in terms of nodal variables facilitates the automatic satisfaction of continuity conditions at element boundaries.

For example, in a triangular element with nodes (i, j, k) at the three vertices, the displacement (u, v) within the element can be written as (Fig. 10.2)

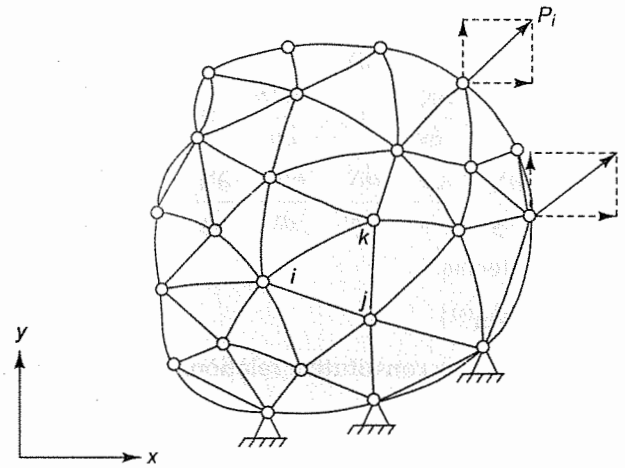

Fig. 10.2 Two-dimensional stress analysis using triangular elements

$$u(x,y) = N_i(x,y)\ u_i + N_j(x,y)\ u_j + N_k(x,y)\ u_k$$
$$v(x,y) = N_i(x,y)\ v_i + N_j(x,y)\ v_j + N_k(x,y)\ v_k$$

where $u_i, v_i, u_j, v_j, u_k, v_k$, are the nodal displacement values and N_i, N_j, N_k are linear shape functions. The strain components can therefore be expressed as

$$\varepsilon_x = \frac{\partial u}{\partial x}$$
$$= \frac{\partial N_i}{\partial x} u_i + \frac{\partial N_j}{\partial x} u_j + \frac{\partial N_k}{\partial x} u_k$$
$$\varepsilon_y = \frac{\partial v}{\partial y}$$
$$= \frac{\partial N_i}{\partial y} v_i + \frac{\partial N_j}{\partial y} v_j + \frac{\partial N_k}{\partial y} v_k$$
$$\gamma_{xy} = \frac{\partial u}{\partial y} + \frac{\partial v}{\partial x}$$
$$= \frac{\partial N_i}{\partial y} u_i + \frac{\partial N_j}{\partial y} u_j + \frac{\partial N_k}{\partial y} u_k + \frac{\partial N_i}{\partial x} v_i + \frac{\partial N_j}{\partial x} v_j + \frac{\partial N_k}{\partial x} v_k$$

The above relations between strain components and the nodal displacements can be written in the matrix form as:

$$\begin{Bmatrix} \varepsilon_x \\ \varepsilon_y \\ \gamma_{xy} \end{Bmatrix} = \begin{bmatrix} \frac{\partial N_i}{\partial x} & 0 & \frac{\partial N_j}{\partial x} & 0 & \frac{\partial N_k}{\partial x} & 0 \\ 0 & \frac{\partial N_i}{\partial y} & 0 & \frac{\partial N_j}{\partial y} & 0 & \frac{\partial N_k}{\partial y} \\ \frac{\partial N_i}{\partial y} & \frac{\partial N_i}{\partial x} & \frac{\partial N_j}{\partial y} & \frac{\partial N_j}{\partial x} & \frac{\partial N_k}{\partial y} & \frac{\partial N_k}{\partial x} \end{bmatrix} \begin{Bmatrix} u_i \\ v_i \\ u_j \\ v_j \\ u_k \\ v_k \end{Bmatrix}$$

which in short form can be written as:

$$[\varepsilon] = [B]\{u^{(e)}\}$$

The stress-strain relation, known as constitutive relation, for a linear isotropic material in plane stress can be written as

$$\begin{Bmatrix} \sigma_x \\ \sigma_y \\ \tau_{xy} \end{Bmatrix} = \frac{E}{1-\nu^2} \begin{bmatrix} 1 & \nu & 0 \\ \nu & 1 & 0 \\ 0 & 0 & \frac{1-\nu}{2} \end{bmatrix} \begin{Bmatrix} \varepsilon_x \\ \varepsilon_y \\ \gamma_{xy} \end{Bmatrix}$$

or in short,

$$[\sigma] = [D]\{\varepsilon\}$$

By using minimization of potential energy of the body or virtual work principle, we can drive the element stiffness matrix as

$$\left[K^{(e)}\right] = \int_{A^{(e)}} [B]^T [D]\ [B]\ h\ dA$$

where h is the thickness of the plate, and the integration is done over the area of the element domain. These element stiffness matrices can be assembled to form global stiffness matrix $[K]$. The applied traction in the form of distributed load can be transformed into nodal loads $\{P\}$. Thus, the finite element equations can be finally written as global equations,

$$[K]\{u\} = \{P\}$$

In addition to the application of the load, it is also necessary to apply a minimum number of displacement boundary conditions to remove the rigid body degrees of freedom and make the finite element equations solvable. Having solved for global nodal displacements, the stress at any point in any element can be evaluated using the stress and nodal displacement relations.

The above procedure for 3-node triangular element can be applied to other elements, such as 4-node rectangle, or 8-node isoparametric elements (Fig. 10.3). As these elements have higher order interpolation functions, they will yield more accurate results. The isoparametric elements can also model elements with curved edges.

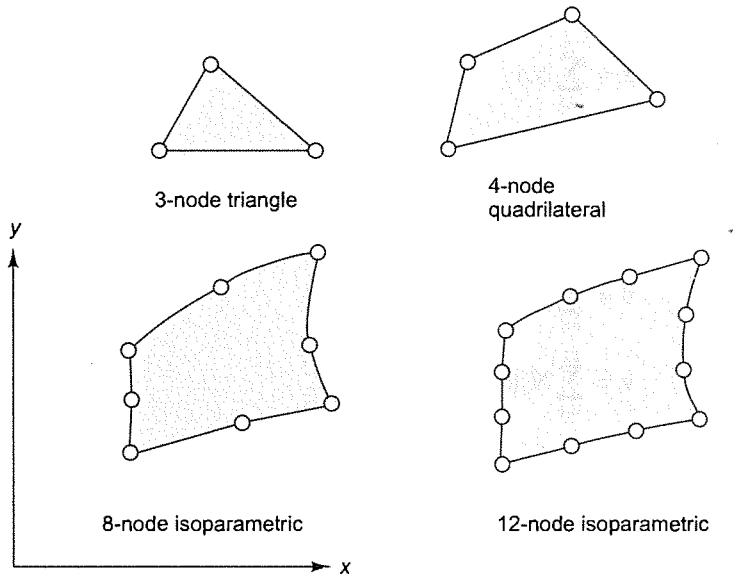

Fig. 10.3 Typical two-dimensional elements

For example, 12-node isoparametric elements have the capability to model quadratic variation of stresses and strains. However, they require mapping and numerical integration technique to evaluate element matrices (Fig. 10.4). In this element, the geometry is described by

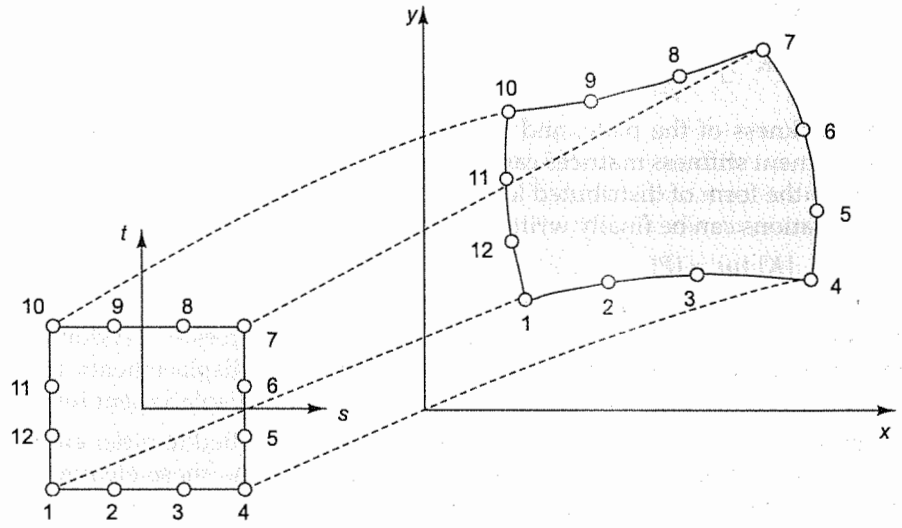

Fig. 10.4 Mapping of 12-node element

$$x = \sum_{i=1}^{12} N_i x_i$$

$$y = \sum_{i=1}^{12} N_i y_i$$

and displacements are given by

$$u = \sum_{i=1}^{12} N_i(s,t)\ u_i$$

$$v = \sum_{i=1}^{12} N_i(s,t)\ v_i$$

where

$$N_1 = \frac{1}{32}(1-t)\ (1-s)\ \left(-10+9s^2+9t^2\right)$$

$$N_2 = \frac{9}{32}(1-t)\ \left(1-s^2\right)\ (1-3s)$$

$$N_3 = \frac{9}{32}(1-t)\ \left(1-s^2\right)\ (1+3s)$$

$$N_4 = \frac{1}{32}(1-t)\ (1+s)\ \left(-10+9s^2+9t^2\right)$$

$$N_5 = \frac{9}{32}(1+s)\ (1-t^2)\ (1-3t)$$

$$N_6 = \frac{9}{32}(1+s)\ (1-t^2)\ (1+3t)$$

$$N_7 = \frac{1}{32}(1+s)\ (1+t)\ (-10+9s^2+9t^2)$$

$$N_8 = \frac{9}{32}(1+t)\ (1-s^2)\ (1+3s)$$

$$N_9 = \frac{9}{32}(1+t)\ (1-s^2)\ (1-3s)$$

$$N_{10} = \frac{1}{32}(1+t)\ (1-s)\ (-10+9s^2+9t^2)$$

$$N_{11} = \frac{9}{32}(1-s)\ (1-t^2)\ (1+3t)$$

$$N_{12} = \frac{9}{32}(1-s)\ (1-t^2)\ (1-3t)$$

10.2 Direct Methods to Determine Fracture Parameters

The stress and strain fields in 2-D crack problems can be determined, in general, by using the triangular, quadrilateral or isoparametric elements. The elements may be 3-node or 6-node triangles, 4-node quadrilaterals or 8-node isoparametric elements as shown in Fig. 10.3. Out of all these the 8-node isoparametric elements can model complex geometries and can have a quadratic interpolation of displacement variation.

Making use of the expressions for the displacements and the stresses near the crack tip, we can use the value of σ_{ij} at any point near the crack tip to determine the value of K_I, K_{II} as follows:

$$u_i = K_I\sqrt{\frac{r}{2\pi}}f_i^{I}(\theta) + K_{II}\sqrt{\frac{r}{2\pi}}f_i^{II}(\theta) + K_{III}\sqrt{\frac{r}{2\pi}}f_i^{III}(\theta), \qquad i = 1,\ldots,3$$

$$\sigma_{ij}(r,\theta) = \frac{K_I}{\sqrt{2\pi r}}g_{ij}^{I}(\theta) + \frac{K_{II}}{\sqrt{2\pi r}}g_{ij}^{II}(\theta) + \frac{K_{III}}{\sqrt{2\pi r}}g_{ij}^{III}(\theta)$$

where $f_i^{I}, f_i^{II}, f_i^{III}$ and $g_{ij}^{I}, g_{ij}^{II}, g_{ij}^{III}$ are functions of θ.

For example, for a Mode I case, we know the stress, strain or displacement field for plane strain as follows:

$$\sigma_x = \frac{K_I}{\sqrt{2\pi r}}\cos\frac{\theta}{2}\left(1-\sin\frac{\theta}{2}\sin\frac{3\theta}{2}\right)\text{fs}$$

$$\sigma_y = \frac{K_I}{\sqrt{2\pi r}}\cos\frac{\theta}{2}\left(1+\sin\frac{\theta}{2}\sin\frac{3\theta}{2}\right)$$

$$\tau_{xy} = \frac{K_I}{\sqrt{2\pi r}}\sin\frac{\theta}{2}\cos\frac{\theta}{2}\cos\frac{3\theta}{2}$$

$$u = 2(1+\nu)\frac{K_I}{E}\sqrt{\frac{r}{2\pi}}\cos\frac{\theta}{2}\left(1-2\nu+\sin^2\frac{\theta}{2}\right)$$

$$v = 2(1+\nu)\frac{K_I}{E}\sqrt{\frac{r}{2\pi}}\sin\frac{\theta}{2}\left(2-2\nu+\cos^2\frac{\theta}{2}\right)$$

Therefore, K_I can be determined from the known stress, strain or displacement field as

$$K_I = \sigma_{ij}\frac{\sqrt{2\pi\, r}}{g_{ij}^I(\theta)}$$

or from displacement field as

$$K_I = \frac{u_i\sqrt{2\pi}}{\sqrt{r}\, f_i^I(\theta)}$$

Ideally, K_I and K_{II} determined from the stress value at any point near the crack tip should give the correct K_I and K_{II} values. However, there are certain limitations of simple elements to represent large stress gradients. The stress gradient near the crack tip is very high and, theoretically, stress becomes singular at the crack tip. To represent such large stresses and stress gradients reasonably well, we need to employ a very fine mesh near the crack tip. Watwood [10.4] made some studies of center cracked specimen using triangular and rectangular elements (Fig. 10.5). He evaluated K_I

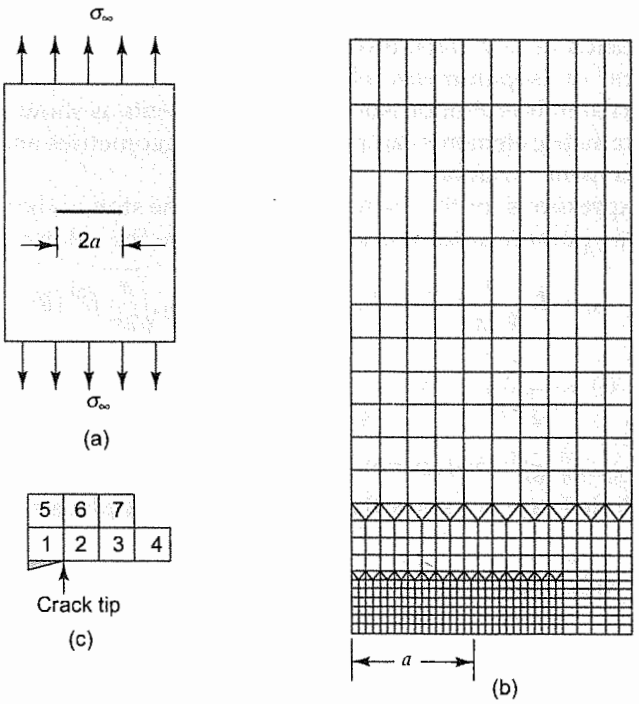

Fig. 10.5 (a) Geometry and load on centre cracked panel, (b) finite element idealization of upper right hand quadrant by Watwood [10.4], 478 Elements, 478 nodal points, and (c) blow up near the crack tip

using the stress values in various elements in the neighborhood of the crack tip; they are listed in Table 10.1. It is clear from Table 10.1 that K_I ranges from 5 to 18.5 while the theoretical value is 5.82.

TABLE **10.1** K_I determined through σ_x, σ_y or τ_{xy} in various elements of centre cracked specimen (Fig. 10.5)

Element No.	K_I		
	σ_x	σ_y	τ_{xy}
1	2.37	12.5	8.4
2	3.4	5.5	18.5
3	2.6	5.8	5.05
4	2.28	6.5	4.2
5	---	7.2	6.1
6	---	5.8	3.85
7	1.56	6.1	5.62

Very near the crack tip the finite element solution tends to be inaccurate due to its inability to model singular nature of stresses accurately. An improved evaluation of K_I can be done from the plot of K_I vs. r. Thus, K_I can be extrapolated to find K_I at $r = 0$ for a fixed θ (Fig. 10.6). Using this approach, Chan et al. [10.5] determined that the K_I value with coarse mesh (area of element is 3.1×10^{-4}) was within an error of 11% and with fine mesh (area of element is 1.2×10^{-4}) the value was within an error of 5% compared to Westergaard solution.

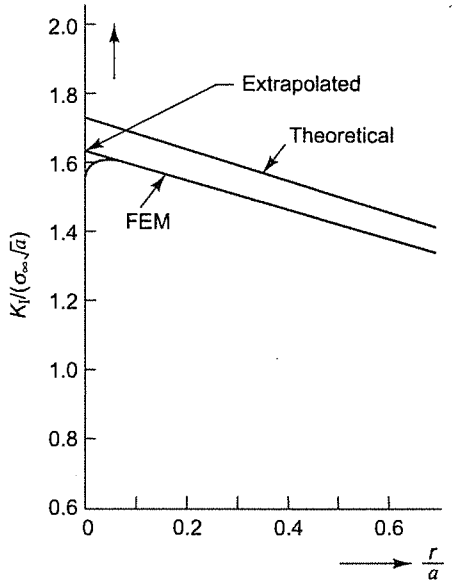

Fig. 10.6 Results of finite element calculations for infinite plate with central crack, Chan et al. [10.5]

The drawback of the above mentioned direct methods is that they require very fine mesh in the vicinity of the crack tip which involves large amount of computational complexity.

10.3 Indirect Methods to Determine Fracture Parameters

There are several indirect methods which do not use crack tip stress formulae directly. They make use of the knowledge of crack behavior in finite element analysis which will markedly improve the accuracy of the results.

10.3.1 J-Integral Method

As given in Eq. (6.1), J-Integral is defined as

$$J = \int_{\Gamma} \left(W dx_2 - T_i \frac{\partial u_i}{\partial x_1} ds \right)$$

where $W = \int_0^{\varepsilon} \sigma_{ij} d\varepsilon_{ij}$ is the strain energy density and T_i is the traction. The contour Γ starts from one crack surface and goes on to the other crack surface surrounding the crack tip (Fig. 6.2). This integral value can be evaluated on a path which is slightly away from the crack tip. Thus, the stress and the displacement values on the integration path Γ are not much affected by the modeling inaccuracies of the crack tip stresses.

A typical path in a finite element analysis is shown in Fig. 10.7. The path is taken along the nodes on the element's edges. The strain energy density values at nodes are obtained as extrapolation of the values at the Gauss points within the elements. The values of the traction vector T_i are the external forces for the region enclosed by Γ as a free body. Chan et al. [10.5] applied this method to the analysis of a compact test specimen. The resulting stress intensity factor K_I is quite accurate and has an error of only 3.5%.

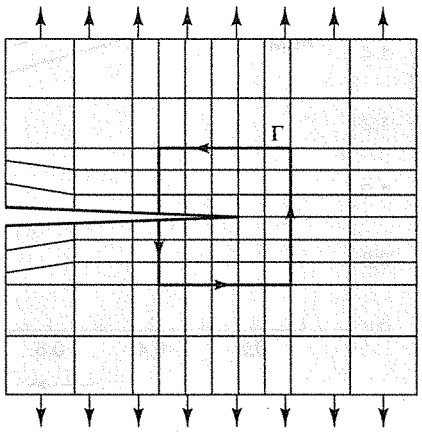

Fig. 10.7 A rectangular elements mesh and path of integration Γ for the J-integral

10.3.2 Energy Release Rate Method

This involves the evaluation of energy in the cracked body for two slightly different crack configurations, say, a and $a + \Delta a$. Let Π and $\Pi + \Delta\Pi$ be the potential energies of the plate, respectively (Fig. 10.8). Then, the energy release rate G_I can be written as

$$G = -\frac{\Delta\Pi}{B\Delta a}$$

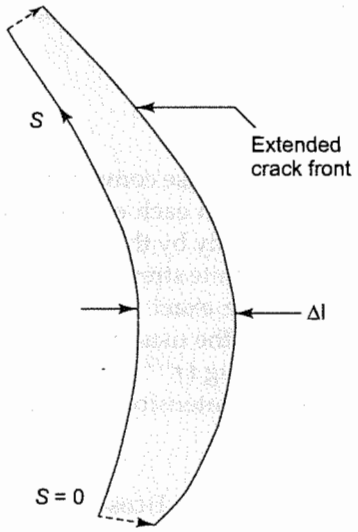

Fig. 10.8 Growth of embedded crack

where B is the thickness of the plate. Watwood [10.4] applied this method to analyze a center cracked panel of finite size. The G_I can be written in terms of K_I using the relation $K_I = \sqrt{G_I E}$ for a plane stress case of linear isotropic material. The results are compared with those obtained by Isida [10.6] in Table 10.2. It can be seen that the error is within 2%. This method can also be applied to a 3-dimensional case to evaluate fracture parameters of the embedded cracks. An average value of energy release rate G is given by (Fig 10.8):

$$G_{av} = -\frac{\Delta\Pi}{\int \Delta l(s)ds}$$

TABLE 10.2 K_I obtained by FEM through energy release approach

a/W	K_I/σ		*Difference*
	FEM	*Theoretical**	
0.188	4.86	4.96	2%
0.254	5.90	6.00	1.7%
0.317	6.90	7.01	1.6%

* Isida [10.6]

10.3.3 Stiffness Derivative Method

This technique evaluates the change in the potential energy $\Delta\Pi$ in finite element analysis which uses the change in stiffness of the plate ΔK for the two configurations of the crack. The difference in the potential energies is given by:

$$\Delta\Pi = \frac{1}{2}\mathrm{u}^T\Delta K\mathrm{u} + \left(\mathrm{u}^T K - P^T\right)\Delta\mathrm{u}$$

where P are the nodal loads. This is suitable for 3-dimensional problems as the crack can advance in multiple ways.

10.3.4 Singular Element Method

All the mentioned approaches discussed so far use conventional elements which either can model constant stress or linear stress variation within each element. Modeling of large stress gradients near the crack tip can be improved significantly by the employment of a very fine mesh. But they are inadequate to model the theoretically infinite stress at the crack tip. Singular finite elements are a special class of elements which have the exact interpolation functions to model the stress singularity. In these elements, in addition to the usual nodal displacements as degree of freedom, there will be displacement functions involving ($r^{1/2}$) terms. These are associated with additional degrees of freedom directly giving the stress intensity factors K_{I} and K_{II}. Using Gifford and Hilton [10.7] these additional terms are

$$\mathrm{u}_{s\mathrm{I}} = \frac{1}{4\mu}\sqrt{\frac{r}{2\pi}}\left\{\cos\theta\left[(2\kappa-1)\cos\frac{\theta}{2}-\cos\frac{3\theta}{2}\right]-\sin\theta\left[(2\kappa+1)\sin\frac{\theta}{2}-\sin\frac{3\theta}{2}\right]\right\}$$

$$\mathrm{u}_{s\mathrm{II}} = \frac{1}{4\mu}\sqrt{\frac{r}{2\pi}}\left\{\cos\theta\left[(2\kappa+3)\sin\frac{\theta}{2}+\sin\frac{3\theta}{2}\right]+\sin\theta\left[(2\kappa-3)\cos\frac{\theta}{2}+\cos\frac{3\theta}{2}\right]\right\}$$

$$\mathrm{v}_{s\mathrm{I}} = \frac{1}{4\mu}\sqrt{\frac{r}{2\pi}}\left\{\sin\theta\left[(2\kappa-1)\cos\frac{\theta}{2}-\cos\frac{3\theta}{2}\right]+\cos\theta\left[(2\kappa-1)\sin\frac{\theta}{2}-\sin\frac{3\theta}{2}\right]\right\}$$

$$\mathrm{v}_{s\mathrm{II}} = \frac{1}{4\mu}\sqrt{\frac{r}{2\pi}}\left\{\sin\theta\left[(2\kappa+3)\sin\frac{\theta}{2}+\sin\frac{3\theta}{2}\right]+\cos\theta\left[(2\kappa-3)\cos\frac{\theta}{2}+\cos\frac{3\theta}{2}\right]\right\}$$

where μ is shear modulus and

$$\begin{aligned}\kappa &= (3-4\nu) && \text{for plane strain}\\ &= (3-\nu)/(1+\nu) && \text{for plane stress.}\end{aligned}$$

The total displacement in the singular element is the summation of the regular expressions and the terms derived due to singular terms are as follows:

$$\mathrm{u} = \sum_{i=1}^{12} N_i\mathrm{u}_i + K_{\mathrm{I}}\mathrm{u}_{s\mathrm{I}} + K_{\mathrm{II}}\mathrm{u}_{s\mathrm{II}}$$

$$v = \sum_{i=1}^{12} N_i v_i + K_I v_{sI} + K_{II} v_{sII}$$

The singular elements are employed adjacent to the crack tip. Outside these singular elements, the usual conventional elements are used.

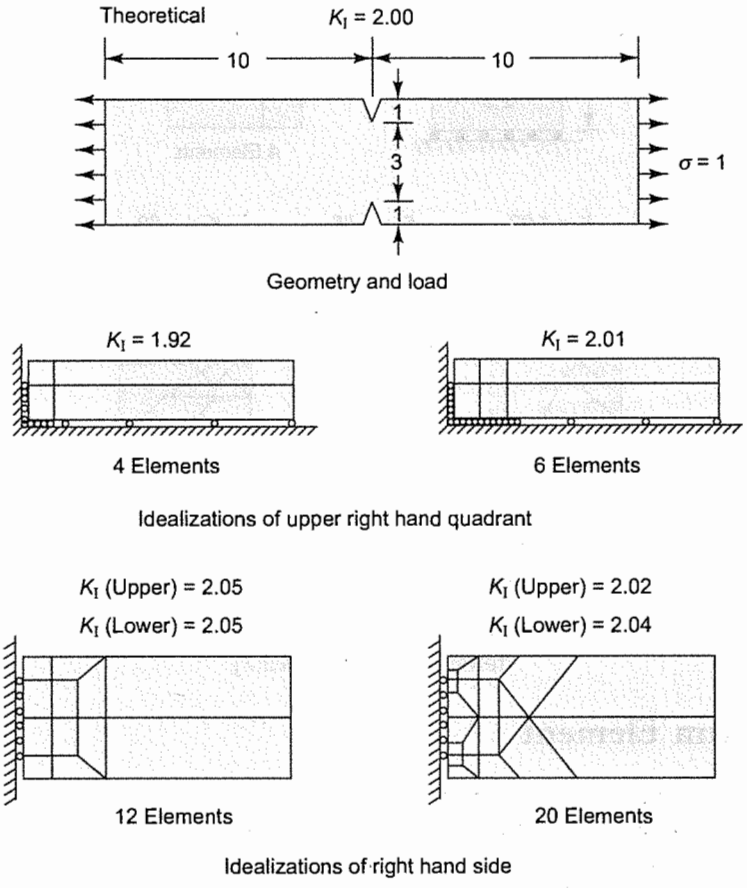

Fig. 10.9 Geometry and idealizations for double edge notch tension test specimen [10.7]

This singular element approach to a double edge notched specimen (Fig. 10.9) yields quite accurate results using only a few elements [10.7]. With a 4-element mesh, the stress intensity factor K_I was evaluated as 1.92, and with a 6-element mesh the K_I value was obtained as 2.01 while the exact value is 2.00 [10.8]. For a single edge notch at an angle of 45° (Fig. 10.10) 4-element analysis gave the values of K_I and K_{II} as 1.79 and 0.85 and 7-element mesh yielded 1.92 and 0.90 respectively while the exact values are 1.86 and 0.88 [10.9].

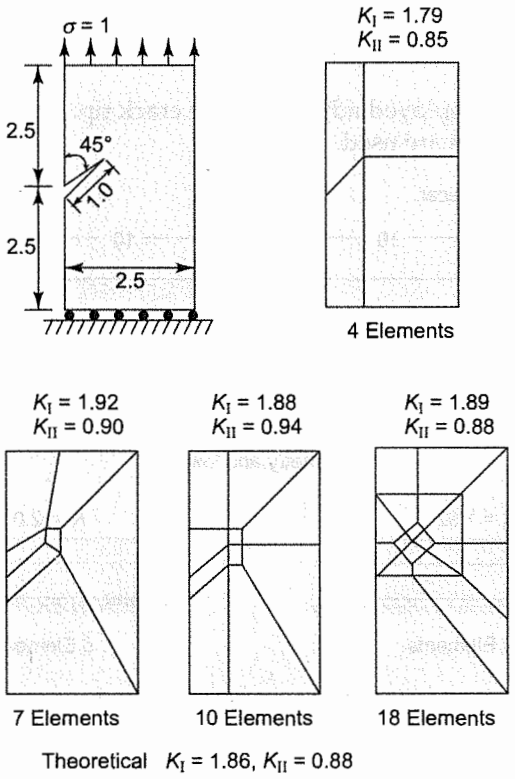

Fig. 10.10 Geometry, idealizations, and results for 45° slant crack in tensile specimen [10.7]

10.3.5 Barsoum Element

An easier simulation of crack tip singularity can be achieved with the help of Quarter-Point element technique which is known as Barsoum Element [10.10]. In this special method, the usual isoparametric 6-node triangle or 8-node isoparametric quadrilateral elements are employed. As shown in Fig. 10.11, mid-side nodes on the two adjacent sides are shifted towards the corner node to the quarter point location. For these locations of the mid nodes, the Jacobian becomes singular at the corner node, thus making displacement derivates infinite and consequently stresses and strains become infinite as well. It can be shown that the variation of stresses along the two sides of the elements is according to $1/\sqrt{r}$.

On the other hand, if all the three nodes on the side of an 8-node quadrilateral element are collapsed to one node (giving the same node number) then the stress (or strain) varies as $1/\sqrt{r}$ along any radial line emanating from crack tip. To model the crack tip singularity the mesh

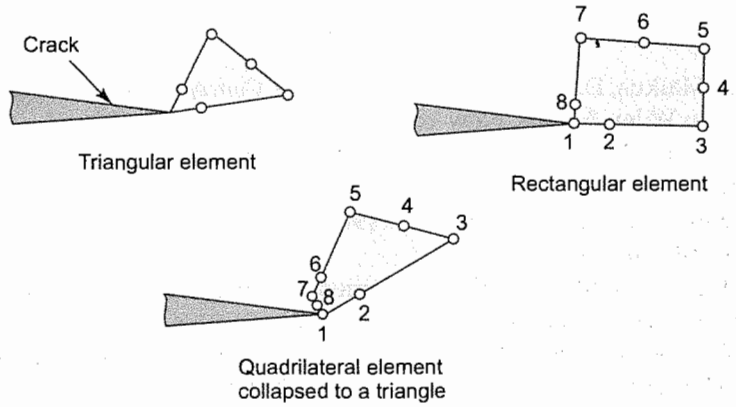

Fig. 10.11 Quarter point elements

arrangement can be taken to be as shown in the Fig. 10.12. Observe that all the mid side nodes adjacent to the crack tip are at quarter point locations. From the displacement field solution the stress intensity factor K_I, in a Mode I case, can be calculated as per the following relation,

$$K_I = \frac{2\mu}{\kappa + 1}\sqrt{2\pi}\left(\frac{4v_B - v_C}{\sqrt{L}}\right)$$

where v_B, v_C are the displacement in the y direction behind the crack tip.

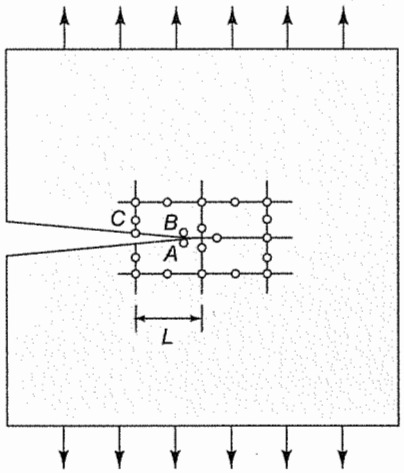

Fig. 10.12 Quarter point elements around a crack tip

It has been demonstrated that K_I found by this method is within 2% of the theoretical solutions. Accuracy of the finite element calculation can be improved if the neighboring elements are also modeled to have the terms depicting the stresses for a crack with its tip outside the element.

Finally, finite element method can be applied to study fracture in the case of elastoplastic materials and impact loads. Dynamic crack propagation can also be simulated well but the propagation simulation procedures are still in progress.

REFERENCES

10.1 Cook, R.D., Malkus, D.S. and Plesha, M.E. (1989). *Concepts and Applications of Finite Element Analysis*, John Wiley & Sons, New York.

10.2 Reddy, J. N. (1993). *An Introduction to the Finite Element Method*, McGraw-Hill, Inc., New York.

10.3 Zienkiewicz, O.C. and Taylor, R. L. (1989). *The Finite Element Method*, Vols. I and II, McGraw-Hill, Inc., London.

10.4 Watwood Jr., V. B. (1969). "The Finite Element Method for Prediction of Crack Behaviour", *Nuclear Engineering and Design*, 11, pp. 323–332.

10.5 Chan, S. K., Tuba, I.S. and Wilson, W.K. (1970). "On the Finite Element Method in Linear Fracture Mechanics," *Engineering Fracture Mechanics*, 2, pp. 1–17.

10.6 Isida, M. (1955). "On the Tension of a Strip with a Central Elliptical Hole," *Transactions of Japanese Society of Mechanical Engineering*, 21, pp. 507–518.

10.7 Gifford, Jr. L. N. and Hilton, P. D. (1978). "Stress Intensity Factors by Enriched Finite Elements," *Engineering Fracture Mechanics*, 10, pp. 486-496.

10.8 Brown Jr. W.F. and Srawley, J.E. (1966). "Plane Strain Crack Toughness Testing of High Strength Metallic Materials," *ASTM Special Technical Publication*, 410.

10.9 Bowie, O.L. (1973). "Solutions of Plane Crack Problems by Mapping Techniques," *Mechanics of Fractures*, Vol. I, (Ed.) G. C. Sih, Noordhoff, Leyden, pp. 1-66.

10.10 Barsoum, R.S. (1976). "On the Use of Isoparametric Elements in Linear Fracture Mechanics," *International Journal for Numeric Methods in Engineering*, 10, pp. 25-38.

Chapter

11

Mixed Mode Crack Initiation and Growth*

... I do not understand the reason why it is that the correct laws of physics seem to be expressible in such a tremendous variety.

Richard Feynman

11.1 Introduction

In the previous chapters, we have studied crack growth under Mode I loading. Over the past many years considerable research work has been devoted and fracture mechanics principle based designs are developed using Mode I fracture theories. This may be mainly so, because Mode I failure predominates for homogeneous isotropic materials. In the particular case of opening mode, loading is applied in the direction normal to the crack faces and the crack grows parallel to the faces, i.e., in a self-similar manner. But, in many practical situations, loading is of mixed mode type, that is, combination of all the three Irwin's modes—opening mode, in plane shear sliding mode and out of plane tearing mode. For conservative fracture based design estimates, one needs to characterize the crack under mixed mode loading.

Studies are carried in the mixed mode condition in order to find the crack extension direction, critical load (or critical crack dimension) and stability of the crack path. Various models have been proposed to characterize the mixed mode crack. Essentially, the models proposed are based either on energy or stresses. Various models for initiation and growth of a crack subjected to Mode I and Mode II loading are presented in this chapter within the scope of linear elastic fracture mechanics.

11.2 Fracture Surface

Fracture surface is a locus of points in K_I–K_{II} space where the combined action of K_I and K_{II} attains a material dependent critical value. For a crack in a plane problem subjected to mixed mode loading, the fracture surface can be taken in a general functional form as:

* Contributed by Prof. Raju Sethuraman, Department of Mechanical Engineering, IIT Madras.

$$f(K_I, K_{II}, K_{Ic}, K_{IIc}) = 0 \tag{11.1}$$

where K_I and K_{II} are Mode I and Mode II stress intensity factors, K_{Ic} and K_{IIc} are critical values of K_I and K_{II}. The function describing the fracture surface is commonly considered in a polynomial or power law form and is expressed in a non-dimensional form as:

$$\left(\frac{K_I}{K_{Ic}}\right)^a + \left(\frac{K_{II}}{K_{IIc}}\right)^b = 1 \tag{11.2}$$

In the above equation the exponents a and b are material dependent constants. Equation (11.2) was applied by Wu [11.1] for predicting the crack behavior in a mixed mode condition for composites. He obtained the values of material constants a and b as equal to 1 and 2 respectively for the behavior of a crack in wood. Different values have to be used for material constants a and b if one needs to apply Eq. (11.2) for various composites.

Based on energy principles fracture surface function can be assumed to be quadratic in K_I and K_{II}. It can be expressed as:

$$C_{11}K_I^2 + 2C_{12}K_I K_{II} + C_{22}K_{II}^2 = C \tag{11.3}$$

where C_{11}, C_{12} and C_{22} are material dependent constants to be evaluated through experiments and C is a real number constant.

Experimental results observed by Erdogan and Sih [11.2] follow ellipse like distribution as shown in Fig. 11.1. This kind of distribution is a subset of the form given in the Eq. (11.3). Later, Broek [11.3] proposed a model which takes the following form:

$$\left(\frac{K_I}{K_{Ic}}\right)^2 + \left(\frac{K_{II}}{K_{IIc}}\right)^2 = 1 \tag{11.4}$$

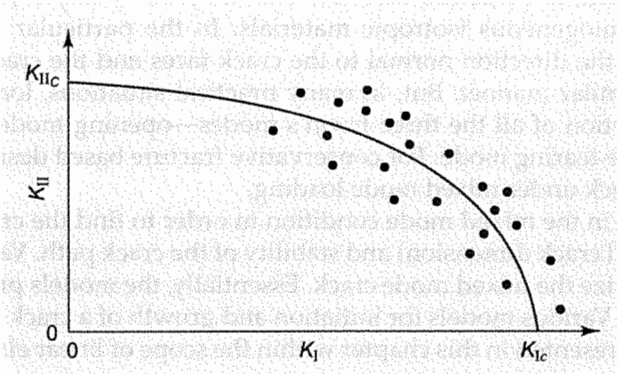

Fig. 11.1 A typical failure surface based on experiment [11.2]

It was observed by Broek that the failure surface given by Eq. (11.4) closely approximates the fracture behavior of mixed mode for most of the engineering materials.

11.3 Mixed Mode Crack Propagation Criteria

In this section the following criteria are presented:

- Modified Griffith Criterion
- Maximum Tangential Stress (MTS) Criterion
- Strain Energy Density (SED) Criterion.

11.3.1 Modified Griffith Criterion

In the Modified Griffith Criterion, the concept of energy balance is extended to include energy release rates associated with all the modes. Total energy release rate for a crack in a plate subjected to Mode I and Mode II loading is given as:

$$G = G_I + G_{II} \tag{11.5a}$$

where

$$G_I = \alpha \frac{K_I^2}{E} \tag{11.5b}$$

$$G_{II} = \alpha \frac{K_{II}^2}{E} \tag{11.5c}$$

$\alpha = 1$ for plane stress

$= 1 - \nu^2$ for plane strain

According to this criterion, crack extension will occur in the direction where total energy release rate is maximum and the extension will occur when the maximum energy release rate reaches a critical value. The critical value depends on the material considered.

Crack Extension Direction

A crack in a plate with an inclination of β degree with ordinate subjected to remote loading σ_0 is shown in Fig. 11.2. A polar coordinate system is considered at the crack tip. For various hypothetical crack extension directions, $\theta(-\pi < \theta < \pi)$, the associated strain energy release rates G_θ is evaluated and is plotted as a function of θ as shown in Fig. 11.3. The crack extension direction θ_c corresponding to the $G_\theta^{\max}$ is obtained by maximizing the G_θ using

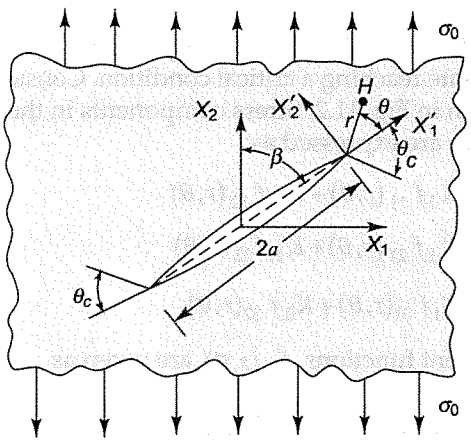

Fig. 11.2 Mixed mode crack subjected to remote loading σ_0

$$\frac{\partial G_\theta}{\partial \theta} = 0 \quad \text{and} \quad \frac{\partial^2 G_\theta}{\partial \theta^2} < 0 \tag{11.6}$$

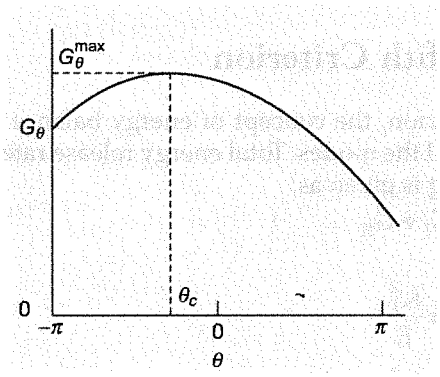

Fig. 11.3 Variations of energy release rate with crack extension direction

Critical Condition

Crack extension will occur when G_θ^{max} reaches a critical value of strain energy release rate G_c, that is,

$$G_\theta^{max} \geq G_c \tag{11.7}$$

The material dependent critical value G_c is obtained from pure Mode I loading. Employing Eq. [11.5(b)], we obtain

$$G_c = \frac{\alpha K_{Ic}^2}{E} \tag{11.8}$$

where K_{Ic} is the critical Mode I stress intensity factor.

11.3.2 Maximum Tangential Stress Criterion

Maximum Tangential Stress Criterion (MTS) was proposed by Erdogan and Sih [11.2] based on a certain component of stress state reaching a critical condition. Consider a crack subjected to Mode I and Mode II loading as shown in Fig. 11.2. Stress components in the vicinity of crack tip (Point H) using polar coordinate system are expressed as:

$$\sigma_{rr} = K_I f_{11}(r,\theta) + K_{II} f_{12}(r,\theta) \tag{11.9}$$

$$\sigma_{\theta\theta} = K_I f_{21}(r,\theta) + K_{II} f_{22}(r,\theta) \tag{11.10}$$

$$\tau_{r\theta} = K_I f_{31}(r,\theta) + K_{II} f_{32}(r,\theta) \tag{11.11}$$

where the coordinate dependent functions $f_{ij}(r,\theta)$ are given as

$$f_{11}(r,\theta) = \frac{1}{\sqrt{2\pi r}}\left(\frac{5}{4}\cos\frac{\theta}{2} - \frac{1}{4}\cos\frac{3\theta}{2}\right)$$

$$f_{12}(r,\theta) = \frac{1}{\sqrt{2\pi r}}\left(-\frac{5}{4}\sin\frac{\theta}{2}+\frac{3}{4}\sin\frac{3\theta}{2}\right)$$

$$f_{21}(r,\theta) = \frac{1}{\sqrt{2\pi r}}\left(\frac{3}{4}\cos\frac{\theta}{2}+\frac{1}{4}\cos\frac{3\theta}{2}\right)$$

$$f_{22}(r,\theta) = \frac{1}{\sqrt{2\pi r}}\left(-\frac{3}{4}\sin\frac{\theta}{2}-\frac{3}{4}\sin\frac{3\theta}{2}\right)$$

$$f_{31}(r,\theta) = \frac{1}{\sqrt{2\pi r}}\left(\frac{1}{4}\sin\frac{\theta}{2}+\frac{1}{4}\sin\frac{3\theta}{2}\right)$$

$$f_{32}(r,\theta) = \frac{1}{\sqrt{2\pi r}}\left(\frac{1}{4}\cos\frac{\theta}{2}+\frac{3}{4}\cos\frac{3\theta}{2}\right)$$

According to MTS criterion, crack extension will occur in the direction where tangential stress component $\sigma_{\theta\theta}$ at an infinitesimal radial distance r_0 from the crack tip is maximum and the extension will take place when the maximum tangential stress reaches a critical value which is a material dependent parameter.

Crack Extension Direction

Consider a crack in a mixed mode loading condition as shown in Fig. 11.2. Around the crack tip an infinitesimal circle with radius r_0 is constructed such that $r_0/a << 1$ (Fig. 11.4). Along the circumference of the circle, $\sigma_{\theta\theta}$ is maximized and the corresponding θ_c is evaluated using

$$\frac{\partial \sigma_{\theta\theta}}{\partial \theta} = 0 \tag{11.12a}$$

$$\frac{\partial^2 \sigma_{\theta\theta}}{\partial \theta^2} < 0. \tag{11.12b}$$

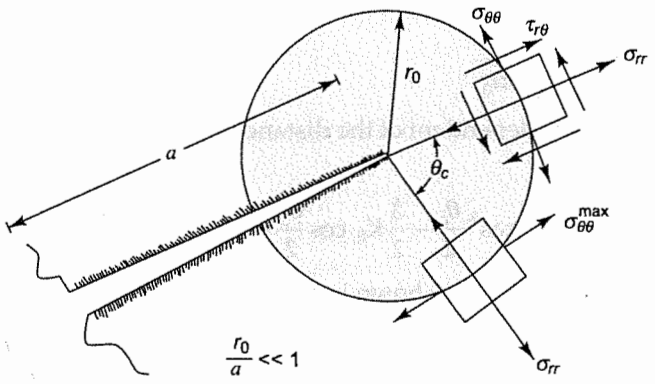

Fig. 11.4 Crack extension direction for MTS criterion

Substituting $f_{21}(r, \theta)$ and $f_{22}(r, \theta)$ in Eq. (11.10), we obtain the expression for $\sigma_{\theta\theta}$ as

$$\sigma_{\theta\theta} = \frac{K_I}{4\sqrt{2\pi r}}\left(3\cos\frac{\theta}{2}+\cos\frac{3\theta}{2}\right)-\frac{3K_{II}}{4\sqrt{2\pi r}}\left(\sin\frac{\theta}{2}+\sin\frac{3\theta}{2}\right) \tag{11.13}$$

Applying the condition of Eq. (11.12a) in the above equation and replacing θ by crack extension direction θ_c, we have

$$K_I\left(\sin\frac{\theta_c}{2}+\sin\frac{3\theta_c}{2}\right)+K_{II}\left(\cos\frac{\theta_c}{2}+3\cos\frac{3\theta_c}{2}\right)=0 \tag{11.14}$$

This expression can further be simplified by trigonometric manipulation to:

$$K_I \sin\theta_c + K_{II}\left(3\cos\theta_c - 1\right) = 0 \tag{11.15}$$

Note here that the stress components σ_{rr} and $\sigma_{\theta\theta}$ are becoming principal stresses in the direction of θ_c on the considered circle. This can be verified by substituting expressions of $f_{13}(r, \theta)$ and $f_{23}(r, \theta)$ in Eq. (11.11) to have

$$\tau_{r\theta} = \frac{1}{4\sqrt{2\pi r}}\left[K_I\left(\sin\frac{\theta_c}{2}+\sin\frac{3\theta_c}{2}\right)+K_{II}\left(\cos\frac{\theta_c}{2}+\cos\frac{3\theta_c}{2}\right)\right] \tag{11.16}$$

Using Eq. (11.14) the above equation gives

$$\tau_{r\theta} = 0$$

Critical Condition

To obtain $\sigma_{\theta\theta}^{\max}$, the maximum value of $\sigma_{\theta\theta}$ corresponding to crack extension direction, we replace θ by θ_c in Eq. (11.13). Also, we manipulate trigonometric relations to obtain:

$$\sigma_{\theta\theta}^{\max} = \frac{K_I}{\sqrt{2\pi r_0}}\cos^3\frac{\theta_c}{2}-\frac{3}{2}\frac{K_{II}}{\sqrt{2\pi r_0}}\cos\frac{\theta_c}{2}\sin\theta_c \tag{11.17}$$

Crack extension occurs when $\sigma_{\theta\theta}^{\max}$ reaches a critical value σ_c which is a material dependent constant; σ_c is usually obtained from pure Mode I loading where $\theta_c = 0$ and $K_I = K_{Ic}$, that is,

$$\sigma_c = \frac{K_{Ic}}{\sqrt{2\pi r_0}} \tag{11.18}$$

For obtaining failure surface independent of the distance r_0, we substitute Eq. (11.18) in Eq. (11.17) to have

$$K_I\cos^3\frac{\theta_c}{2}-\frac{3}{2}K_{II}\cos\frac{\theta_c}{2}\sin\theta_c = K_{Ic} \tag{11.19}$$

Fracture surface based on Eq. (11.19) is shown in Fig. 11.5.

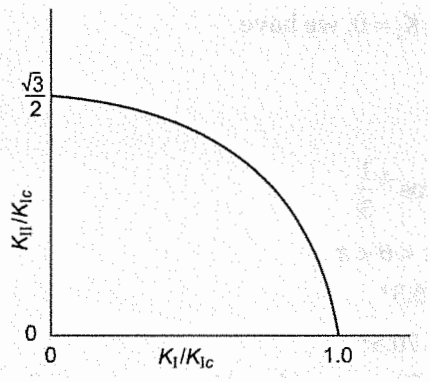

Fig. 11.5 Fracture surface based on maximum tangential stress criterion

Example 11.1 Consider an infinite plate with a center crack of length $2a$. Find crack extension direction and critical condition for the crack extension using MTS criterion for (i) pure Mode I loading as shown in Fig. 11.6(a), and (ii) pure Mode II loading as shown in Fig. 11.6(b). The critical stress intensity factor in Mode I, determined experimentally, is K_{Ic}.

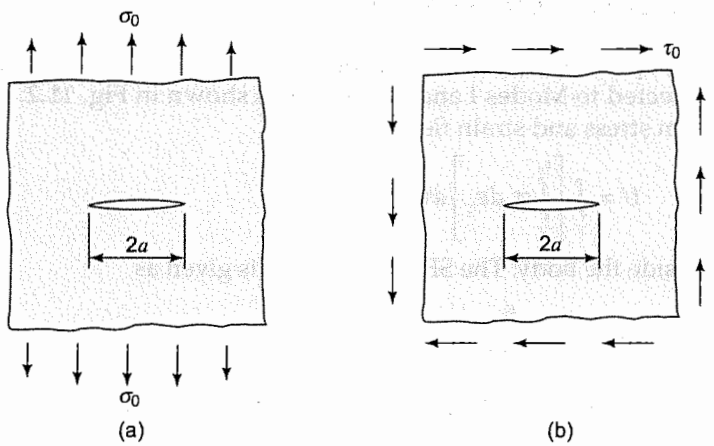

Fig. 11.6 Figures of Examples 11.1 and 11.2 of centre crack plane problems subjected to (a) pure Mode I loading and (b) pure Mode II loading

Solution: (i) Invoking Eq. (11.15) for K_{II}, we have

$$K_I \sin\theta_c = 0$$

yielding

$$\theta_c = 0$$

The critical condition for crack extension is obtained by substituting θ_c in Eq. (11.19) to have

$$K_I = K_{Ic}$$

which, of course, is the expected value.

(ii) Invoking Eq. (11.15), for $K_I = 0$, we have

$$K_{II}\left(3\cos\theta_c - 1\right) = 0$$

yielding

$$\theta_c = \cos^{-1}\frac{1}{3}$$

There are two solutions for $-\pi < \theta < \pi$,

$$\theta_c = 70.5°$$

$$\theta_c = -70.5°$$

The second solution ($\theta_c = -70.5°$) is considered because it satisfies Inequality (11.12b). The critical condition for crack extension is obtained by substituting $\theta_c = -70.5°$ in Eq. (11.19) to have

$$K_{II} = -\frac{2}{3}\frac{K_{Ic}}{\cos\left(\theta_c/2\right)\sin\theta_c} = \frac{\sqrt{3}}{2}K_{Ic}$$

11.3.3 Strain Energy Density Criterion

Based on energy principles, Sih [11.4, 11.6] proposed Strain Energy Density [SED] criterion. Consider a crack subjected to Modes I and II loading as shown in Fig. 11.2. Total strain energy U can be obtained from stress and strain field as:

$$U = \int_V \left[\int_0^{\varepsilon_{ij}} \sigma_{ij} d\varepsilon_{ij}\right] dV \tag{11.20}$$

where V is a region inside the body. The SED function W is given as

$$W = \frac{dU}{dV} = \int_0^{\varepsilon_{ij}} \sigma_{ij} d\varepsilon_{ij} \tag{11.21}$$

For plane linear elasticity problems W can be written in the following form in terms of stress components

$$W = \frac{(1+\nu)}{2E}\left[\frac{\kappa+1}{4}\left(\sigma_{11}+\sigma_{22}\right)^2 - 2\left(\sigma_{11}\sigma_{22} - \tau_{12}^2\right)\right] \tag{11.22}$$

where

$$\kappa = 3-4\nu \qquad \text{(for plane strain)}$$

$$= (3-\nu)/(1+\nu) \qquad \text{(for plane stress)}$$

The Cartesian stress components in the vicinity of crack tip in terms of polar coordinate system are given as:

$$\sigma_{11} = K_I f_{11}(r,\theta) + K_{II} f_{12}(r,\theta) \tag{11.23}$$

$$\sigma_{22} = K_I f_{21}(r,\theta) + K_{II} f_{22}(r,\theta) \tag{11.24}$$

$$\tau_{12} = -K_I f_{31}(r,\theta) + K_{II} f_{32}(r,\theta) \tag{11.25}$$

where the coordinate dependent functions $f_{ij}(r,\theta)$ are given as

$$f_{11}(r,\theta) = \frac{1}{\sqrt{2\pi r}}\cos\frac{\theta}{2}\left(1-\sin\frac{\theta}{2}\sin\frac{3\theta}{2}\right)$$

$$f_{12}(r,\theta) = -\frac{1}{\sqrt{2\pi r}}\sin\frac{\theta}{2}\left(2+\cos\frac{\theta}{2}\cos\frac{3\theta}{2}\right)$$

$$f_{21}(r,\theta) = \frac{1}{\sqrt{2\pi r}}\cos\frac{\theta}{2}\left(1+\sin\frac{\theta}{2}\sin\frac{3\theta}{2}\right)$$

$$f_{22}(r,\theta) = \frac{1}{\sqrt{2\pi r}}\sin\frac{\theta}{2}\cos\frac{\theta}{2}\cos\frac{3\theta}{2}$$

$$f_{31}(r,\theta) = \frac{1}{\sqrt{2\pi r}}\sin\frac{\theta}{2}\cos\frac{\theta}{2}\cos\frac{3\theta}{2}$$

$$f_{32}(r,\theta) = \frac{1}{\sqrt{2\pi r}}\cos\frac{\theta}{2}\left(1-\sin\frac{\theta}{2}\sin\frac{3\theta}{2}\right).$$

Substituting Eqs. (11.23)–(11.25) in Eq. (11.22), the SED function is obtained with some algebraic manipulation in terms of stress intensity factor as:

$$W = \frac{1}{\pi r}\left[g_{11}K_{\mathrm{I}}^2 + 2g_{12}K_{\mathrm{I}}K_{\mathrm{II}} + g_{22}K_{\mathrm{II}}^2\right] \tag{11.26}$$

where

$$g_{11} = \frac{1}{16\mu}(1+\cos\theta)(\kappa-\cos\theta)$$

$$g_{12} = \frac{1}{16\mu}\sin\theta\left[2\cos\theta-(\kappa-1)\right]$$

$$g_{22} = \frac{1}{16\mu}\left[(\kappa+1)(1-\cos\theta)+(1+\cos\theta)(3\cos\theta-1)\right]$$

$$\mu = \frac{E}{2(1+\nu)}$$

Strain energy density function poses singularity of order one at the crack tip. Sih proposed a strain energy density factor S in a quadratic form which is independent of the coordinate r ; it is defined as:

$$S(\theta) = \left(g_{11}K_{\mathrm{I}}^2 + 2g_{12}K_{\mathrm{I}}K_{\mathrm{II}} + g_{22}K_{\mathrm{II}}^2\right)/\pi \tag{11.27}$$

According to SED criterion, crack extension will occur in the direction of minimum strain energy density $S(\theta)$ and the extension will occur when the $S(\theta)$ reaches a critical value S_c which is a material dependent parameter.

Crack Extension Direction

Consider a crack in a mixed mode loading condition as shown in Fig. 11.2. Along the circumference of a circle with radius r_0 strain energy density is minimized and the corresponding θ_c is evaluated using conditions:

$$\frac{\partial W}{\partial \theta} = 0 \quad \text{and} \quad \frac{\partial^2 W}{\partial \theta^2} > 0 \tag{11.28}$$

or,

$$\frac{\partial S}{\partial \theta} = 0 \quad \text{and} \quad \frac{\partial^2 S}{\partial \theta^2} > 0 \tag{11.29}$$

Substituting Eq. (11.27) in Eq. (11.29), we obtain

$$\left[2\cos\theta-(\kappa-1)\right]\sin\theta\, K_I^2+2\left[2\cos 2\theta-(\kappa-1)\cos\theta\right]K_I K_{II} + \left[(\kappa-1-6\cos\theta)\sin\theta\right]K_{II}^2 = 0 \tag{11.30}$$

$$\left[2\cos 2\theta-(\kappa-1)\cos\theta\right]K_I^2+2\left[(\kappa-1)\sin\theta-4\sin 2\theta\right]K_I K_{II} + \left[(\kappa-1)\cos\theta-6\cos 2\theta\right]K_{II}^2 > 0 \tag{11.31}$$

By knowing values of the stress intensity factors for a given problem, crack extension direction can be obtained from the solution to Eq. (11.30), subject to the condition given by Inequality (11.31).

Critical Condition

Crack extension will occur when minimum value of strain energy density function (S_{min}) reaches a critical value of strain energy density factor S_c. Thus, the condition is expressed as:

$$(S_{min}) \geq S_c \tag{11.32}$$

The material dependent critical value S_c is usually obtained by using Eq. (11.27) for a pure Mode I loading with $\theta_c = 0°$ and $K_I = K_{Ic}$ as

$$S_c = \frac{(1+\nu)(\kappa-1)}{4\pi E} K_{Ic}^2 \tag{11.33}$$

Thus, Inequality (11.32) can be expressed as

$$S_{min} \geq \frac{(1+\nu)(\kappa-1)}{4\pi E} K_{Ic}^2 \tag{11.34}$$

for a crack to become critical.

Example 11.2 Consider again the infinite plate of Fig. 11.6 with a center crack of length $2a$. Find crack extension direction and critical condition for crack extension using SED criterion for (i) pure Mode I loading and (ii) pure Mode II loading. The critical stress intensity factor in Mode I, determined experimentally, is K_{Ic} and Poisson's ratio of the material is $\nu = 0.3$.

Solution: (i) Involving Eq. (11.30) for K_{II} for pure Mode I, we obtain

$$\left[2\cos\theta_c - (\kappa - 1)\right]\sin\theta_c = 0$$

This equation yields two solutions:

$$\theta_c = 0$$

$$\theta_c = \cos^{-1}\left(\frac{\kappa - 1}{2}\right)$$

Substituting $\theta_c = 0$ in the left hand side of Inequality (11.31), we obtain

$$\text{LHS} = \left[2 - (\kappa - 1)\right] K_I^2 \tag{11.35}$$

where

$$\kappa = 3 - 4\nu = 1.8 \qquad \text{(for plane strain)}$$

$$\kappa = (3 - \nu)/(1 + \nu) = 2.08 \qquad \text{(for plane stress)}$$

Equation (11.35) simplifies to

$$\text{LHS} = 1.2K_I^2 > 0 \qquad \text{(for plane strain)}$$

$$\text{LHS} = 0.92K_I^2 > 0 \qquad \text{(for plane stress)}$$

Hence, Inequality 11.31 is satisfied. It can be shown that the second solution does not satisfy Inequality 11.31. Therefore, $\theta_c = 0$ is considered. To find the critical condition, we substitute $\theta_c = 0$ in Eq. (11.27) to have:

$$S_{\min} = g_{11} K_I^2 = \frac{(\kappa - 1)}{8\pi\mu} K_I^2$$

$S_{\min}$ is substituted in Inequality 11.34 to obtain:

$$\frac{(\kappa - 1)}{8\pi\mu} K_I^2 \geq \frac{(1 + \nu)(\kappa - 1)}{4\pi E} K_{Ic}^2$$

which simplifies to yield the expected result $K_I \geq K_{Ic}$.

(ii) Invoking Eq. (11.30), for pure Mode II loading, we have:

$$\left[(\kappa - 1) - 6\cos\theta_c\right]\sin\theta_c = 0$$

yielding two solutions:

$$\theta_c = 0$$

$$\theta_c = \cos^{-1}\left(\frac{\kappa - 1}{6}\right)$$

In the above two solutions, $\theta_c = \cos^{-1}\left(\frac{\kappa - 1}{6}\right)$ is considered because it satisfies the condition of Inequality (11.31). For a plane strain case with $\nu = 0.3$,

$$\kappa = 1.8$$

$$\theta_c = \cos^{-1}\left(\frac{0.8}{6}\right) = -82.3°$$

Substituting θ_c in Eq. (11.27), we have:

$$S_{\min} = \frac{1+\nu}{96E}\left(-\kappa^2 + 14\kappa - 1\right) K_{II}^2 .$$

To find critical condition for crack extension in pure Mode II, we substitute $S_{\min}$ in Eq. (11.34) to have:

$$K_{II} \geq \left(\frac{24(\kappa-1)}{-\kappa^2+14\kappa-1}\right)^{1/2} K_{Ic}$$

It is worth noting here that MTS criterion is same for plane stress and plane strain because it is stress based. On the other hand, SED criterion depends on conditions of plane stress or plane strain because it accounts for stresses as well as displacements.

11.4 An Example of Mixed Mode

In the previous section, all three criteria have been discussed and relevant equations and inequalities have been developed. In this section, we consider an example of mixed mode which is solved by MTS criterion as well as by SED criterion.

Example 11.3 Consider an infinite plate with a crack of length $2a = 80$ mm, inclined at angle β with the applied tensile stress σ_0 as shown in Fig. 11.7. K_{Ic} of the material is known to be 40 MPa$\sqrt{\text{m}}$, its elastic constants are $E = 200$ GPa and $\nu = 0.3$, and the plate is subjected to plane strain. (i) Determine initial crack extension direction using MTS and SED fracture criteria for $\beta = 60°$, (ii) find the applied stress σ_0 corresponding to the crack initiation using MTS and SED fracture criteria for $\beta = 60°$ and, (iii) determine relations θ_c vs. β and critical σ_0 vs. β for both fracture criteria for β varying between 10° and 90°.

Solution: State of stress with respect to axes X_1' and X_2' is (Fig. 11.7)

$$\sigma_{11}' = \sigma_0 \cos^2\beta$$
$$\sigma_{22}' = \sigma_0 \sin^2\beta$$
$$\tau_{12}' = \sigma_0 \sin\beta\cos\beta$$

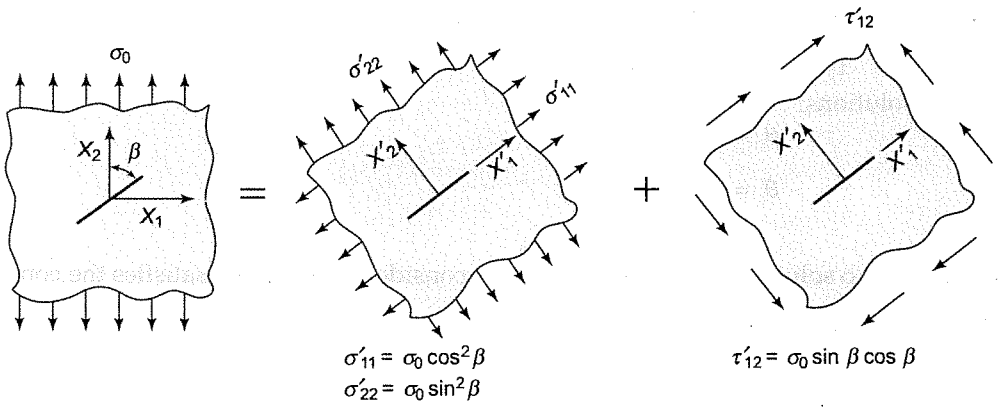

Fig. 11.7 Angled crack subjected to remote uniaxial tensile load

Stress component σ'_{22} loads the crack in pure Mode I and component τ'_{12} in pure Mode II, whereas the effect of σ'_{11} can be neglected. Thus, we have

$$K_I = \sigma_0 \sqrt{\pi a} \sin^2 \beta$$

$$K_{II} = \sigma_0 \sqrt{\pi a} \sin \beta \cos \beta$$

(i) To find initial crack extension direction for $\beta = 60°$:

$$K_I = \sigma_0 \sqrt{\pi a} \sin^2 60° = \frac{3}{4} \sigma_0 \sqrt{\pi a}$$

$$K_{II} = \sigma_0 \sqrt{\pi a} \sin 60° \cos 60° = \frac{\sqrt{3}}{4} \sigma_0 \sqrt{\pi a}$$

Substituting K_I and K_{II} in Eq. (11.15) for applying MTS criterion, we obtain

$$\sqrt{3} \sin \theta_c + (3 \cos \theta_c - 1) = 0$$

This equation can be solved by trial and error. It is convenient to make a small program on computer. Out of the two roots within the range $-\pi < \theta < \pi$, the one that satisfies Inequality (11.12b) is

$$\theta_c = -43.2°$$

Similarly, to find θ_c for SED criterion, we substitute K_I and K_{II} in Eq. (11.30) for plane strain $(\kappa = 1.8)$ to obtain:

$$3(\cos \theta_c - 0.4) \sin \theta_c + 2\sqrt{3} (\cos 2\theta_c - 0.4 \cos \theta_c) + (0.4 - 3 \cos \theta_c) \sin \theta_c = 0$$

Through trial and error approach this equation yields:

$$\theta_c = -40.5°$$

(ii) To find critical applied stress σ_0^{crit} corresponding to crack initiation:

To determine σ_0^{crit} through MTS criterion we substitute K_I and K_{II} in Eq. (11.19) to have:

$$\frac{\sigma_0^{crit} \sqrt{\pi \times 0.040}}{4} \left[3 \cos^3 \left(\frac{-43.2°}{2} \right) - \frac{3\sqrt{3}}{2} \cos \left(\frac{-43.2°}{2} \right) \sin (-43.2°) \right] = 40$$

yielding $\sigma_0^{crit} = 111$ MPa.

For finding σ_0^{crit} through SED criterion, we substitute K_I, K_{II} and θ_c in Eqs (11.27) and (11.33) to have:

$$S_{min} = \frac{0.008286}{E} \left(\sigma_0^{crit} \right)^2$$

$$S_c = \frac{132.4}{E}$$

which, on substitution in Inequality 11.34, gives:

$$\sigma_0^{crit} = 126.4 \text{ MPa}$$

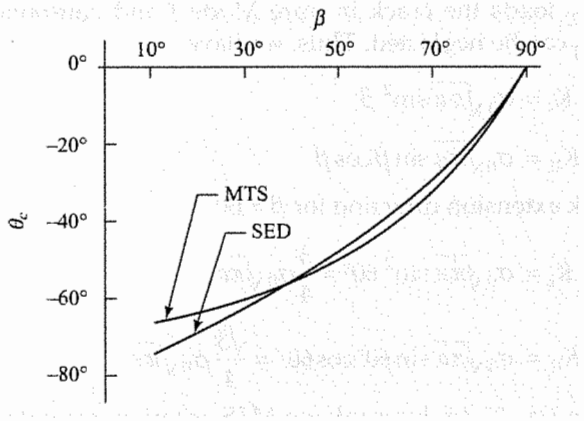

Fig. 11.8 Critical angle θ_c vs. crack orientations angle β of Example 11.3 for MTS and SED fracture criteria

(iii) Similar to parts (i) and (ii), θ_c and σ_0^{crit} are determined for various values of angle β using the computer program. Figure 11.8 shows the relation between crack extension direction θ_c and crack inclination angle β. For the pure Mode I case of $\beta = 90°$, the critical angle θ_c turns out to be 0°, representing, as expected, crack growth in self-similar manner. As β decreases from 90° and the Mode II component starts increasing, deviation of the crack angle (θ_c) from the crack plane increases. Figure 11.9 shows the dependence of critical applied stress σ_0^{crit} on the crack inclination angle β. Obviously $\beta = 90°$ is worst possible crack orientation angle which shows the lowest value of σ_0^{crit}.

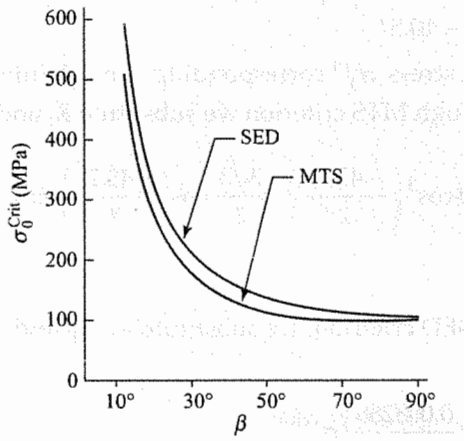

Fig. 11.9 Relation between critical load σ_0^{crit} and crack angle β of Example 11.3

11.5 Crack Growth

For LEFM analysis, one of the three criteria, presented in this chapter, may be chosen for predicting the initiation of the crack extension. In comparison to Modified Griffith Criterion, MTS Criterion and SED Criterion are more popular among investigators. Furthermore, MTS criterion is strictly stress-based and its analysis does not depend on the condition of plane stress and plain strain. SED criterion deals with strain energy and therefore conditions for predicting crack growth direction and critical applied stress depend on whether the plate is subjected to plane strain or plane stress.

The path of a finite crack growth in a mixed mode case can be predicted by successive application of the fracture criterion. When the given external loading situation reaches the critical stage through a chosen criterion, the existing crack is extended in the predicted critical direction through a small distance. For the newly extended crack configuration we apply the chosen criterion again and criticality of the current (updated) loading configuration is checked. If the loading is critical, the crack is extended and the above procedure is repeated. If the condition is subcritical, the crack growth stops.

References

11.1 Wu, E.M. (1967). "Application of Fracture Mechanics to Anisotropic Plates," *Journal of Applied Mechanics*, 34, pp. 967–974.

11.2 Erdogan, F. and Sih, G. C. (1963). "On Crack Extension in Plates under Plane Loading and Transverse Shear, Transaction of ASME," *Journal of Basic Engineering*, 85, pp. 519–527.

11.3 Broek, D. (1974). *Elementary Engineering Fracture Mechanics*, Noordhoff, Leiden.

11.4 Sih, G.C. (1973). "Methods of Analysis and Solutions of Crack Problems," *Mechanics of Fracture*, Vol. I, (Ed.) G. C. Sih, Noordhoff, Leiden.

11.5 Sih, G.C. (1973). "Some Basic Problems in Fracture Mechanics and New Concepts," *Engineering Fracture Mechanics*, 5, pp. 365–377.

11.6 Sih, G.C. (1974). "Strain Energy Density Factor Applied to Mixed Mode Crack Problems," *International Journal of Fracture*, 10, No. 3, pp 305–321.

Chapter

12

Crack Detection through Non-Destructive Testing

Archimedes was given the task of determining if King Hiero's goldsmith was embezzling gold during the manufacture of the king's crown...Baffled, Archimedes went to take a bath and observed from the rise of the water that he could calculate the volume of water. Allegedly, Archimedes went running through the street naked shouting, "Eureka! Eureka!"

Wikipedia

12.1 Introduction

There are defects in the materials of real life components, which act as cracks. In fact, manufacturing of a component is not ideal. There are always defects of several kinds like voids and inclusions. Welding, a common technique to join components, is a very aggressive technique. It generates various kinds of defects in the weldment and in the heat affected zones. Thus, all critical components must be checked through non-destructive techniques (NDT) to detect potentially dangerous cracks.

It is common practice to apply a factor-of-safety during the designing of a work-piece. The major uncertainty is due to the presence of manufacturing defects. If the work-piece is scanned with an NDT to rule out dangerous cracks, its integrity is assured and reliability is improved. The designer can afford to choose a lower factor-of-safety. These days, NDT has been improved to the extent that almost defect free components can be manufactured for crucial applications. However, a designer should justify the cost involved.

Many process plant operators and machine users now perform scheduled inspection at a regular interval rather than act after a failure. NDT is very effective in identifying those defects which may grow and cause catastrophic failure in a component. These defects can either be repaired or else the component itself can be replaced. This kind of quality assurance is found to be economical in the long run.

In certain crucial components such as space vehicles, airplanes, nuclear plants, dams, etc., online monitoring of defects is recommended. To achieve it, sophisticated technologies have been developed; many of them use large data handling capabilities of modern computers. These days many non-destructive tests are available, from very simple to very sophisticated. This chapter discusses some of the commonly used non-destructive test methods. They are:

- Examination through human senses,
- Liquid penetration method,
- Ultrasonic testing,
- Radiographic imaging,
- Magnetic particle inspection.

12.2 Examination through Human Senses

In many cases, a defect in a component can be detected in an initial investigation using human senses such as sight, smell, hearing, etc. Field technicians working with a machine usually know the possible locations where a crack is most likely to grow and may become unstable. Also, these people with some experience develop a keen and acute sense of observation.

12.2.1 Visual Inspection

A human eye is a marvelous device provided by nature. It is capable of detecting even minute changes in the intensity of light. For most crack detections, an initial cleaning of the surface is required. My friend, Vijay, is an expert on rolling mills. Once Vijay was consulted by a production firm to determine why the rolled sheets of a rolling machine were no longer maintaining the uniform thickness. I accompanied him to the site; Vijay looked at the rolling mill and then asked for a cleaning cloth. The frame which houses the rollers is a crucial component. It was found to be oily and dusty. Vijay cleaned the portion of the frame between the main rollers and observed a fatigue crack growth. The crack had still not achieved the critical length required for catastrophic failure but had decreased the stiffness of the frame considerably. The firm owner was advised to reinforce the frame so that the crack could be arrested and the frame could regain its original stiffness.

Several optical aids are used to facilitate the detection of a crack. Most of these devices have their own light source to properly illuminate the area under investigation. The simplest optical device is a convex lens known as the magnifying lens. To investigate the surface for a crack the lens is moved in or out to focus on the surface. A magnification of 2 to 3 usually facilitates crack detection. To detect minor cracks or scratches, an optical microscope is used, usually of 10 magnifications. A microscope with a higher magnification of 100x, 500x or 1000x can also be used but the depth of the field and the area of view are reduced considerably.

An endoscope is a more sophisticated optical device which has its own source of light so that the surface can be illuminated and scanned for cracks. The surface is adequately illuminated by the light carried through flexible optical fibers. Also, a subminiature closed circuit TV camera is installed at the front portion of the endoscope. The pictures are then carried back with the help of another set of optical fibers to a computer screen. Because of high optical efficiency of optical fibers, an endoscope can view surfaces up to 4–5 meter away. Endoscopes are useful for a wide range of applications like

detecting cracks in the internal surfaces of boilers, pipes, reactors, and heat exchangers. For example, once I visited a company making cylinders to store nitrogen and oxygen gases at very high pressures. I found that the internal surface of each cylinder was being thoroughly checked with an endoscope.

12.2.2 Investigation through Hearing

Polymer composite laminates are initially investigated by a coin test. A metal coin (e.g. one rupee coin) is tapped on the surface of a polymer composite component. The noise of the tap changes wherever interlaminar separation is present. With no interlaminar damage, the sound waves go all the way up to the rear end of the laminate and then return back, thus taking a long time to return. This corresponds to a low frequency noise. When interlaminar cracks are present, some sound waves are reflected from the surfaces of the interlaminar separation and return back early giving a higher frequency noise. The difference in the frequencies can be quite easily detected. However, a component passing the coin test is usually checked further through a rigorous NDT like ultrasonic investigation before it is finally approved.

Up till very recent time, all axles of locomotive passenger compartments were tested on all big stations during a long railway journey. Now, with the availability of more reliable components, frequent checking is not required. The axles are inspected in the yard of destination station. A trained person taps one end of the axel with a small hammer to hear the frequency. A higher frequency note would cause alarm and the compartment with a defective axle is taken out of the train-rack for a rigorous NDT. In short, appearance of a crack in a component does produce new sound frequencies and a trained person can sense the danger.

12.2.3 Detection through Smell

One good example is the leakage in an LPG cooking stove. In reality, there is no smell in LPG but an artificial smell is introduced so that if there is a leakage any where, a housewife can smell the gas and be alarmed. In most cases, the damage occurs in the plastic pipe taking the gas from the cylinder to the stove as it gets aged and cracked.

In making a high pressure cylinder, the design is usually made to have a leak before break. A semi-elliptical crack extends mostly in depth from the internal surface towards external surface. A stage comes when the semi-elliptical crack grows and becomes a through-the-thickness-crack. The design is made such that the through-the-thickness-crack is not critical. However, there will be a leakage of the gas or liquid and the crack is detected.

12.2.4 Other Simple Methods

I visited a steel plant which was making tubes as one of the several products. Each tube was tested by first closing its ends and then filling it with a liquid (e.g., water). The pressure of the liquid was increased to 30–40 % higher than the designed pressure. The pressure of the filled system was monitored with a pressure gauge for a specified time (e.g., 15 minutes) to explore whether the pressure decreases. A flow through a leak will make the pressure drop fast as the liquid does not compress much and even a small loss of liquid will decrease the pressure quickly. Such pressure difference tests are adopted for checking various systems. If a system stores high pressure gas, its leakage is often detected by applying a soap water solution on the suspected place and watch the bubbles come out.

12.3 Liquid Penetration Inspection

Liquid penetration inspection is a simple technique for non-destructive testing and is one of the most widely used techniques. It detects cracks which are exposed to a surface. The technique can be used on the surface of a wide variety of materials. It is quite reliable and is capable of identifying cracks of very small width, even cracks of just a few microns (μm).

12.3.1 Principle

An appropriate penetrant liquid with an excellent wetting capability is made to enter into the cavity of a crack through the capillary action. It is worth noting here that widths of most cracks in work-pieces of real life are so thin that cracks can not be observed through naked eyes. Figure 12.1(a) shows one such crack: dashed lines depict the existence of a crack which is invisible to human eyes. When a penetrant is applied on the surface it starts entering the crack [Fig 12.1(b)]. The penetration into a very narrow crack cavity is slow and thus takes time, known as dwell time. The penetrant contains a bright colour dye, usually red, to provide enough contrast for decorating the crack.

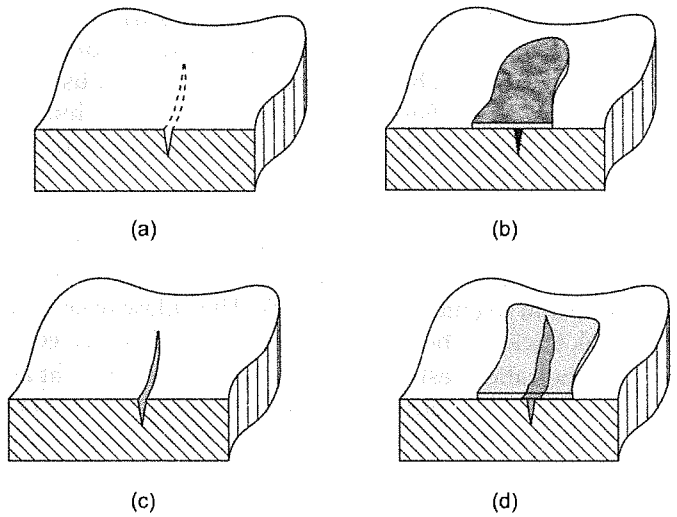

Fig. 12.1 (a) A thin crack having an opening on the surface but invisible, (b) a penetrant is spread on the surface which enters in to the cavity of the crack, (c) the penetrant is wiped out but crack is still invisible and (d) spreading of developer brings colored penetrant out of the crack cavity to make of crack look wider and visible

The excess penetrant is wiped off from the surface, leaving only the liquid within the crack cavity. Although the crack is filled with a colored liquid [Fig. 12.1(c)], the crack can not be seen yet in most cases because the crack mouth is very narrow (a few μm only).

Another liquid, a developer, is applied on the surface which is a good solvent for the penetrant liquid. As a result, a part of the penetrant comes out of the crack cavity and diffuses into the developer's layer on the surface [Fig.12.1 (d)]. In fact, the developer's layer works like a blotting

paper. Thus, a colored line with a reasonable width appears at the mouth of the crack opening. The colored line can now be easily observed by the investigator.

12.3.2 Procedure

Before applying the penetrant, the surface of the work-piece is made free of scales, flakes, paint, dirt, grease, other chemicals, etc. If the surface is not cleaned, the penetrant will have difficulty entering the crack cavity. However, abrasive cleaning methods should be avoided. Sand blasting must not be done as the particles are likely to fill the crack opening. Usually, a good solvent is used to clean the surface. Then, the surface should be dried so as to let the cleaning solvent evaporate out and to facilitate the entering of the penetrant inside the crack.

A penetrant is usually a water based liquid containing a bright dye, usually red. It can be petroleum based also. A supplier usually provides a kit of mutually compatible chemicals—a penetrant, a developer and useful solvents. It is important that the penetrant and the other chemicals do not react with the surface of the work-piece. Filling of the crack cavity through capillary action takes time and, therefore, the layer of penetrant should be allowed to remain on the surface for some time. The dwell time is usually 20 minutes or so.

At the end of the dwell time, the penetrant is cleaned from the surface. The surface should be cleaned thoroughly. If the traces of the penetrant remain on the surface, they will be decorated too along with the crack cavity when the developer is applied and the identification of a crack may become difficult. The cleaning should not be overdone also, as it can cause the loss of the penetrant from the cavity of the crack. For water-based penetrants, a simple wiping of the surface with a cloth damped with water is suitable. Or the work-piece may be washed in water. For petroleum based penetrants, oil or chlorine based solvents may be used.

A developer which is a good solvent of penetrant is applied on the surface. The developer is usually a liquid but in certain cases a solid powder is also used. The penetrant takes time to come out of the crack cavity and get soaked into the developer. This dwell time is approximately same as the dwell time taken by the penetrant to enter into the crack. The sideway spread of the bright colored dye makes the crack line look thicker. Then, the crack can be easily detected with naked eyes.

Chemicals used in dye penetration tests are usually sold in convenient aerosol cans. Thus, the chemicals can be easily sprayed on the surface to be examined for crack detection. Because of the low cost of chemicals and their availability in convenient aerosol spray cans, the dye penetration technique is very popular.

12.3.3 Crack Observation

The crack should be observed in bright day light or in a well illuminated place. The wavelength of red light lies between 0.63 and 0.76 μm which is adequate for detecting most cracks. It is important to know that to identify a geometric feature, it has to be greater than or equal to $\lambda/2$ where λ is the wavelength of the light source. An analogy is that when a horse crosses a field, he does not feel the small pits or bumps on the surface of the ground. But, if a mouse runs over the ground he has to go up and down with the unevenness of the surface. However, if the width of a crack is expected to be quite small, a fluorescent dye is used in the penetrant in place of the red colour dye. The cracks are then observed under dark conditions using ultraviolet (UV) rays whose wavelength is substantially smaller (in the range of 0.35 to 0.4 μm).

The dye penetrant examination can be performed on a variety of materials, ferrous and non-ferrous metals, polymers, ceramics, and glass, etc. However, the technique is not suitable for porous materials because pores that are opened to the surface will light up and it would be difficult to identify the cracks.

For thin components, through-the-thickness-cracks are identified easily as the penetrant passes from the front free surface to the rear free surface (Fig. 12.2).

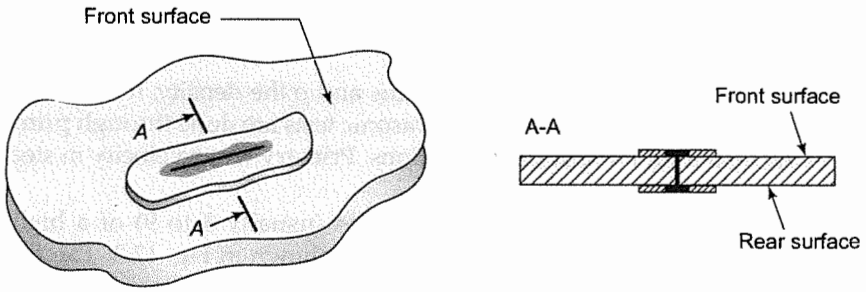

Fig. 12.2 Detecting a through-the-thickness crack

To summarize, the liquid penetration inspection is inexpensive, simple to use, reliable and versatile to inspect work-components of many kinds of materials. But it can detect only those cracks which are exposed on the surface. For fully embedded cracks, other non-destructive techniques should be used.

12.4 Ultrasonic Testing

Ultrasound tests in medical diagnostic centers are now quite popular and many of us have undergone scanning of our body organs. Ultrasonic testing to detect crack in a hardware component is based on the same principle. In fact, the ultrasonic tests were first developed for hardware materials and later on modified to perform ultrasound diagnosis of human body.

Ultrasonic testing is non-invasive, simple, inexpensive and very versatile. The technique is capable of detecting fully embedded cracks as well as surface cracks. Ultrasonic detectors are now made very compact and can be easily taken to inspect defects in fields. Also, defects can be easily identified in many kinds of materials like metals, polymers, wood, ceramics, polymer composites, etc.

12.4.1 Principle

The ultrasonic testing is similar to a search light being used to locate a thief. If there is no thief, the light gets reflected from a wall across the street. In case, there is a thief, the light will be reflected from the thief as well as from the wall.

In case of a search light, optical light waves emanate and detect objects, where as in ultrasonic tests, stress waves (also known as the sound waves) propagate within the work-piece to be investigated. When a stress wave propagates through a solid or a liquid, a particle vibrates from its usual position and makes the neighboring particle move. Thus, the energy propagates from one particle to another with sound wave velocity.

There are several kinds of stress waves in a material but two prominent ones are, (i) longitudinal or primary waves in which the particles move in the direction of energy propagation, and (ii) shear or secondary waves in which particles move normal to the direction of energy propagation. Usually, the velocity of longitudinal waves is designated by c_1 and the velocity of shear waves by c_2. They can be determined with the help of following expressions

$$c_1 = \sqrt{E/\rho}$$

$$c_2 = \sqrt{G/\rho}$$

where E is theYoung's modulus, G the shear modulus and ρ the density. It is to be noted that c_1 is greater than c_2 as E is larger than G. Majority of ultrasonic tests are done through primary waves but secondary waves are also used for special applications. Primary wave velocity in steel is quite high (about 5140 m/s).

In ultrasonic testing, a bunch of stress wave pulses (usually 3 to 9) of a high frequency is introduced on the surface of a work-piece by a probe as shown in Fig. 12.3. The frequency of the pulse-bunch is high, usually in the range of 0.5–15 MHz. This frequency is much higher than our capability of hearing whose upper limit is only 0.02 MHz. Thus, ultrasonic testing is inaudible to human ears. Most of the stress waves of a pulse-bunch reflect back from the rear face of a work-piece since there is air beyond it and very little energy is transmitted to air particles. In fact, for waves propagating in solids and liquids, the air can be regarded as vacuum. The reflected pulses are received by the probe and are quite weak in magnitude. The probe sends them to an instrument for amplification and processing. If a defect exists in the work-piece, the pulse-bunch is reflected from the defect with a shorter flight time.

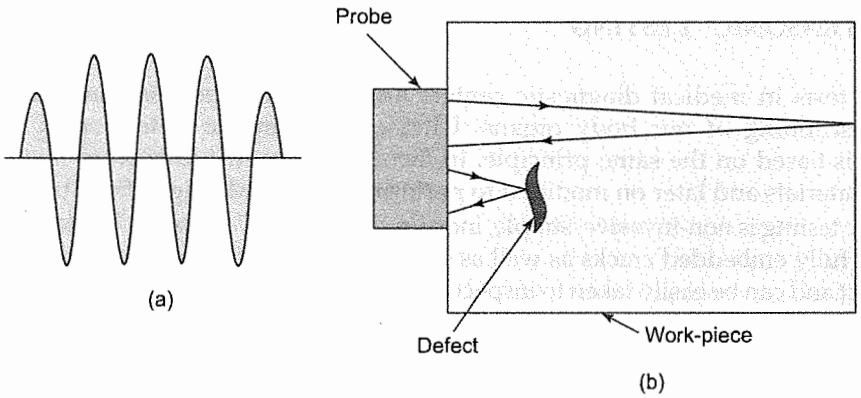

Fig. 12.3 (a) A bunch of high frequency pulses, (b) a probe transmitting high frequency pulses to a work-piece and receiving reflections from the rear surface and a defect

It is inconvenient to deal with a bunch of high frequency pulses. Therefore, pulses are rectified and smoothened as shown in Fig. 12.4; the smoothened pulse is known as echo. The incident pulses on the work-piece are also rectified and smoothened to have a primary echo (bang). Figure 12.5 shows the primary echo, the echo from the rear surface and the echo from a defect. Appearance of an echo between the primary echo and the echo of the rear surface gives two important informations, (a) there is a defect in the material, and (b) how deep is the defect. Figure 12.5 shows

an echo from a defect with round trip flight time of t_1. Then, the distance of the defect from the front surface is $c_1 t_1/2$.

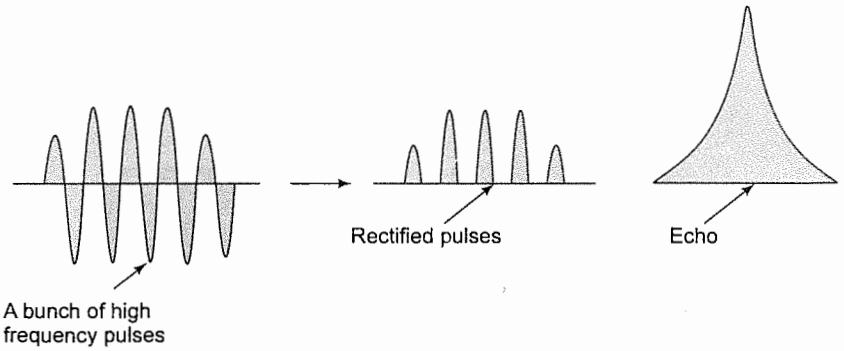

Fig. 12.4 A burst of high frequency pulses rectified and smoothened to have an echo

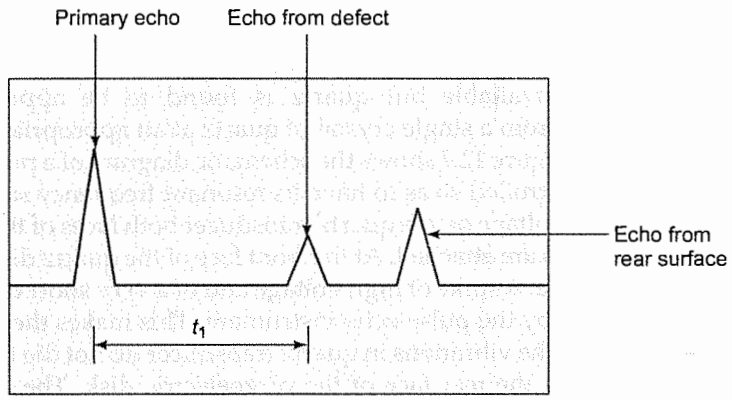

Fig. 12.5 Echoes recorded on an oscilloscope display or a computer

Ultrasonic testing requires high frequency of pulses because the defect size should be larger than the half of the wavelength ($\lambda/2$) of elastic waves. For example, wavelength of sound wave propagation for 5 MHz probe is about 1 mm in steel. This kind of pulse frequency can detect flaws having geometrical features large than 0.5 mm. If a probe of 1 MHz frequency is used on a steel component, defects smaller than 2.5 mm will not be detected. On the other hand, wavelength of 1 MHz probe in a polymer like epoxy is close to 1.6 mm and defects of sizes smaller than 0.8 mm are not detectable.

12.4.2 Equipment

There are mainly three major units of an ultrasonic test setup, (i) probe, (ii) pulse-echo instrument, and (iii) display oscilloscope (or computer) as shown in Fig. 12.6. The probe is the most crucial unit and will be taken up first.

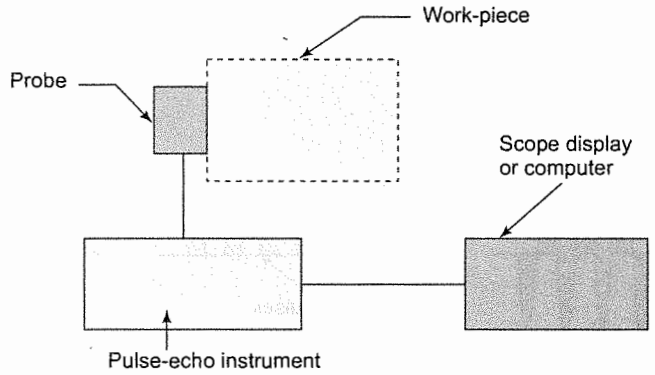

Fig. 12.6 Hardware elements of an Ultrasonic Detector

Probe

The transducer in the probe is a thin disk of a piezoelectric material which converts a voltage signal into stress pulses. These stress pulses are transmitted to the surface of the work-piece. There are several piezoelectric materials available but quartz is found to be appropriate for most applications. The thin disk is cut from a single crystal of quartz at an appropriate angle (X-cut for generating longitudinal waves). Figure 12.7 shows the schematic diagram of a probe. The thickness of the quartz disk is precisely controlled so as to have its resonant frequency same as the desired frequency of the probe. To apply voltage on the quartz transducer both faces of the thin quartz disk are electroplated and electric wires are attached. At the front face of the quartz disk a wear resistant plate is fixed as shown in the figure. A spike of high voltage and of a very short duration (≈10 ns) is applied on the quartz transducer by the pulse-echo instrument. This makes the piezoelectric disk vibrate at its resonant frequency. The vibrations in quartz transducer do not die fast and, therefore, a damping material is applied on the rear face of the piezoelectric disk. The damping material helps in suppressing the vibrations of the disk and thus, only a bunch of a few pulses passes into the work-piece.

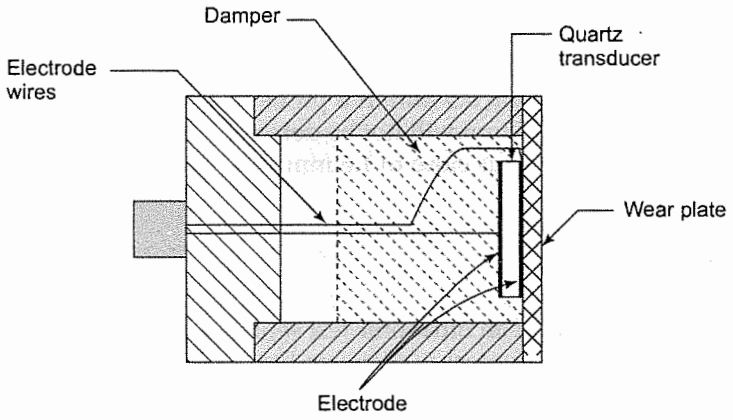

Fig. 12.7 Schematic diagram of a probe with quartz transducer, sound absorbing damper and wear plate

A kit of ultrasonic flaw detector comes with probes of different frequencies. Depending upon the material to be tested, an appropriate probe is chosen. The wavelength of sound waves is usually maintained between 1 and 10 mm within the work-piece.

The piezoelectric disk also works as a transducer to record the echoes coming back to it. The stress of an echo develops voltage across the faces of the piezoelectric disk. The electric signal thus generated is weak and needs to be amplified.

A material known as couplant is required to propagate the sound waves from the probe to the surface of the work-piece. Usually, a viscous oil, grease, glycerin or water is used as couplant. The couplant should be quite inert to avoid damage to the surfaces of the work-piece and the probe.

Pulse-Echo Instrument

As already stated, the pulse-echo instrument generates a spike of high voltage and of a very short duration at a regular interval. This spike resonances the piezoelectric disk which, in turn, passes a bunch of pulses into the specimen as the primary echo (main bang).

The sound wave inside the material is dissipated due to several mechanisms (to be discussed subsequently). Once all the echoes of a main bang die, a new spike of identical nature is generated. The new spike again triggers the oscilloscope and the echo response is repeated. This kind of repetition at a regular interval creates a stable display on an oscilloscope or computer screen.

An amplifier in the pulse-echo instrument amplifies the weak signal of the echo received by the probe. Also, the instrument filters the undesirable noise picked up by the probe before the echo is displayed on an oscilloscope screen. Some professionals like to use a computer in place of oscilloscope display. It has the advantages that a large number of test information can be stored, an echo can be magnified and minute features can be studied.

Transmission Losses

As the pulse propagates in the material, there are transmission losses and the intensity of the stress waves is attenuated because of several causes: (i) there is a divergence of stress waves which in turn makes the echo weak,(ii) there is a scattering of stress waves due to inhomogeneities present in real life material such as inclusions of second phase particles, voids, shrinkage cracks, grain boundaries, etc., and (iii) there exist hysteresis which convert mechanical energy of sound waves into heat. If the transmission losses are high, the echo from the rear surface of the work-piece will be of poor quality. Losses of high frequency stress waves are more and therefore a high frequency probe may not be appropriate for testing thick components. A low frequency probe can be used on a thick work-piece as the transmission losses are low. However, it can not detect minute defects as the wavelength of the sound wave is long. On the other hand, a high frequency probe can detect defects of smaller sizes. An experienced or trained operator chooses a probe of a right frequency for the given job.

Transmission losses are much higher in polymers in comparison to losses in metals. Then, a single probe with pulse-echo capability may not work. In such situations, two probes are used, a transducer transmitter and a transducer receiver, as shown in Fig 12.8. Most polymer composite laminates are tested with the help of this arrangement.

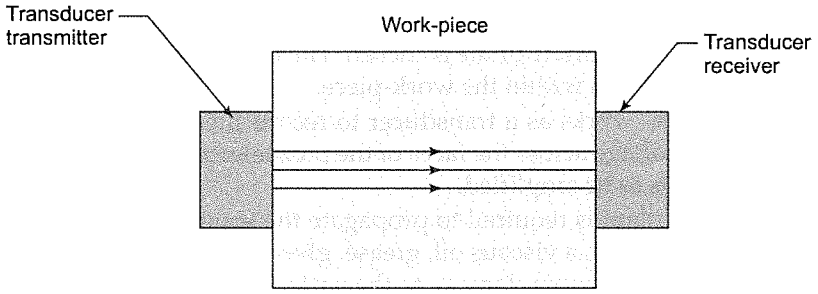

Fig. 12.8 Two probes Ultrasonic Detector

12.4.3 Immersion Inspection

A component is completely immersed in water or other suitable liquids and tested for flaws. The testing can be done through a transmitter-receiver transducers or through a single probe using pulse-echo principle. The immersion method is convenient for testing a large number of work-pieces. The method has an additional advantage that the couplant is uniform over the entire surface of a work-piece.

From the geometric point of view, there are three kinds of inspections–A-Scan, B-Scan and C-Scan. A-Scan investigates flaws at a point of the work-piece. If the probe is moved in a line and echo response is continuously monitored it is called a B-Scan. C-Scan is useful in scanning the full area of a component as the probe is moved first along a line, say parallel to x-axis, then, it is shifted laterally by a small amount along y-axis and again scanned in x-direction. The procedure is carried out to cover the entire area. Figure 12.9 shows a C-scan of an impacted polymer composite panel. The empty space corresponds to the signals not received by the receiving transducer. In the impacted panel, this corresponds to delamination caused by the impact induced damage.

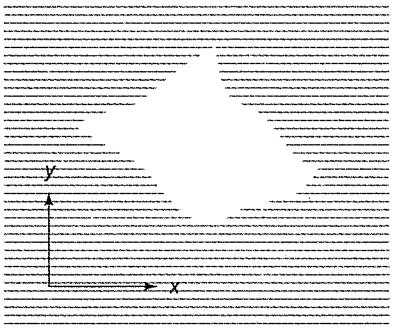

Fig. 12.9 C-scan showing delamination in a polymer composite laminate

Once, I visited a company which was making large panels of polymer composites to be used in airplanes. They had a setup specially made for detecting crack in a panel. In the set up, a jet of water hit the left face of a panel which also transmitted ultrasonic waves to the panel. On the right face of the panel, another jet of water was made to hit the panel in the same line. This water jet was connected to a receiving transducer. The transmitting and receiving transducers moved in unison to do the C-scan of the work-piece.

The ultrasonic testing is very versatile and has been adopted for various applications by devising special elements. For example, a work-piece can be scanned at an angle using an angular probe whose transducer usually works on shear wave propagation. In short, ultrasonic test is a widely used non-destructive technique. It is simple to use, relatively inexpensive, quick and portable. The technique can detect surface as well as fully embedded defects.

12.5 Radiographic Imaging

Working of radiographic imaging is similar to that of a camera with a flash light which we use in daily life. The flash sends a predetermined amount of light and the reflected light from the objects is recorded on a photographic film installed inside the camera. The film records the contrast of the light reflected from the various objects in the view. In radiography, the difference is that the recording film is separate from the radiographic source and is placed behind the work-piece.

In radiographic imaging, electromagnetic waves (X-rays or γ-rays) of very short wavelength are transmitted through a work-piece. If the material of the work-piece is not uniform, the transmission of electromagnetic waves will be absorbed differently and there will be contrast on the recording film. For example, if there is an embedded void in the work-piece, the electromagnetic waves will not be absorbed while propagating through the void and thus reduction in the intensity will be less. Consequently, the film will be exposed more on the portion that corresponds to void location.

X-rays or γ-rays are both electromagnetic waves but are produced using different sources. Each has its own strength and limitations (to be discussed subsequently). For radiographic imaging, both waves behave in same manner to detect defects.

12.5.1 Contrast through Absorption Rate

X-rays or γ-rays propagate with the velocity of light. Their frequencies are extremely high and consequently their wavelengths are extremely small, usually ranging between 1 nm and 1×10^{-6} nm. They are capable of passing through any material because of the presence of spaces between atoms. Also, an atom itself is spacious as its nucleus is quite small. Radiographic waves are like a mouse which can go through small holes in a wall, whereas light waves with longer wavelength are like a cat which cannot pass through.

X-rays or γ-rays are progressively absorbed as they propagate in a material. The absorption rate (attenuation) depends on the material being tested; it is high in a dense material. The progressive absorption is the key to radiographic imaging. An inclusion or a void will affect the intensity of radiation on the recording film, thus creating contrasts.

12.5.2 Imaging through X-rays

X-rays are produced in high vacuum within a tube made of glass or ceramic. When the cathode is heated by passing current through it, electrons are emitted. A very high voltage is applied between the cathode and the anode target as shown in Fig. 12.10. Depending upon the application, an X-ray tube is designed with voltage in a high range from 20 kV to 20 MV. The electrons, accelerated by the high voltage, impact the target producing X-rays. The target is known as focal point and is usually made of a hard material like tungsten. Most of the kinetic energy of the impacting electrons

is converted into heat. Thus, a proper cooling of the target is required. Also, the target cannot be very small to avoid its overheating. The finite size of target plays an important role in affecting the sharpness of imaging. This aspect will be discussed subsequently. A window of low absorbing material (beryllium, aluminum) is provided for the exit of the X-rays from the tube. The X-rays radiation spreads as shown in Fig. 12.11. X-rays pass through a work-piece to a recording film.

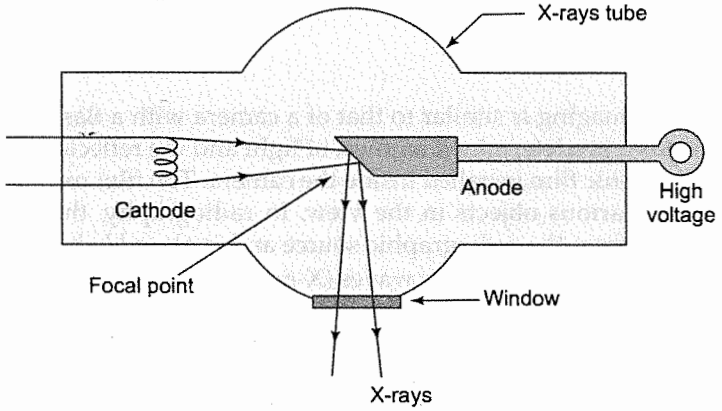

Fig. 12.10 X-ray setup

Penetration Ability and Exposure

Absorption of X-rays is high in thick or dense materials. To have an appropriate intensity of X-rays for a given material and a given thickness of a work-component, suitable anode-voltage is selected for the X-rays tube. For example, X-rays generated by 150 kV can penetrate 30 mm thick steel plate and 80 mm thick aluminum plate. Similar to a photographic camera, right exposure is given for imaging defects. Too much or too little exposure will not give a proper contrast on the recording film. Usually, an exposure is measured as $E = At$, where A is the filament current of cathode and t the exposure time.

Loss of Sharpness of an Image

The image of a defect may not be sharp due to two considerations:

(i) *Geometric unsharpness:* The focal point works more like a point source from where X-rays start spreading as shown in Fig. 12.11. However, as discussed earlier, it is difficult to have the focal point very small; usually its size is between 2 mm × 2 mm and 5 mm × 5 mm. Due to the finite size of the focal point, X-rays from the edge of a defect fall on a finite width of the recording film, giving rise to a blurring of the edge (Fig. 12.12). The blurring can be minimized by placing the focal point far away from the work-piece and the recording film very close to the rear surface of the work-piece.

(ii) *Effect on radiation on recording film:* High density radiation interacts with the recording film which has a thin layer of a silver halide as a main constituent to record the amount of exposure. The radiographic exposure dislodges electrons from silver halide emulsion. These electrons fly to cause ionization of adjacent silver halides causing blurring of the edges of a defect. One can use low sensitivity film with a thinner spread of silver halide to suppress

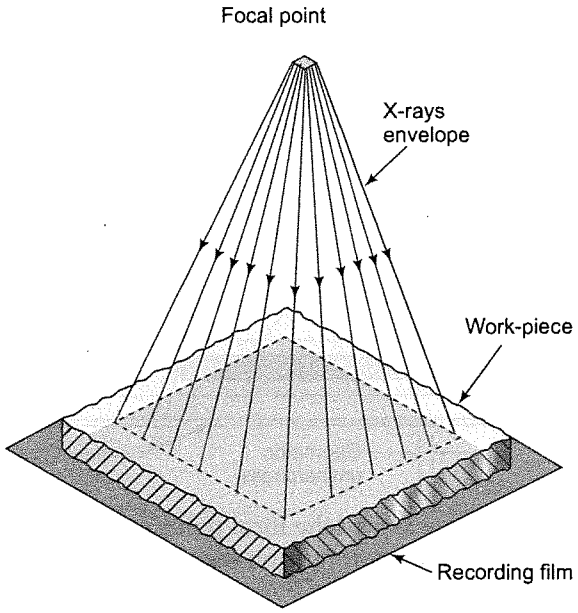

Fig. 12.11 X-rays falling on a work-piece with a film placed close to its rear surface

the blurring. But then, the exposure time on the film would have to be higher, thus creating a condition of give and take.

12.5.3 Imaging through Gamma Rays

A gamma rays source is an unstable nucleus that continuously emits radiation similar to the radiation of X-rays. Several kinds of gamma sources are used but the most common are Cobalt 60 and Iridium 192. The energy level of radiation is quite high, in the wide range of 100 keV to 1 MeV. Because of their smaller wavelength, they are capable of penetrating dense and thick materials. Sources of γ-rays are supplied by a national atomic commission (i.e., Bhabha Atomic Reactor Center, Mumbai in India). They are supplied in sealed capsules of dimensions ranging between 0.3 mm $\times$ 0.3 mm and 6 mm $\times$ 6 mm.

The gamma imaging of defects in a material is similar to X-ray imaging with associated problems of contrast, blurring and optimum exposure. However, a gamma source is small and can be inserted into a small cavity. For example, a gamma source can be placed within a pipe of small internal diameter; the radiation sensitive film is then placed at the outside surface of the pipe.

A γ-source continuously emits radiation and, thus, has a limited life, a few months to a few years depending upon the type of γ-rays source. It is worth noting that X-rays emission is broadband, that is, radiation has a wide range of wavelength. In contrast, γ-rays emission is monochromatic. Also, in comparison to X-rays, the number of disintegration per unit time is much less in γ-rays and, therefore, substantially longer exposure time is required.

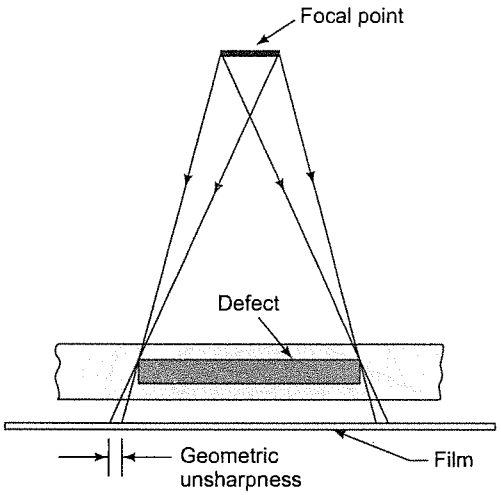

Fig. 12.12 The finite size of the focal point develops geometric unsharpness on the film

12.5.4 Strong Points of Radiographic Imaging

- Can detect defects in almost all materials including dense steel.
- X-rays and γ-rays can penetrate thick components and detect cracks.
- No surface preparation of a work-piece required.
- Sources of γ-rays are very compact to use.

12.5.5 Limitations of Radiographic Imaging

- The technique is relatively expensive. Sophisticated equipment is required for X-rays and a source of γ-rays has a limited life.
- Access to both front and rear surfaces is needed.
- Very tight cracks (very small space between the crack faces) are difficult to be detected. Also, minute discontinuities are not detected.
- Radiographic imaging gives no idea of how deep the defect is.
- Sharpness may be a concern in interpreting the images.
- A thin defect (e.g. a thin disk) normal to the propagation direction of X-rays or γ-rays is not recorded with good contrast as the progressive absorption through the defect is small creating only small contrast.
- X-rays or γ-rays are high energy electromagnetic waves and may cause injuries to workers. Each worker in a radiographic unit has to carry a badge which progressively monitors the radiation exposure to his body.

In short, radiographic imaging deals with powerful high frequency and very low wavelength electromagnetic waves which pass through all kinds of materials. A defect absorbs the radiation differentially and is recorded on a sensitive recording film with a different contrast.

12.6 Magnetic Particle Inspection

Magnetic particle inspection is capable of detecting surface and subsurface cracks in a work-piece made of ferromagnetic materials such as most steels, nickel and cobalt. The technique is simple to use, inexpensive, quick, sensitive, and reliable. However, inspection is limited to ferromagnetic materials only.

12.6.1 Principle

A strong magnetic flux is generated within a work-piece. A defect disturbs the lines of force and creates leakage of magnetic flux out of the surface of the work-piece. When minute magnetic particles are sprayed, they get deposited on the surface at points which are close to the crack. This happens because the disturbed magnetic flux passes through the particles. Figure 12.13 (a) shows a crack open to the surface. Some magnetic particles may enter inside the cavity of the crack and allow some magnetic flux pass through them. But most of the disturbed flux passes through a ridge of particles which builds up at the mouth of the crack. It is worth noting that the width of the particle ridge is much wider than the width of the crack mouth. Thus, the cracks can be observed easily. This concept is similar to one used in liquid penetration test where the coloured penetrant comes out of the crack cavity and spreads on the sides to make the crack visible.

A subsurface crack which is not too deep inside the surface (usually within 6 mm) is also detectable. In Fig.13 (b), a fully embedded crack disturbs the magnetic flux and part of it tends to leak out. When magnetic particles are sprayed, they get deposited on the surface to facilitate magnetic lines of force pass through them. However, the deposition of magnetic particles due to a subsurface crack is diffused whereas a surface crack shows clear and sharp deposition of particles.

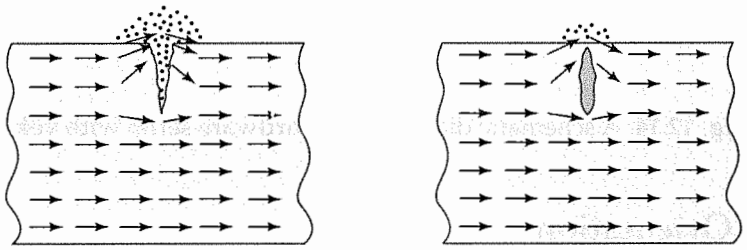

Fig. 12.13 Magnetic flux through work-pieces, (a) a particle ridge is built up over the mouth of a surface crack, and (b) magnetic particles are deposited due to a subsurface crack

12.6.2 Sensitivity

Magnetic particle inspection is quite sensitive and can detect cracks as small as 0.02 mm deep. Also, it is capable of detecting surface cracks with opening as small as 0.002 mm (2 μm). However, the ratio of the depth to width of the crack should be large (>5). A shallow crack with a wide opening having depth/width ratio of the order of one does not really disturb the magnetic flux and therefore magnetic particles do not get deposited.

12.6.3 Hardware

The technique is versatile and many kinds of hardware models have been developed for different geometry of work-pieces. A schematic diagram of a general purpose test setup is shown in Fig. 12.14. Its flexible yokes can clamp a large variety of work-pieces. The coil develops a longitudinal magnetic flux in the work-piece. The work-piece in the figure shows a corner crack identified by magnetic particle inspection.

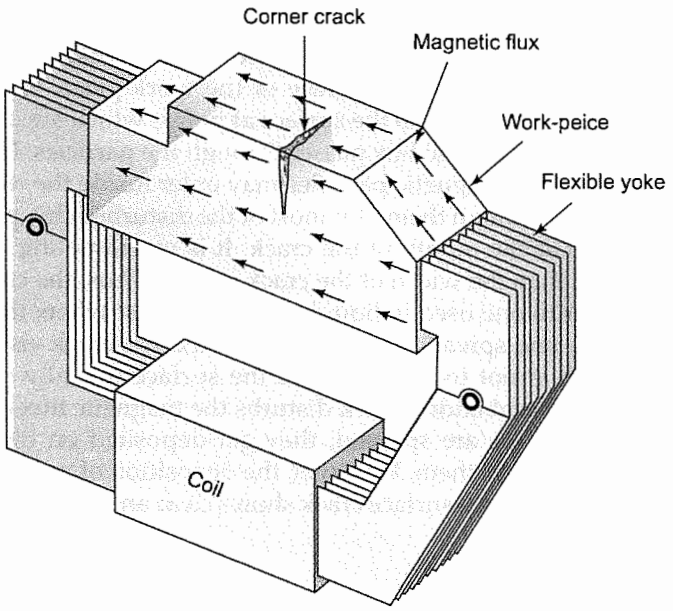

Fig. 12.14 A schematic diagram of a hardware setup with yokes

12.6.4 Flaw Orientation

Flaws normal to the magnetic flux direction disturb the magnetic lines of the force the most. On the other hand, if a thin long crack is aligned to the magnetic flux direction, it would not be detected. Usually, flaw orientations between 45° and 90° are detected. Thus, to detect all the cracks, the work-piece should be tested in several orientations. For example, if defects are to be detected in a tube, two kinds of magnetic flux should be generated. In Fig.12.15 (a), a coil is wound around the tube generating longitudinal magnetic flux. The configuration detects cracks normal to the axes of the tube. In Fig. 12.15 (b), a conductor rod is passed through the interior of the tube generating circular flux. This kind of flux would detect cracks parallel to the axis of the tube.

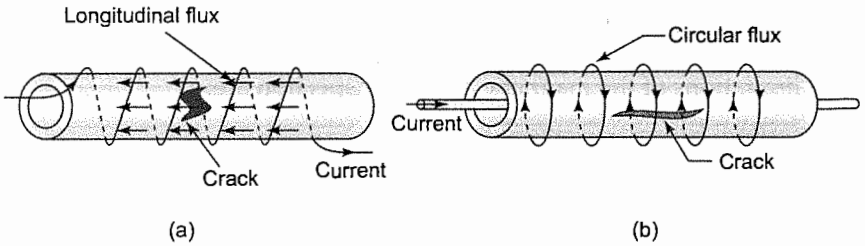

Fig. 12.15 (a) Wound coils around a tube generating axial lines lines of force and (b) a conducting rod inserted inside the tube generating circular flux

12.6.5 Magnetic Ink Powder

Particles used are minute in size (about 6 μm) and are made of a suitable ferromagnetic material with good permeability like pulverized iron oxide (Fe_3O_4), carbonyl iron powder (pure iron), etc. There are two ways of applying the magnetic particles, (i) wet and (ii) dry. In the wet route, particles are suspended in water or oil and are applied on the component. In dry particle route, air is the carrier which sprays particles on the surface.

Magnetic particles inspection can be performed even if there is a thin paint on the surface of the work-piece and particles. Thus, particles are often coloured with black or red thin paint. Also, the work-piece may be painted with a thin coat of white colour so that the build up of black or red coloured particles on a defect is easily observed.

Fluorescent particles are also used, especially to detect hair line cracks. Fluorescent particles are prepared by applying a thin coat of a fluorescent material on the surface of the ferromagnetic particles. Then, the observation is made under dark conditions using UV light. In comparison to crack detection through ordinary magnetic particles, the illumination of a crack through fluorescent particles is vastly superior.

12.6.6 Voltage Source

Three kinds of voltage sources are used: (i) DC, (ii) AC, and (iii) Half Wave Rectification (HWAC). A DC source gives full penetration and is suitable to detect both surface and sub-surface cracks. An AC source works well with surface cracks. A HWAC source works well with dry particles as ripples in magnetic flux keep on vibrating the particles making them more visible.

12.6.7 Demagnetization

Often, a work-piece needs to be demagnetized to avoid confusion in detecting defects. There are several ways but one good method is to place the work-piece in reverse magnetic field and reduce the magnitude gradually to zero.

12.6.8 Strength and Limitations

The strength and limitations of the magnetic particle inspection are:

Strength

- Simple to use.
- Inexpensive.
- Rugged equipments.
- Sensitive enough to detect even hairline cracks.
- No elaborate surface preparation of the work-piece required; only degreasing is adequate, especially on machined and electroplated surfaces. However, rust, scale, etc., should be removed.
- No elaborate safety required.
- Quite dependable if a component can be checked in several directions.

Limitations

- Only work-pieces made of ferromagnetic materials can be inspected.
- Only surface or subsurface defects are detectable
- Orientation of a crack with the direction of magnetic flux is important.
- Often, demagnetization of a component is required.

In short, the magnetic particle inspection is a powerful technique to detect surface or subsurface defects in ferromagnetic materials. The technique is inexpensive and simple to use.

12.7 Concluding Remarks

Fracture mechanics is applicable only when a crack exists in a work-piece. Real materials have many defects like voids, inclusions, cracks, etc. But most of them are subcritical and safe. Reliable non-destructive test methods are required to assure safety of components. These days, many non-destructive test techniques are available. However, only some of the widely used methods are discussed in this chapter. Also, only the basics of various NDTs are covered in this chapter; for in-depth details and various sophistications, readers are recommended to refer to advanced material.

Some time back, I met a German expert whose team developed an experimental test setup to check a locomotive wheel for defects with ultrasonic testing at 21 locations. The testing of the wheels is done at a fast pace so that all the wheels of a train rack can be tested within an hour. Such preventive testing can save many human lives. Thus, the modern philosophy is to avoid, to the maximum possible extent, a catastrophic failure by regularly checking the critical components through non-destructive testing.

REFERENCES

12.1 Mix P. E. (2005). *Introduction to Nondestructive Testing*, John Wiley & Sons, Inc., New Jersey.
12.2 Raj, Baldev, Jayakumar, T. and Thavasimuthu, M. (1997). *Practical Nondestructive Testing*, Narosa Publishing House, New Delhi.
12.3 Boving, K. G. (1989). *NDE Handbook*, Butterworths, London.
12.4 Hemelrijck, D.V. and Anastassopoulos, A. (1996). *Non Destructive Testing*, A.A. Belkema, Rotterdam.
12.5 Halmshaw, R. (1996). *Introduction to the Non-Destructive Testing of Welded Joints*, Woodhead Publishing Ltd. Cambridge.
12.6 Cartz, L. (1995). *Nondestructive Testing*, ASM International, Material Park.
12.7 Bray, D.E. and Stanley R.K. (1989). *Nondestructive Evaluation*, McGraw-Hill Book Company, New York.
12.8 http://www.ndt-ed.org/index_flash.htm

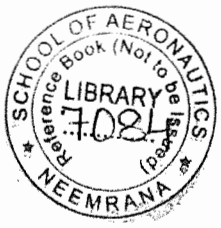

Index

Author's Profile

Prof. Prashant Kumar was till recently with the Department of Mechanical Engineering, Indian Institute of Technology, Kanpur. He has over three decades of teaching and research experience. A B. Tech. in Mechanical Engineering from IIT Kanpur, he has M.S. in Design from University of California, Berkeley, USA. He worked as a Design Engineer in Los Angeles for over two years. In 1976, he obtained his Ph. D in Mechanics of Solids from Brown University, USA.

Prof. Prashant Kumar has published a number of papers in international and national journals and magazines. He has worked on sponsored projects on fracture aspects of polymer composites. He has been a consultant to many industries around Kanpur and national organizations like HAL Korwa, ADE Bangalore and ADA Bangalore.

Prof. Prashant Kumar was the founder Head of Department of newly created Design Programme at IIT Kanpur from year 2002 to 2005. Earlier, he was Head of Department of Mechanical Engineering from year 1998 to 2001.